Development of Corrosion Resistant Conducting Polymer Coating for Aircraft Applications

Submitted in partial fulfillment of the requirements

of the degree of

Doctor of Philosophy

from the
Indian Institute of Technology, Bombay, India
and
Monash University, Australia

by

Gunjan Gupta

Supervisors:

Prof. A. S. Khanna (IIT Bombay)

Dr. Nick Birbilis (Monash University)

The course of study for this award was developed jointly by
the Indian Institute of Technology, Bombay and Monash University, Australia
and given academic recognition by each of them.
The programme was administered by The IITB-Monash Research Academy

(June 2013)

Copyright Notices

Notice 1

Notice 2

APPROVAL SHEET

This thesis entitled **"Development of Corrosion Resistant Conducting Polymer Coating for Aircraft Applications"** by **Gunjan Gupta** is approved for the degree of Doctor of Philosophy.

Examiners

[redacted]

[redacted]

[redacted]

Chairman

Date : 18/06/2013

Place : Mumbai

DECLARATION

I declare hereby that this written submission represents my ideas in my own words and where others' ideas or words have been included, I have adequately cited and referenced the original sources. I also declare that I have adhered to all principals of academic honesty and have not misrepresented or fabricated or falsified any idea/data/fact/source in my submission. I understand that any violation of the above will be cause for disciplinary action from the authority and can also evoke penal action from the sources which have thus not been properly cited or from whom proper permission not taken when needed.

(Gunjan Gupta)

Roll No. 09416401 (IIT Bombay)

I.d. No. 22343288 (Monash University)

Date: 18.06.2013

Place: IIT Bombay, Mumbai

ACKNOWLEDGEMENTS

This section is as special to me as to those who feature in this, who have supported me in every possible way to reach as far as this big moment, so close to my PhD, and I feel privileged to express my gratitude and appreciation to them.

I am truly indebted to Prof. A S Khanna with whom I completed my M.Tech dissertation as well, for bringing me from one of the most prized jobs in India to this PhD programme with a belief that I could do this. I am extremely glad to have had the opportunities to learn from him and work with him. Dr. Nick Birbilis gave me tremendous opportunities to go beyond the boundaries and figure out more science in the challenging topic. His support in every step of the process made the journey fairly easy. I express my deepest gratitude and appreciation to both my supervisors, who admitted me to work on this challenging topic, for fostering and stimulating critical thinking and providing every small and big support through every thick and thin.

The IITB-Monash Research Academy is thankfully acknowledged for selecting me through the rigorous process. The Academy staffs have been very cooperative and supportive in simplifying the paper work related to research, granting support for international conference. I thank Head of the department, staff of Materials Engineering, Monash University for their immense support and cooperation during my three month Melbourne stay. I would also like to thank Dr. Rajeev Gupta from Monash University for his help during the experimental works. I would thank Dr. A.B. Cook for his guidance and suggestions in my drafting technical paper.

My colleagues and friends at both institutes have been pillars during the entire period and beyond and deserve due acknowledgement. I thank Rama, Narayani, Garima, Ruchi, Swati and Karan for their support during laboratory works. I express my heartfelt thanks to all my friends and departmental staffs at Mumbai and Melbourne for being companions for most of my time spent in the two cities and making life simple for me.

I would also like to thank my research committee members Prof. R.S. Raman and Prof. A.S.Panwar for taking time out of their busy schedule to serve in my committee, review my report and provide valuable comments and suggestions on the work.

Last but certainly not the least, I would like to thank my family for their love and support during my research. I especially would like to thank my husband Mr. Sandeep Khandelwal whose understanding, love and support is indispensable for the successful completion of my research work.

Abstract

Epoxy based conducting polymer coatings were prepared by using polyaniline (Pani), modified with lignosulfonate (LGS) dopant for the aircraft AA2024-T3 alloy. High-strength, light-weight alloys such as AA2024-T3 is widely used for the skin construction of an aircraft. This type of coating resulted in enhancement of conductivity upto 4.88 S/cm compared to 10^{-8} S/cm for epoxy alone. However such a combination Pani-LGS loses its conductivity with time because of the loss of the dopant. Therefore, the Pani-LGS was further modified by grafting with another polymer i.e. poly(acrylamide co acrylic acid) which maintained the conductivity for longer duration by preventing the loss of dopant. The modification of Pani-LGS with poly (acrylamide co acrylic acid) exhibited conductivity of 3.9 S/cm but maintains it for longer time and showed 1200h salt spray test. The aim of the present work was to achieve conductivity of 5-10 S/cm and corrosion resistance equivalent to 2000h salt spray pass for the coating and hence, further improvements were made with the addition of montomorillonite clay (MMT), aluminium oxide nanoparticles (Al_2O_3) and graphene (G) to the coating. Other properties of these developed conducting coating, such as corrosion resistance, weathering resistance and mechanical properties were also studied. It was found that the modified coating system had better conductivity (8.76 S/cm in case of graphene), corrosion resistance (2400 h salt spray passes) and enhanced mechanical properties. Detailed stepwise mechanism of various modifications has been proposed which helps in overcoming the defects created by aggressive environment, by both barrier protection and anodic protection of conducting polymer coatings.

Content

List of Tables

List of Figures

Chapter 1 Introduction

Conducting polymers have recently been studied as a new class of materials for the corrosion protection of metals. Conducting polymer coatings are environmental friendly coatings. It can substitute any heavy metal containing compound. The polymer's conductive nature provides an electroactive interaction with the metal surface and forms a passivation layer between the metal surface and the polymer coating. Therefore, it functions as a barrier coating as well as provides anodic protection to the underlying metal substrate.

Corrosion of metals creates one of the major problems in the maintenance of aircraft, particularly in areas where adverse environmental or weather conditions exist. Corrosion is an important issue for an aircraft because it can be expensive to remove, lead to reduced readiness of the aircraft and can also create a safety hazard. High-strength, light-weight alloys such as AA2024-T3 is widely used for the skin construction of an aircraft. The most common problem of this alloy is that it forms a non protective oxide on their surfaces because of copper, zinc and other metal contamination and is susceptible to corrosion under continued exposure to aggressive environments. The current technology to protect AA2024-T3 aluminium alloys is by chemical conversion coating using chromates (primer) and epoxy (top coat). These chromates based coatings give excellent corrosion protection, but are becoming unpopular due to their adverse environmental effects. Another problem with these alloys is due to lightening/electrical thundering which can cause damage to internal components of the aircraft. In order to protect the aircraft alloy from aggressive environment and electrical thundering damage, conducting polymeric coatings can be of best benefit.

Conducting polymers are used as an alternative to the environmental hazardous chromate based coatings. Conducting polymers like polyaniline (Pani), polypyrrole (PPy), polythiophene have been shown to provide adequate conductivity and protection against corrosion for aluminium alloys. Polyaniline has played a significant role in corrosion protection because of its high environmental stability, low cost and simple polymerization process. Several methodologies have been proposed for the application of conducting polymer coatings such as a primer alone or as a primer with epoxy top coat. Epoxy resins are used as

binder in protective coatings because of their excellent adhesion, corrosion resistance, and excellent mechanical and thermal properties. Polyaniline when added to epoxy matrix, have shown to enhance the overall properties of epoxy. From literature, it was found that dopant play an important role in the conductivity of the polyaniline. Polyaniline alone cannot provide sufficient conductivity as well as corrosion protection. Lignosulfonate dopant is used to increase the conductivity of Pani but long term exposure to any aggressive environment, increases the susceptibility of loss of dopant and consequently decreases the conductivity of polyaniline. Double stranded conducting polymers serves as viable solution for the problem of dopant loss and improves the conductivity and corrosion resistance of polyaniline based coatings. Incorporation of nanoparticles (montmoronillite clay (MMT), aluminium oxide (Al_2O_3) and graphene (G)) will further enhances the strength, corrosion resistance, thermal stability, conductivity and mechanical properties of the conducting polymer coatings.

Chapter 2 Literature Survey

Corrosion is defined as the deterioration of metal in presence of an external environment. It begins on the surface of the metal involving two chemical changes; metal that is attacked undergoes an anodic change and corrosive agent undergoes a cathodic change. Pure aluminium forms native oxide passivating layer which results in excellent corrosion protection [1]. However, pure aluminium metal does not have enough mechanical strength for structural and constructional applications. Improved strength is achieved by Cu, Mg, or Si in aluminium alloys. These types of high-strength, light-weight alloys such as AA2024-T3 are widely used for the skin construction of an aircraft. The most common problem of these alloys is that they form a non protective oxide on their surfaces because of copper, zinc and other metal contamination and are susceptible to corrosion under continued exposure to aggressive environments [2].

Leblance et al. studied the corrosion behavior of AA2024-T3 and the interactions between individual inclusions were investigated using atomic force microscopy-based techniques. The results showed that Al-Cu-Fe-Mn intermetallic particles were cathodic in nature and interacted strongly with their surroundings. For large exposed areas, it was found that pitting initiated at a few Al_2CuMg particles, which became active upon film breakdown even though scanning kelvin probe force microscopy measurements in air showed they were noble with respect to the matrix prior to the exposure. Accelerated matrix dissolution took place for exposed areas containing a large area fraction of AlCu-Fe-Mn inclusions. The location of the cathodic sites had a strong influence on the local chemistry of the environment and controlled the corrosion behavior of the surface [3].

The current technology to protect AA2024-T3 aluminium alloys is by chemical conversion coating using chromates. These coatings give excellent corrosion protection, but are becoming unpopular due to their adverse environmental properties. Chromium ions are carcinogenic in nature and their contamination with water leads to environment and human health issues like nausea, vomiting, headache and dizziness [4-7]. The use of chromate containing compounds has been limited since 1982 and EPA (Environmental Protection Agency) has issued a

regulation that chromate based coatings should be replaced by environmentally friendly alternatives. Since the release of this federal mandate, much of the collaborative work has been done in the academic, industrial and governmental sectors to provide an apt method for corrosion control of aluminium alloys [4]. Another problem is of lightening/electrical thundering which can cause damage to aircraft. In order to protect the aircraft alloy from aggressive environment and electrical thundering damage conducting polymeric coatings are planned.

Several methodologies have been proposed for the application of conducting polymer coatings such as a primer alone or as a primer with conventional top coat or as an additive to paint formulation, blended with conventional polymer coatings [8]. Polyaniline has played a significant role in corrosion protection because of its high environmental stability, low cost and simple polymerization process [9-14]. One drawback with these materials is their low solubility, caused by π stacking of conjugation, resulting in poor processability in the finished polymers. Use of dopants such as HCl, H_2SO_4 in case of polyaniline produces materials with high conductivity but does not provide solubility. Replacing these dopants with larger functionalized organic dopants such as 10-camphorsulfonic acid (CSA), dodecylbenzenesulfonic acid (DBSA) and lignosulfonic acid (LGS) increases the solubility of conventional conducting polymer. Several formulations are available of Pani doped with CSA [8], DBSA [9-10], TSA [11] and LGS [12]. Dopants in Pani can play an important role in corrosion protection due to the formation of a metal-dopant interface [15,16]. Recently the natural polymeric acid, the derivatives of natural polymer lignin and cellulose have drawn attention as dopant for conducting polymers due to their biocompatibility and biodegradation [17-21]. The use of LGS as a dopant in conducting polymer coatings is new for the corrosion protection of aluminium alloys.

Dopants, used for modifying conducting polymers, are usually lost due to the action of heat, moisture, and rain water, and once the dopant is lost, polymer loses its electrical conductivity and redox activity. Double stranded conducting polymers solve these problems of material instability and improve the corrosion resistance and conductivity [21]. The double stranded conducting polymer comprises a strand of conducting polymer complexed to a polyelectrolyte. Polyelectrolyte has two functional groups, carboxylic acid that balances the charge on the conducting polymer and provides adhesion with metal and another acrylamide group modify the physical and chemical properties of the polymer. The material stability is

improved because the polymeric dopant is strongly coupled with the polyaniline chain, thus the dopants are not lost due to heat, moisture and rain water. Another problem with conducting polymer is that they are hard, brittle solid with very low adhesion to the substrate. This can be solved by blending the conducting polymer with an insulating resin (epoxy binder) to form a coating that can easily adhere to the surface of a substrate [22-23].

2.1 Chromate Based Coatings

Chromate conversion coatings are commonly used on aluminium surface in order to improve the corrosion resistance, provide desirable surface finish and adequate paint adhesion characteristics [8, 9]. Chromate epoxy primers are often used for corrosion control of iron and aluminium structural alloys. Jie He et al. studied the comparison between chromated epoxy and plain (nonchromated) epoxy coating on steel and aluminium substrates by scanning vibrating electrode technique (SVET), also known as the current density probe. The SVET was used to map the current flowing in and around the defect while the sample was immersed in either 3% NaCl (steel) or in dilute Harrison solution (aluminium). Both steel and aluminium substrates coated with the chromated epoxy exhibited a significant delay in onset of corrosion, compared with substrates coated with nonchromated epoxy. This observation is an important aspect for the long term protection mechanism of chromate-based coatings, leading to passive and more resilient films than that produced in the absence of chromate [11].

Due to environmental concerns and adverse health effects there is an intensive effort to find suitable replacements for chromate-based coatings. Many coating formulations have failed to produce the level of protection that chromates provide, therefore researchers have moved to more advanced technologies for improved protection. Some of the newer alternatives include low temperature cationic plasma deposition, sol-gel and ceramic coatings, various inorganic and organic inhibitors and conducting polymers including some based on double helical structures.

2.2 Polymers to conducting polymers

Polymers were originally thought of as electrical insulators, not electrical conductors. However, in the early 1960s Pohl, Katon and others synthesized and characterized polymers (some conjugated) with conductivities in the semiconductor range. Ultimately, the belief that

polymers are all poor conductors was shattered by the discovery of iodine-doped polyacetylene which exhibited electrical conductivity many orders of magnitude higher than neutral polyacetylene. This discovery was made in 1976 by Hideki Shirakawa, Alan MacDiarmid and Alan Heeger; for which they received the 2000 Nobel Prize in Chemistry. The discovery of electrically conducting polymers (ECPs) triggered the development of a new multidisciplinary field known as "synthetic metals" [24-27]. ECPs can be synthesized both by chemical and electrochemical methods. There are three conducting states of ECPs:

1. Neutral (uncharged), where ECPs are insulators or semiconductors
2. Oxidized (p-doped) where electrons are removed from the backbone, and
3. Reduced (n-doped) (least common), where electrons are added to the backbone of the neutral polymer.

The ability to control the level of conductivity in polymers has given researchers the tools to tailor properties to specific needs and devices. ECPs have potential applications in many diverse areas as actuators, supercapacitors/batteries, molecular electronics, electrochromic windows/displays, transistors, photovoltaics, bio/chemical sensors and corrosion protection. Corrosion protection using electroactive polymers was first suggested by MacDiarmid in 1985. ECPs undergo transition from insulating to the conducting state through several doping techniques [28-32]. Following are the reasons to choose conducting polymer coating in replacement to chromate based coatings:

- Conductive polymers substitute any heavy metal containing compound.
- The polymer's conductive nature provides an electroactive interaction with the metal surface and forms a passivation layer between the metal surface and the polymer coating. Therefore, it functions as a barrier coating as well as surface conversion agent, similar to the chromate coatings.
- Conducting polymers should be able to stop pitting corrosion, which is one of the most severe features of corrosion for aircraft.
- Conducting polymer coatings are environmental friendly coatings

2.3 Conducting Polymers

Conducting polymers (CP) are composed of conjugated chains containing π delocalized electrons along the polymer backbone of C, H and heteroatoms such as N and S [33-36]. Their unique π conjugation properties impart electrical conductivity at room temperature. Depending on the type of charge transport carrier, conductive polymers can be classified into two main groups; ionically and electronically conducting polymers. Polyethylene oxide with lithium perchlorate is an example of an ionically conductive polymer where the ions are responsible for the conduction of electricity. These polymers are mainly used as an electrolyte in solid state batteries [37-41]. Graphite containing coatings and polyaniline are typical examples of electronically conductive polymers. This class of polymer can be further divided into extrinsically and intrinsically conducting polymers (ICP). Extrinsically conductive polymers conduct electricity due to presence of conductive fillers such as graphite, carbon fibre and metal particles, where as ICP (polyaniline) conduct electricity due to their inherent property of conjugation. The latter is a term used for the presence of alternate single (sigma) and double (sigma and π) bonds in polymer molecules. The carbon atoms along the ICP backbone have sp^2 hybridizations (three sp^2 orbitals in the plane and pz orbital out of plane). In sp^2 hybridization, the pz orbital of the adjacent carbon atoms overlap each other and form additional π bonds, and the sp^2 orbitals form the sigma bonds. The energy difference between the highest occupied molecular orbital (HOMO) and the lowest unoccupied molecular orbital (LUMO) is smaller in the case of π bonds compared to the sigma bonds that provide the semi-conducting behaviour, and the optical absorption properties are in or near the visible spectral range. This π-π overlap causes the delocalization of electrons that provide the pathway for the free electron charge carriers to move along the polymer chain. ECPs are semiconductive polymers that can be doped and converted into electrically conductive forms [42-44]. The intrinsic conductivity of conducting polymers is very less typically in the range of 10^{-6} S/cm. Conductivity of conducting polymer is increased by doping i.e. by simple chemical or electrochemical oxidation or reduction by appropriate reagent. These reagents are called as dopants [45-48]. Due to the excellent electrical properties and plastic nature of conducting polymers, they have been proposed for applications such as antistatic coating, corrosion inhibition coatings, electrochromic display, sensors, light-emitting diodes, capacitors, light weight batteries, and gas permeation membranes, etc [49-52]. Among these applications, Pani attracted much attention for corrosion inhibition of metals.

2.4 Polyaniline (Pani)

Polyaniline (Pani) is one of the conductive polymers used in coating that have been intensively investigated. Pani has several advantages over most current CPs. The advantages are: (a) easy chemical and electrochemical polymerization, (b) easy doping and re-doping by treatment with standard aqueous acid and base and (c) high resistance to environmental degradation and chemicals [53-57]. Pani is commonly prepared by chemical polymerization of the aniline monomer using $(NH_4)_2S_2O_8$ in hydrogen chloride solution. The polymer can also be prepared by electropolymerization of the monomer. Pani can exist in four different oxidation states: leucoemeraldine, pernigraniline, emeraldine base (intermediate form) and emeraldine salt (conductive form) (Fig. 2.1) [58- 62]. Pani is prepared as the emeraldine salt (ES) from both chemical and electrochemical polymerization techniques. This form (ES) is soluble in organic solvents such as N, N-dimethylformamide, N,N-dimethylacetamide and l-methyl-2-pyrrolidinone.

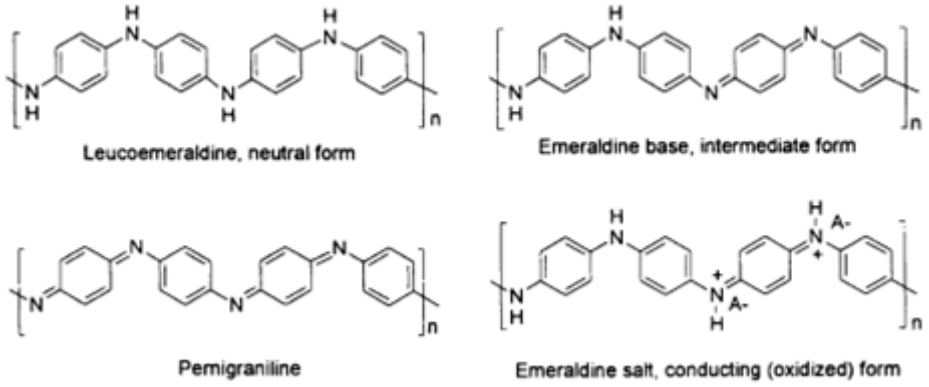

Fig. 2.1: Four forms of Pani [61]

This form of polyaniline has also been investigated for its corrosion control properties. ECPs are the redox-active materials with equilibrium potentials that are positive relative to those of aluminium, similar to the potential of chromate and provide corrosion protection [63-65] (Table 2.1). The reaction sequence for the passivation (oxide layer formation) and corrosion protection induced by polyaniline layer is shown in Fig. 2.2. In acidic medium, EB (emeraldine base) converts to ES (Fig. 2.3). Then, the mechanism involves Fe oxidation by polyaniline, which is thereby reduced to LE (leucoemeraldine). Further oxidation of Fe (II) to Fe (III) and re-oxidation of LE to EB occur both by oxygen; and Fe_2O_3 deposition by resulting OH^- [66].

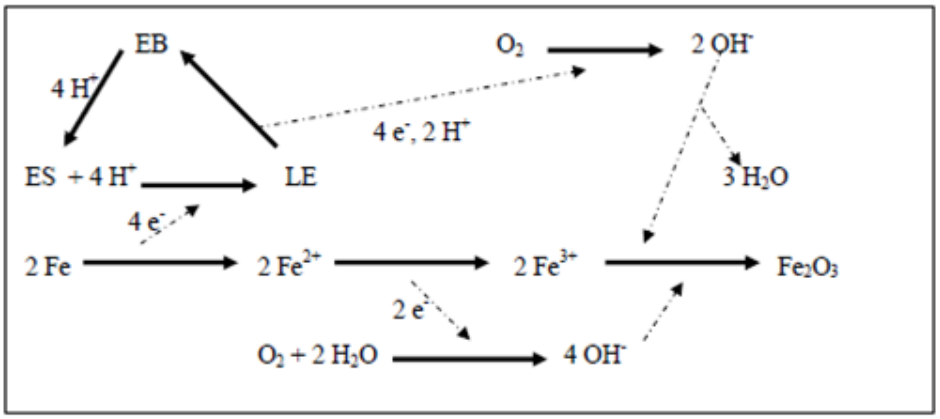

Fig. 2.2: Mechanism of formation of passive layer on metal with Pani coating [66]

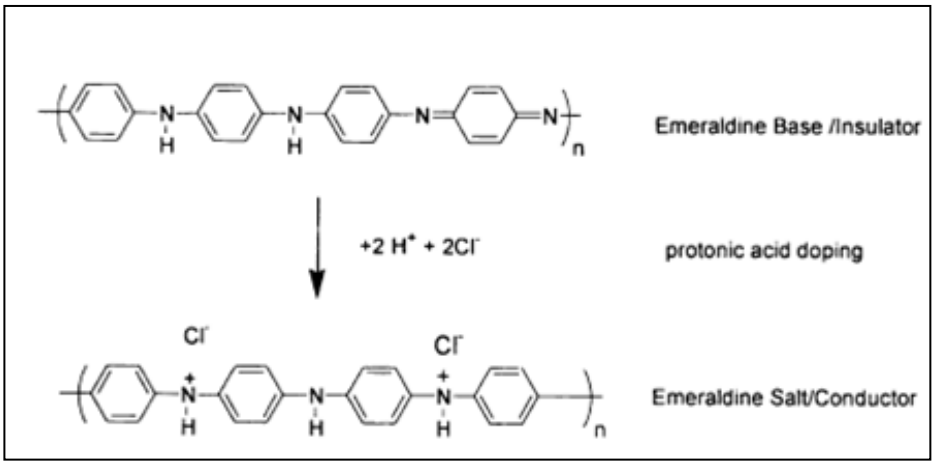

Fig. 2.3: Protonic acid doping [66]

Table 2.1: Reduction potential for a variety of redox couples [65]

Redox couple	Reduction potential (vs. SHE at pH 7)
Mg/Mg^{2+}	−2.36
Al/Al_2O_3	−1.96
Zn/Zn^{2+}	−0.76
Fe/Fe^{2+}	−0.62
H_2/H_2O	−0.41
H_2O/O_2	+0.82
CrO_4^{2-}/Cr_2O_3	+0.42
Polypyrrole	−0.1 to +0.3[a]
Polyaniline	+0.4 to +1.0[a]
Polythiophene	+0.8 to +1.2[a]

[a]For the ECPs, an approximate range of electroactivity is provided, the actual reduction potentials depending on the dopant (counterion) and doping level, the electrolyte and other experimental variables. These potential ranges can be further modified (through electronic or steric effects) by placing appropriate substituents on the polymer ring system

Williams et al. studied the mechanism of corrosion inhibition on AA2024-T3 by polyaniline. It was reported that under conditions of high humidity, where significant water activity exists at the metal-coating interface, oxide formation occurs via below reaction:

$$2Al^{3+} + 3H_2O \rightarrow Al_2O_3 + 6H^+$$

Given the arguments for Pani re-oxidation presented above, the overall mechanism for oxide growth may be represented in Fig.2.4. The balanced generation of H^+ and OH^- ions in this reaction scheme implies a conservation of proton activity within the coating so that a high turnover number is expected for the cyclic re-oxidation of Pani LB to Pani-pTS [67].

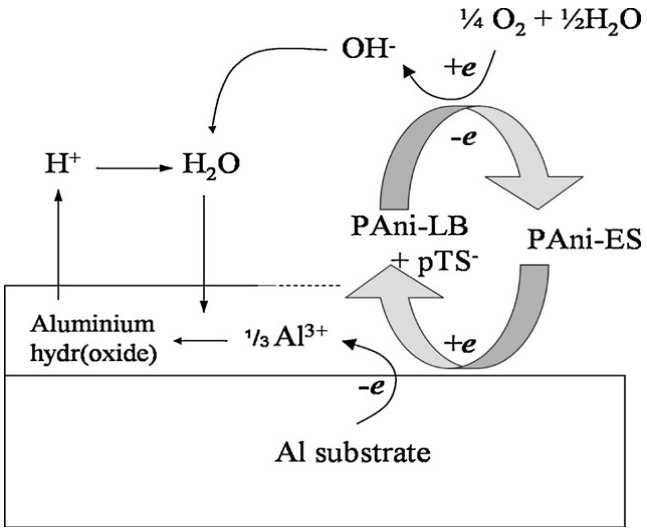

Fig 2.4: Mechanism of Pani ES induced oxide film growth on aluminium [67]

Tallman et al. reported the use of conducting polymer coatings for corrosion protection of ferrous and non-ferrous alloys [4]; and conducting polymers such as polyaniline (Pani) have been reported to provide corrosion protection to aluminium alloys [5]. It is reported that galvanic interaction occurs between aluminium and coatings containing the oxidized and conducting form of Pani, the emeraldine salt (ES), which is usually formed by doping the non-conducting emeraldine base (EB) with an organic acid. The galvanic interaction between Pani ES and the aluminium substrate lead to polarization of the aluminium substrate to more positive potentials with the formation of Pani EB and subsequent release of the dopant anion. Various explanations of the way in which galvanic interaction imparts protection have been proposed: formation of a protective Pani induced oxide layer formed via the cyclic reduction of Pani ES to Pani EB with subsequent re-oxidation of the latter by O_2, resulting into the formation of a passivating salt film at the Pani metal interface leading to the suppression of O_2 reduction as a result of a shift to more positive potentials. Work on iron has shown that the

nature of the dopant determines the nature of Pani induced layer, be it an oxide or salt layer. Dopants therefore do not aid in the formation of an oxide layer at defects but dictate the nature of the film formed (oxide or salt) under intact regions of the coating. It has also been suggested that dopant anions can act as inhibitors in their own right and that the protection from Pani ES containing coatings results from the release of the inhibitor anion at coatings defects as a result of Pani ES being reduced to Pani LB – no re-oxidation occurs in this case unless of course the Pani LB becomes detached from the metal surface. Owing to these reactions, Pani coatings can offer corrosion protection via being active in the modification of micro-environment [6-7].

T. Wang et al. [68] electrodeposited polyaniline (Pani) on aluminium AA1100 electrode from tosylic acid as an anti-corrosion primer using a potentiostat method. The electrodeposited Pani film on AA1100 was tested using potentiodynamic polarisation in 0.5 M NaCl solution. As shown in Fig. 2.5, aluminium electrode with Pani film exhibits passive behaviour and the pitting potential E_{pit} is −0.52 V, which is 0.13 V more positive than that of bare AA1100 alloy (-0.65V). This suggests that Pani film improved protection to localized corrosion of AA1100. It can also be found that Pani coated AA1100 produced a larger cathodic current than bare AA1100 electrode.

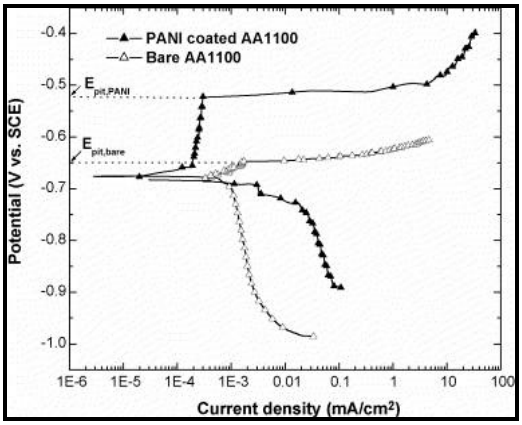

Fig. 2.5: Potentiodynamic polarisation curves of bare and Pani coated AA1100 [66]

Kunal G. Shah et al. [69] compared the corrosion behaviour of coated and uncoated Al2024. The Fig. 2.6 shows comparison of Tafel plots of galvanostatically coated polyaniline and bare Al-2024. Fig. 2.7 shows a Tafel plot of galvanostatically coated polyaniline at 4 mA/cm^2 for different reaction times along with the bare (control). As seen in Fig. 2.7, both the bare and the coated samples show similar cathodic behaviour but significantly differ in the anodic

behaviour. It was shown that the anodic slope changes from 18.49 x 10^{-3} V/decade for the control to 52.27 x 10^{-3} V/decade for the aniline-coated sample. This shows that the coating acts as a barrier. There was significant reduction in corrosion current and corrosion rate by polyaniline coating (Table 2.2). The I_{corr} decreases from 1.703 µA for the control to 0.543 µA for the polyaniline-coated sample. The corrosion rate was decreased from 0.023 mmpy for the control to 0.0074 mmpy for the polyaniline coated aluminium (Table 2.2). The corrosion rate for the coated sample was nearly threefold times lower than that of the control. As shown in Fig. 2.7 I_{corr}, corrosion rate, and the corrosion potential are dependent on the reaction time at which the sample was coated. The E_{corr} for the coated samples was much higher than that of the control which shows noble behaviour of aluminium substrate.

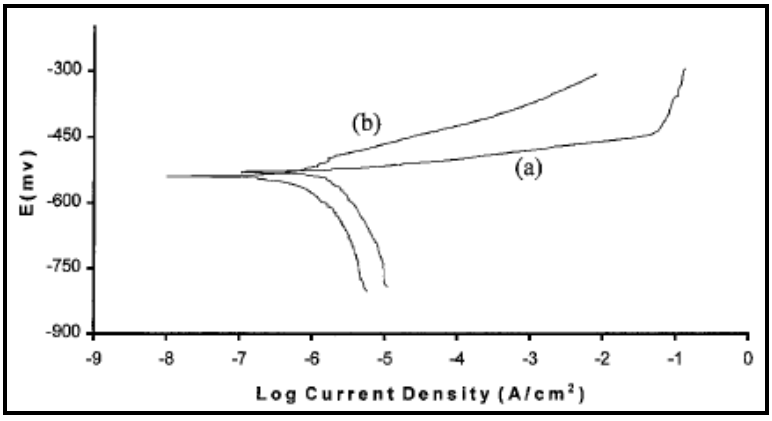

Fig. 2.6: Tafel plots (a) Bare Al-2024 (b) polyaniline-coated Al-2024 [69]

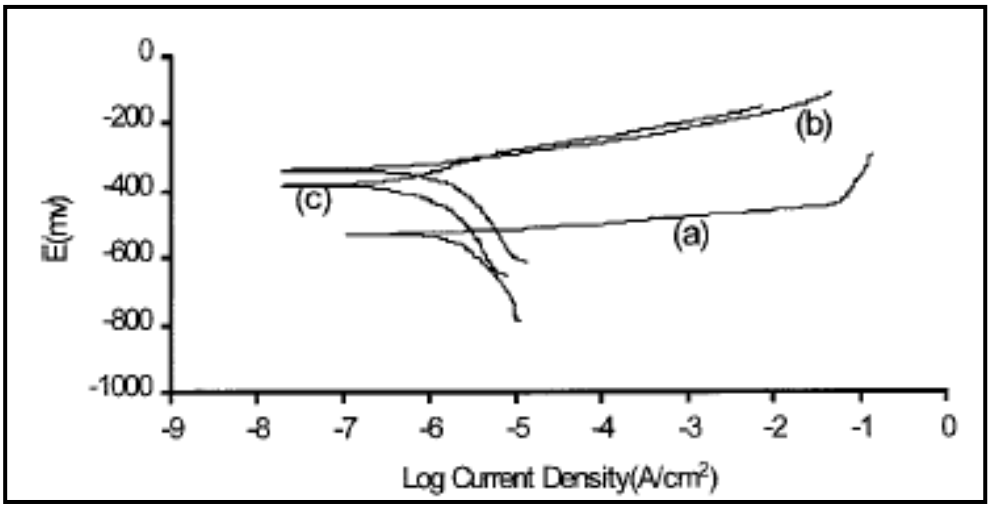

Fig. 2.7: Polyaniline coated on Al-2024 at different reaction times (a) Control (b) 5 min (c) 10 min [69]

Table 2.2: Comparison of I_{corr} and Corrosion Rate for Pani Coated and Uncoated Al-2024 [69]

Sample	Corrosion rate (mmpy)	Corrosion current ($\mu A/cm^2$)
Control (Bare Al2024)	2.3×10^{-2}	1.703
Polyaniline coated Al2024	7.4×10^{-3}	5.4×10^{-1}

There are still some unsolved problems concerning its structure and property due to its complexity in molecular structure and poor solubility in common organic solvents. However, conventional Pani polymer have several weaknesses with regards to its application as anti corrosion coatings and are mentioned as below:

1. Lack of processability, material and chemical instability
2. Difficulty in adjusting the properties of polymer to enhance the adhesion to metal & to the top coat
3. Due to the rigid nature of its backbone it is insoluble in common solvents such as toluene, xylene and chloroform and it is soluble only in special solvents like 1-methyl 2-pyrrolidinone (NMP) and N, N-dimethylformamide (DMF).

The reason for the lack of processability comes from the fact that conducting polymers are π conjugated polymers. The delocalised n-electronic structure leads to a stiff polymer chain and strong inter-chain attraction. Thus, the conventional conducting polymers cannot be easily dissolved, melted or blended with other polymers. Pani is a difficult material to process under normal conditions [70-73].

2.5 Effect of Dopant

Use of dopants such as HCl and H_2SO_4, increase conductivity with several hundred S/cm without interrupting intermolecular interactions and thus does not provide soluble doped materials. Replacing these small dopants with larger functionalized organic dopants such as 10-camphorsulfonic acid (CSA), 2-acrylamido-2-methyl-1-propanesulfonic acid (AMPSA), or dodecylbenezenesulfonic acid (DBSA) increases the solubility of the conjugated polymers. This is due to improved polymer-to-polymer interactions and polymer-solvent interactions through the large organic functionalities attached to the inorganic moiety [74]. Doping PANI

with CSA and processing from a polar solvent such as m-cresol has resulted in films with conductivities as high as 400 S/ cm. Other sulfonic acids are also effective as dopants, including polyelectrolytes, diesters of sulfophthalic acid, sulfosuccinic acid and lignosulfonic acid [75, 76]. Lignosulfonate (LGS) is an inexpensive by product from pulp processing industries. It has an aromatic network polymer with exhibit versatility in performance as scale inhibitor, water reducer, drilling and mud thinner, composites, building materials, dispersant, corrosion inhibitor and fuel cells. Incorporation of larger (more hydrophobic) dopants into conducting polymers such as dodecylsulfonate, lignosulfonate or benzenesulfonate, results in formation of materials that do not readily undergo ion exchange. The use of sulfonated aromatics is known to impart materials with good mechanical properties [76].

The mentioned below are different types of doping techniques:

1. Chemical Doping

It can be done by exposing CP to a solution or vapour of the dopant. In chemical doping the ionization potential of CP should be small enough and dopant should have a redox potential suitable for oxidation/reduction.

2. Electrochemical Doping

In electrochemical doping the CP is generally subjected to the applied potential generally in solution. Due to application of positive potential to CP, the dopant anion moves in from solution into the CP towards the delocalized charge site causing anionic doping (p type doping) and vice versa.

3. Ionic Irradiation

Ionic irradiation is a completely different process that involves bombarding a polymer film with high energy ions. The ions strip electrons from the polymer atoms along their path. These electrons react with the polymer to create a conductive layer several microns thick at the surface of the irradiated region. The exact mechanism of this process is still unclear [76].

Ufana Riaza et al. [77] compared corrosion protective performance of nanostructured methyl orange (MO) doped polyaniline (PANI) and camphorsulphonic acid (CSA) doped poly (1-naphthylamine) (PNA) dispersed polyurethane-based composite coatings against mild steel (MS). The influence of the dopant on the passivation of metal was analyzed using two different dopants. The corrosion protective performance of the coatings against MS was

evaluated by the physico-mechanical properties and corrosion rate measurements. The CSA-PNA coatings were found to exhibit promising corrosion resistance performance. It was observed that CSA was found to be a better dopant than MO in the formation of a dense protective passive iron oxide/dopant layer. At the Los Alamos National Laboratory (LANL) and the John F. Kennedy Space Centre (KSC), researchers demonstrated that doped Pani coatings inhibited corrosion of carbon steel. The NASA-KSC tests were conducted in a 3.5 wt % NaCl/0.1 M HCl environment using ca. 0.005-cm-thick films of Pani doped with p-toluenesulfonic acid on carbon steel. These tests were conducted in acid solutions to mimic the acid environment of the space shuttle launch site. The coupons were coated with Pani and doped to increase the conductivity of the samples. The Pani coated coupons were coated with an epoxy topcoat and the Pani /epoxy coating performed significantly better than the epoxy topcoat alone. These results were used by researchers at LANL-KSC to develop CP coatings to resist the corrosive effects of acid vapour generated during space shuttle launches [66].

L. Shao et al. [36] synthesized natural polymer lignosulfonate (LGS) with polyaniline to form environmental friendly material. The conductivity and thermal stability were improved at certain contents of LGS in LGS-Pani. Lignosulfonate (LGS) is composed of functionalized phenylpropane units connected through alkyl and aryl ether linkages. An inexpensive by-product from pulp processing industries, LGS has become increasingly valuable for its multi-purpose ability to improve performance of petroleum derived chemicals like resins, plastics and fillers. This aromatic network polymer has found applications in numerous industrial areas because of its versatile dispersing, binding, complexing, and emulsifying properties. Additionally, lignosulfonate doped polyaniline (LGS-Pani) is environmentally friendly. The effects of the LGS mass percent in the feeds on the conductivity of the resulting polymers are presented in Fig. 2.8 when no LGS was introduced. As Fig. 2.8 shows, with increasing LGS mass fraction, the conductivity was enhanced in the earlier stage and weakened later. There was a maximum conductivity of 5.00 S/cm at a mass fraction of 11.4 wt%. Significantly, this conductivity exceeded the highest reported in polymer acid-doped Pani systems. Fig. 2.9 shows the interactions between Pani and LGS.

Anionic dopants are easily lost or segregated and lead to material instability. Dopants are lost due to heat, moisture, and rain water etc., once the dopant is lost the polymer loses its electrical conductivity, processability and its electroactivity. Because of the lack of processability, conducting polymers cannot be used as paint like coating on aluminium. There

have been recent developments to improve the processability of conventional conducting polymers. So, conducting polymers are modified by groups. But, these efforts were not successful because the substituent group interferes with the conformation of the conducting polymer backbone and decrease its electronic conductivity. Surfactant dopants have been used to render the polymer soluble. Although the polymer was soluble in organic solvents, it still suffered from instability and the problem of dopant loss. The double stranded conducting polymers solve the problems with material instability and processability [78, 55].

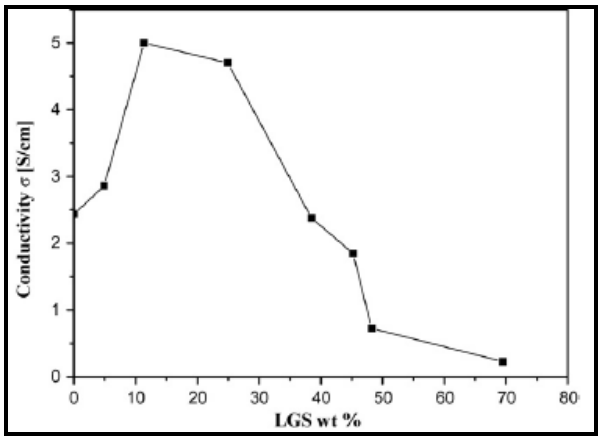

Fig. 2.8: Effect of LGS mass fraction on the conductivity of the doped polymer [36]

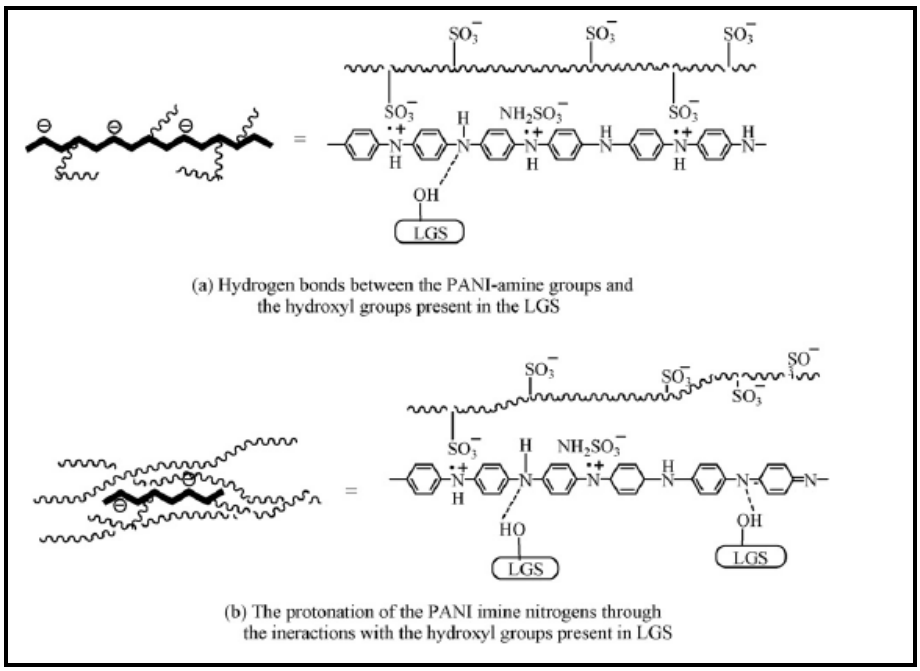

Fig. 2.9: Interactions between Pani chain and LGS [36]

2.6 Double Stranded Conducting Polymer (DSCP)

Double stranded conducting polymers (DSCP) designed to be used as anti corrosion coating for aluminium alloys, behave differently from that of the traditional polymeric paints. The traditional polymeric paints function as a barrier to ion transport between metal and environment and physically seal the surface without chemical reactions. DSCP interacts strongly with the metal surface to promote the formation of a protective passive layer. DSCP coating works similar to that of anodization or chromate conversion than the traditional polymer barrier paints [79]. It is tolerant to scratch damage when compared to chromate coating and the barrier paint coatings. DSCP comprises a strand of a conducting polymer complexed to a polyelectrolyte. The polyelectrolyte is selected from polymers with anionic functional groups such as carboxylic acid or sulfonic acid group or its salt form, for example poly (styrene sulfonic acid) or its salt form, poly (acrylic acid) or its salt form, poly(2-acrylamido -2-methyl-1-propenesulfoic acid) or its salt form, poly (butadiene-maleic acid) or its salt form, poly (methyacrylic acid) and complex [80]. The polyelectrolytes comprises of two functional groups, "A" and "R". "A" functional group balances the charge on the conducting polymer and adhesion to the metal while "R" functional groups modify the physical and chemical properties of the polymer. The A functional groups are anionic functional groups, preferably carboxylates and sulfonates. The R functional groups are used to increase adhesion to substrates, decrease swelling in moisture environment, provide adhesion or binding to top coat, allow blending with other polymers and provide adjustment of glass transition temperatures. The R functional group consists of methylacrylate, ethylacrylate, acrylamide, methylvinylether, ethylvinylether [5, 81-83].

Mechanistic studies suggest that DSCP coatings can be effective in reducing pitting corrosion and crevice formation. Pitting corrosion and crevice formation are significantly safety concerns for aircrafts as they weaken the aircraft structure without giving an alarming appearance. In principal, a self repairing DSCP coating could be more elastic and less fragile than the traditional aluminium oxide passive film. It gives better resistance to stress crack corrosion than the traditional passive oxide layers. Reduced vulnerability to stress will also contribute to safety of aircrafts, automobiles and bridges. The structure is analogous to the double stranded structure of DNA in which two strands of polymers are twisted together and substantial inter strand binding leads to stability of the molecular complex. The double stranded polymer complex offers an advantage over other conductive polymer coatings

because the complex can be rendered soluble in any solvent and paint can be applied to the surface via any method such as spraying, dipping or brushing. Additionally, the second strand of the complex is an acidic group. The carboxylic acid groups on this strand provide excellent adhesion properties for the polymer coating on metal surface. Their ability to protect a scratched surface is achieved by the mentioned two ways:

1. Tolerance to imperfection or pinholes during the initial coating or painting
2. Tolerance to wear and scratching during usage. This translates into cost saving for the original equipment manufacturer and a reduction of cost for repairing during the service life of the coated metal.

The material's stability is improved because the polymeric dopant is strongly coupled with the polymeric chain, thus the dopants are not lost due to heat, water or solvent. It is stable in ambient temperature and found to be thermally stable till 290^{o}C [78].Anionic functional groups can serve two advantageous purposes:

1. As dopants for conducting polymer, they balance the mobile positive charge on conducting polymer and since these are covalently bonded, they are less susceptible to loss due to heat or wash out.
2. As binding groups to the passive layer on metal that contain Al^{+3} sites (functional groups enhance the adhesion of the coating onto the metal substrate).

The earliest work involving polyaniline on aluminium alloy appears to be by Racicot and co-workers. A molecular complex of polyaniline with a polyanion was synthesized by a template-guided synthesis, yielding a ''double-strand'' polyaniline [82]. The polyanion can be selected so as to impart desirable properties to the coating material, such as increased solubility in common solvents and improved adhesion to the substrate and/or topcoat. Electrostatics and molecular entanglement holds the complex together and, consequently, there is little tendency for the polyaniline to lose dopant and conductivity. Double-stranded PANI has been used with success in marine and aggressive environments [82]. Linfeng Sun et al. [83] synthesized and characterized double stranded molecular complex made of polyaniline and polymeric anion dopant as shown in Fig. 2.10. The molecular complex is advantageous in several respects: (a) it offers good stability of the conductive state (b) the second strand improve material processability and for adjustment of properties to satisfy demands in applications. The two strands of polymers are tightly bonded. The complex does not decompose or unwind in acid, base, solvent, mild oxidant, reductant, or by heat. In

contrast, under the same conditions the single-strand polyaniline loses its dopant and becomes nonconductive.

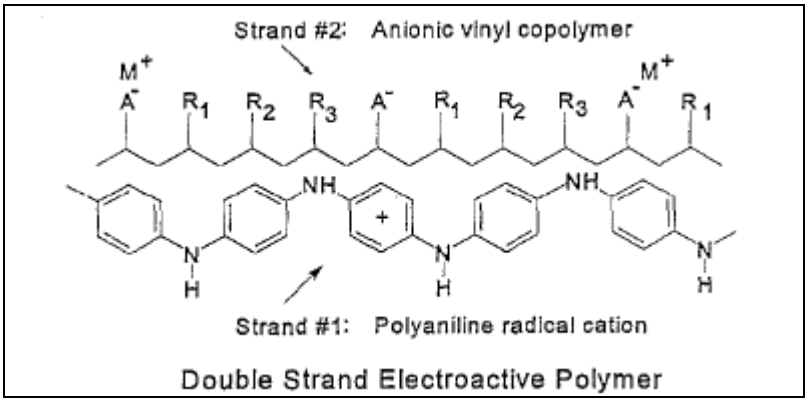

Fig. 2.10: Double stranded molecular complex of polyaniline and polyanion [83]

Robert Racicot et al. [84] achieved corrosion protection of aluminium alloys by using a double-stranded polyaniline as a surface conversion coating. Electrochemical impedance spectroscopy measurements show that the conducting polymer coated AA7075 alloy is highly resistant to corrosion. Mechanistic studies indicate that the conducting polymer is not a barrier polymer coating, but it chemically converts the surface of the alloy to form a passive layer that protects the metal from corrosion. The use of double-stranded polyaniline facilitates a formulation for coating and provides good adhesion to the metal surface. The electrochemical impedance spectroscopy (EIS) studies suggest that conducting polymer is competitive with the Alodine-600 chromate chemical conversion. Samples immersed in 0.5N NaCl solution were monitored periodically by EIS. Fig. 2.11 shows an example of the comparison between Alodine 600 and the double stranded polyaniline coating on the aluminium alloy AA7075-T6. The low-frequency impedances of both coatings are high (10^5 ohm) indicating that the performance of the conducting polymer is comparable to that of the Alodine chemical conversion. When the samples were exposed to the doubly corrosive solution of salt and acid (pH 3.6), the conducting polymer performs better than Alodine-600. In this acidic media, the chromate conversion coating is no longer protective and the impedance value decreased to a non-protective level. In contrast, the corrosion resistance remained high for the double-stranded polyaniline coated samples. Fig. 2.12 shows the comparison at the initial stage (3 days) of the EIS tests in pH 3.6 buffered 0.5 N NaCl solutions. For the polyaniline-converted AA7075 surface, the low frequency charge transfer resistance approaches 10^6 ohm and the impedance remains high after three weeks. The Alodine-600 chromate conversion sample is

far less resistant to corrosion in this acidic salt environment. The low frequency impedances of these chromate samples decrease by one order of magnitude within the first three days of the test and continue to decrease to that of an unprotected sample.

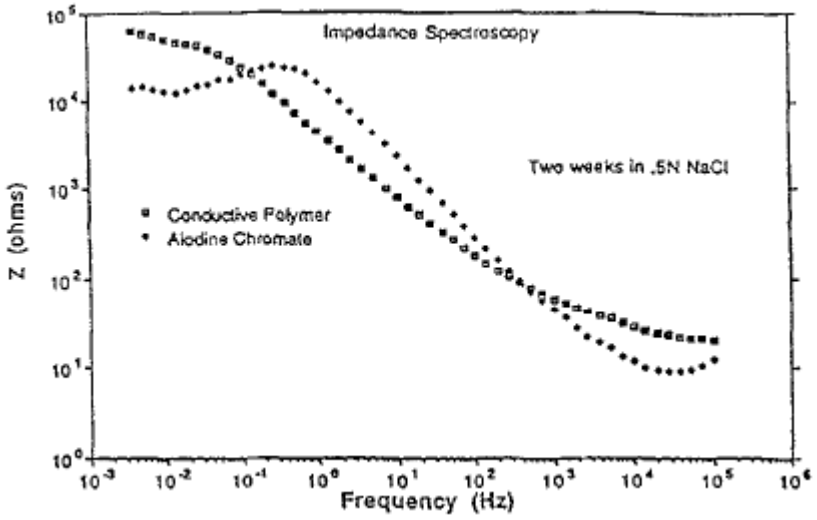

Fig. 2.11: EIS measurements of DSCP treated sample and the Alodine 600 chromate conversion samples on AA7075 [84]

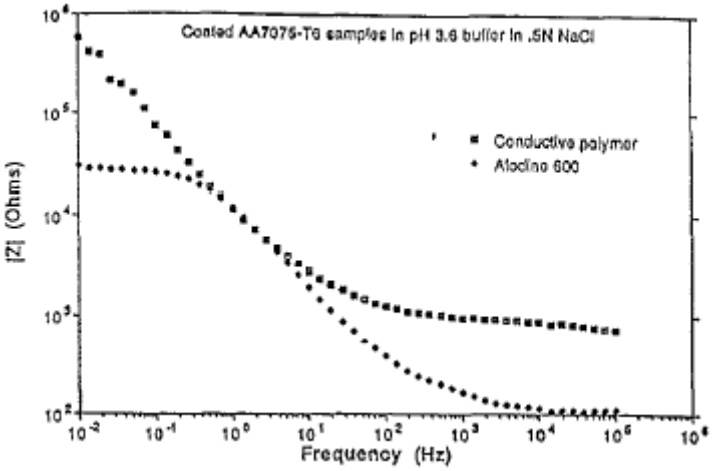

Fig. 2.12: EIS measurements of DSCP treated sample and Alodine 600 chromate after 3 days immersion in acidic salt solution [84]

The advantages of the double-stranded complex are the following:

(1) The conductive state of the polymer is very stable because the polymeric dopant is part of a stable complex

(2) With proper choice of the polymeric dopant, the conductive polymer can be dispersed in solvents to be used as a coating material

(3) The polymeric dopant provides sites for function & ion to achieve good adhesion to metal and to the top coat.

Qunhui Sun et al. [85] synthesized the dendritic superstructure of polyaniline using a water-soluble polyelectrolyte copolymer as the support matrix. In his synthesis poly(acrylic acid) (PAA) had been used as a dopant in polyaniline biosensor for glucose measurement. Nanofibers and nanotubes were usually obtained via a complex formation between the Pani (polycation) and PAA (polyanion). It was pointed out that the aniline monomer was first attracted to the PAA backbone through either hydrogen bonding or columbic attraction. This gives rise to the possibility of forming an aniline copolymeric nucleus that is favorable for the growing of one-dimensional Pani. In this regard, the PAA main chain may be considered as a polymer template for the nanofiber growth. In comparison, however, when an A–B–A three-block copolymeric amphiphile is used in the Pani's formation, Pani nanoparticles are usually formed. In this case, moreover, the globular micelle from the A–B–A copolymer acted as a template and finally resulted in the granular architecture formation of the Pani.

2.7 Nanoparticles

Nanoparticles are generally considered to be a number of atoms or molecules bonded together with radius of 100nm [86]. In typical nanomaterials, the majority of the atoms located on the surface of the particles, whereas they are located in the bulk of conventional materials. Nanomaterials represent almost the ultimate in increasing surface area and they are chemically very active because the number of surface molecules or atoms is very large compared with the molecules or atoms in the bulk of the materials. Substances with high surface areas have enhanced physical, chemical, mechanical, optical and magnetic properties and this can be exploited for a variety of structural and non-structural application. Nanoparticles / fillers find application in wear-resistant, erosion-resistant and corrosion resistant [87, 88]. Dispersed nanoparticles (alumina, zinc oxide and silica) can also improve corrosion resistance. This is accomplished through cathodic protection. Due to the large surface area, nanoparticles are often more efficient than micro particles, resulting in lower concentration necessary to obtain good results. These improvements can include high modulus, increased strength and heat resistance, corrosion resistance, increased biodegradability of biodegradable polymers, thermal stability, and mechanical properties. Montmorillonite (MMT), hectorites and saponites are the most commonly used layered

silicate. Montmorillonite (MMT) clay is an interesting host material because of their ready availability, small particle size, and well-known susceptibility for intercalation [89]. Nanoparticles are uniformly distributed throughout the coating, thus providing the resin or coating with a continuous, solid, protective network layer of Al_2O_3 or SiO_2. The nanoparticles also form a unique elastomeric structure within the coating, and create a denser, more compact film structure. Cathodic protection is a technique used to inhibit corrosion by supplying an electrical charge that suppresses the electrochemical reaction. If correctly applied, corrosion can be stopped completely. In its simplest form it is achieved by attaching a sacrificial anode, thus making the iron, steel or aluminium the cathode in the cell formed. Nanoparticles have a large amount of electrons on their surface, which can create this sacrificial anode. Nanocomposites with homogeneously dispersed graphene in the polymer matrix also exhibited good barrier properties. The N_2 and He permeation rate were suppressed several-fold by the addition of functionalized graphene because of the formation of a 'tortuous path' in the presence of graphene in the nanocomposites. The graphene-based polymer nanocomposites showed good EMI shielding efficiency. The review of conducting polymer/graphene nanocomposites highlighted their potentials applications in the coming years for biomedical application, such as ultraminiaturised low cost sensors for the analysis of blood and urine. Conducting polymer/graphene composites can also be used as electrode materials in a range of electrochromic devices. The polymer/graphene flexible electrode has some commercial applications in LEDs, transparent conducting coatings for solar cells and displays. The other commercial applications of graphene polymer composites are: lightweight gasoline tanks, plastic containers, more fuel efficient aircraft and car parts, stronger wind turbines, medical implants and sports equipment. The discovery of graphene as a nanofiller has opened a new dimension for the production of light weight, low cost, and high performance composite materials for a range of applications [89].

2.7.1 Montmorillonite nanoclay

Montmorillonite Clay belongs to the smectite family. Because of its suitable layer charge density, montmorillonite clay is nowadays the most widely used clay as nanofiller. Depending on the strength of interfacial interactions between polymer matrix and layered silicate, three different types of PLS nanocomposites are shown in Fig. 2.13.

1. ***Intercalated nanocomposite***: The insertion of a polymer matrix into the layered silicate structure occurs in a crystallographically regular fashion, regardless of the clay to polymer

ratio. Intercalated nanocomposites are normally interlayer by a few molecular layers of polymer.

2. ***Flocculated nanocomposite***: Conceptually this is same as intercalated nanocomposites. However, silicate layers are sometimes flocculated due to hydroxylated edge-edge interaction of the silicate layers.

3. ***Exfoliated nanocomposite***: The individual clay layers are separated in a continuous polymer matrix by an average distance that depends on the clay loading. Usually, the clay content of an exfoliated nanocomposite is much lower than that of an intercalated nanocomposite [89-90].

The model crystallographic structure for montmorillonite clay consists of two fused silica tetrahedral sheets sandwiching an edge-shared octahedral sheet of either aluminium or magnesium hydroxide (Fig. 2.14). Isomorphous substitutions of Si^{+4} for Al^{+3} in the lattice structure and of Al^{+3} for Mg^{+2} in the octahedral sheet cause an excess of negative charges within the montmorillonite layers. These negative charges are counterbalanced by cations such as Ca^{+2} and Na^{+} situated between the layers. Due to the high hydrophilicity of the clay, water molecules can also be present between the layers [90]. When the microstructure of montmorillonite clay was observed on a larger scale, each layer can be seen as a high aspect ratio lamella about 100-200 nm in diameter and 1 nm in thickness. Five to ten lamellae are associated by interlayer ions in primary particles of dimensions 8-10 nm in the transverse direction which, in turn, form a larger irregular aggregate with the dimensions of 0.1-10 μm in diameters.

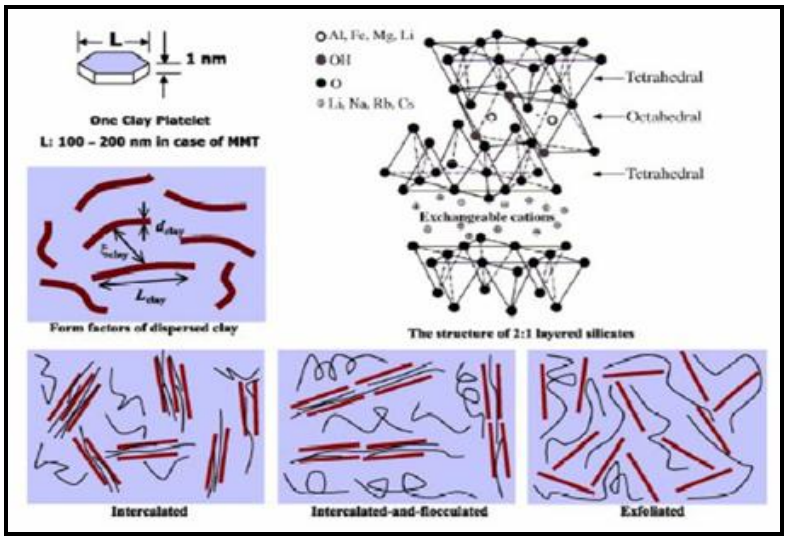

Fig. 2.13: Types of polymer/layered silicate nanocomposites [89]

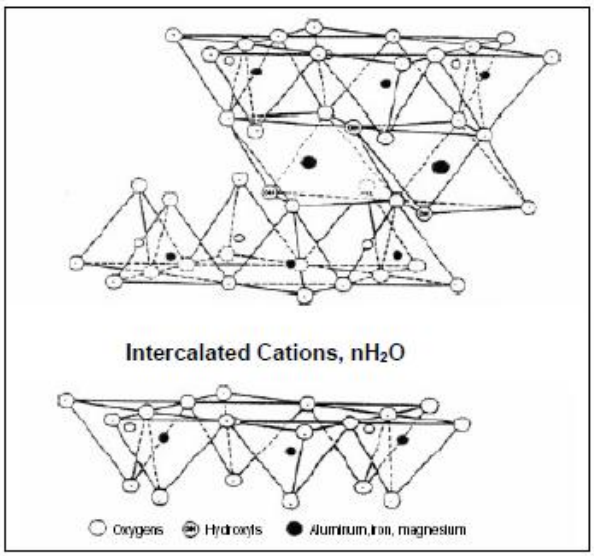

Fig. 2.14: Crystallographic structure of montmorillonite clay [90]

Stacking of the layers lead to a regular van-der waals gap between the layers called the interlayer or gallery. In order to improve the dispersion clay in a polymer, different compatibilizing agents are used in the synthesis of nanocomposites. Cloisite additives consist of organically modified, layered magnesium aluminium silicate platelets which allow complete dispersion into matrix. The organic modifier that is added in Cloisite 30B is MT (methyl, tallow, bis-2-hydroxyehtyl, quaternary ammonium) A typical structure of Closite Clay is shown below in Fig. 2.15 [91].

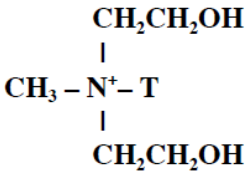

Where, T is Tallow (~65% C18; ~30% C16; ~5% C14)

Fig. 2.15: Cloisite 30B clay [91]

The most popular are the alkylammonium ions because they can be exchanged easily with the ions situated between the layers. Montmorillonite exchanged with long chain alkylammonium ions can be dispersed in polar organic liquids, forming gel structures with high liquid content. Montmorillonite (MMT) clay was selected as the host because of its important advantages:

(a) The galleries normally occupied by hydrated cations that balance the charge deficiency is generated by the isomorphous substitution in the tetrahedral sheets. The monomer (aniline)

can be introduced into the galleries easily by ion exchange and are hardly separated from the galleries.

(b) It is an inactive inorganic host without redox character, so the polymerization can be controlled.

(c) It is a well-ordered host in two dimensions, after the intercalation of monomer extrinsic initiator can enter and initiate the polymerization in the interlayer. While in the three-dimensional ordered host a similar method is unrealistic due to the blocking traffic channel [92].

Jui-Ming Yeh et al. [93] prepared a series of nanocomposite materials that consisted of emeraldine base of polyaniline and layered montmorillonite (MMT) clay by effectively dispersing the inorganic nanolayers of MMT clay in organic polyaniline matrix via in-situ polymerization. Organic aniline monomers were first intercalated into the interlayer regions of organophilic clay hosts and followed by one-step oxidative polymerization. Polyaniline-clay nanocomposites (PCN) in the form of coatings with low clay loading (e.g., 0.75 wt %) on cold-rolled steel (CRS) were found much superior in corrosion protection over those of conventional polyaniline. Corrosion protection of sample-coated CRS coupons was observed from the values of corrosion potential (E_{corr}), polarization resistance (R_p), corrosion current (I_{corr}), and corrosion rate (R_{corr}), as listed in Table 2.3. The CRS coupon coated with EB of polyaniline shows a higher E_{corr} value than the uncoated CRS. However, it exhibits a lower *E*corr value than the specimen coated with PCN materials. For example, the CLAN075-coated CRS has a high corrosion potential of ca. -555 mV at 30 min. Even after 5 h measurement, the potential remained at ca. -560 mV. Such E_{corr} value implies that the CLAN075-coated CRS was nobler toward the electrochemical corrosion compared to the EB of polyaniline. The CLAN075-coated CRS shows a polarization resistance (R_p) value of 2 x 10^4 /cm^2 in 5 wt % NaCl, which were about 2 orders of magnitude greater than the uncoated CRS.

The Tafel plots for (a) uncoated, (b) Pani-coated, (c) CLAN025-coated, (d) CLAN05-coated, and (e) CLAN075- coated CRS are shown in Fig. 2.16. The corrosion current (i_{corr}) of CLAN075-coated CRS is ca. 2.4 A/cm^2, which is correspondent to a corrosion rate (R_{corr}) of ca. 4.46 mpy (Table 2.3). Electrochemical corrosion current values of PCN materials as coatings on CRS were found to decrease gradually with further increase in clay loading.

Table 2.3: Tafel data of Pani-MMT Clay Nonocomposite Materials [93]

compound code	feed composition (wt %)		inorganic content found in product[b] (wt %)	electrochemical corrosion measurements			
	polyaniline	MMT		E_{corr} (mV)	R_p (kΩ·cm^2)	i_{corr} (μA/cm^2)	R_{corr} (MPY)
bare				−641	0.8	44.4	86.1
PANI	100	0	0	−590	3.4	12.0	23.3
CLAN025	99.75	0.25	0.70	−581	13.7	2.9	5.6
CLAN05	99.50	0.50	1.50	−568	15.4	2.7	5.2
CLAN075	99.25	0.75	3.80	−555	20.0	2.4	4.5
CLAN1	99.00	1.00	4.70	−551	36.2	1.1	2.1
CLAN3	97.00	3.00	7.10	−543	57.9	0.5	1.0

[a] Saturated calomel electrode was employed as reference electrode. [b] As determined from TGA measurements.

From the DSC measurements as in Fig. 2.17, it was found that the incorporation of MMT clay into polyaniline resulted in a large increase in the crystalline temperature (heating scan) relative to pure polyaniline. This behavior was expected and associated with the strong heterogeneous nucleation effect of the large clay particles in the PCN system. As the loading of MMT clay is increased, the crystalline temperature of PCN materials became higher.

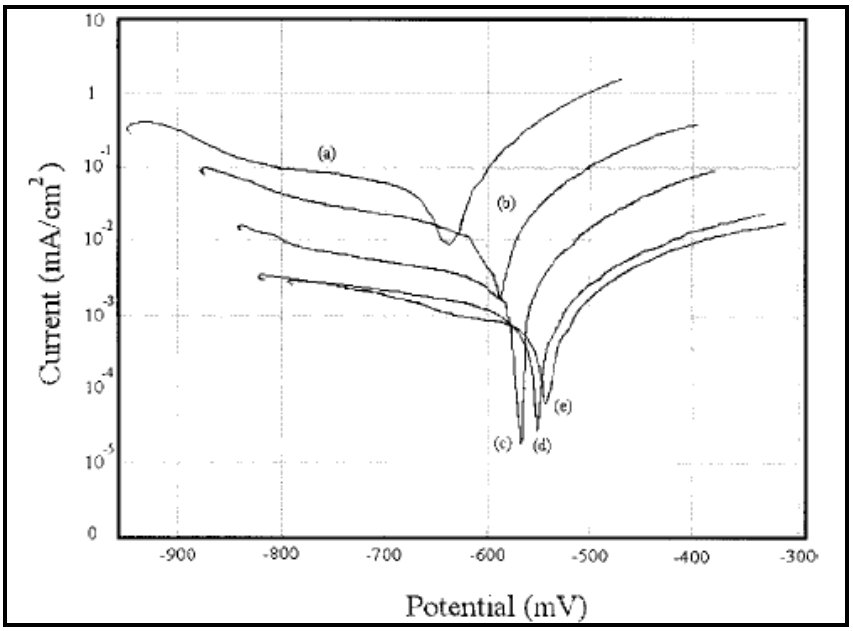

Fig. 2.16: Tafel plots (a) uncoated (b) Pani-coated (c) CLAN025-coated (d) CLAN05-coated and (e) CLAN075-coated CRS [93]

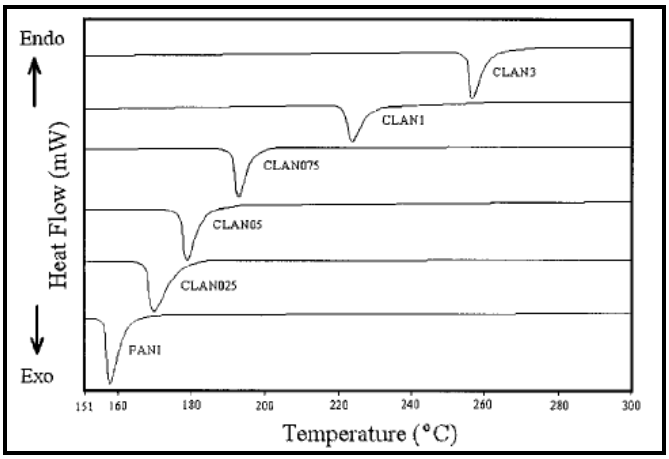

Fig. 2.17: DSC curves of polyaniline and a series of polyaniline-clay nanocomposite materials [93]

Hyung Min Lee et al. [94] synthesised novel nanocomposite materials of conducting polyaniline (Pani) and Na-montmorillonite (MMT) via microemulsion polymerization. Microemulsions are macroscopically homogenous mixtures consisting of oil, water and surfactant. The X-ray diffraction analysis showed that the d-spacing of the Pani-MMT nanocomposites became wider than that of pristine Na-montmorillonite, showing that the PANI was successfully intercalated into the Na-montmorillonite layers. FT-IR spectra of the nanocomposites also confirmed characteristic peaks of both Pani and MMT. SEM images (Fig. 2.18) of the Pani-MMT nanocomposite indicated that the polymerization occurs mainly between the clay layers. Fig. 2.19 shows the XRD results for the Na-montmorillonite, pure Pani, and Pani-MMT nanocomposite. The variation of the d-spacing (001) of the clay was calculated from the observed peaks by using the bragg equation. The d-spacing in the direction of pristine MMT is about 1.18 nm.

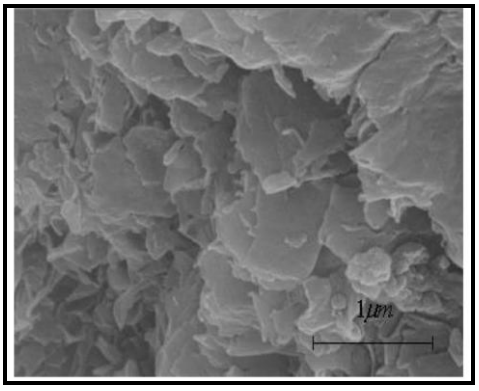

Fig. 2.18: SEM image of Pani-MMT nanocomposite [94]

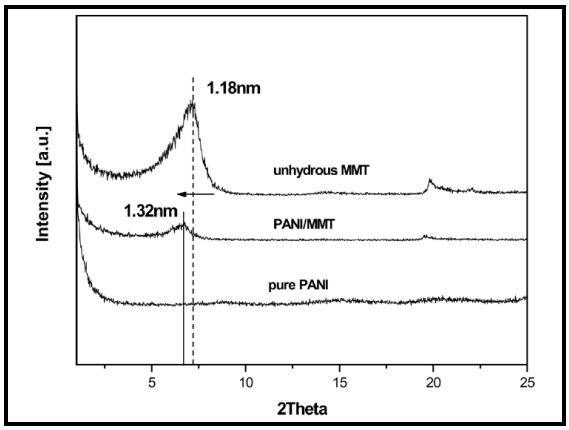

Fig. 2.19: XRD for Na-MMT, pure Pani and Pani-MMT nanocomposite [94]

After polymerization, the diffraction peak of the Pani-MMT nanocomposite was shifted to a lower angle. The d-spacing of nanocomposite was increased up to 1.32 nm. This result demonstrated the insertion of PANI between the clay layers. FT-IR spectra of Pani-MMT nanocomposite is shown in Fig. 2.20. The band at 1570 cm^{-1} is assigned to the C=N stretching, and those at 1305, 1245 cm^{-1} are associated with the C-N stretching modes. These peaks are ascribed to the formation of Pani. The strong peaks of 1041, 915 cm^{-1} and the peak at 840 cm^{-1} were estimated to be the characteristic vibrations of polymerized Polyaniline-Montmorillonite Nanocomposite MMT. H. M. Lee and H. J. Choi revealed that pristine MMT has a flaky texture reflecting its layered structure. It is possible to notice that the morphology of Pani-MMT nanocomposite was similar to that of pristine MMT, demonstrating that the polymerization occurs mainly between the clay layers.

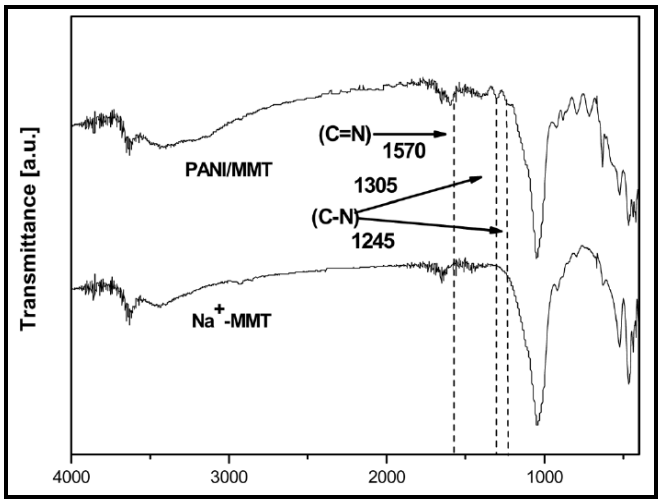

Fig. 2.20: FT-IR spectra of Na-MMT and Pani-MMT nanocomposite [94]

2.7.2 Aluminium oxide

Alumina, Al_2O_3, is a ceramic metal oxide of great importance as building material, refractory material, attributed to its high strength, corrosion resistance, chemical stability, low thermal conductivity, and good electrical insulation. One phase of alumina, the γ-phase is widely used as catalyst, catalyst support and adsorbent because it's high porosity and surface area. It is conventionally prepared by heating the hydrated trihydroxides, gibbsite and bayerite, to temperature of >1000^{o}C to obtain the α-alumina, corundum, a material with great hardness and low surface area. The trihydroxides, gibbsite, bayerite, both are $Al(OH)_3$. nH_2O and the monohydroxyl oxide, boehmite, $AlO(OH)\cdot\alpha H_2O$, have the monoclinic crystal structure with similar lattice parameters (*a*=0.866 nm, *b*=0.506 nm, *c*=0.983 nm, β=94°34′ in boehmite, *a*=0.868 nm, *b*=0.507 nm, *c*=0.972 nm, β=94°34′ in gibbsite, and *a*=0.867 nm, *b*=0.506 nm, *c*=0.942 nm, β=90°26′ in bayerite. In the process of heat treatment, the trihydroxide undergoes a series of transformations. It loses the water of hydration, then dehydroxalate at < 300ºC to form the monohydroxyl oxide boehmite, AlO(OH), which on further heating to increasingly higher temperatures, changes to the transition aluminas, including the η-, γ-, δ-, and θ-phases, which then transform finally to the α-form. These transition alumina are crystalline solids with high porosity and surface areas as well as acidic and basic properties, which make them suitable as adsorbents, catalyst, and catalyst support and fabricated into filtration membranes as well as used as fillers or components in polymer/ inorganic composite materials with enhanced mechanical properties. The conventional alumina as obtained are usually powder of particulates. These could be fabricated into alumina fibers by various methods, through melt growth techniques including the internal crystallization method and extrusion, electrospraying and electrospinning have been developed for producing Al_2O_3 fibers. More recently, interest in nano-materials and nanotechnology has spurred a flurry of investigations on the preparation and the applications of nano-materials including that of inorganic oxides such as aluminium oxide [95].

2.7.2.1 Aluminium oxide nanoparticles in coatings

The effect of alumina in polyaniline, diglycidyl ether of bisphenol A type epoxy resin, carbon fiber and epoxy resin composite has been studied recently. Generally it has been found that the present of low loading of alumina nanoparticles and nanofibers tend to enhance the thermal and mechanical properties of the polymer matrix. In many instances the strength of

the composites are below the strength of neat resin due to non-uniform particle size distribution and particle aggregation. Ash et.al studied the mechanical behavior of alumina particulate/poly(methyl methacrylate) composites. They concluded that when a weak particle matrix interphase exists, the mode of yielding for glassy, amorphous polymers changes to cavitational to shear, which leads to a brittle-to ductile transition. Two challenges have been observed to be overcome to facilitate the enhancement of the properties of the polymer substrate. First is the need to disperse the nanoparticles and nanofibers uniformly throughout the polymer substrate and secondly to facilitate the interaction between the nanofibers and the molecules of the polymer substrate. At low loading the nanoparticles could be distributed uniformly across the substrate. However at high loading, there is the tendency for the fibers to clusters together and hence limit the enhancement of the mechanical properties and in fact lowered it. It has also been observed that while the tensile strength increases with reduction in particles size for micron-scale particles, the tensile strength decreased with reduced particle size for nano-scale particles. The changes were attributed not to the strength of bonding between the particulate with the matrix but more to the poor dispersion of particles. Attempts to meet the second challenge involve functionalizing alumina particles such as in the on fiber and epoxy resin composites. The functionalizing of the alumina surfaces is meant to enhance the miscibility of the alumina particles in the polymer substrate and also the facilitate bridging between alumina surfaces with the substrate [95].

2.7.3 Graphene

Graphene is two dimensional carbon nanofiller with a one atom thick planar sheet of sp^2 bonded carbon atoms that are densely packed in a honeycomb crystal lattice (Fig.2.21). Graphene, a single atomic monolayer of graphite, possesses a unique combination of properties that are ideal for corrosion inhibiting coating in applications such as microelectronic components (e.g., interconnects, aircraft components, and implantable devices) [96]. Graphene is predicted to have remarkable properties, such as high thermal conductivity, superior mechanical properties and excellent electronic transport properties. These intrinsic properties of graphene have generated enormous interest for its possible implementation in a myriad of devices. These include future generations of high speed and radio frequency logic devices, thermally and electrically conducting reinforced nanocomposites, ultra-thin carbon films, electronic circuits, sensors, and transparent and flexible electrodes for displays and solar cells. Graphene is chemically inert, stable in ambient

atmosphere up to 400^0C. Graphene is being widely investigated across a number of fields due to its unique structural and electrical properties [97, 98]. Anran Liu et al. [99] observed the conductivities of graphene sheets (conductivity) 1.1×10^3 S m^{-1} into polypyrrole greatly improved the conductivity of the composite. Thus, the conductivity of the composite film is increased with graphene content. Graphene, as nanofiller, may be preferred over other conventional nanofillers (Na-MMT, Al_2O_3, CNT, ZnO_2 etc.) owing to high surface area, aspect ratio, tensile strength, thermal conductivity and electrical conductivity, EMI shielding ability, flexibility, transparency, and low CTE.

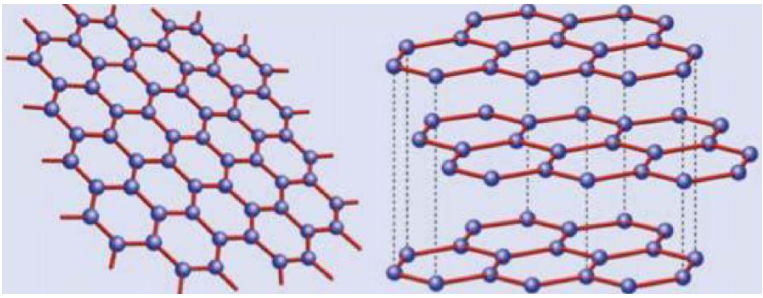

Fig. 2.21: Graphene (honeycomb lattice) [98]

In a recent study, Prasai et al. [100] have reported that graphene coating improves the corrosion resistance of Cu by seven times. However, the electrochemical experiments were performed in a less aggressive electrolyte. Electrochemical impedance spectroscopy measurements suggest that while graphene itself is not damaged, the metal under it is corroded at cracks in the graphene film (Fig. 2.22). Tafel analysis was conducted to quantify the corrosion rates of samples with and without graphene coatings (Fig. 2.23). These results indicate that copper films coated with graphene grown via chemical vapour deposition are corroded seven times slower in an aerated Na_2SO_4 solution as compared to the corrosion rate of bare copper. Tafel analysis reveals that nickel with a multilayer graphene film grown on it corrodes twenty times slower while nickel surfaces coated with four layers of mechanically transferred graphene corrode four times slower than bare nickel. These findings establish graphene as the thinnest known corrosion-protecting coating.

Chen et al. [101] have demonstrated that graphene can inhibit the oxidation of the underlying copper metal. He reported that graphene coating improves the oxidation resistance of Cu and Cu/Ni alloy in air, and the chemical resistance of these alloys in 30% hydrogen peroxide, but do not elaborate on electrochemical protection of these metals. Sreevatsa et al. [102] provided

a qualitative description of graphene as an ionic barrier for steel, but the electrochemical tests did not show any considerable improvement in corrosion resistance.

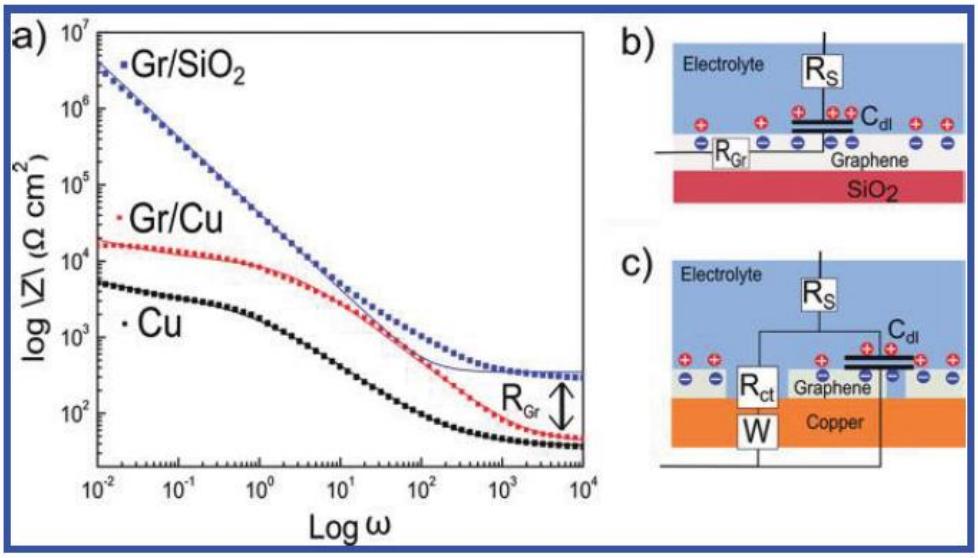

Fig. 2.22: (a) Bode magnitude plot of Gr/SiO2, Cu and Gr/Cu samples, (b) Equivalent circuit model used in modeling Gr/SiO2 devices (c) Equivalent circuit model for Cu and Gr/Cu devices [100]

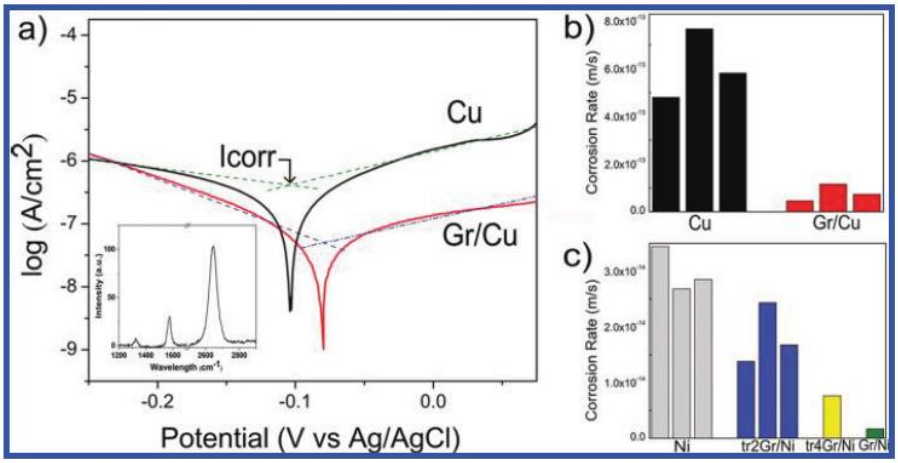

Fig. 2.23: (a) Tafel plots of Cu and Gr/Cu samples, (b) Corrosion rates of Cu and Gr/Cu samples extracted from tafel plots, (c) Corrosion rates of bare Ni samples and the samples where graphene was transferred onto Ni substrate [100]

Kirkland et al. [103] discussed the possibility of graphene as a corrosion barrier based on com mercially available graphene-coated Cu that probably did not have the desired surface coverage. Polarization curves for graphene coated Cu samples displayed a comparatively small decrease in the anodic reaction rate (Fig. 2.24) accompanied by a larger reduction in the

rate of cathodic reactions, i.e. $2H_2O + O_2 + 4e^- \rightarrow 4OH^-$. The i_{corr} was reduced, with a concomitant negative shift in the E_{corr} of approximately −0.15 V. In this case the graphene is acting primarily as an inhibitor of the cathodic reaction, which is in contrast to the dominant mechanism acting upon the Ni surface.

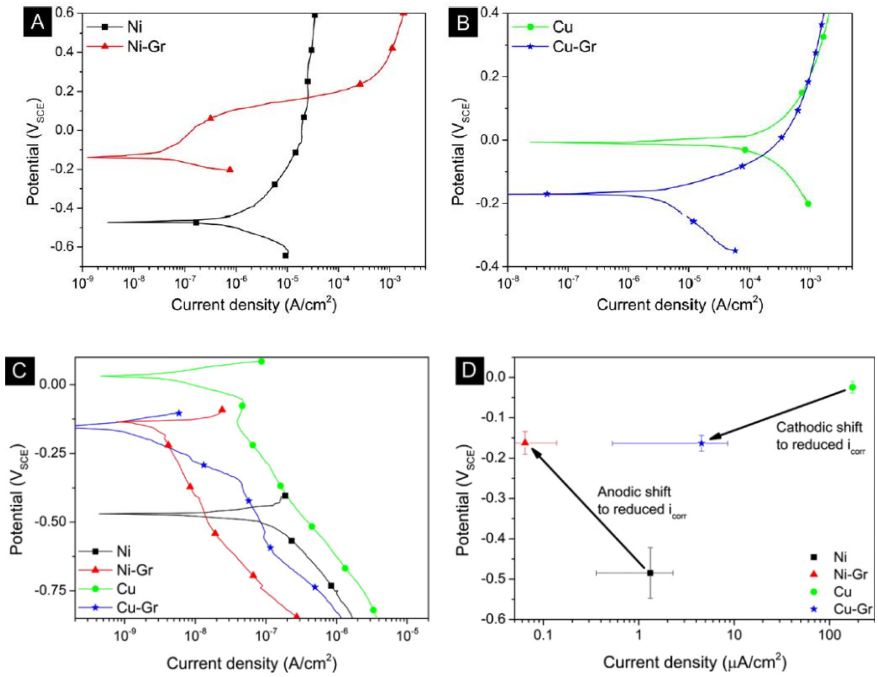

Fig. 2.24: Anodic polarisation curves of Ni and Ni-Gr (A) Cu and Cu-Gr (B) cathodic polarisation curves for all samples (C) E_{corr} vs I_{corr} for coated and uncoated Cu samples, with respective shifts are indicated [103]

R.K.Singh Raman et al. [104] demonstrated that the graphene coatings can dramatically decrease anodic and cathodic current densities to protect Cu metals from electrochemical degradation in an aggressive electrolyte (Fig. 2.25).

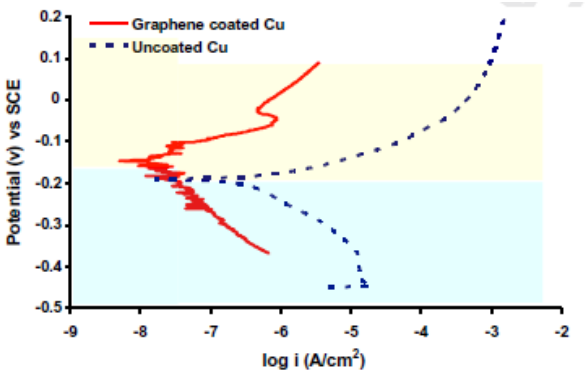

Fig. 2.25: Potentiodynamic polarisation of the graphene coated and uncoated Cu [104]

2.8 Double Stranded Conducting Polymer Nanocomposites

C. Basavaraja [45] et al. investigated the thermal stability of polyaniline–poly-N-isopropylacrylamide-co-acrylic acid/alumina aqueous dispersions in the presence of dodecyl benzenesulfonic acid. The TGA curves and DSC thermograms of Pani–PNA, Pani–PNA/Al_2O_3 (10%), and Pani–PNA/ Al_2O_3 (30%) are shown in Fig. 2.26 and 2.27 respectively. The TGA curves of these samples exhibit three steps of mass losses. The initial loss below 100^0C is assigned to the gradual evaporation of moisture/PNA. The second loss around 250-500^0C is due to the thermo-chemical decomposition of the chemically active organic materials (DBSA) mainly at 150-300 and 250-500^0C. The mass loss for Pani–PNA and Pani–PNA/ Al_2O_3 is very slow under 500^0C, which slightly increases with the increase in the content of Al_2O_3. Above this temperature, degradation proceeds rapidly. The third stage starts in the range of 500-600^0C, which implies a complete decomposition of organic polymers leaving only the oxide particles whose degradation occurs at a higher temperature. The incorporation of Al_2O_3 in the polymer matrix shows increased thermal stability. Pani–PNA shows a residual weight of 35% at 600^0C, which increases after the introduction of Al_2O_3 into Pani–PNA. The Pani–PNA/ Al_2O_3 (10%) matrix shows a residual weight of 41%, which subsequently increases to 45% for the Pani–PNA/Al_2O_3 (30%) composite.

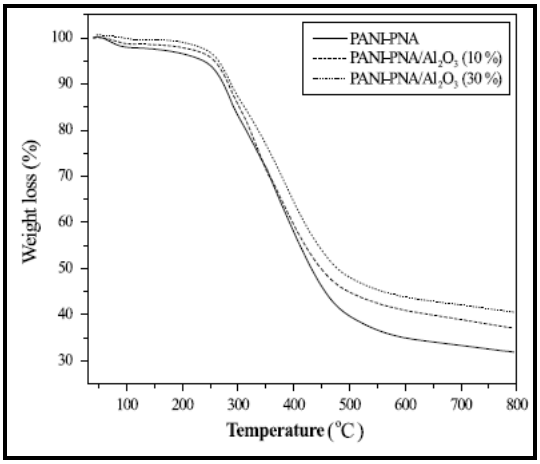

Fig. 2.26: TGA curve of Pani–PNA, Pani–PNA/ Al_2O_3 (10%) and Pani–PNA/ Al_2O_3 (30%) films [45]

There are three endothermic peaks in the curves of Fig. 2.27 (a) and (b) for Pani–PNA, Pani–PNA/ Al_2O_3 (10%). The first one is at 50–160^0C because of the removal of moisture/PNA. The second peak at 280–450^0C results from the removal of DBSA. The third at 500–600^0C is

due to the complete removal of chemically active organic molecules. Fig. 2.27 for Pani–PNA/ Al_2O_3 (30%) differs significantly from Fig. 2.27 a and b, as these endothermic peaks are minimized due to the higher content of oxide particles confirming the structural changes after the incorporation of Al_2O_3. Since the degradation process of Al_2O_3 is much higher than that of the polymer matrix, it does not appear in the degradation curve. The higher thermal degradation of composites after the incorporation of Al_2O_3 indicates that it has a positive influence on the thermal stability of the composites and inhibits their fast degradation. Aircraft coating also affected by various temperature conditions (low to high) in the environment. Thermal analysis tells about the stability of coating from low temperature to high temperature.

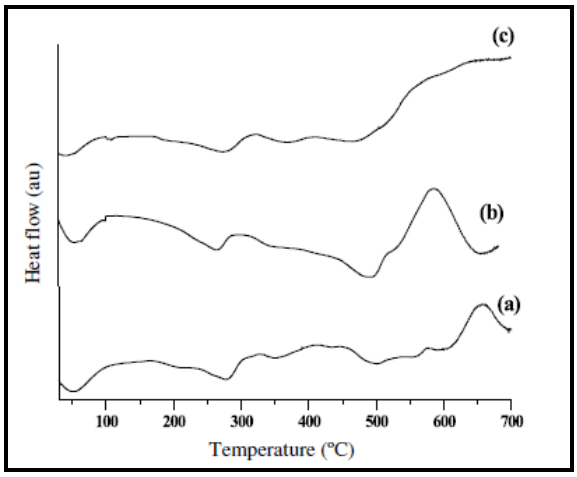

Fig. 2.27: DSC thermograms for (a) Pani–PNA (b) Pani–PNA/ Al_2O_3 (10%) (c) Pani–PNA/ Al_2O_3 (20%) and Pani–PNA/ Al_2O_3 (30%) [45]

2.9 Epoxy conducting polymer nanocomposites

Out of various resins, epoxy resins are used for a wide variety of protective coatings because of their excellent adhesion, good mechanical and thermal properties, easy processing and their notable chemical resistance under different aggressive environments, such as wet and high humidity conditions. It is used as a matrix in coating for applications in automotive, aerospace, marine, electronics, construction and recreational industries. There are mainly three different approaches to synthesize polymer-clay nanocomposites, melt intercalation, solution and in situ polymerization [85, 105]. In *melt intercalation process* thermoplastic polymer is mechanically mixed with organophilic clay at elevated temperatures. The polymer chains are then intercalated between the individual silicate layers of the clay. This process is

becoming increasingly popular since the resulting thermoplastic nanocomposites may be processed by conventional methods such as extrusion and injection molding. In the *solution method*, the organoclay as well as the polymer are dissolved in a polar organic solvent. The entropy gained by desorption of the solvent molecules allows the polymer chains to diffuse between the clay layers. After evaporation of the solvent, an intercalated nanocomposite structure is obtained. This strategy can be used to synthesize epoxy-clay nanocomposites but the large amount of solvent required is a major disadvantage. The *in situ polymerization* approach was the first strategy used to synthesize polymer clay nanocomposites and is a convenient method for the thermoset-clay nanocomposites. It is very similar to the solution method except that the role of the solvent is replaced by a polar monomer solution. Once the organoclay has been swollen in the monomer, the curing agent is added and total exfoliation of clay occurs in favourable cases.

Solange de Souza [106] studied corrosion protection of different metal with polyaniline acrylic blend. Fig. 2.28 shows the schematic diagram of the mechanism of metal passivation by polyaniline acrylic blend coating. For Fe/Pani (CSA)–PMMA electrode, the protective behaviour of the coating based on Pani (CSA) – PMMA blend is clearly shown in the Fig. 2.29 by the stabilization of potential arrow at ca. −0.4 $V_{(SCE)}$ for 85 days, even after the addition of a corrosive 0.1 mol L^{-1} NaCl solution to the electrolytic bath. The physical meaning of the initial OCP (Eoc≅0.4 $V_{(SCE)}$) corresponds to the equilibrium potential of the oxidized polymer (emeraldine oxidation state) that, after approximately 4 h, diminishes to ca. -0.4 $V_{(SCE)}$ (equilibrium potential of the reduced polymer, leucoemeraldine oxidation state. The OCP values of both bare Fe, Cu and Ag electrodes are also indicated in the Fig. 2.29 for comparison (arrows at −0.56, −0.03 and 0.28 $V_{(SCE)}$, respectively). The protective behaviour of the coating based in Pani(CSA)–PMMA blend is due to the presence of Pani(CSA) and not to the acrylic matrix (PMMA). In essence, measures of OCP as a function of time for Fe/PMMA electrode show that, after a few h in acidic medium, the potential evolves to the value corresponding to iron dissolution. This showed that the PMMA alone did not exhibit significant barrier property and did not hinder the attack of corrosive solution to the metal substrate.

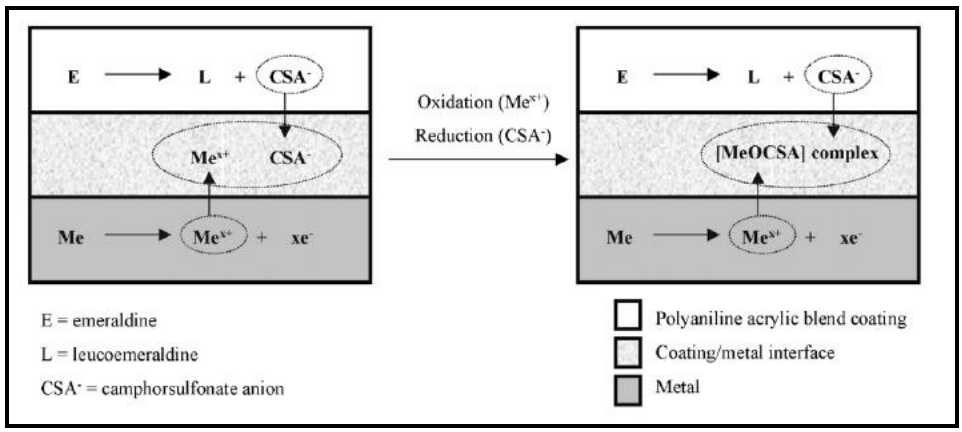

Fig. 2.28: Schematic diagram of the mechanism of metal passivation by polyaniline/ acrylic blend coating [106]

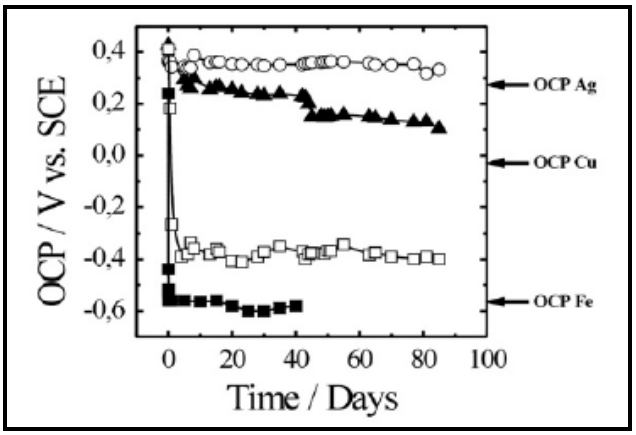

Fig. 2.29: OCP for (□) Fe/Pani(CSA)–PMMA electrode, (■) Fe/PMMA electrode, (▲) Cu/Pani(CSA)–PMMA electrode and (○) Ag/Pani(CSA)–PMMA electrode [106]

2.10 Aim and Objectives of the Research

From the literature survey, conductivity was found to be 10 S/cm that can be achieved by using various dopants and conducting polymers. Thus it was clear from the literature that researchers have reached to the above mentioned conductivity. However, such system was not applied on to the metals and their suitable corrosion protection mechanism along with the conductivity has not been developed yet. So our aim is to develop an anticorrosive coating formulation with all coating properties like gloss, UV, mechanical along with the conductivity of 5-10 S/cm.

In this research work, we have chosen epoxy as base matrix and mixed polyaniline particles into it for the proper coating system. Alone polyaniline with epoxy system will not provide

the desirable conductivity, so various dopants are added to enhance the conductivity. Therefore three systems were developed for achieving the above mentioned conductivity and excellent corrosion resistance. The systems are as follows:

1. Lignosulfonate doped with polyaniline (Pani-LGS) conducting polymer which was not earlier studied for the conductivity and corrosion protection of metals.
2. Grafting the above lignosulfonate doped polyaniline system with polyelectrolyte i.e.poly(acrlamide co acrylic acid) (Pani-PAmAc) to prevent the dopant loss and maintain the conductivity for longer time.
3. Modifying the grafted system with various nanoparticles (MMT/Al_2O_3/G) to achieve excellent corrosion and mechanical properties.

The research work carried out is as follows:

- Synthesis of lignosulfonate doped polyaniline (Pani-LGS) conducting polymer particles by chemical polymerization method.
- Synthesis of polyaniline with poly (acrylamide co-acrylic acid) in presence of lignosulfonate dopant (Pani-PAmAc) by chemical polymerization method.
- Synthesis of Pani-PAmAc with different nanoparticles like montmorillonite nanoclay (MMT), aluminium oxide (Al_2O_3) and graphene (G).
- Characterisation of synthesized particles using various techniques like SEM, FTIR, TEM,TGA and check the electrical conductivity of the particles.
- Formulation of proper coating system by using Pani-LGS, Pani-PAmAc, Pani-PAmAc-MMT, Pani-PAmAc-Al_2O_3 and Pani-PAmAc-G particles in the epoxy matrix.
- Uniform application of the coating over the aircraft AA2024-T3 alloy.
- Optimisation of Pani-LGS in the epoxy system.
- Optimisation of different molar ratio of Pani and PAmAc in the coating system.
- Structural and Morphological studies of the coating using FTIR, SEM and AFM.
- Thermal analysis of the coating using TGA studies.
- Electrical conductivity of the coating using four probe conductivity meter and broadband dielectric spectrometer at room temperature and variance in temperature, respectively.
- Performance evaluation of the coating using polarization method, EIS, salt spray test and UV-weatherometer at different immersion time in 0.6M NaCl.

- Mechanical properties such as hardness, adhesion, tensile and % elongation properties were studied.
- Detailed discussion of possible mechanism of corrosion inhibition using various formulated conducting polymer coatings.

The work mainly focused in understanding the corrosion behaviour at different immersion time and electrical conductivity on temperature variance of conducting polymer coatings. Other additional properties were also studied to fulfil the requirement of the coating.

Chapter 3 Experimental Work

In the present work, synthesis of epoxy based lignosulfonate doped polyaniline coatings was carried out. This was further modified with polyelectrolyte (PAmAc) and nanoparticles such as MMT/Al_2O_3/G. The aim of the study was to examine the electrical conductivity, adhesion and corrosion resistance. The details of the materials used, experimental methodology for synthesis of modified polyaniline, characterization techniques and performance evaluation are given below.

3.1 Materials

Aniline, acrylic acid, acryl amide, N,N'methylbisacrylamide, ammonium persulphate (APS) and lignosulfonic acid (LGS) were procured from Sigma Aldrich (India). Epoxy resin-bisphenol A (EEW 600) and polyamide hardener were obtained from Huntsman Chemicals (India). De-foamer (BYK A530), wetting agent (BYK 333) and dispersant (BYK 9076) were supplied by BYK chemicals (India). Montmorillonite clay (Cloisite 30B) was purchased from Southern Clay Products Inc. (USA). Al_2O_3 nanoparticles were supplied by Reinste Nano Ventures Private Limited (India) and graphite flake from Caltron Clays & Chemicals Private Limited (India). Sodium nitrate, sulphuric acid, potassium permanganate, hydrogen peroxide, phosphorus pentaoxide, sodium borohydride, sulfanilic acid, hydrazine, m-cresol and acetone were received from Merck (India) and used without further purification. AA2024-T3 aluminium samples were provided by Airport Metals (Australia) with the nominal chemical composition shown in Table 3.1.

Table 3.1: Chemical composition (wt %) of AA2024-T3 aluminium alloy

Si	Fe	Cu	Mn	Mg	Cr	Zn	Ti	Al
0.07	0.16	4.19	0.62	1.40	0.01	0.07	0.03	Bal

3.2 Synthesis of Conducting Polymer [Polyaniline (Pani-LGS)]

Pani-LGS was synthesised by chemical oxidative polymerisation of 0.08M solution of aniline in aqueous 0.02M HCl using 0.04 M ammonium persulfate (APS) [23, 30, 37]. The aniline solution was initially stirred for 6 h at room temperature and then maintained at 5ºC. Drops of APS were slowly added to the solution to precipitate polyaniline. A dark green colour ensures the complete polymerisation and precipitation of aniline (Fig. 3.1). The solution was then filtered and washed with distilled water; then de-doped in NH_4OH solution, filtered and dried again in a vacuum oven. The dried material (the emeraldine base (EB) of Pani) was re-doped via exposure to a 0.02M LGS solution. The solution was stirred for 4 h at room temperature, then filtered and dried in vacuum oven at 60ºC for 24 h to yield lignosulfonate doped polyaniline. It is emphasised that the above process evolved from significant experimental work to allow reproducible and quality synthesis.

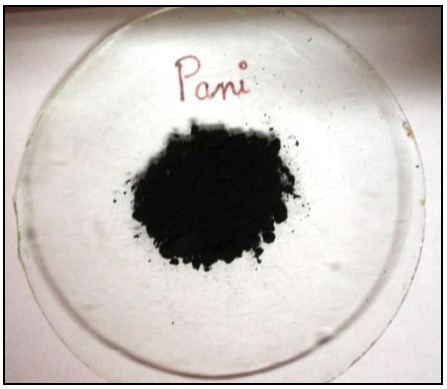

Fig. 3.1: Synthesised Pani-LGS particles

3.3 Synthesis of Double Stranded Conducting Polymer [Polyaniline-Poly (acrylamide-co-acrylic acid) (Pani-PAmAc)]

Synthesis of polyelectrolyte (PAmAc) was carried out using acrylamide (Am), acrylic acid (Ac), N,N'methylbisacrylamide (MBA) (crosslinking agent) and ammonium persulphate (APS) (oxidant) in 300 ml distilled water in a three necked round bottom flask at 70ºC under nitrogen atmosphere with stirring at 300 rpm for 2 h. The transparent liquid converts to milky white microgel as shown in Fig. 3.2 and this conversion indicates the completion of the reaction. The obtained solution was cooled and aniline and LGS were added slowly as

mentioned in Table 3.2 with constant stirring for 6 h at room temperature followed by addition of APS solution at 0- 4ºC. The molar ratio of aniline to acidic group was varied from 0.5 to 2. The colour of the liquid changed from orange to green after 5 h and finally to dark green colour at the end of 24 h. The solution was then filtered and washed with distilled water and methanol several times until the filtrate become colourless and dried at 60ºC for 24 h (Fig. 3.3).

Fig. 3.2: Synthesised PAmAc microgel

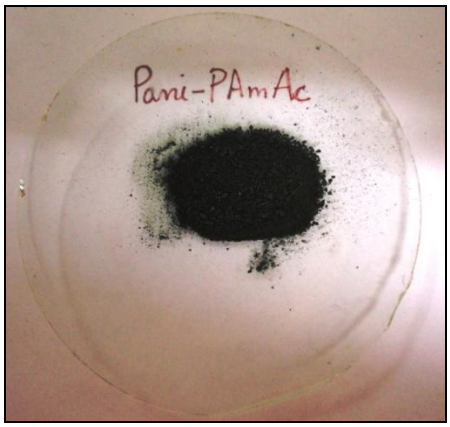

Fig. 3.3: Synthesised Pani-PAmAc particles

In this process the aniline molecules bind to poly(acrylamide co acrylic acid) by hydrogen bonding and the anilinium ions may get strongly attracted by the electrostatic force from the ionized portion of the polyelectrolyte. In this emulsified [poly (acrylamide co acrylic acid):(An)] adduct, the polyelectrolyte molecule serves two roles: (1) It serves as a template polymer that binds the aniline monomer (2) It serves as an emulsifier that helps to absorb the

aniline monomers in the interior of the emulsified particle. This process is called as template guided chemical polymerisation.

Table 3.2: Composition and designation of different molar ratio of Polyaniline-Poly(acrylamide-co-acrylic acid)[Pani-PAmAc]

Synthesis of PAmAc				Molar Ratio (Pani: Acid)	Aniline (mole)	LGS (mole)	APS (mole)	Pani-PAmAc Designation
Acryl amide (mole)	Acrylic acid (mole)	MBA (mole)	APS (mole)					
0.66	0.04	0.026	0.013	1:0.5	0.08	0.02	0.04	1Pani0.5PAmAc
1.33	0.08	0.053	0.026	1:1	0.08	0.02	0.04	1Pani1PAmAc
2.00	0.12	0.080	0.040	1:1.5	0.08	0.02	0.04	1Pani1.5PAmAc
2.66	0.16	0.106	0.053	1:2	0.08	0.02	0.04	1Pani2PAmAc

3.4 Synthesis of Double stranded Conducting Polymer Nanocomposites (Conducting polymer, Polyelectrolyte and Nanoparticles)

3.4.1 Polyaniline-Poly (acrylamide-co-acrylic acid)-Montmorillonite [Pani-PAmAc-MMT]

10 gm of MMT clay and 0.02 mole of lignosulfonate was added to 300 ml of HCl (1.0 M), aqueous solution in 500 ml three necked round bottom flask under ice bath and stirred vigorously with a magnetic stirrer for 30 min. To this solution 0.66 mole acrylamide (Am), 0.04 mole acrylic acid (Ac), 0.026 mole N,N'methylbisacrylamide (MBA) (crosslinking agent) and 0.013 mole ammonium persulphate (APS) (oxidant) were added and stirred at 300 rpm at 70ºC under nitrogen atmosphere for 2 h (Fig. 3.4).

Fig. 3.4: Synthesis setup

The growing radical propagates further on the MMT surface and crosslinks into a microgel by the copolymerisation of PAmAc and Pani. The -COOH group of Ac helps to adsorb aniline monomers onto the MMT-PAmAc microgels. The obtained microgel was cooled and 0.08 mole aniline was added slowly with constant stirring followed by a dropwise addition of 0.04 mole APS solution at 0-5ºC. The reaction was carried out for 7-8 h. The addition of oxidant (ammonium persulfate, APS) initiates the oxidative polymerisation of Pani in the system. After then, the resulting precipitate was filtered and washed thoroughly with distilled water and methanol several times until the filtrate become colourless and dried under vacuum at 60ºC for 24 h (Fig. 3.5).

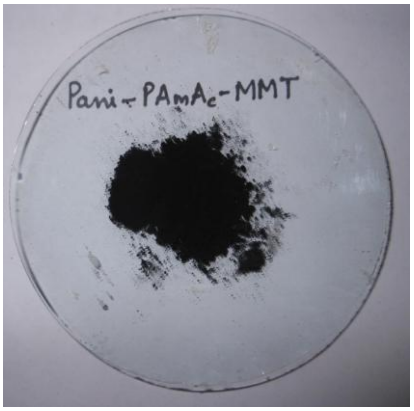

Fig. 3.5: Synthesised Pani-PAmAc-MMT particles

3.4.2 Polyaniline-Poly(acrylamide-co-acrylic acid)-aluminium oxide nanoparticles [Pani-PAmAc-Al_2O_3]

10 gm of Al_2O_3 and 0.02 mole of lignosulfonate was added to 300 ml of HCl (1M), aqueous solution in 500 ml three necked round bottom flask under ice bath and stirred vigorously with a magnetic stirrer for 30 min. To this solution 0.66 mole acrylamide (Am), 0.04 mole acrylic acid (Ac), 0.026 mole N,N'methylbisacrylamide (MBA) (crosslinking agent) and 0.013 mole ammonium persulphate (APS) (oxidant) were added and stirred at 300 rpm at 70ºC under nitrogen atmosphere for 2 h. The growing radical propagates further on the Al_2O_3 surface and crosslinks into a microgel by the copolymerization of PAmAc and Pani. The -COOH group of Ac helps to adsorb aniline monomers onto the Al_2O_3-PAmAc microgels. The obtained microgel was cooled and 0.08 mole aniline was added slowly with constant stirring followed by a dropwise addition of 0.04 mole APS solution at 0-5ºC. The reaction was carried out for 7-8 h. The addition of oxidant (ammonium persulfate, APS) initiates the oxidative polymerization of Pani in the system. After then, the resulting precipitate was filtered and washed thoroughly with distilled water and methanol several times until the filtrate become colourless and dried under vacuum at 60ºC for 24 h (Fig. 3.6) [95].

Fig. 3.6: Synthesised Pani-PAmAc-Al_2O_3 particles

3.4.3 Polyaniline-Poly(acrylamide-co-acrylic acid)-sulfonated graphene nanoparticles [Pani-PAmAc-G]

Graphite oxide was prepared by Hummers' method from graphite flake [96]. Graphite oxide were ultrasonicated in distilled water and purified by dialysis. Sulfonated graphene (G) were prepared from graphite oxide according to a method reported by Samulski and co-workers [98]. 10 ml of sulfonated graphene**,** 0.66 mole acrylamide (Am), 0.04 mole acrylic acid (Ac), 0.026 mole N,N'methylbisacrylamide (MBA) (crosslinking agent) and 0.013 mole ammonium persulphate (APS) (oxidant) were added to 300 ml of water in 500 ml three necked round bottom flask and stirred at 300 rpm at 70ºC under nitrogen atmosphere for 2 h. The growing radical propagates further on the graphene surface and crosslinks into a microgel by the copolymerisation of PAmAc and Pani. The -COOH group of Ac helps to adsorb aniline monomers onto the graphene -PAmAc microgels. The obtained microgel was cooled and 0.08 mole aniline and 0.02 mole lignosulfonate were added slowly with constant stirring followed by a dropwise addition of 0.04 mole APS solution at 0-5ºC. The reaction was carried out for 7-8 h. The addition of oxidant (ammonium persulfate, APS) initiates the oxidative polymerisation of Pani in the system. After then, the resulting precipitate was filtered and washed thoroughly with distilled water and methanol several times until the filtrate become colourless and dried under vacuum at 60ºC for 24 h (Fig. 3.7).

Fig. 3.7: Synthesised Pani-PAmAc-G particles

3.5 Coating Formulation

3.5.1 Coating Formulation of Pani/Epoxy

Pani-LGS/Epoxy coatings were prepared by subjecting Pani-LGS particles in m-cresol to ultrasound for 5 h. The resulting solution was filtered to eliminate solid residue. This solution was subsequently mixed with epoxy and polyamide as curing agent. Different amounts of Pani-LGS solution were added to epoxy as shown in Table 3.3.

3.5.2 Coating Formulation of Pani-PAmAc/Epoxy

Pani-PAmAc/Epoxy coatings were prepared by subjecting different molar ratios of Pani and PAmAc particles in m-cresol to ultrasound for 5 h. The resulting solution was filtered to eliminate solid residue. This solution was subsequently mixed with epoxy and polyamide as curing agent (Table 3.4).

3.5.3 Coating Formulation of Pani-PAmAc-MMT/Epoxy

Pani-PAmAc-MMT/Epoxy coatings were prepared by ultrasonicating 5 wt% Pani-PAmAc-MMT particles in 10 ml m-cresol for 5 h. The resulting solution was filtered to eliminate solid residue. The solution was subsequently mixed with 75 gm epoxy and 25 gm polyamide hardner. 20 ml of xylene as a solvent, deformer, wetting agent were added in the formulated resin and then stirred for 15 minutes.

3.5.4 Coating Formulation of Pani-PAmAc-Al_2O_3/Epoxy

Pani-PAmAc- Al_2O_3/Epoxy coatings were prepared by ultrasonicating 5 wt% Pani-PAmAc-Al_2O_3 particles in 10 ml m-cresol for 5 h. The resulting solution was filtered to eliminate solid residue. The solution was subsequently mixed with 75 gm epoxy and 25 gm polyamide hardner. 20 ml of xylene as a solvent, deformer, wetting agent were added in the formulated resin and then stirred for 15 minutes.

3.5.5 Coating Formulation of Pani-PAmAc-G/Epoxy

Pani-PAmAc-G/Epoxy coatings were prepared by ultrasonicating 5wt% Pani-PAmAc-G particles in 10 ml m-cresol for 5 h. The resulting solution was filtered to eliminate solid residue. The solution was subsequently mixed with 75 gm epoxy and 25 gm polyamide hardner. 20 ml of xylene as a solvent, deformer, wetting agent were added in the formulated resin and then stirred for 15 minutes.

Table 3.3: Composition and Designation of Pani/Epoxy Coating

S.No.	Epoxy (gm)	Pani (gm)	Hardner (gm)	Additives (gm)	Xylene (ml)	Coating Designation
1.	75	0	25	0.2	20	Epoxy
2.	75	1	25	0.2	20	1Pani/Epoxy
3.	75	2	25	0.2	20	2Pani/Epoxy
4.	75	5	25	0.2	20	5Pani/Epoxy
5.	75	10	25	0.2	20	10Pani/Epoxy
6.	75	20	25	0.2	20	20Pani/Epoxy

Table 3.4: Composition and Designation of Pani-PAmAc/Epoxy Coating

S.No.	Epoxy (gm)	Pani-PAmAc (gm)	Hardner (gm)	Additives (gm)	Xylene (ml)	Coating Designation
1.	75	0.5 (1Pani0.5PAmAc)	25	0.2	20	1Pani0.5PAmAc/Epoxy
2.	75	0.5 (1Pani1PAmAc)	25	0.2	20	1Pani1PAmAc/Epoxy
3.	75	0.5 (1Pani1.5PAmAc)	25	0.2	20	1Pani1.5PAmAc/Epoxy
4.	75	0.5 (1Pani2PAmAc)	25	0.2	20	1Pani2PAmAc/Epoxy

3.6 Pretreatment of aluminium AA2024-T3 alloys

AA2024-T3 substrates were polished to 1200 grit. The samples were then conditioned by degreasing in a solution of 5g/dm^3 (NaOH), 30g/dm^3 (Na_2CO_3), and 20g/dm^3 ($Na_3PO_4 \cdot 10H_2O$), at 50ºC for 40 sec then rinsing with 5% (NaOH), at 50ºC for 30 sec and 10% (HNO_3), at room temperature for 15 sec and final rinsing with distilled water.

3.7 Application of Coating over AA2024-T3 Substrate

AA2024-T3 panels were coated with the formulated coating system and cured at room temperature for 12 h, followed by curing at 60ºC for 12 h. The average dry coating thickness was measured using Elektrophysik coating thickness gauge as shown in Table 3.5 (Model Exacto FN, Type 1800202).

Table 3.5: Thickness of formulated coating systems

Coating Designation	Thickness (µm)
Epoxy	12±2
1Pani/Epoxy	13±3
2Pani/Epoxy	15±2
5Pani/Epoxy	15±2
10Pani/Epoxy	15±2
20Pani/Epoxy	16±3
1Pani0.5PAmAc/Epoxy	20±2
1Pani1PAmAc/Epoxy	18±3
1Pani1.5PAmAc/Epoxy	19±4
1Pani2PAmAc/Epoxy	21±2
Pani-PAmAc-MMT/Epoxy	25±3
Pani-PAmAc-Al_2O_3/Epoxy	25±5
Pani-PAmAc-G/Epoxy	24±3

3.8 Characterization of synthesised polymer

3.8.1 Scanning Electron Microscopy

The morphology of polymer particles were studied through scanning electron microscopy (SEM) at 1nA beam current, 10 kV accelerating voltage, 10 mm working distance using secondary electron detector in a Hitachi S3400 N microscope.

3.8.2 Transmission Electron Microscop

The morphology of the samples was examined through transmission electron microscopy (TEM). The aqueous solution of samples were ultrasonicated and collected on Cu grid. Microscopic investigations were carried out by Philips CM 200 TEM at 200 kV.

3.8.3 Conductivity Measurements

A pellet of Pani-LGS (diameter: 10mm, thickness: 3mm) was prepared by compression at a 0.3 GPa at room temperature for conductivity measurement. Electrical conductivity was measured by Broadband Dielectric Spectrometer (BDS) provided by Novocontrol GmbH, Germany at temperature 223 K to 423K with a step of 20 K and room temperature electrical conductivity was analysed using a four-point probe (VEECO FPP-5000) meter.

3.8.4 TGA Analysis

Thermal properties were determined by SDT Q 600 TGA at heating rate of 10ºC/ min from 30ºC to 900ºC under nitrogen atmosphere.

3.9 Characterization of Coating

3.9.1 Scanning Electron Microscopy

Surface morphology of coatings were studied through scanning electron microscopy (SEM) at 1nA beam current, 10 kV accelerating voltage, 10 mm working distance using secondary electron detector in a Hitachi S3400 N microscope

3.9.2 Atomic force microscopy

AFM analysis of the coated sample before and after corrosion was performed using Nanoscope IV AFM/MFM (Veeco Dimensions 3100 SPM with Nanoscope IV controller, Digital Instruments). Samples were analyzed in contact mode using standard non-conductive silicon nitride probe having sharp fine tip at the end.

3.9.3 Thermogravimetric analysis (TGA)

Thermal analysis was carried out by SDT Q 600 TGA at heating rate of 10ºC/ min from 30ºC to 900ºC under nitrogen atmosphere.

3.10 Performance evaluation of the coating

3.10.1 Conductivity Measurements

Electrical conductivity was measured by Broadband Dielectric Spectrometer (BDS) provided by Novocontrol GmbH, Germany at temperature 223 K to 423K with a step of 20 K and room temperature electrical conductivity was analysed using a four-point probe (VEECO FPP-5000) meter.

3.10.2 Corrosion protection properties

Electrochemical studies were carried out by potentiodynamic polarisation and electrochemical impedance spectroscopy (EIS), using a Bio-logic VMP3 Potentiostat/Galvanostat. For electrochemical testing a three-electrode cell incorporating a saturated calomel reference electrode (SCE) and a platinum mesh counter electrode. The test area of the working electrode was in all cases 1 cm^2. All polarisation and EIS measurements preceded by immersion for 1 day prior to the electrochemical test in order to achieve potential and environmental stabilization. EIS spectra were acquired in the frequency range from 10^6 Hz to10^{-2} Hz with AC amplitude of 10 mV. The data were fit by EC Lab software.

3.10.3 Adhesion Test

The adhesion of coatings was evaluated using Cross-hatch test as per ASTM D 3359.

3.10.4 Salt Spray Test

Corrosion resistance of coated panels was also examined by using salt spray test as per ASTM B117 specifications with 5wt% aqueous NaCl solution at 35 ± 2ºC.

3.10.5 UV–weatherometer Measurements

Accelerated weathering of coated specimen was carried out to simulate outdoor weathering using combination of UV light and water condensation (ASTM-G63). Damage caused by the weathering cycle was assessed using visual assessment, colour change and gloss measurement. The coated panels exposed in UV-weatherometer were characterized for color change (dE) and gloss retention using a spectrometer (BYK-Gardener Spectrometer) equipped with Color-Lab Quality Control software.

3.10.6 Mechanical Properties of the coating

The mechanical properties of the films were determined using universal testing machine. An average value of at least five replicates of each material was taken. Hardness of the coatings was measured by pencil hardness test (ASTM D3363).

Chapter 4 Results and Discussion

4.1 Characterization of Polyaniline (Pani) and its modification with copolymer (Pani-PAmAc) particles

4.1.1 Scanning Electron Microscopy of Pani and Pani-PAmAc particles

The SEM micrographs of Pani and Pani-PAmAc particles are shown in Fig.4.1. Pani forms large aggregate consisting of many small particles whereas the surface of Pani-PAmAc is smooth and homogeneous. SEM micrograph shows that Pani is porous in nature which becomes compact when uniformly impregnated in the PAmAc microgel [77].

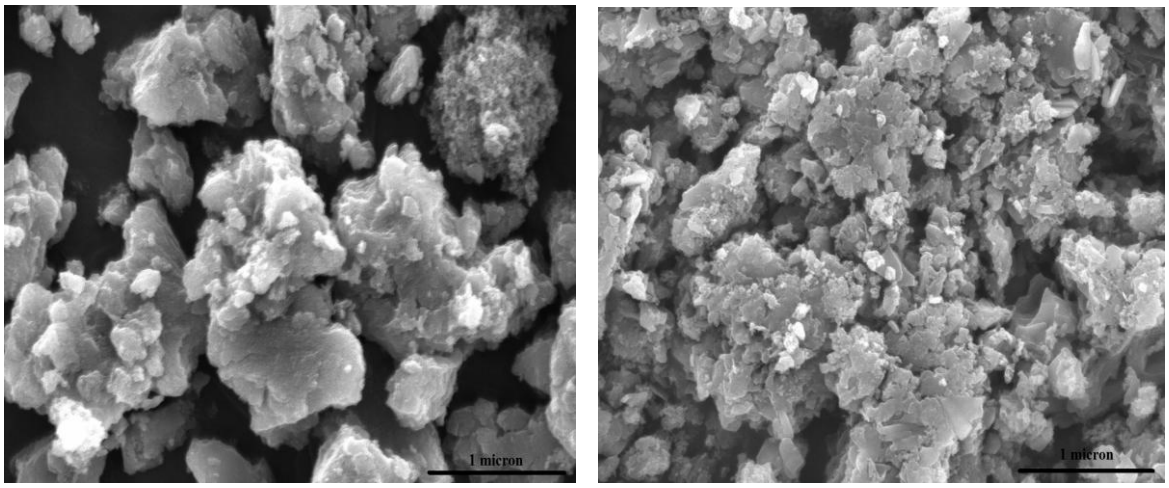

(a) **(b)**

Fig. 4.1: SEM micrographs of (a) Pani and (b) Pani-PAmAc

4.1.2 Transmission Electron Microscopy of Pani and Pani-PAmAc particles

Fig. 4.2 shows the TEM micrographs of Pani and Pani-PAmAc composite polymer particles. Pani particles appear as a globular structure. This globular pattern was randomly distributed among the matrix of the PAmAc as shown in Fig 4.2 (b). The average diameter of Pani-PAmAc particles increased slightly from the Pani particles ($\sim$ 10 -15 nm) to $\sim$ 30-35 nm.

PAmAc particles are water soluble, so it starts polymerizing in aqueous medium leading to the formation of larger aggregates [79].

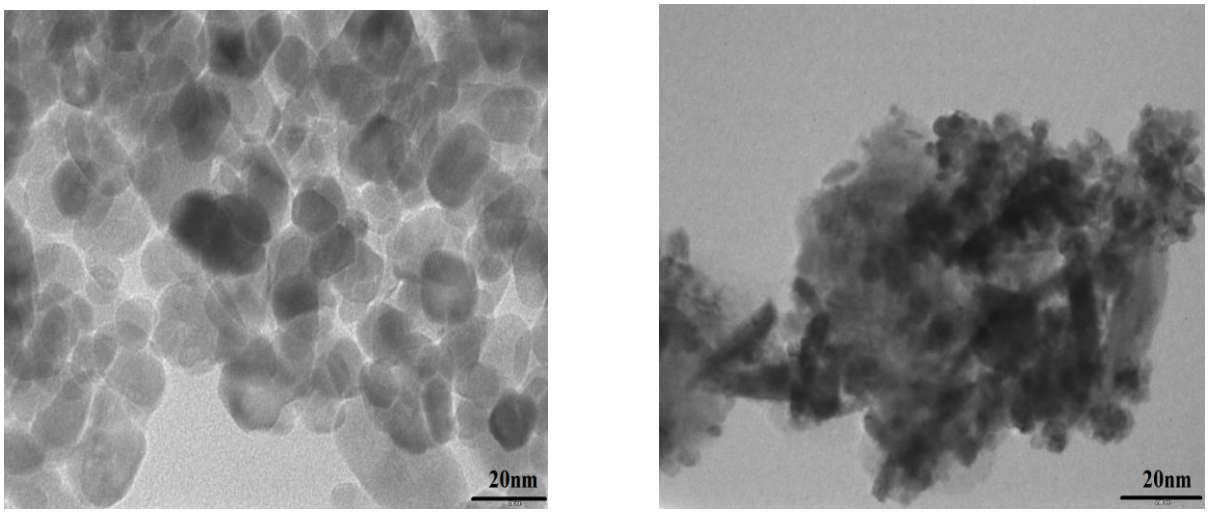

(a) **(b)**

Figure 4.2: TEM micrographs of (a) Pani (b) Pani-PAmAc

4.1.3 Conductivity Measurements of Pani and Pani-PAmAc particles

The room temperature conductivity of Pani and Pani-PAmAc particles were 6.48 S/cm and 5.9 S/cm, respectively as shown in Fig. 4.3. It was found that the incorporation of copolymer (PAmAc) into Pani decreases the conductivity due to its insulating nature

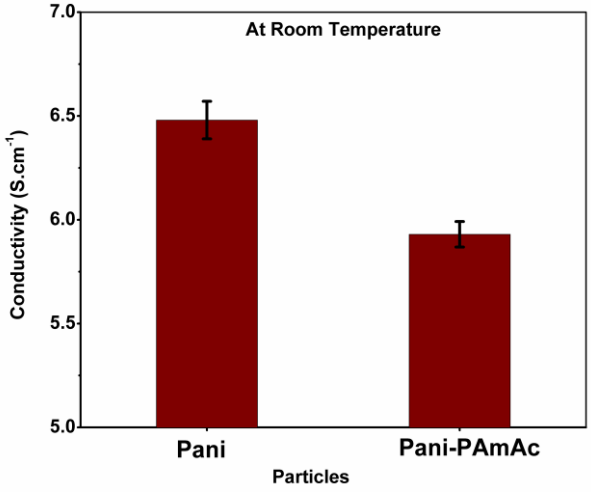

Fig. 4.3: Room temperature conductivity of Pani and Pani-PAmAc

. Fig. 4.4 shows the temperature dependence on electrical conductivity of Pani and Pani-PAmAc particles. The temperature dependent conductivity was measured from 223 K to 423K. The electrical conductivity of particles increases with increase in temperature due to thermal excitation of electrons. It was assumed LGS dopant has a positive influence on the temperature dependent conducting property of Pani, which enhanced the mobility of conducting particles at higher temperature.

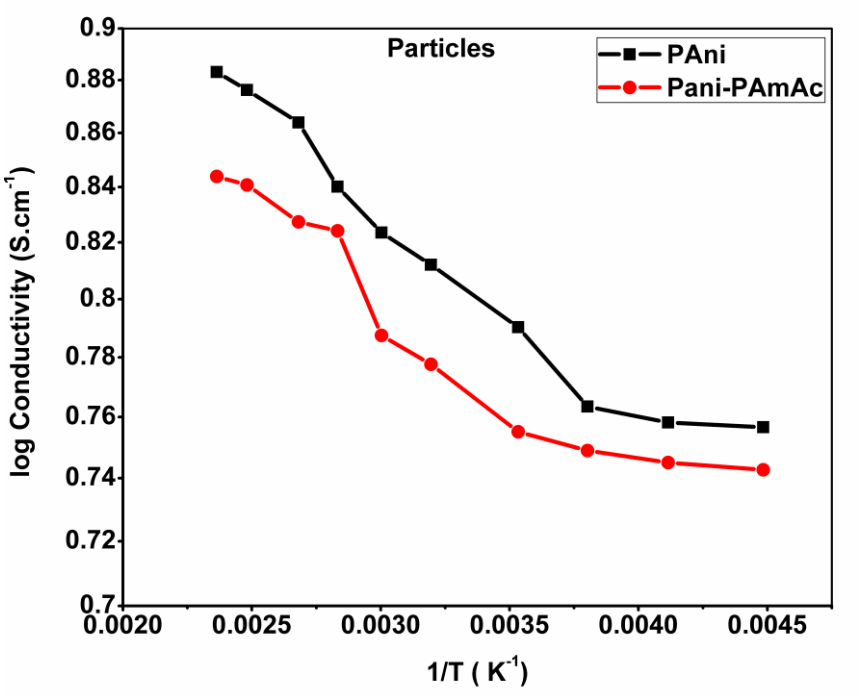

Fig. 4.4: Logarithm conductivity vs. inverse temperature of Pani and Pani-PAmAc

4.1.4 Thermal Analysis of Pani and Pani-PAmAc particles

Fig. 4.5 shows TGA curves for Pani, PAmAc and Pani-PAmAc. The initial mass loss upto 170°C is due to loss of water which is much prominent in Pani. A sharp mass loss beginning at nearly 350°C and continuing till about 600°C is observed which presumably corresponds to large scale thermal degradation of Pani chains. For PAmAc moisture release takes place at a slow rate over the temperature range of 40–200°C responsible for successive release of absorbed moisture and bound (H-bonded) water. A relatively high mass loss range then follows upto 400°C which corresponds to cyclisation of PAmAc chains and associated liberation of NH_3. A much sharper mass loss zone appears over the temperature zone of 400–500°C accounting for large scale thermal degradation with the liberation of H_2, CO and NH_3. The TGA curve of Pani-PAmAc composite does not really show an average behaviour. The

rate of mass loss is the least over the initial zone i.e. up to 250°C, due to loss of water molecules. The major losses of weight were observed over two temperature ranges, beginning around 250–300ºC and 300–400ºC. The first decrease of mass was mainly due to the loss of dopant molecules (LGS). The second weight loss at the higher temperature indicates a structural decomposition of the polymer. The sharp decomposition between 400–500°C for the composite resembles the same as for PAmAc. TGA data indicate that the Pani-PAmAc composites as obtained from a stable aqueous solution in the presence of PAmAc are far from being physical blends of Pani and PAmAc. This overall confirms that the synthesised Pani-PAmAc has good thermal stability, better than that of Pani and Pani-PAmAc homopolymers [17, 18, 50, and 72].

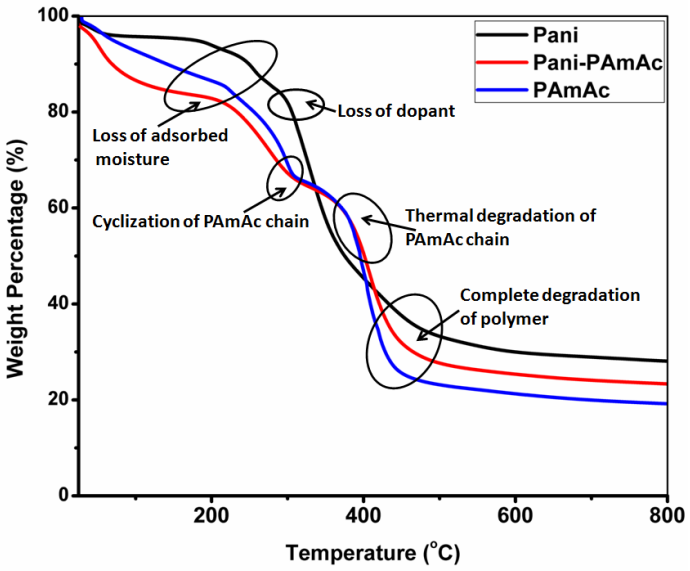

Fig 4.5: TGA Curve of Pani, PAmAc and Pani-PAmAc

4.2 Characterization of double stranded conducting polymer nanoparticles [Polyaniline-Poly(acrylamide co-acrylic acid)-MMT/Al_2O_3/G]

4.2.1 Scanning Electron Microscopy of Pani-PAmAc-Nanoparticles

Fig. 4.6 shows the SEM micrographs of Pani-PAmAc-MMT, Pani-PamAc-Al_2O_3 and Pani-PamAc-G. Pani-PamAc-MMT. (Fig. 4.6a) shows the granular structure along with flaky texture of MMT clay. It shows that the particles are in agglomerated form and their average size was found to be around 200nm. From Fig. 4.6b, it was found the size of 150-200nm spherical structure of Pani-PamAc-Al_2O_3. In Fig. 4.6c, Pani-PamAc was grown on the surface of a graphene-based nanosheet, due to adsorption of aniline molecules on the graphene sheets

via electrostatic and p-p interactions. Pani-PamAc-G exhibit particle size of 50-70 nm shows compact structure due to aggregation of particles.

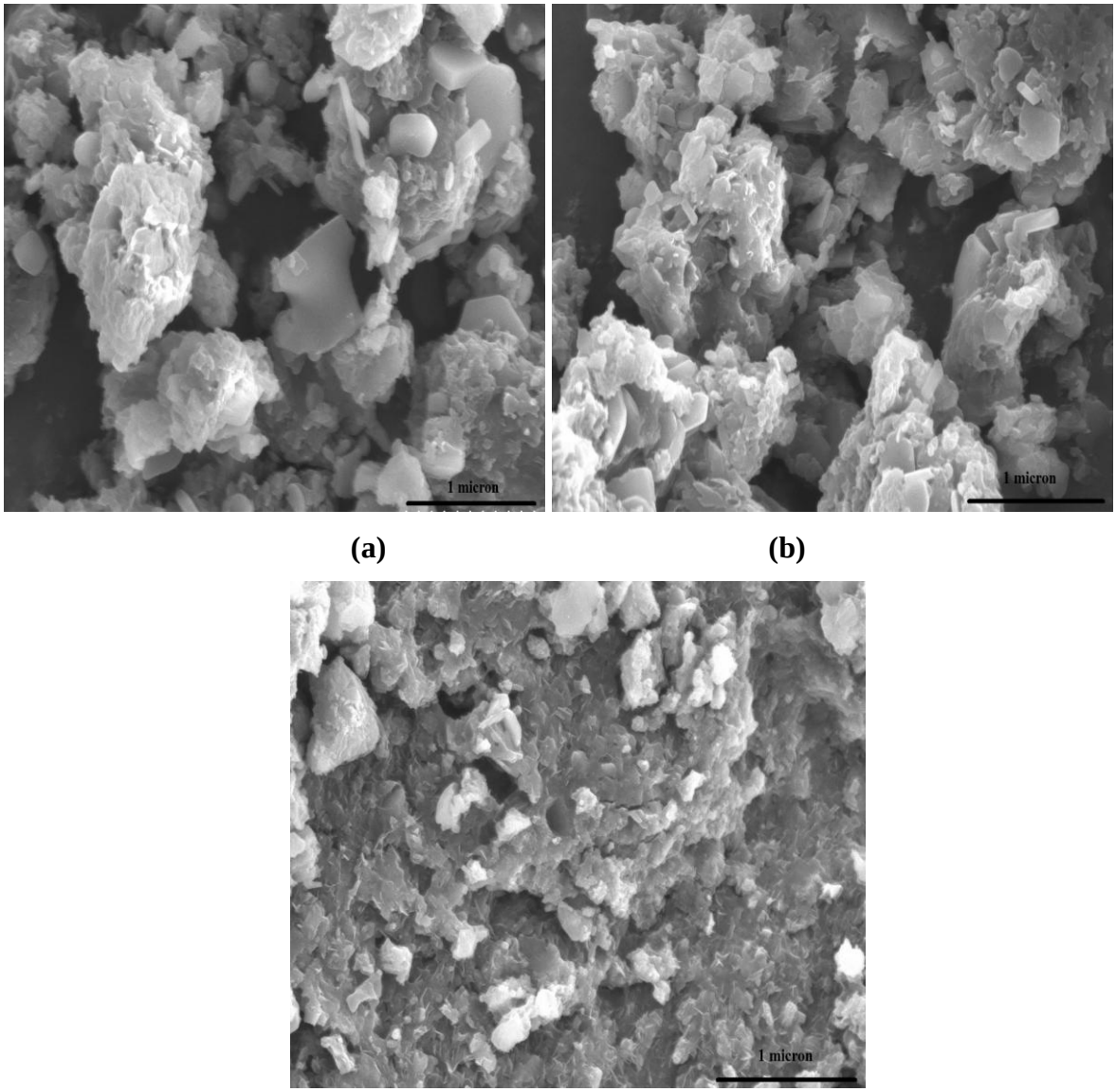

(a) **(b)**

(c)

Fig. 4.6: SEM micrographs of (a) Pani-PAmAc-MMT (b) Pani-PAmAc-Al_2O_3 (c) Pani-PAmAc-G (1microns)

4.2.2 Transmission Electron Microscopy of Pani-PAmAc-Nanoparticles

The actual structure and size of the Pani-PAmAc-nanocomposites was confirmed by TEM. Fig. 4.7 shows the TEM micrographs of Pani-PAmAc-MMT, Pani-PAmAc-Al_2O_3 and Pani-PAmAc-G. From Fig. 4.7a, the dark black lines represent the lamellar stacks of silicate layer

of MMT clay. TEM image of Pani-PAmAc-MMT show the lamellar-like particles were composed of small spherical Pani-PAmAc particles having size of 60-50 nm.

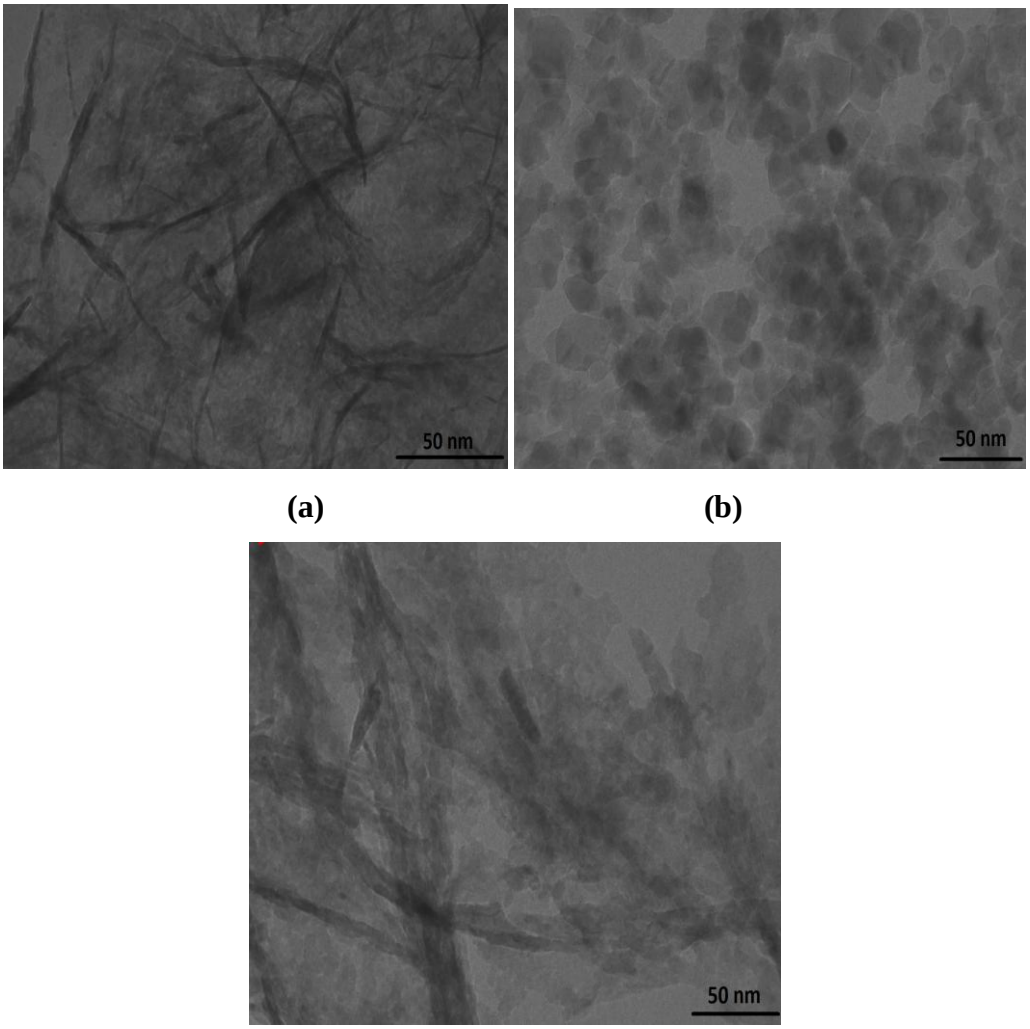

(a) **(b)**

(c)

Fig. 4.7: TEM images of (a) Pani-PAmAc-MMT (b) Pani-PAmAc-Al_2O_3 (c) Pani-PAmAc-G (50 nm)

Pani-PAmAc- Al_2O_3 shows the dark color globular structure of Pani-PAmAc was embedded in the surface of spherical alumina particles with diameter ranging from 20 to 30 nm in Fig. 4.7b. Pani-PAmAc-G shows the randomly distribution of 40- 50nm sheet like structure, in which globular Pani particle are embedded into it as shown in Fig. 4.7c shows the folded morphology of small fragments of graphene.

4.2.3 Electrical Conductivity of Pani-PAmAc-Nanoparticles

The room temperature conductivity of Pani-PAmAc-MMT, Pani-PAmAc-Al_2O_3 and Pani-PAmAc-G nanoparticles were 6.20, 6.16 and 14.76 S/cm, respectively as shown in Fig. 4.8. Fig. 4.9 shows the temperature dependence on electrical conductivity of Pani-PAmAc-MMT, Pani-PAmAc-Al_2O_3 and Pani-PAmAc-G nanocomposites. The temperature dependent conductivity was measured from 223 K to 423K. It was noted that the electrical conductivity of the nanoparticles increases with the increase in temperature. The electrical conductivity of Pani-PAmAc-MMT nanoparticles depends on the nature of both the host clay and the guest Pani-PAmAc. The electrical conductivity of Pani-PAmAc-MMT was lower than that of pure Pani (6.48 S/cm) because of the existence of individual silicate layers with insulting character. The conductivity of Pani-PAmAc-Al_2O_3 increases with increase in temperature due to thermal excitation of electrons. The electrical conductivity of Pani-PAmAc-Al_2O_3 was lesser than that of pure Pani. This can be ascribed to the conformational changes of Al_2O_3 that make hopping difficult and thereby reduce conductivity. It was found that the incorporation of graphene into Pani-PAmAc greatly improved the conductivity of the nanoparticle due to its inherent conducting nature. The conductivity of graphene was due to its π-conjugated orbital system which imparts very high conductivity to the material. The electrical conductivity is perhaps the best indicator of the extent to which graphite oxide has been reduced to graphene. Graphite oxide and graphite flakes are not conductive because it lacks an extended π-conjugated orbital system.

The conductivity behaviour depending on temperature can be ascribed by two mechanisms for electrical conduction in the particles. Arrhenius theory is attributed to excess thermal energy at high-temperature region (373–423 K) to excite electrons to the conduction band (thermal process). The other mechanism takes place in the low temperature region (223–353K) and is attributed to the hopping process, in which the excited electrons in this region lose their ability to make a transition to the conduction band with lowering temperature. Thus, the electron attempts to find a state of similar energy by tunnelling beyond its nearest neighbours to hop into more distant sites. This hopping leads to a greater selection of possible energy levels of electrons. The behaviour of DC conductivity in this region is called variable range hopping (VRH), which is expressed in Mott's theory [115,117].

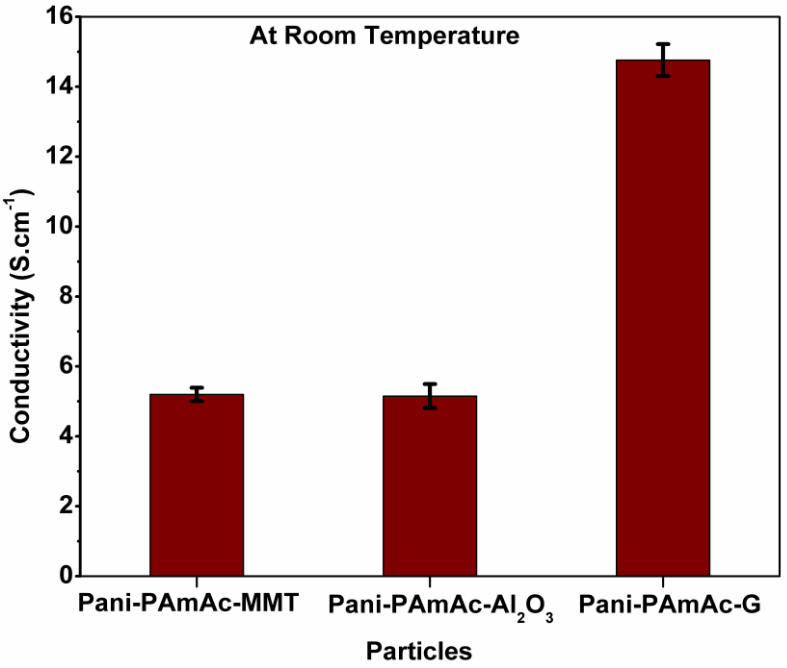

Fig. 4.8: Room temperature conductivity of Pani-PAmAc-MMT, Pani-PAmAc-Al_2O_3 and Pani-PAmAc-G nanoparticles

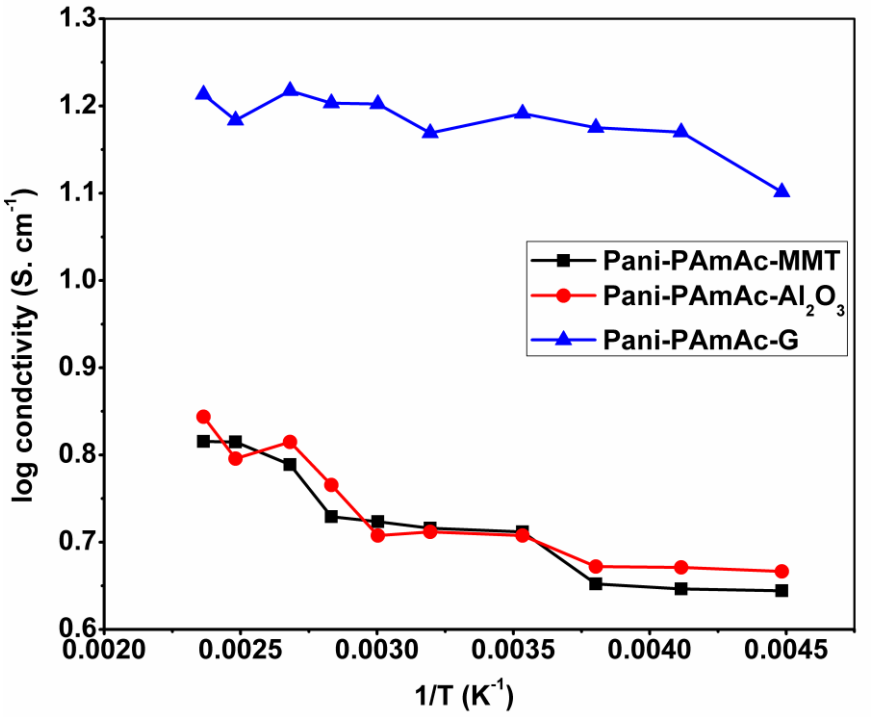

Fig. 4.9: Logarithm conductivity vs. inverse temperature of Pani-PAmAc-MMT, Pani-PAmAc-Al_2O_3 and Pani-PAmAc-G nanoparticles

4.2.4 Thermogravimetric analysis (TGA) of Pani-PAmAc-Nanoparticles

Aircraft coating affected by various temperature conditions (low to high) in the environment.Using thermogravimetric analysis (TGA), the thermal stability can be characterized by the change in coating weight as a function of temperature. Weight loss measurements can be performed at various temperatures. TGA provides a possibility of evaluating the weight loss under many time-temperature conditions; this can be used for predicting the thermal stability of coatings.

The TGA curves of the Pani-PAmAc-MMT, Pani-PAmAc-Al_2O_3 and Pani-PAmAc-G nanoparticles are shown in Fig.4.10. It is clear from the figure that all the samples have a little mass loss around 180ºC due to the removing of adsorbed water. From 210 to 410°C, Pani-PAmAc-Al_2O_3 showed about 24% mass loss, possibly due to the release of its functional groups such as -SO_3H and -COOH. At 900°C, Pani-PAmAc-Al_2O_3 still kept about 42% weight residual, indicating the excellent thermal stability of Al_2O_3. The TGA curve of Pani-PAmAc-MMT exhibited about 44% weight loss in the temperature scale of 220 to 440°C and 20% weight residual at 900°C. The TGA curve of Pani-PAmAc-G exhibited about 43% weight loss in the temperature scale of 210 to 440°C and 5% weight residual at 900°C.

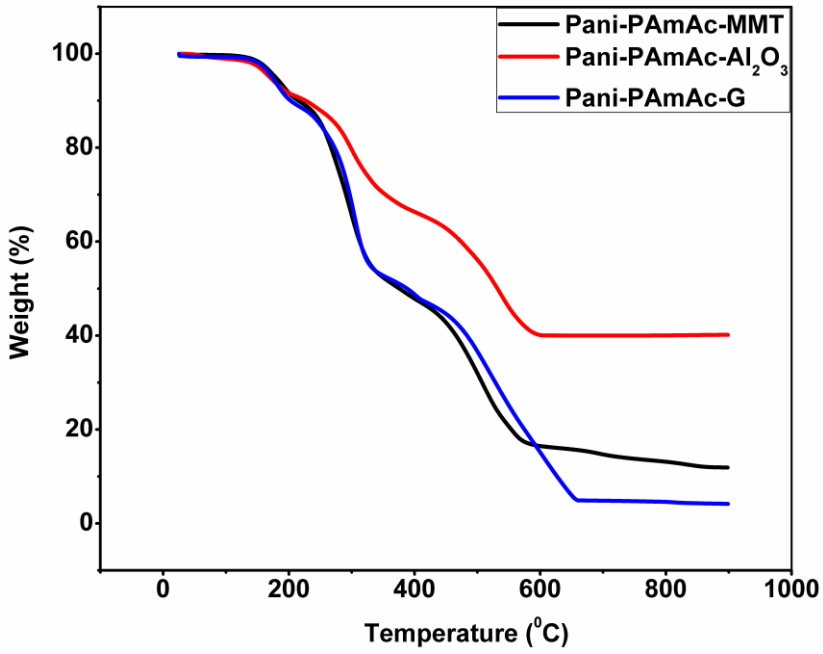

Fig. 4.10: TGA curve of Pani-PAmAc-MMT, Pani-PAmAc-Al_2O_3 and Pani-PAmAc-G nanoparticles

4.3 Characterisation of Pani-LGS/Epoxy Coating

4.3.1 Scanning Electron Microscopy (SEM) of Pani-LGS/Epoxy coating

The SEM characterisation of Pani/Epoxy coatings are seen in Fig. 4.11. Neat epoxy shows air gaps in the coating that continuously disappear as the concentration of Pani-LGS in epoxy increases. 2% Pani-LGS and 5% Pani-LGS coatings exhibited a smooth and homogeneous dispersion of particles. When the content was above 5% the particles agglomerated.

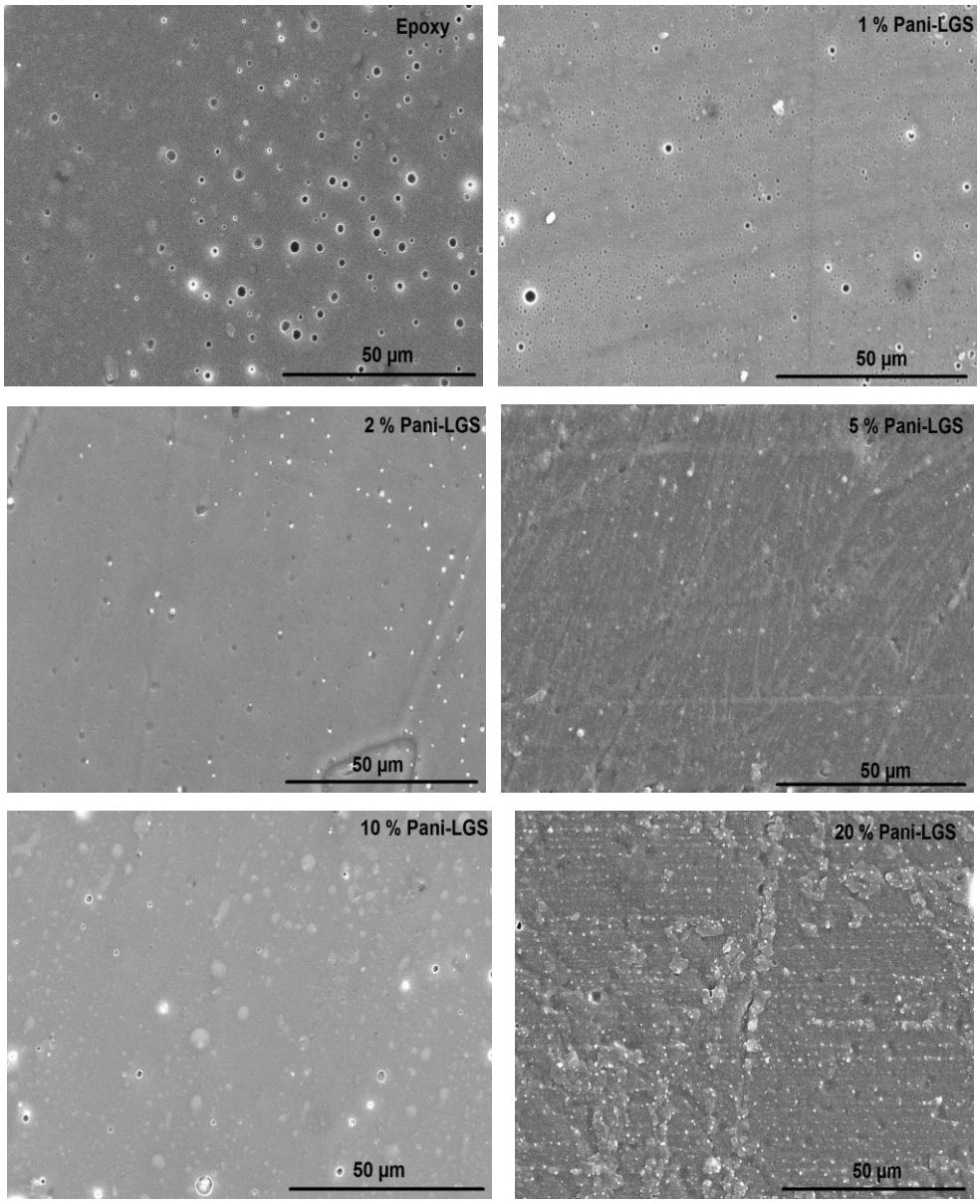

Fig. 4.11: Scanning Electron micrographs of Pani-LGS/Epoxy coatings (SE at 1000x magnification)

SEM micrographs of Pani/Epoxy coatings after 720 h of salt spray exposure revealed numerous large pits and surface damage formed after corrosion on the surface of epoxy, 1% Pani and 2% Pani samples (Fig. 4.12). However, a 5% Pani/Epoxy coating was compact and smooth in morphology - with no cracks evident, even after salt spray exposure. Few small corrosion pits and white corrosion product deposits were observed in 10% Pani-LGS and 20% Pani-LGS coated samples.

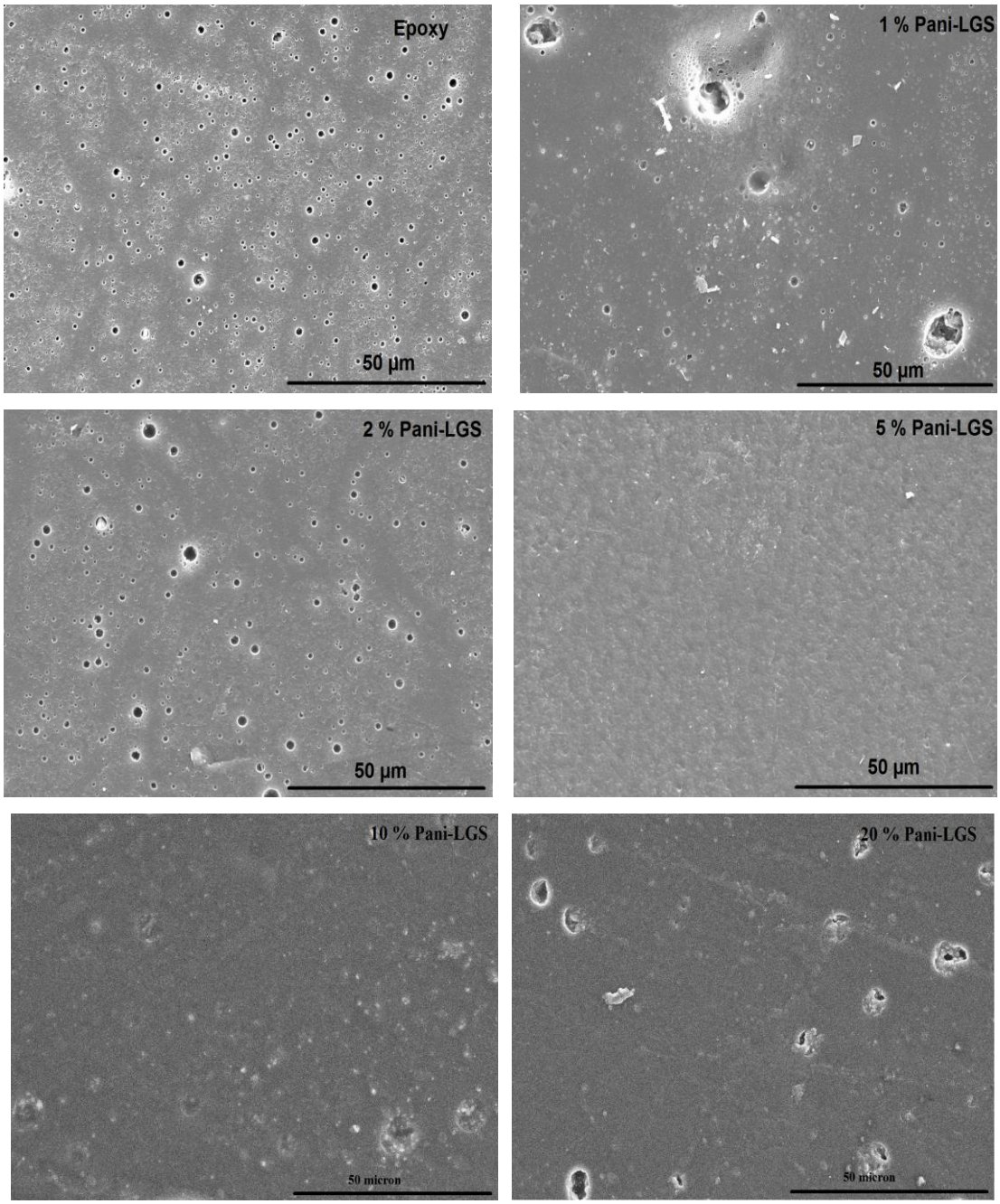

Fig. 4.12: Scanning Electron micrographs of Pani-LGS/Epoxy coatings after 720 h salt spray exposure (SE at 1000x magnification)

4.3.2 Atomic Force Microscopy of Pani-LGS/Epoxy coating

AFM were performed to understand the particle distribution and surface roughness of the coatings at the micro and nano level. Fig. 4.13 (a-f) shows the AFM images of different concentration of Pani-LGS/Epoxy coatings. All coatings are crack free and low roughness values. Epoxy shows very low roughness value as compared to Pani containing epoxy coatings due to absence of polyaniline particles which increase the surface roughness of the coating. At low concentration of polyaniline particles are uniformly distributed as shown in Fig. 4.13 (a-d) but as the concentration of the particles increases agglomeration was clearly observed in Fig. 4.13 (e and f) and this was also confirmed by the increase in roughness value of 10% Pani and 20% Pani epoxy coatings. The root-mean square (RMS) values of surface roughness determined by AFM were 3.81± 0.9, 4.20±1.1, 4.53±0.7, 5.95±0.9, 6.21±1.3 and 8.71±1.7nm for epoxy, 1%Pani, 2%Pani, 5%Pani, 10%Pani and 20% Pani coatings, respectively.

Fig. 4.14 (a-f) shows the AFM images of series of Pani-PAmAc/Epoxy coatings after 720 h salt spray exposure, respectively. The RMS values were 27.75±1.6, 23.38±1.4, 21.11±1.9, 19.29±1.5, 22.63±0.9 and 26.20±1.2nm for epoxy, 1%Pani, 2%Pani, 5%Pani, 10%Pani and 20% Pani coatings, respectively. It was found that blisters or some uniform pits formed on the coating surface after 720 h of salt spray exposure and increase the roughness values. The AFM study detected the high roughness value in the epoxy coating and on increaseing the concentration of polyaniline the roughness value decreases. However, at higher concentration of polyaniline, the high roughness value was observed due to corrosion product and presence of pits on the surface.

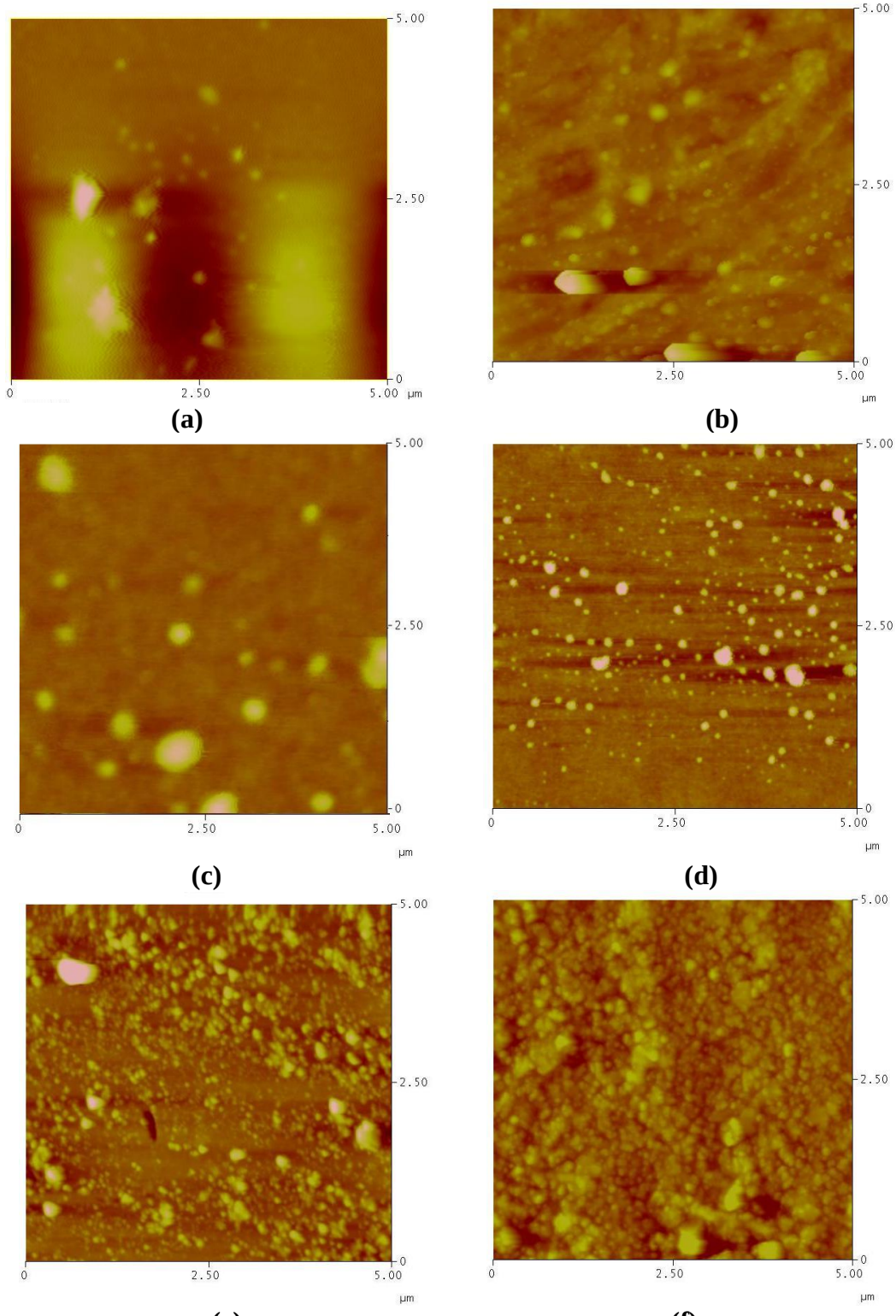

Fig. 4.13: AFM images of (a) Epoxy (b)1% Pani (c) 2% Pani (d) 5%Pani (e) 10% Pani (f) 20% Pani Coatings (5 microns)

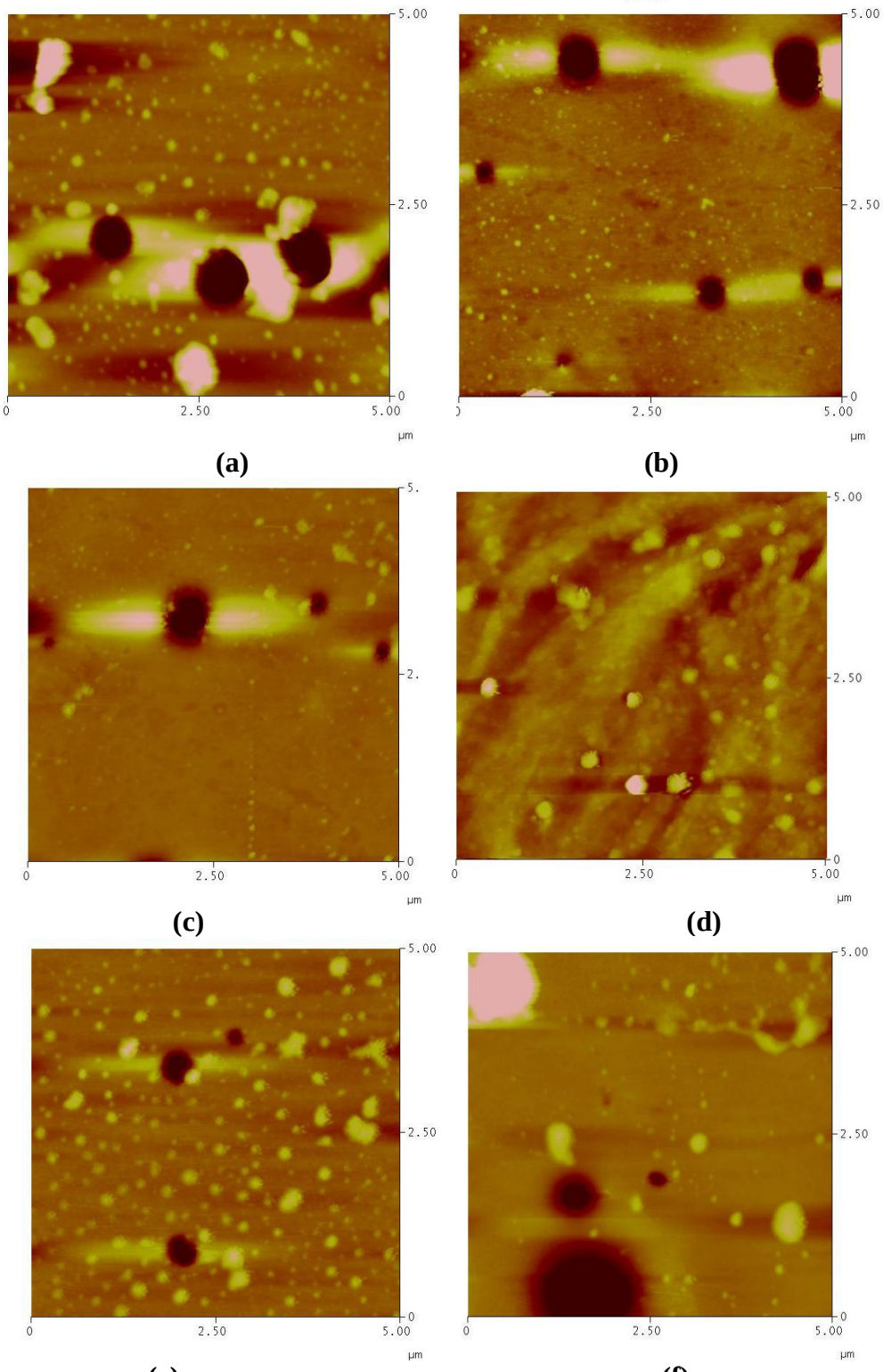

Fig. 4.14: AFM images of (a) Epoxy (b) 1% Pani (c) 2% Pani (d) 5%Pani (e) 10% Pani (f) 20% Pani Coatings after 720 h salt spray exposure (5 microns)

4.3.3 TG Analysis of Pani-LGS/Epoxy coating

TGA curve of Epoxy and various loading of Pani/Epoxy blends are presented in Fig. 4.15. All curves show a typical behaviour of epoxy coating. Pani/Epoxy blends show high degradation temperature as compared to Epoxy. The curves of various loadings will exhibit same decomposition behaviour. The decomposition process of epoxy starts at 190ºC with three subsequent decays being observed at 160ºC, 210ºC and 350ºC. A small weight loss before 210ºC was due to loss of volatile and moisture and finally undergoes a complete degradation around 600ºC.

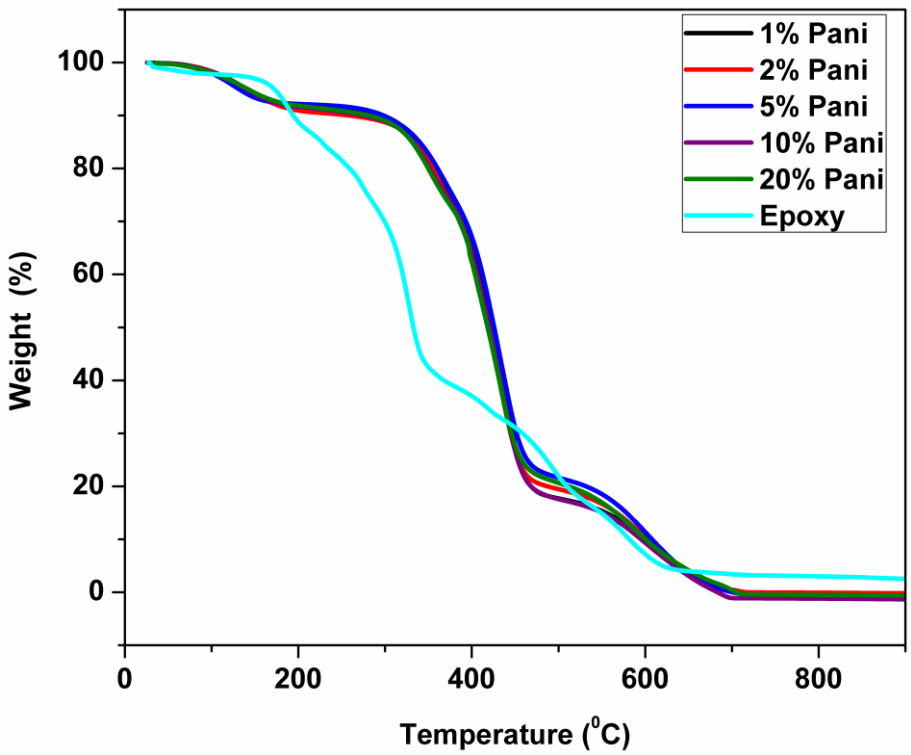

Figure 4.15: TGA Curves of Pani/Epoxy Coating

TGA curves of Pani/Epoxy samples exhibit three steps of mass losses. The decomposition process of Pani/Epoxy starts at 170ºC with subsequent decays being observed at 210ºC, 320ºC, 480ºC and 710ºC. TGA curves show a small weight loss below 170ºC, caused by the loss of adsorbed water and oligomers. The weight loss between 170ºC to 320ºC corresponds to release of sulfonate groups. The weight loss in the range of 320–480°C temperature may be due to the structural decomposition of Pani particles. The value of decomposition process at 480°C was different at various loading conditions in epoxy base. The final degradation of polymer takes place at 690°C.The percentage weight loss at 320ºC of epoxy and various

loading of Pani/Epoxy coatings was observed 50% and 10%, respectively. Hence, it may be concluded that on addition of Pani increases the thermal stability of the epoxy system [17, 18, 72, and 80].

4.3.4 Electrical Conductivity of Pani-LGS/Epoxy coating

The room temperature conductivity of Epoxy, 1% Pani, 2% Pani, 5% Pani, 10%Pani and 20% Pani coatings were 10^{-8}, 2.16, 4.44, 4.59, 4.88 and 4.23 S/cm, respectively as shown in Fig. 4.16. As the concentration of Pani-LGS increases the amount of conducting particles increases in the epoxy matrix which thereby lead to increase in conductivity. The amount of Pani-LGS was limited to 10%. Beyond this concentration, the dispersion of the Pani particles into epoxy matrix was very difficult, when the content of Pani-LGS reached to 10wt%, the conductivity of the hybrid decreased thereafter due to agglomeration of Pani particles and resulting in interruption in conducting pathway.

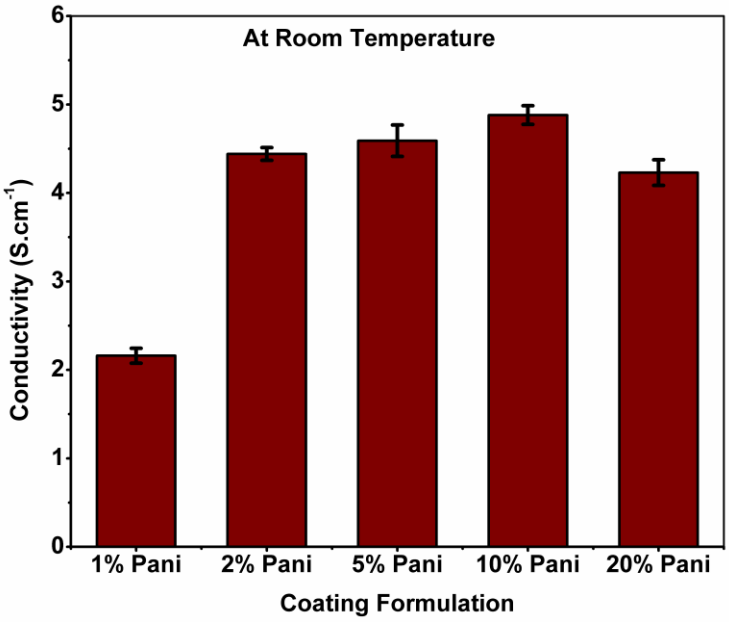

Fig. 4.16: Room temperature conductivity of different loading of Pani-LGS/Epoxy coatings

Fig. 4.17 shows the temperature dependence on electrical conductivity of various loading of Pani-LGS/Epoxy coatings. The temperature dependent conductivity was measured from 223 K to 423K. It was noted that the electrical conductivity of the coating increases with the increase in temperature. 1% Pani shows relative lower conductivity as compared to other Pani

concentration. This was due to less number of conducting particles are available for the electrical conductivity. The continuous pathway was not available for the conducting of electrons. Electrical properties depend on the polymer matrix, processing method and filler type. On increasing the temperature the movement of electron charge carriers also increases.

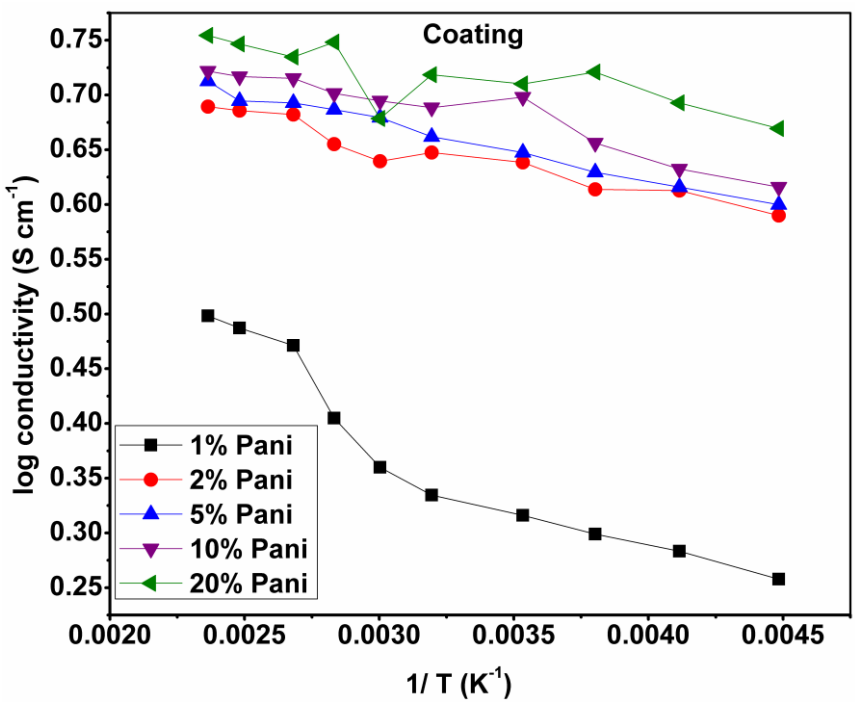

Fig. 4.17: Logarithm conductivity vs. inverse temperature of different loading of Pani-LGS/Epoxy coatings

4.3.5 Corrosion protection of Pani-LGS/Epoxy coatings

The corrosion protection behaviour of coatings was examined in 0.6M NaCl using potentiodynamic polarization and EIS studies. pH was maintained at 7 for the test solutions.

The potentiodynamic polarization curves for AA2024-T3, epoxy coated and various composition of Pani-LGS coated AA2024-T3 in 0.6M NaCl are shown in Fig. 4.18. The corrosion potential of all Pani-LGS formulations except 5% Pani-LGS were shifted in the positive direction compared to that of the bare AA2024-T3. The E_{corr} increased from -907 mV_{SCE} for the AA2024-T3 to about -511 mV_{SCE} for the 1%Pani-LGS coating. However, the E_{corr} value obtained from 5% Pani-LGS was -475 mV_{SCE}. The corrosion current densities and corrosion rate values were determined by extrapolation of the linear portions of the anodic and cathodic slopes of tafel curves. The values of the corrosion potential (E_{corr}), corrosion

current density (i_{corr}) and protection efficiency (PE) obtained from tafel curves of bare AA2024-T3,epoxy and Pani-LGS coatings are summarized in Table 4.1. From the measured corrosion current density values, the protection efficiency was obtained from the following equation [34],

$$\textbf{Protection efficiency (\%)} = (i_{corr}(uc) - i_{corr}(c)) / i_{corr}(uc) * 100$$

Where, i_{corr} and $i_{corr(c)}$ are the corrosion current density values in the absence and presence of the coating, respectively.

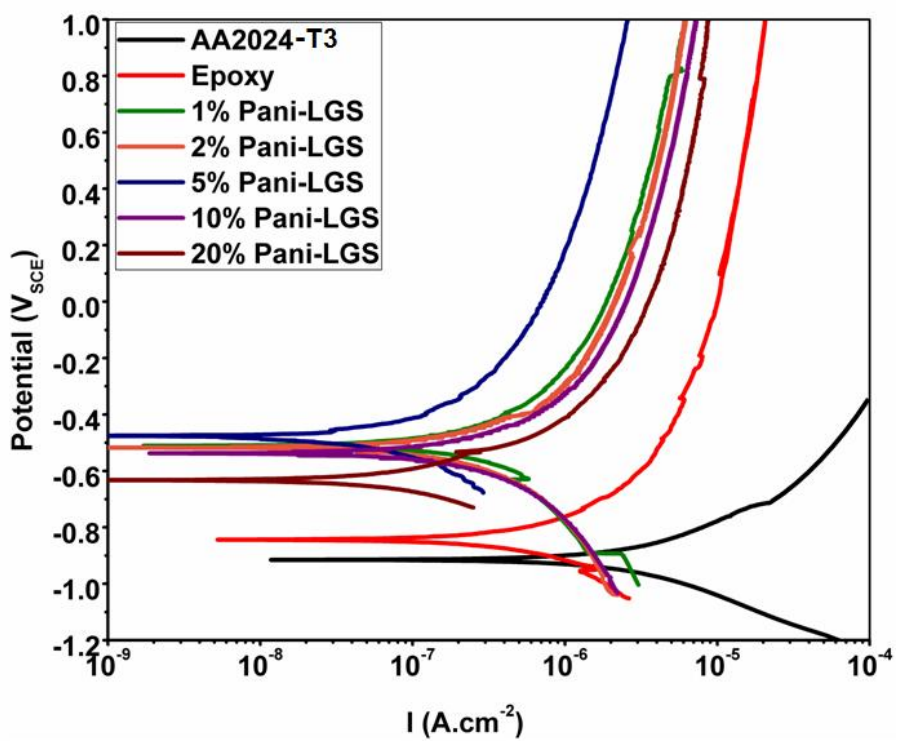

Fig. 4.18: Potentiodynamic polarisation curves of Pani-LGS/Epoxy coatings at initial immersed stage in 0.6M NaCl solution

The i_{corr} values decreased significantly on increasing the concentration of Pani-LGS into the coating and then increased after 5% Pani-LGS. The i_{corr} value of AA2024-T3 was 42.56μA cm^{-2} which decreased to 5.61μA cm^{-2} for epoxy. This shows that epoxy had potential to decreased i_{corr} by one order of magnitude. For 2% Pani-LGS i_{corr} value was 0.71μA cm^{-2} whereas for 5% Pani-LGS i_{corr} value decreased to 0.13μA cm^{-2} and then again increased to 0.85μA cm^{-2} for 10% Pani-LGS. From the results it was found that the optimized concentration of Pani-LGS is the required criteria for the protection of AA2024-T3

alloy from the corrosion. On increasing the concentration, corrosion current density decreased but after reaching 5% Pani-LGS the value again increased because of the formation of agglomerated particles of Pani-LGS in the coating due to its high concentration. As a result, there is decease in admittance of the aggressive species to the AA2024-T3 surface and therefore a decrease in i_{corr} was observed in 5% Pani-LGS.

Table 4.1: Electrochemical Parameters of AA2024-T3, epoxy and various Pani-LGS loadings coatings on AA2024-T3 alloy in 0.6M NaCl solution

Compositions	***i_{corr} ($\mu A/cm^2$)(Std. Dev.)***	***E_{corr} (m V $_{SCE}$)(Std. Dev.)***	***P_E (%)***
AA2024-T3	42.56 (0.58)	-907 (1.2)	-
Epoxy	5.61 (0.06)	-842 (1.3)	86.6
1% Pani-LGS	1.70 (0.11)	-511 (4.4)	95.9
2% Pani-LGS	0.71 (0.09)	-537 (5.2)	98.3
5% Pani-LGS	0.13 (0.02)	-475 (2.3)	99.7
10% Pani-LGS	0.85 (0.16)	-512 (1.3)	98.0
20% Pani-LGS	0.94 (0.13)	-620 (4.2)	97.8

Electrochemical impedance spectroscopy was also used to evaluate the corrosion activity of epoxy coating and different loading of Pani-LGS coatings. Fig. 4.19 shows the impedance behaviour of AA2024-T3, epoxy and various Pani-LGS/epoxy loadings at initial period of immersion in 0.6M NaCl. In the initial immersion, the value of $|Z|_{0.01\ Hz}$ of bare AA2024-T3 alloy was found to be 0.02 MΩ cm^2. The epoxy coated sample has $|Z|_{0.01\ Hz}$ of 0.9 MΩ cm^2, which is one order of magnitude higher than that of bare substrate. For Pani-LGS coating, the value was increased to 300 MΩ cm^2 at 5% loading which were four orders of magnitude higher than that of bare and three magnitudes higher than that of epoxy coating. At various Pani-LGS loading the values comes different. As we increase the concentration of Pani-LGS the impedance value increases but after an optimum concentration these particles agglomerate into the coating matrix resulting in decrease in the impedance. Fig. 4.20 shows the impedance of epoxy and various Pani-LGS/Epoxy loadings after 30 days immersion in 0.6M NaCl. The value of $|Z|_{0.01\ Hz}$ of epoxy coating was 0.01 MΩ cm^2 which was close to AA2024-T3. This shows that after 30 days immersion the epoxy coating lose its potential to protect the substrate in the 0.6M NaCl and diffusion of electrolyte through coating has taken place. For 5% Pani-LGS coating, the value of $|Z|_{0.01\ Hz}$ was decreased from 300 MΩ cm^2 to 60 MΩ cm^2 after 30

days immersion whereas for 2% Pani-LGS value changed 100 MΩ cm^2 to 6 MΩ cm^2. The EIS results indicated that the corrosion protection of optimized concentration of Pani-LGS coatings were more protective than that of epoxy coating.

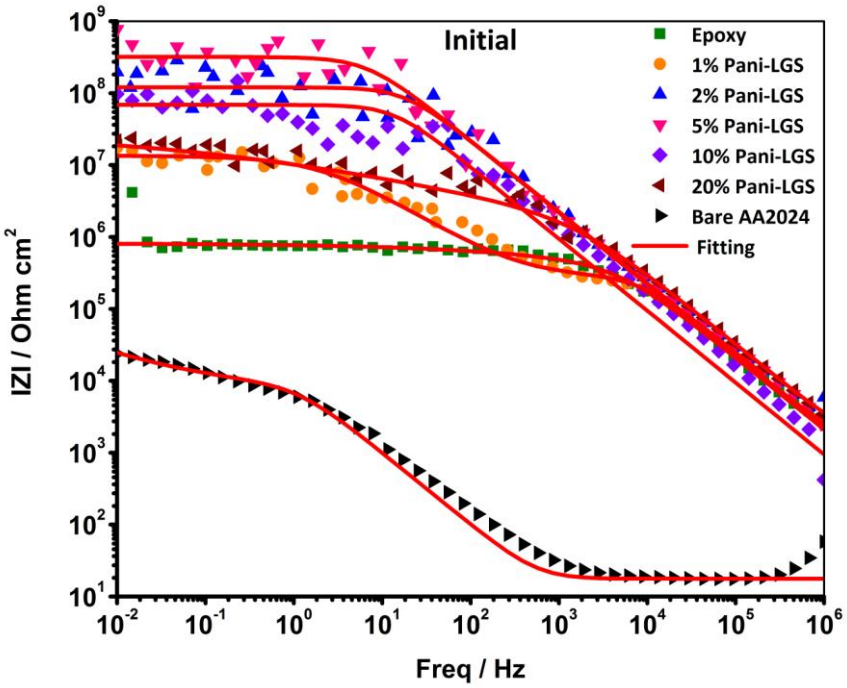

Fig. 4.19: Impedance behaviour of bare AA2024-T3, epoxy and various Pani-LGS/epoxy coated loadings at initial period of immersion

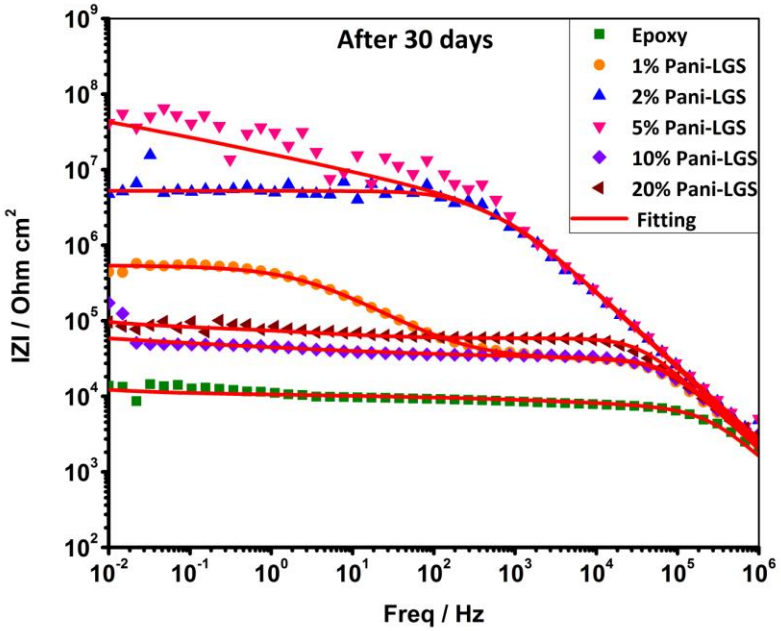

Fig. 4.20: Impedance behaviour of bare AA2024-T3, epoxy and various Pani-LGS/epoxy coated loadings after 30 days of immersion

To understand the corrosion behaviour of the coatings, the EIS data were fitted to electrical equivalent circuit as shown in Fig. 4.21. The circuits contain two RC circuits representing the coating/electrolyte and coating/metal interfaces, respectively. Where R_s is the solution resistance, which was the resistance between the working electrode and the reference electrode, C_c and R_c represent the coating capacitance and coating pore resistance, respectively. Q_{dl} is the constant phase element representing the double layer capacitance and R_t represents the charge transfer resistance. The equivalent circuit, Fig 4.21(b), contains a Warburg element for semifinite diffusion i.e. diffusion in the coating layer.

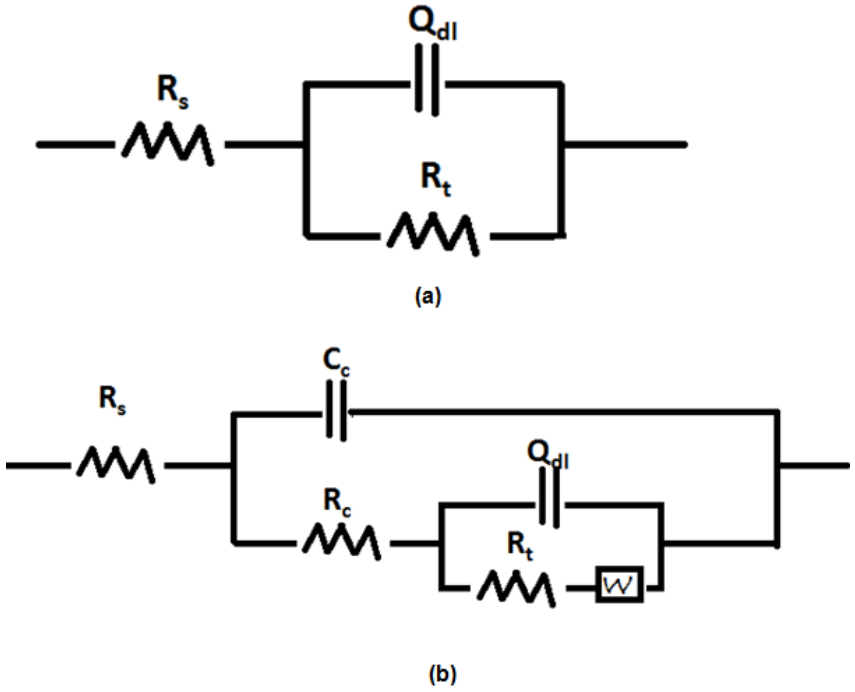

Fig. 4.21: Equivalent electrical circuit for (a) bare AA2024-T3 (b) Epoxy and Pani-LGS coating

Fig. 4.22 shows the coating capacitance, C_c of the epoxy, 2, 5 and 10% Pani-LGS coatings with respect to immersion time in 0.6M NaCl. The coating capacitance of epoxy remains almost constant up to 144 h. The value of coating capacitance increased from 53 $nFcm^{-2}$ to 870 $nFcm^{-2}$ during 168 h of immersion due to diffusion of water into the coating. After that it reached to saturation level for some time and then reached to value of 8300 $nFcm^{-2}$ after 300 h of immersion. However, there is no increment in coating capacitance of 5% Pani-LGS where as 2% and 10% Pani-LGS shows increase in value after 264 h of immersion. At the beginning of the immersion, the value of coating capacitance for 2% Pani-LGS was found to be 7.6 $nFcm^{-2}$ and after immersion to 300 h, it increased to 10 $nFcm^{-2}$. But for 10% Pani-LGS value

changed from 9.1 nFcm^{-2} to 81 nFcm^{-2}. The value of coating capacitance of 5% Pani-LGS coating was 0.3 nFcm^{-2} at the initial period of immersion and 1.2 nFcm^{-2}at 300 h of immersion. The increment of the coating capacitance of epoxy coating was two orders of magnitude higher than that of 5% Pani-LGS eve after 300 h immersion, which implies that 5% Pani-LGS coating adsorbed less water than epoxy coating. This polyaniline may interact with the substrate forming a passive layer that prevents corrosion of the substrate.

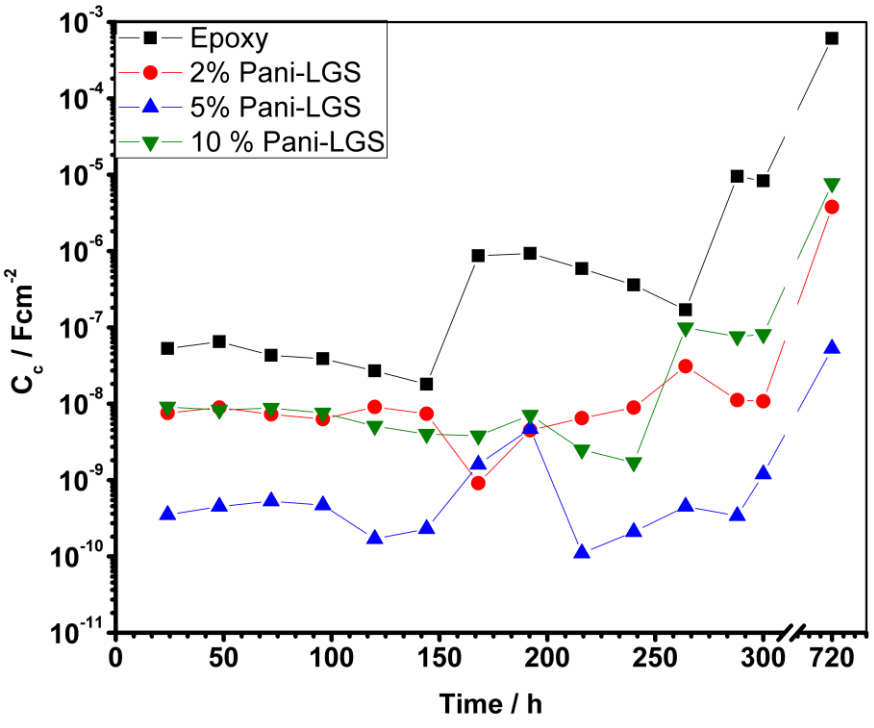

Fig. 4.22: Coating capacitance of the epoxy, 2, 5 and 10% Pani-LGS coatings with respect to immersion time in 0.6M NaCl solution

Fig. 4.23 shows the coating resistance, R_c of the epoxy, 2, 5 and 10% Pani-LGS coatings with respect to immersion time in 0.6M NaCl. R_c is related to electrical resistance to ionic transfer through the coating pores, which reflects the permeability of coating to the electrolyte solution. The value of coating resistance of the epoxy coating rapidly decreased from 8.3 MΩ cm^2 to 0.3 MΩ cm^2 after 96 h of immersion. After 96 h immersion, the coating resistance stabilized at 0.2 MΩ cm^2 due to formation of aluminium oxides product which possibly block the pores and finally value decreased to 0.01 MΩ cm^2. The value of 2% Pani-LGS coating was 120 MΩ cm^2 in the initial immersion period, which was of two orders of magnitude higher than that of epoxy coating. The value increased to 67 MΩ cm^2 after 192 h of immersion and finally to 9 MΩ cm^2 which was same as that of epoxy coating. The coating

resistance value for 10% Pani-LGS changes from 910 MΩ cm^2 to 1.8 MΩ cm^2 after 300 h immersion. However, Rc obtained for 5% Pani-LGS coating is relatively higher than those of the epoxy and other concentration of Pani-LGS coatings. The initial immersion value of Rc for the 5 % Pani-LGS coating was 9100 MΩ cm^2 which further maintained upto 72 h of immersion and then decreased to 120 MΩ cm^2 after 288 h of immersion.

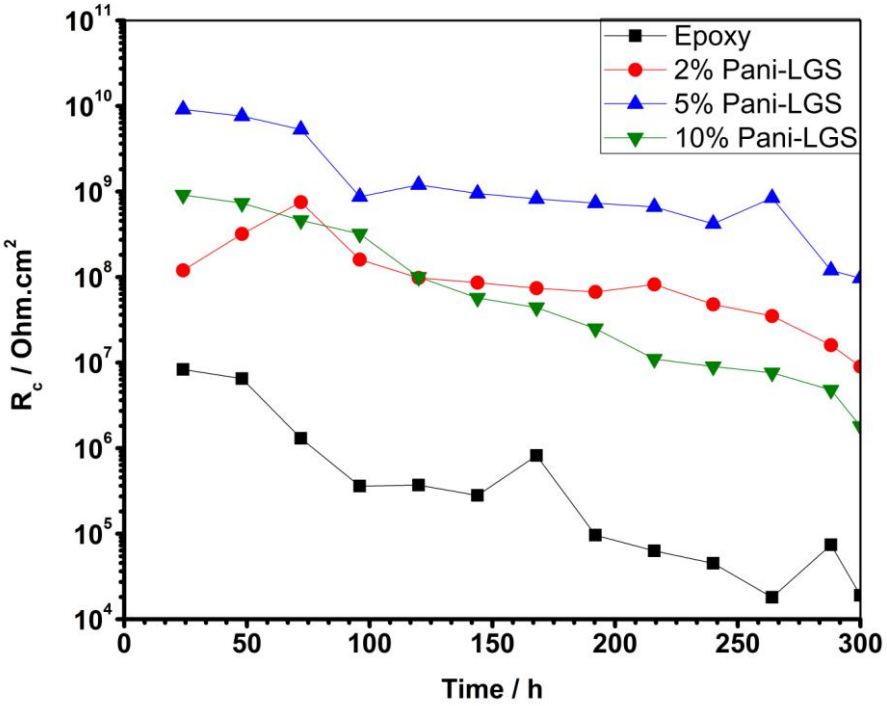

Fig. 4.23: Coating resistance of the epoxy, 2, 5 and 10% Pani-LGS coatings with respect to immersion time in 0.6M NaCl solution

Fig.4.24 shows the charge transfer resistance, R_t of the epoxy, 2, 5 and 10% Pani-LGS coatings with respect to immersion time in 0.6M NaCl. The value of charge transfer resistance, R_t is a measure of the resistance to the electron transfer across the metal surface and is inversely proportional to corrosion rate [35]. The value of R_t for the epoxy coating decreased slowly from 0.9 MΩ cm^2 to 0.7 MΩ cm^2 after 168 h of immersion and reached to final value 0.1 MΩ cm^2 after 300 h of immersion. For the 2 % Pani-LGS coatings the value of R_t gradually decreased from 520 MΩ cm^2 to 84 MΩ cm^2 after 300 h of immersion. Similar observation was observed in 10 % Pani-LGS coating, the value changed from 97 MΩ cm^2 to 16 MΩ cm^2. The value for 5% Pani-LGS coating was 1200 MΩ cm^2 at the initial immersion period, then 980 MΩ cm^2 after 96 h and then stabilized up to 168 h and then decreased again. At last the value reached to 590 MΩ cm^2 after 300 h of immersion, which was of about four

orders of magnitude higher than that of epoxy coatings and one order of magnitude higher than that of 2 % and 10% Pani-LGS coating. The higher value indicates that the corrosion process become difficult in the case of 5 % Pani-LGS coating than that under epoxy coating.

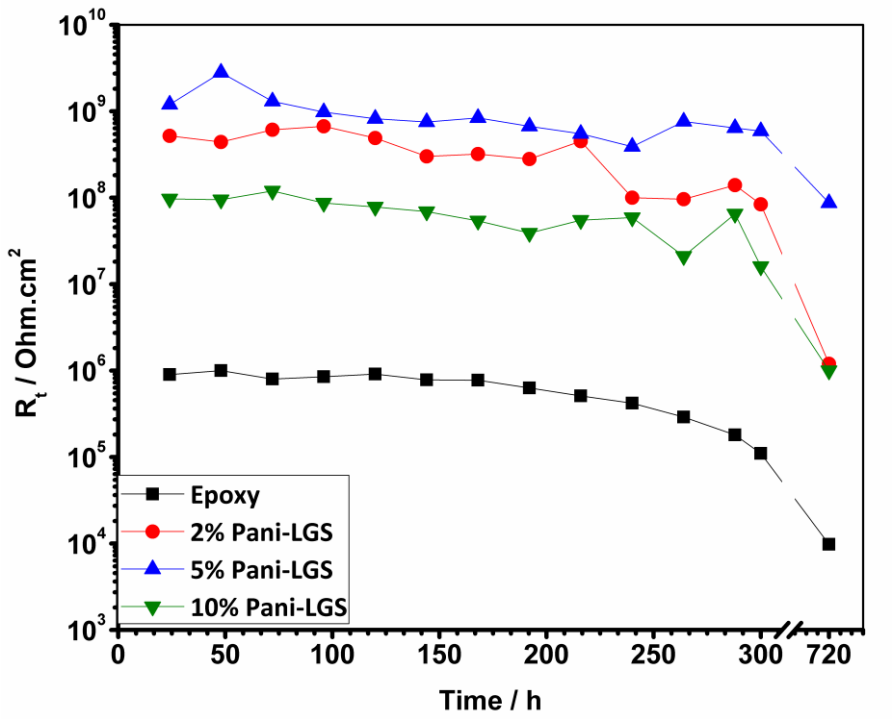

Fig. 4.24: Charge transfer resistance of the epoxy, 2, 5 and 10% Pani-LGS coatings with respect to immersion time in 0.6M NaCl solution

4.3.6 Adhesion Test of Pani-LGS/Epoxy coating

Satisfactory adhesion is a requirement for the coatings to impart corrosion protection. The results of adhesion measurements by the crosshatch method are shown in Table 4.2. It is observed that the adhesion strength of 2 and 5% Pani-LGS was 5B, which is 'Excellent', prior to exposure to 0.6M NaCl. Adhesion strength of 10 and 20% Pani-LGS showed relatively lower values. High content of polyaniline particles results in comparative poor adhesion between the coating and the substrate. This was because of the high volume fractions of Pani-LGS were likely to shatter **t**he compactness of the coating and lead to agglomeration of particles. This could finally result in decrease the polar force in coating matrix, leads to low adhesion value. The adhesion strength of epoxy coating decreased from 5B to 3B, which was due to generation of corrosion pits formed beneath the polyaniline coating. However, there was no effect on the adhesion strength of 2 and 5% Pani-LGS even after 30 days immersion.

Table 4.2: Adhesion test of Epoxy and various loading of Pani-LGS/Epoxy Coatings

Coating System	Adhesion strength (ASTM D3359)	
	Before exposure	After exposure (30 days) (0.6M NaCl)
Epoxy	5B	3B
1% Pani-LGS	5B	4B
2% Pani-LGS	5B	5B
5% Pani-LGS	5B	5B
10% Pani-LGS	4B	3B
20% Pani-LGS	3B	2B

4.3.7 Salt Spray Test of Pani-LGS/Epoxy coating

The coated samples were tested in the salt-fog spray chamber for 720 h as per ASTM B 117 as shown in Fig. 4.25.

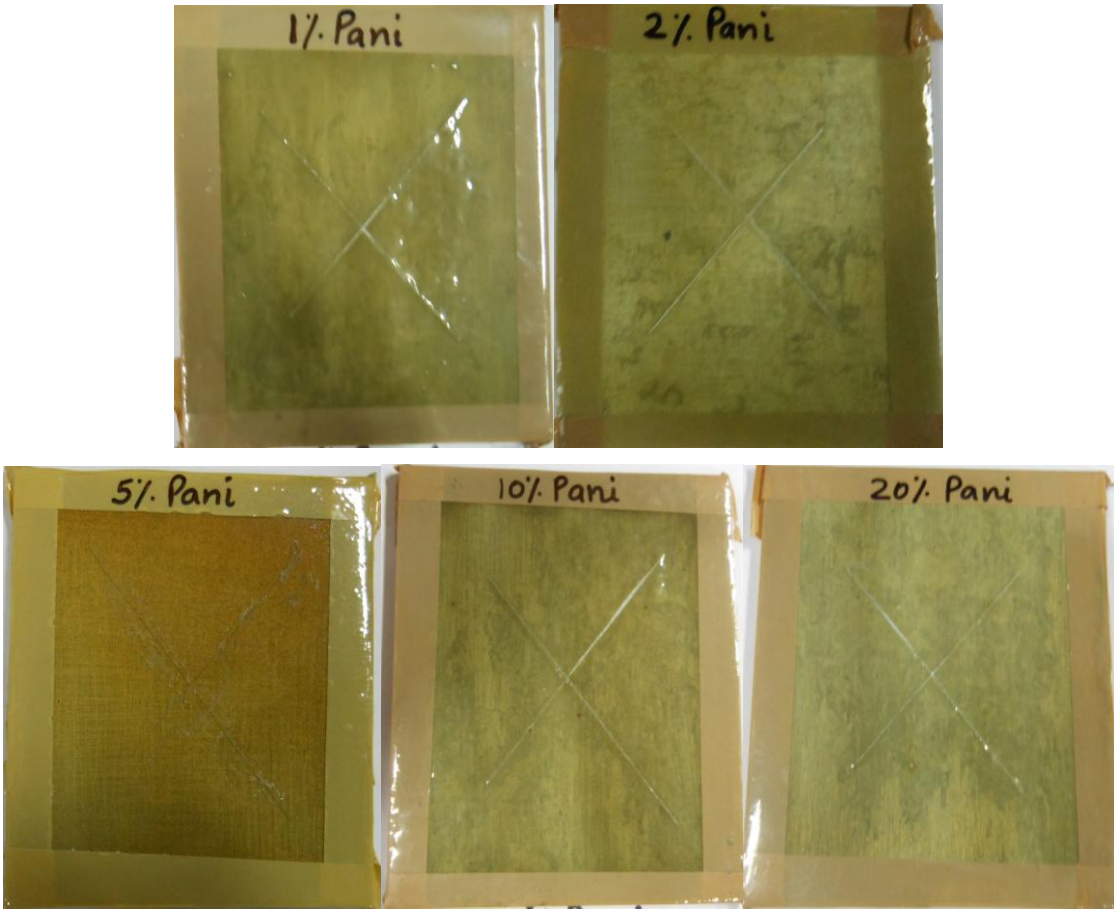

Fig. 4.25: Photographs of Pani-LGS/Epoxy coatings after 720 h to salt spray exposure

2% and 5%Pani/Epoxy coating can withstand upto 720 h of salt spray environment and after that it starts degrading, where as epoxy coated sample start degrading after 300 h. 1% Pani/Epoxy coating was stable upto 450 h but after that it starts degrading very rapidly, indicating that the lower concentration of Pani in epoxy does not give conductive pathway in the insulating coating thereby resulting in poor corrosion resistance. However, 10 and 20 wt% Pani/Epoxy coatings pass 500 h of salt spray. This indicates that good corrosion protection was achieved at 5% optimised concentration of Pani/Epoxy.

4.3.8 UV-Weatherometer of Pani-LGS/Epoxy Coatings (Color change and Gloss retention of coatings)

The UVB-weatherometer shows the damaging effects of sunlight that occur in the short-wavelength range of 313 nm. The epoxy and other formulated coatings, exposed in UVB-weatherometer were studied for change in color (dE) and gloss measurement. dE is a numerical value for color change between the exposed and unexposed samples. The evaluation of dE is based on the CIELAB Color Space Model (Fig. 4.26) and is a highly influential system for measuring color and distinguishing between colors. The CIELAB color space is organized in a cube form.

The L* axis runs from top to bottom with a maximum value of 100, representing a perfect reflecting diffuser and a minimum value of 0, representing black. The a* and b* axes have no specific numerical limits. Positive a* is red, negative a* is green, positive b* is yellow and negative b* is blue. ΔL*, Δa* and Δb* indicate the difference in L*, a*, b* between the exposed and unexposed sample and dE is calculated taking into account these differences and is formulated as [10]:

$$\mathbf{dE^* = [\Delta L^{*2} + \Delta a^{*2} + \Delta b^{*2}]^{1/2}}$$

The color change measurements (dE) and gloss retention was measured using a BYK Spectrophotometer (Fig. 4.27) based on CIE Color Space units.

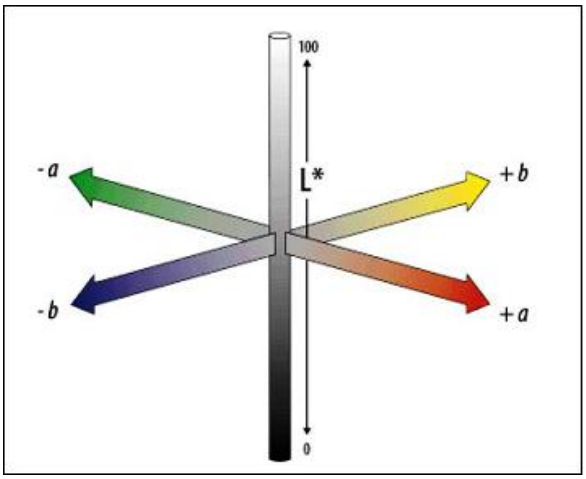

Fig. 4.26: CIELAB color space [27]

Fig. 4.27: Spectrophotometer

Coating systems were subjected to UVB for 720 h. Fig. 4.28 shows the comparative results of change in color of epoxy and Pani-LGS/epoxy formulated systems. The color change decreased by five units on incorporating Pani-LGS particles. 2- 5% Pani-LGS coating system exhibited lowest color change on 360 h UVB exposure. However, colour change decreased by ten units on 720 h UVB exposure. The color change for epoxy coatings was lowered by the incorporation of Pani-LGS particles, suggesting the synthesized Pani-LGS particles possess effective weathering resistant properties. Fig. 4.29 shows the percentage mean gloss retention of epoxy and Pani-LGS/epoxy formulated systems. The % gloss retention increased on addition of Pani-LGS particles. 1-2% Pani-LGS coating system exhibited highest percentage gloss retention on 360 h UVB exposure. However, on increasing the Pani-LGS concentration the value decreases. The percent gloss retention also decreased on further 720 h UVB exposures. Thus optimized concentration of Pani-LGS particles works as an effective UV-blocker and gloss retention in epoxy system.

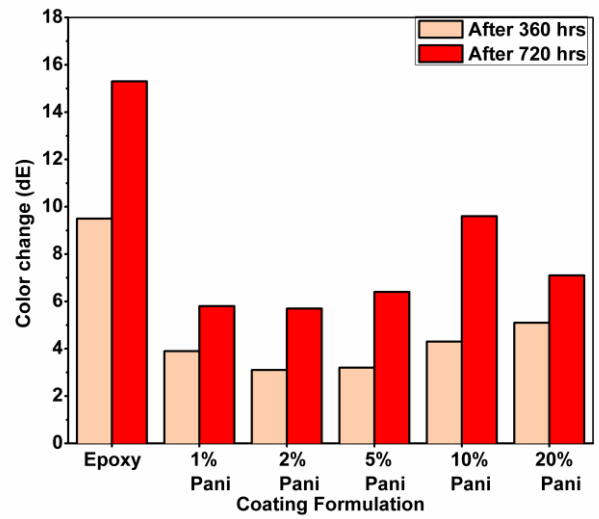

Fig. 4.28: Color change (dE) for various loading of Pani-LGS/Epoxy coatings

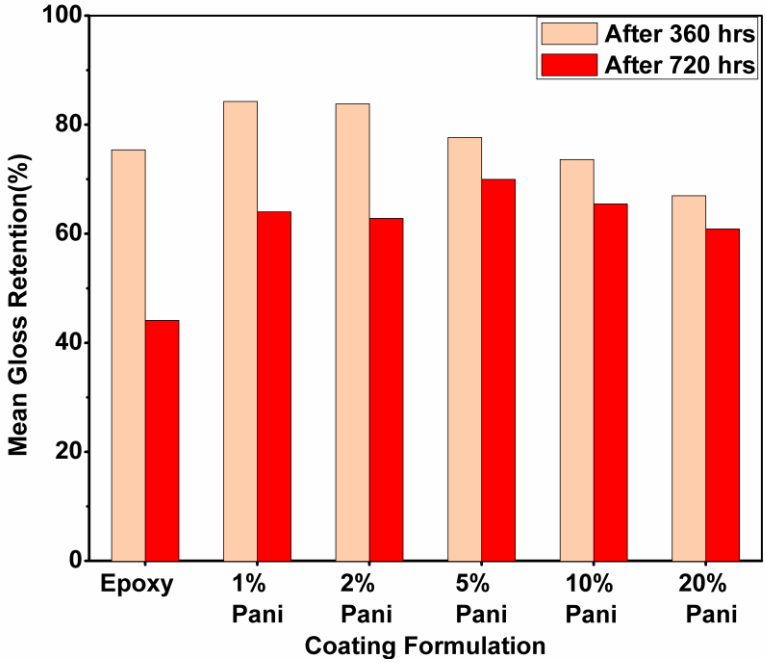

Fig. 4.29: Mean gloss retention (%) for various loading of Pani-LGS/Epoxy coatings

4.3.9 Mechanical Properties of the Pani-LGS/Epoxy Coating

Fig. 4.30 and 4.31 represents the tensile strength and elongation at break against Pani-LGS content in the epoxy films. The epoxy film has high tensile strength (7.2 MPa) and elongation at break (1357%). It was observed that the increase in Pani-LGS concentration resulted in a progressively decrease in tensile strength and elongation at break. The decrease in tensile and elongation properties mainly attributed to:

(1) Pani-LGS is acting as non-reinforcing filler for epoxy matrix mainly because of the brittle nature of polyaniline and also there is significant difference in polarity and crystallinity of two polymers

(2) The presence of Pani-LGS causes some disturbance in the crosslinking formation of epoxy resin.

The hardness values of epoxy and various Pani-LGS/Epoxy films are shown in Table 4.3. Epoxy is a very soft matrix so the hardness of the coating was very low whereas the hardness value increases with increase in Pani content.

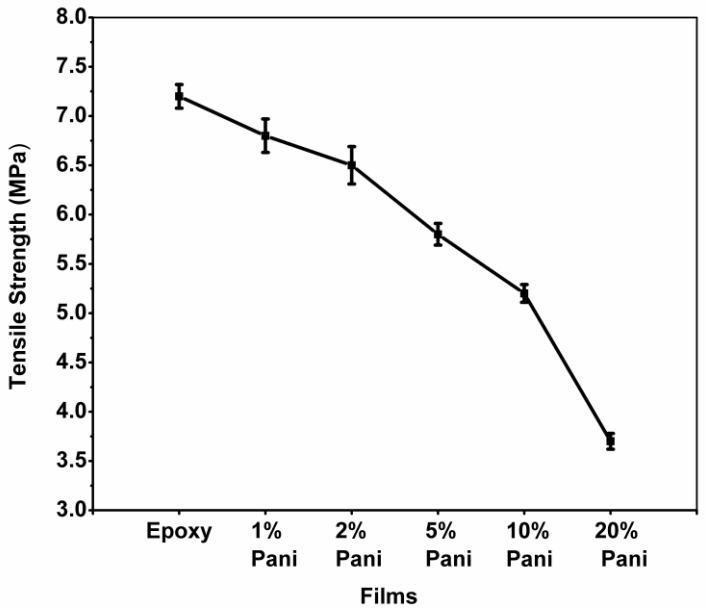

Fig. 4.30: Tensile Strength of Pani-LGS/Epoxy loading films

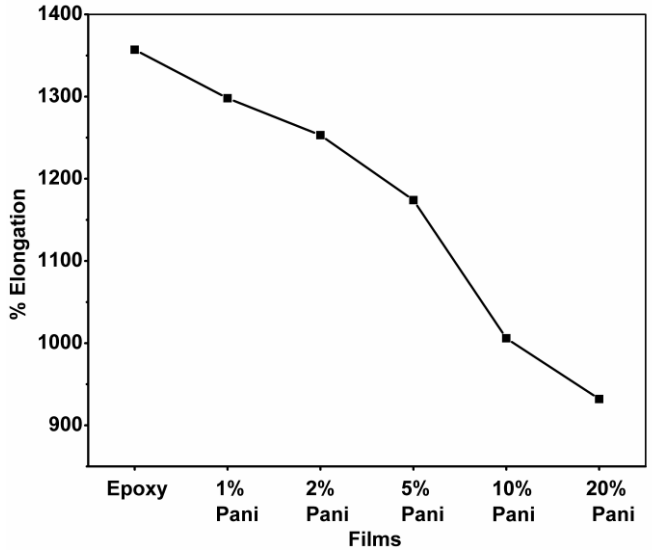

Fig. 4.31: % Elongation of Pani-LGS/Epoxy loading films

Table 4.3: Hardness values of various Pani-LGS/Epoxy loading films

Coating System	Hardness Values
Epoxy	3B
1% Pani-LGS	2B
2% Pani-LGS	B
5% Pani-LGS	2H
10% Pani-LGS	2H
20% Pani-LGS	3H

4.4 Characterisation of Pani-PAmAc/Epoxy Coating

4.4.1 Scanning Electron Microscopy (SEM) of Pani-PAmAc/Epoxy coating

The SEM micrographs of Pani-PAmAc/Epoxy coatings are shown in Fig. 4.32. Pani0.5PAmAc and Pani1PAmAc coatings exhibited smooth and homogeneous morphology. However, non homogeneity morphology of coating was observed in Pani1.5PAmAc and Pani2PAmAc due to excess of polyelectrolyte. From the above results it may be concluded that at low concentration, PAmAc polymer was effectively mixed with the polyaniline whereas higher concentration leads to poor dispersion and agglomeration of the particles in the coating.

Fig. 4.33 (a-d) shows the SEM of different molar ratios of Pani-PAmAc/Epoxy coatings after 1200 h salt spray exposure. Fig. 4.33a shows that even after 1200 h of salt spray exposure Pani 0.5PAmAc exhibited smooth and homogenous morphology. Fig. 4.33b shows very less sign of corrosion with very small pits formation. Pani 1.5PAmAc/Epoxy and Pani2PAmAc/Epoxy coating exhibited localised pits formation as shown in Fig. 4.33c and d. It may be concluded that at higher concentration of PAmAc within the coatings allow the ingress of electrolyte and leads to more pit formation.

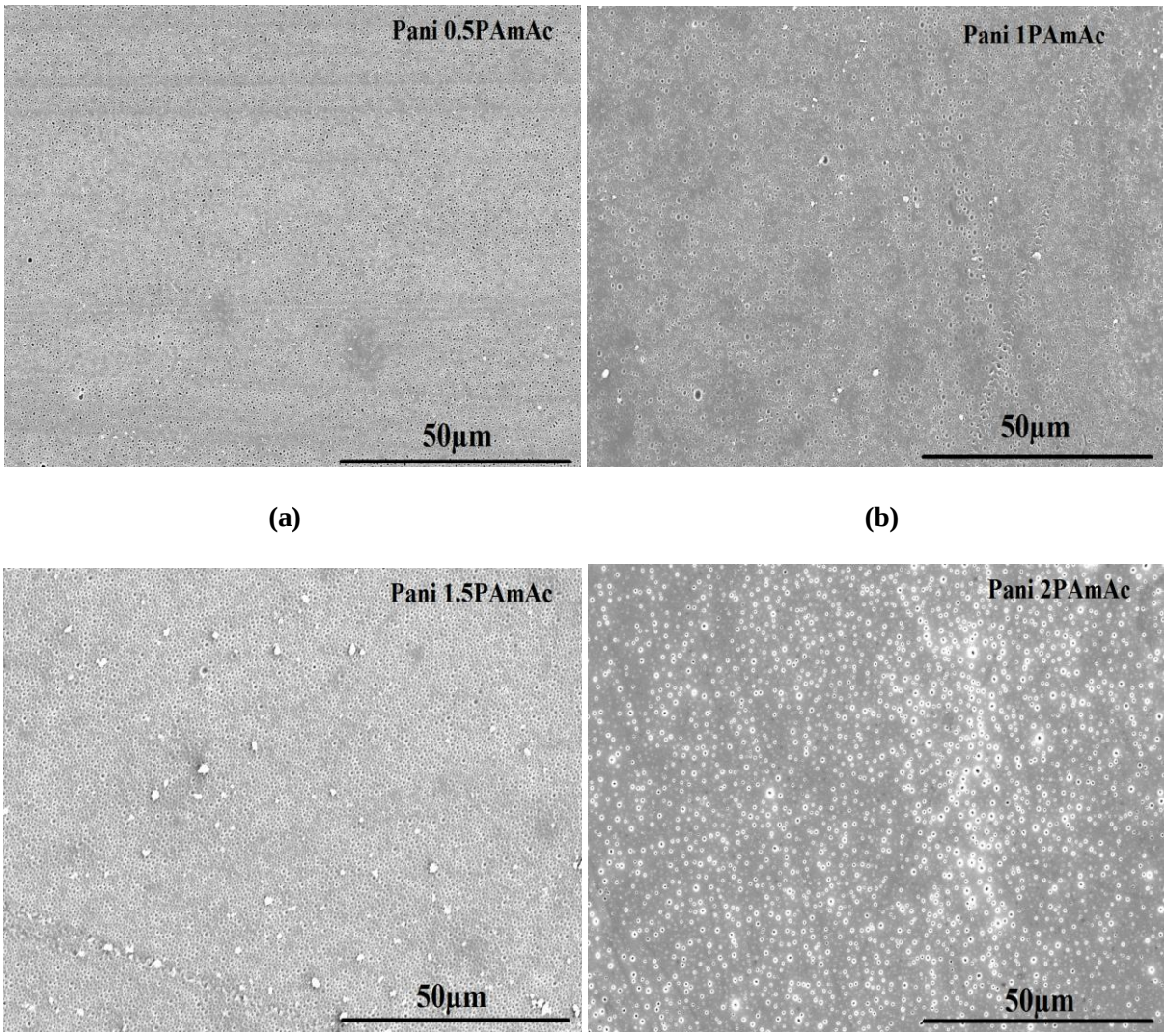

Fig. 4.32: Scanning Electron micrographs of (a) Pani 0.5PAmAc/Epoxy, (b) Pani 1PAmAc/Epoxy, (c) Pani 1.5PAmAc/Epoxy, (d) Pani 2PAmAc/Epoxy Coatings (SE at 1000x magnification)

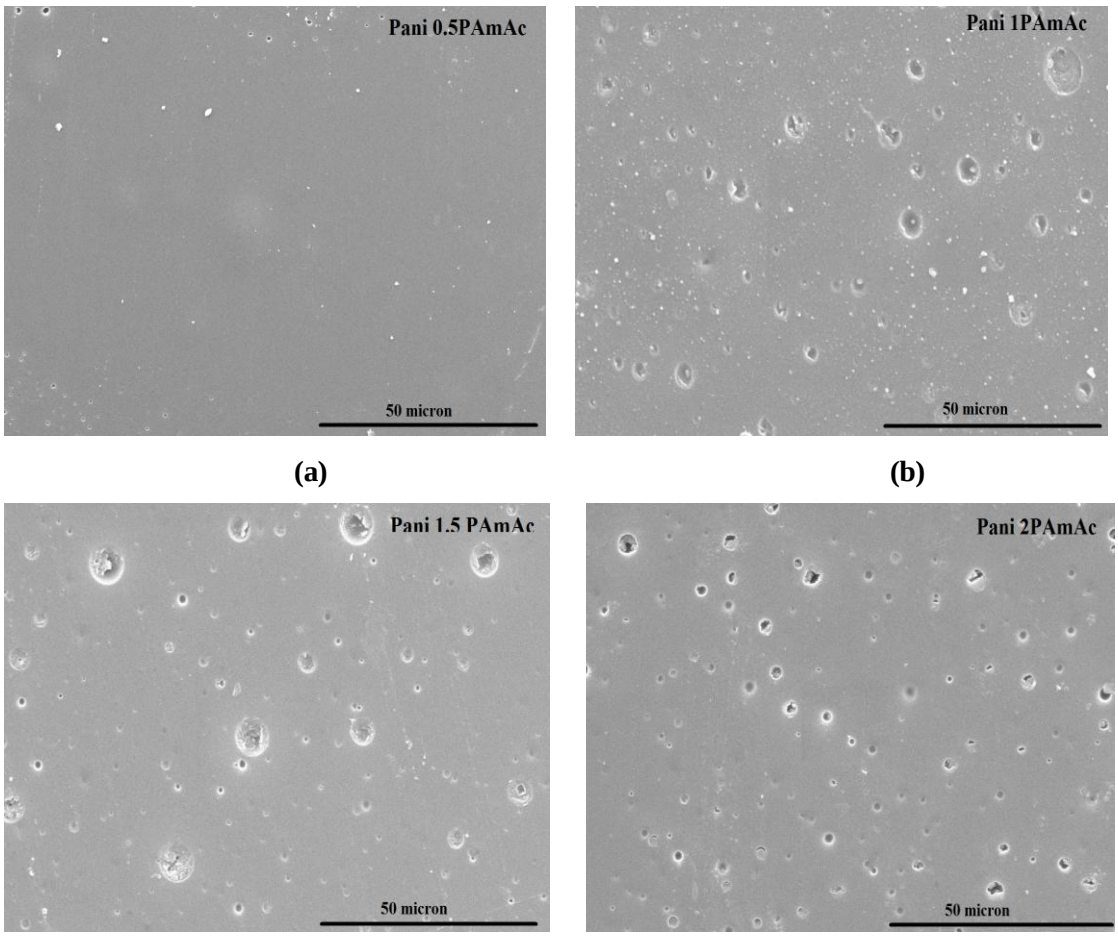

Fig. 4.33: Scanning Electron micrographs of (a) Pani 0.5PAmAc/Epoxy, (b) Pani 1PAmAc/Epoxy, (c) Pani 1.5PAmAc/Epoxy, (d) Pani 2PAmAc/Epoxy Coatings after 1200 h salt spray exposure (SE at 1000x magnification)

4.4.2 Atomic Force Microscopy of Pani-PAmAc/Epoxy coating

AFM was performed to understand the particle distribution and surface roughness of the coatings at the micro and nano level. Fig. 4.34 (a-d) shows the AFM images at different molar ratios of Pani-PAmAc/Epoxy coatings. All coatings are crack free and low roughness values. At low concentration of PAmAc, the coating was comparative smooth and homogeneous as compared to high concentration. At high concentration the agglomeration was clearly visible in the AFM images and leads to increase in roughness values.

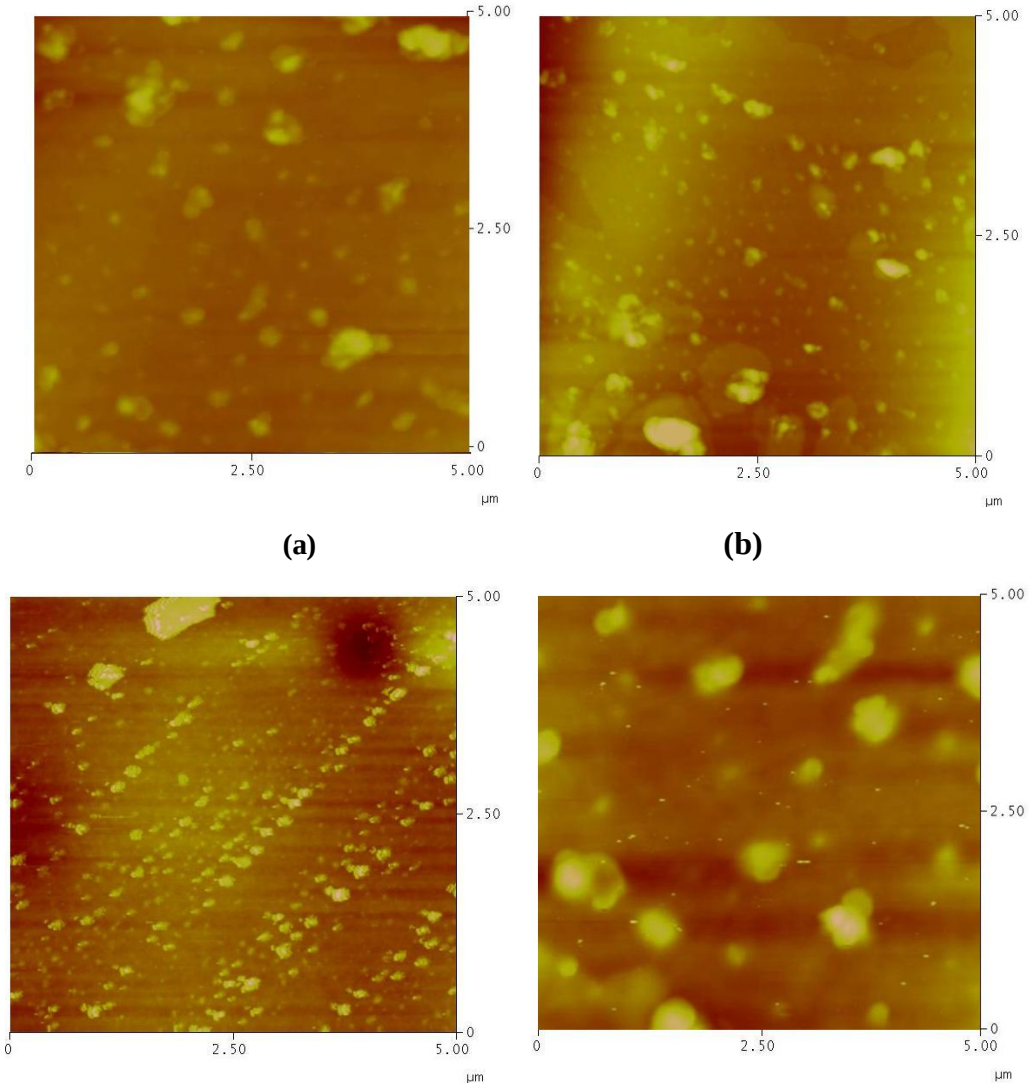

Fig. 4.34: AFM images of (a) Pani 0.5PAmAc/Epoxy, (b) Pani 1PAmAc/Epoxy, (c) Pani 1.5PAmAc/Epoxy, (d) Pani 2PAmAc/Epoxy Coatings (5 microns)

The root-mean square (RMS) values of surface roughness determined by AFM were 4.33±0.3, 4.76±0.6, 5.35±0.9 and 5.94±0.5 nm for Pani0.5PAmAc/Epoxy, Pani1PAmAc/Epoxy, Pani1.5PAmAc/Epoxy and Pani2PAmAc/Epoxy coatings, respectively.

Fig. 4.35 (a-d) shows the AFM images at different molar ratios of Pani-PAmAc/Epoxy coatings after 1200 h salt spray exposure. The root-mean square (RMS) values of surface roughness determined by AFM were 13.17±0.8, 19.83±0.9, 23.19±1.2 and 27.16±1.5nm for Pani0.5PAmAc/Epoxy, Pani1PAmAc/Epoxy, Pani1.5PAmAc/Epoxy and Pani2PAmAc/Epoxy coatings, respectively.

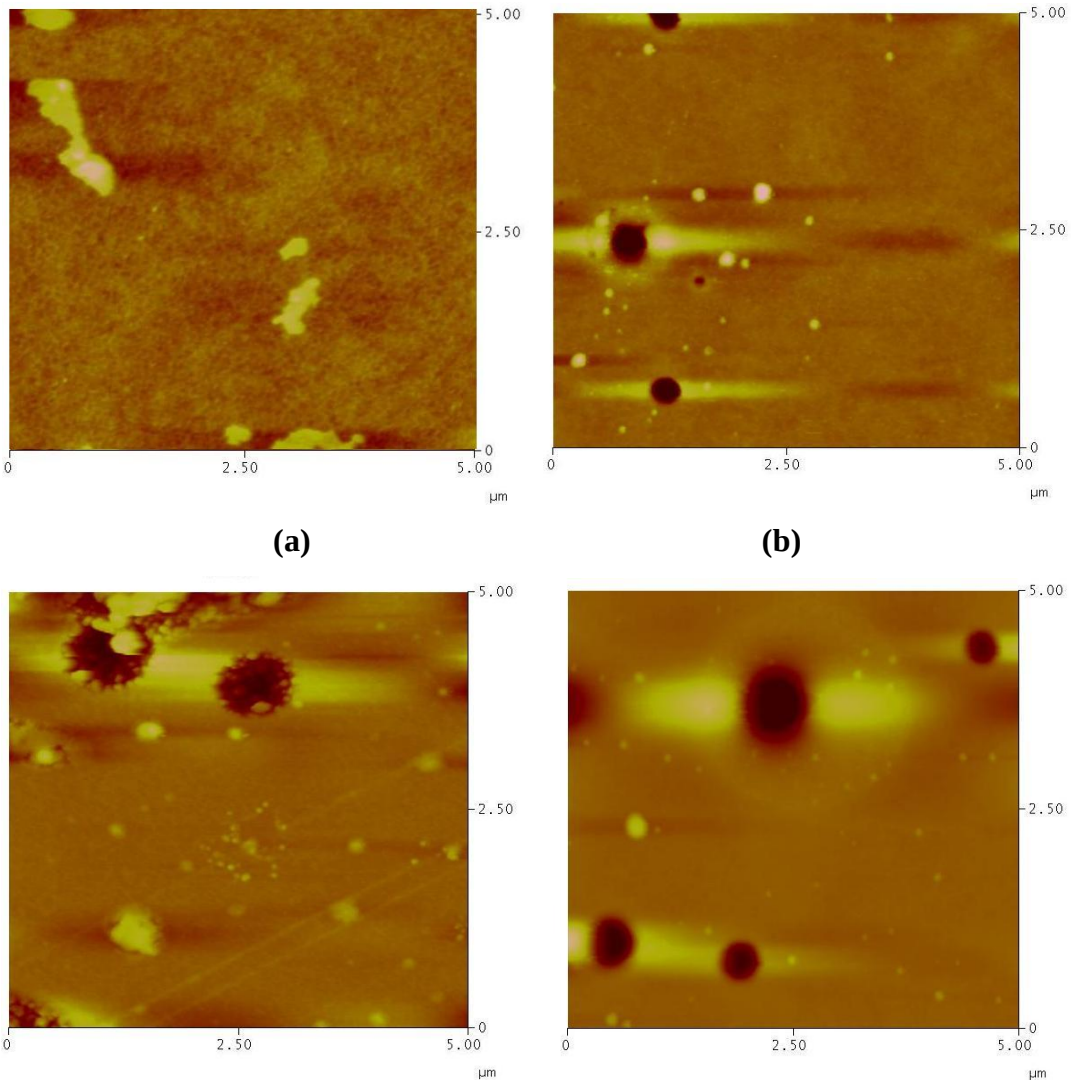

Fig. 4.35: AFM images of (a) Pani 0.5PAmAc/Epoxy, (b) Pani 1PAmAc/Epoxy, (c) Pani 1.5PAmAc/Epoxy, (d) Pani 2PAmAc/Epoxy coatings after 1200 h salt spray exposure (5 microns)

The roughness values of the coatings were increased due to corrosion product or pits formation on the surface. Pits were clearly visible in the AFM images with dark spots. The value of the roughness increases on increasing the concentration of PAmAc which concluded the more corrosion product formation at higher concentration.

4.4.3 TG Analysis of Pani-PAmAc/Epoxy coating

Fig. 4.36 shows the TGA curves at different molar ratios of Pani-PAmAc/Epoxy coatings. TGA curves of Pani-PAmAc/Epoxy samples exhibit similar behavior with three major steps

of mass losses. The TGA thermograms indicate that as the Pani-PAmAc is incorporated in epoxy, a weight loss at around 190ºC is observed which increases minutely, as the concentration of PAmAc increases. The rate of mass loss is least over the initial temperature range i.e. upto 240ºC. The weight loss occurring in the range of 300–410ºC temperature may be due to the structural decomposition of PAmAc where the coatings leave a residue of about 17% at 560ºC. The pure epoxy polymeric film decomposition process starts at 180ºC with three subsequent decomposition decays being observed at 180, 220 and 380ºC and for Pani at 150ºC, 320ºC and 480ºC respectively. This result confirms that the synthesized Pani-PAmAc has good thermal stability, better than that of Pani/Epoxy and Epoxy.

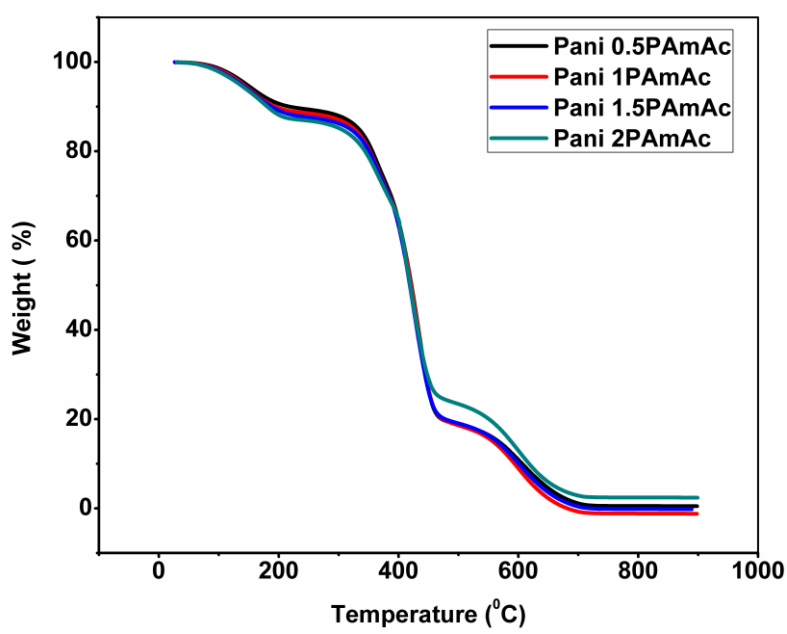

Fig. 4.36: TGA curves of Pani 0.5PAmAc/Epoxy, Pani 1PAmAc/Epoxy, Pani 1.5PAmAc/Epoxy and Pani 2PAmAc/Epoxy coatings

The weight loss in second, third and fourth degradation steps do not follow any systematic trend because of the complex chemical structure of Pani–PAmAc copolymers and their pyrolyzed intermediate products. All Pani-PAmAc/Epoxy formulation shows almost similar trend in thermal degradation but it shows enhancement in thermal properties than that of Pani-LGS/Epoxy formulation due to formation of double stranded conducting polymer which give stiffness to the backbone [50, 80].

4.4.4 Electrical Conductivity of Pani-PAmAc/Epoxy Coating

The room temperature electrical conductivity of Pani0.5PAmAc/Epoxy, Pani1PAmAc/Epoxy, Pani1.5PAmAc/Epoxy and Pani2PAmAc/Epoxy coatings were 3.97, 2.98, 2.68 and 1.87 S/cm, respectively as shown in Fig. 4.37. Once PAmAc polymer was introduced, the conductivity of the coating decreased due to insulating PAmAc matrix. By varying amount of PAmAc from 0.5 to 2, the electrical conductivity at room temperature decreased from 3.97 to 1.87 S/cm. It is known that the Pani particles act as a bridge to facilitate electron transport and the electrical conductivity is strongly depend on the ability to form interconnected conducting network. The electrical conductivity in Pani-PAmAc/Epoxy coating could be maintained due to Pani particles, were coated by the insulating PAmAc layer. Therefore, the electrical conductivity of the Pani-PAmAc/Epoxy coating was lower as compared to Pani-LGS/Epoxy coating.

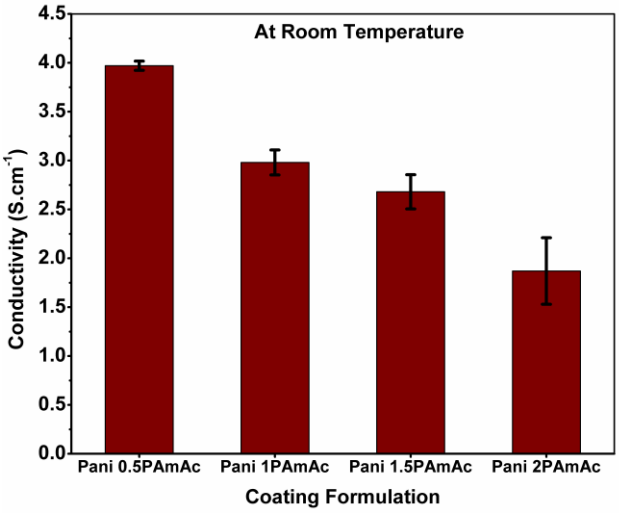

Fig. 4.37: Room temperature conductivity of Pani0.5PAmAc/Epoxy, Pani1PAmAc/Epoxy, Pani1.5PAmAc/Epoxy and Pani2PAmAc/Epoxy coatings

Fig. 4.38 shows the temperature dependence on electrical conductivity at different molar ratios of Pani-PAmAc in coatings. The temperature dependent conductivity was measured at 223 K to 423K. It was noted that the electrical conductivity of the coating increases with the increase in temperature. The conductivity value decreases on increasing the PAmAc concentration. This was due to less number of conducting particles are available for the electrical conductivity. Electrical properties depend on the polymer matrix, processing

method and filler type. On increasing the temperature the movements of electron charge carriers in coating increases.

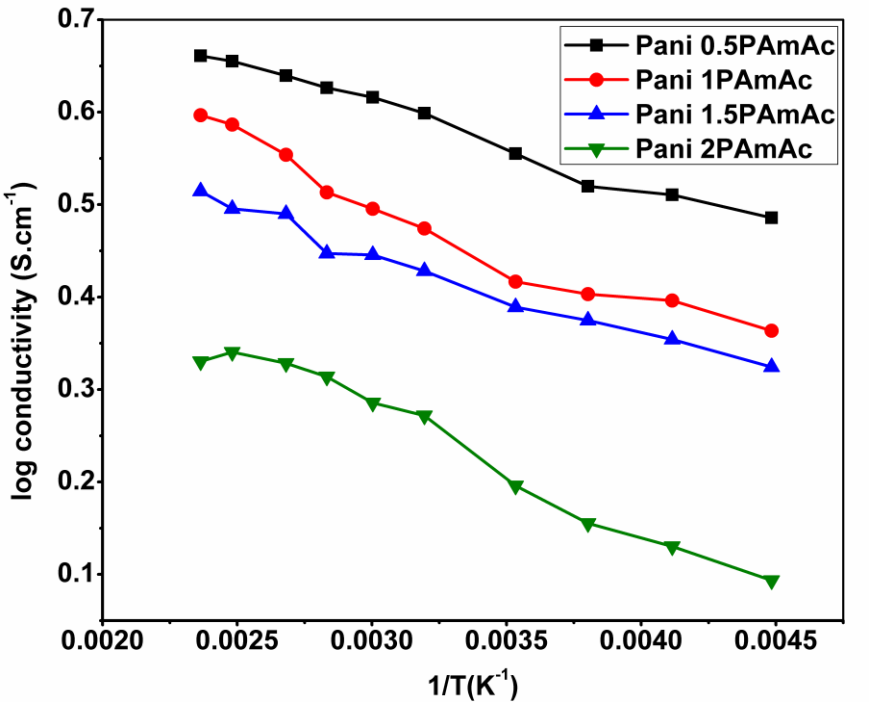

Fig. 4.38: Logarithm conductivity vs. inverse temperature of Pani0.5PAmAc/Epoxy, Pani1PAmAc/Epoxy, Pani1.5PAmAc/Epoxy and Pani2PAmAc/Epoxy coatings

4.4.5 Corrosion protection properties of Pani-PAmAc/Epoxy coating

The corrosion protection behavior of coatings was examined in 0.6M NaCl using potentiodynamic polarization and EIS studies. pH was maintained at 7 for the test solutions.

The potentiodynamic polarization curves for Pani-PAmAc/Epoxy coated AA2024-T3 in 0.6M NaCl are shown in Fig. 4.39. The corrosion potential (E_{corr}) for all the Pani-PAmAc coated AA2024-T3 panels, show noble values than that observed for the bare AA2024-T3, epoxy and Pani/Epoxy coated AA2024-T3 panels. The positive shift in Ecorr indicates the more corrosion protection of the AA2024-T3 surface by the formulated coatings (anodic protection). The electrochemical protection is caused by the increase of the corrosion potential, physical barrier effect and the formation of a protective passive layer on AA2024-T3 surface.

The values of the corrosion potential (E_{corr}), corrosion current density (i_{corr}) and protection efficiency (PE) obtained from Tafel curves of the Pani-PAmAc/Epoxy coatings are summarized in Table 4.4. From the measured corrosion current density values, the protection efficiency was obtained from the following equation [34],

$$\textbf{Protection efficiency (\%)} = (i_{corr}(uc) - i_{corr}(c)) / i_{corr}(uc) * 100$$

Where, i_{corr} and $i_{corr(c)}$ are the corrosion current density values in the absence and presence of the coating, respectively. The i_{corr} values remains constant on varying the molar ratio of PAmAc and Pani. The i_{corr} value of AA2024-T3 was 42.56 μA cm^{-2} which decreased to 0.13 μA cm^{-2} for Pani-LGS/Epoxy and 0.01 μA cm^{-2} for Pani0.5PAmAc/Epoxy. This shows that Pani0.5PAmAc/Epoxy had more corrosion protective value compared to Pani-LGS/Epoxy.

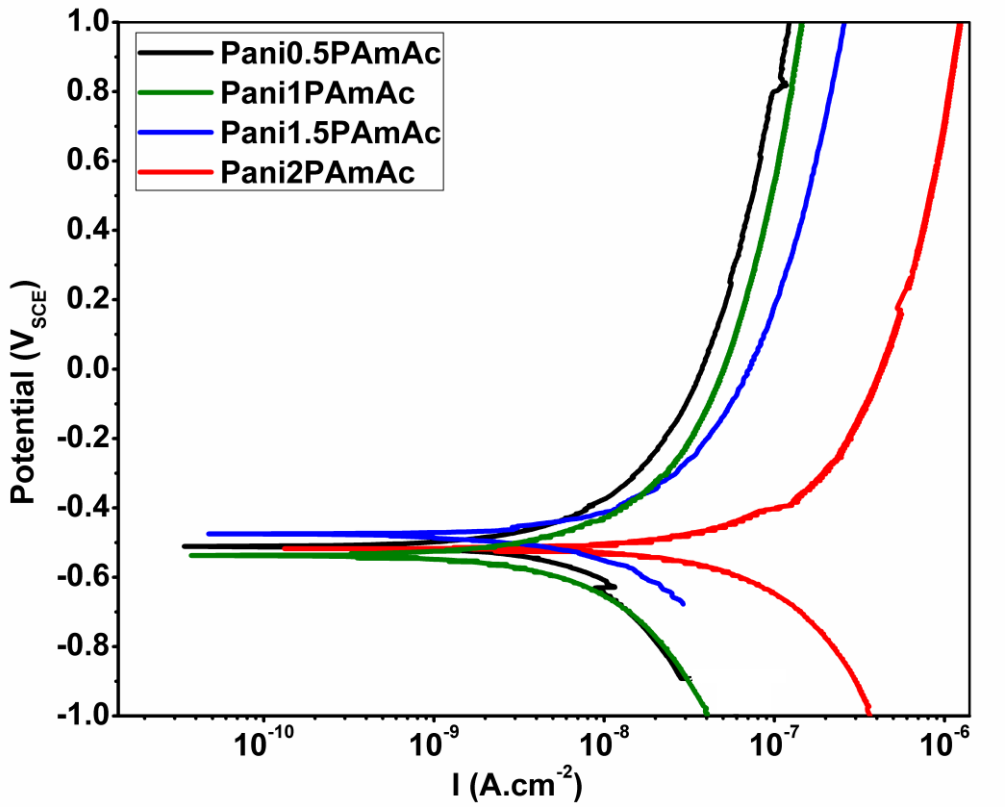

Fig. 4.39: Potentiodynamic polarisation curves of different Pani-PAmAc/Epoxy coatings at initial immersed stage in 0.6M NaCl solution

Table 4.4: Electrochemical Parameters of Pani-PAmAc /Epoxy coated AA2024-T3 alloy in 0.6M NaCl solution

Compositions	i_{corr} ($\mu A/cm^2$) (Std. Dev.)	E_{corr} (m V $_{SCE}$) (Std. Dev.)	P_E (%)
Bare AA2024-T3	42.56 (0.58)	-907 (1.2)	-
Epoxy	5.61 (0.06)	-842 (1.3)	86.6
0.5Pani-LGS/Epoxy	0.13 (0.02)	-475 (2.3)	99.7
Pani 0.5PAmAc/Epoxy	0.01 (0.07)	-507 (0.9)	99.9
Pani 1PAmAc/Epoxy	0.04 (0.41)	-526 (1.2)	99.9
Pani 1.5PAmAc/Epoxy	0.07(0.21)	-482 (1.6)	99.8
Pani 2PAmAc/Epoxy	0.32 (0.22)	-510 (1.3)	99.2

Electrochemical impedance spectroscopy was also used to evaluate the corrosion activity at different molar ratio of Pani-PAmAc in epoxy coatings. Fig. 4.40 shows the impedance behaviour of Pani-PAmAc/Epoxy loadings at initial period of immersion in 0.6M NaCl (after 24 h).

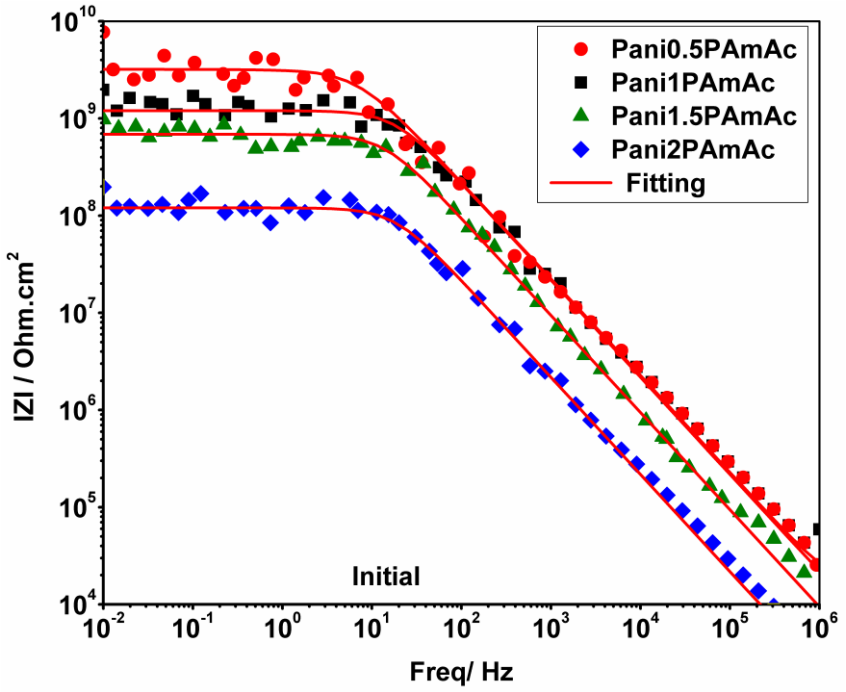

Fig. 4.40: Impedance behavior of Pani-PAmAc /Epoxy coatings at initial immersed stage in 0.6M NaCl solution

In the initial immersion, the value of $|Z|_{0.01\ Hz}$ of Pani-PAmAc/Epoxy coating was decreased on increasing the molar ratios of Pani-PAmAc. The value of bare AA2024-T3 alloy was found to be 0.02 MΩ cm^2. The epoxy coated sample has $|Z|_{0.01\ Hz}$ of 0.9 MΩ cm^2, which is one

order of magnitude higher than that of bare substrate. For Pani-PAmAc/Epoxy coatings, the values were increased by two to three orders of magnitude higher than that of epoxy coating. Pani0.5PAmAc/Epoxy, Pani1PAmAc/Epoxy, Pani1.5PAmAc/Epoxy and Pani2PAmAc/Epoxy coated samples has $|Z|_{0.01\ Hz}$ of 2000 MΩ cm^2, 1000 MΩ cm^2, 600 MΩ cm^2 and 100 MΩ cm^2 respectively.

Fig.4.41 shows the impedance behaviour at different molar ratios of Pani-PAmAc/Epoxy loadings after 30 days immersion in 0.6M NaCl. The value of $|Z|_{0.01\ Hz}$ of Pani0.5PAmAc and Pani1PAmAc coating was almost same to initial immersion values. However, the value of Pani1.5PAmAc and Pani2PAmAc was decreased to 50 MΩ cm^2 and 6 MΩ cm^2, respectively. This may be due to excess of PAmAc units in Pani, which is believed to be responsible for rendering the molecular complex solubility in 0.6M NaCl after 30 days immersion and the coating will show low value of impedance due to diffusion of electrolyte through the coating. This shows that after 30 days immersion in 0.6M NaCl, Pani0.5PamAc and Pani1PAmAc coatings shows higher impedance value and good corrosion protection properties. The EIS results indicated that the corrosion protection of Pani-PAmAc/Epoxy coatings were more protective at lower molar ratio of Pani-PAmAc.

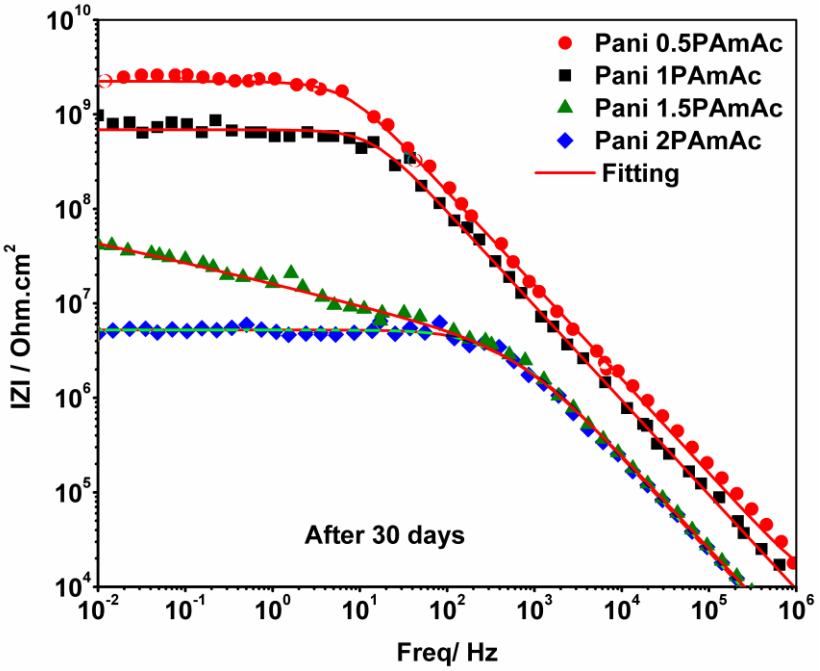

Fig. 4.41: Impedance behavior of Pani-PAmAc /Epoxy coatings after 30 days immersion in 0.6M NaCl solution

Fig. 4.42 shows the impedance behaviour at different molar ratios of Pani-PAmAc/Epoxy coatings after 50 days immersion in 0.6M NaCl. The value of $|Z|_{0.01\ Hz}$ of coating decreased due to diffusion of electrolyte into the coating. The value of Pani0.5PAmAc/Epoxy reached to 300MΩ cm^2, Pani1PAmAc/Epoxy to 20MΩ cm^2, Pani1.5PAmAc/Epoxy to 5MΩ cm^2 and Pani2PAmAc/Epoxy to 0.6MΩ cm^2, respectively. The results show that after 50 days immersion Pani0.5PAmAc/Epoxy coating exhibited high impedance value as compared to other molar ratio of Pani-PAmAc. Improvement in corrosion resistance properties was due to PAmAc which serves the dual functions of being an anticorrosive additive and good adhesion promoter. The strong interaction between the polyaniline and poly(acrylamide co acrylic acid) provides the stability against the loss of ionic dopants. The improved dopant stability in the double-stranded polymeric complex increases the corrosion resistance properties of the coating [91-94]. The diffusion process has started at higher molar ratio of Pani-PAmAc and progress of the electrolyte due to inherent modification of double stranded conducting polymer after 50 days immersion in 0.6M NaCl. The Pani-PAmAc/Epoxy coating will exhibit high corrosion protection performance as compared to Pani-LGS/Epoxy coating. It thus can be concluded that the polyelectrolyte content in Pani-PAmAc/Epoxy coating should be maintained at an optimized concentration for better corrosion resistance.

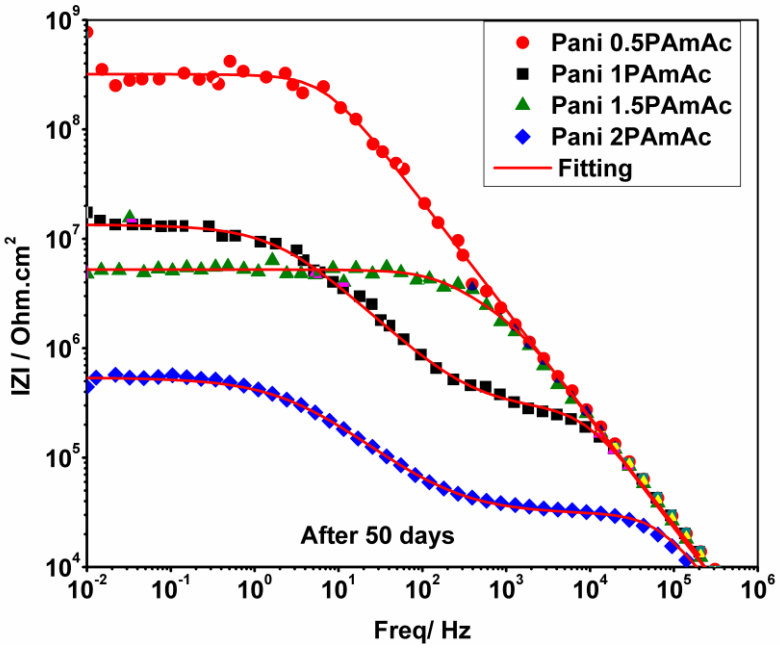

Fig. 4.42: Impedance behavior of Pani-PAmAc/ Epoxy coatings after 50 days immersion in 0.6M NaCl solution

To understand the corrosion behaviour of the coatings, the EIS data were fitted to electrical equivalent circuit as shown in Fig. 4.43. The circuits contain two RC circuits representing the coating/electrolyte and coating/metal interfaces, respectively. Where R_s is the solution resistance, which was the resistance between the working electrode and the reference electrode, C_c and R_c represent the coating capacitance and coating pore resistance, respectively. Q_{dl} is the constant phase element representing the double layer capacitance and R_t represents the charge transfer resistance. The equivalent circuit, Fig 4.43(b), contains a Warburg element for semifinite diffusion i.e. diffusion in the coating layer.

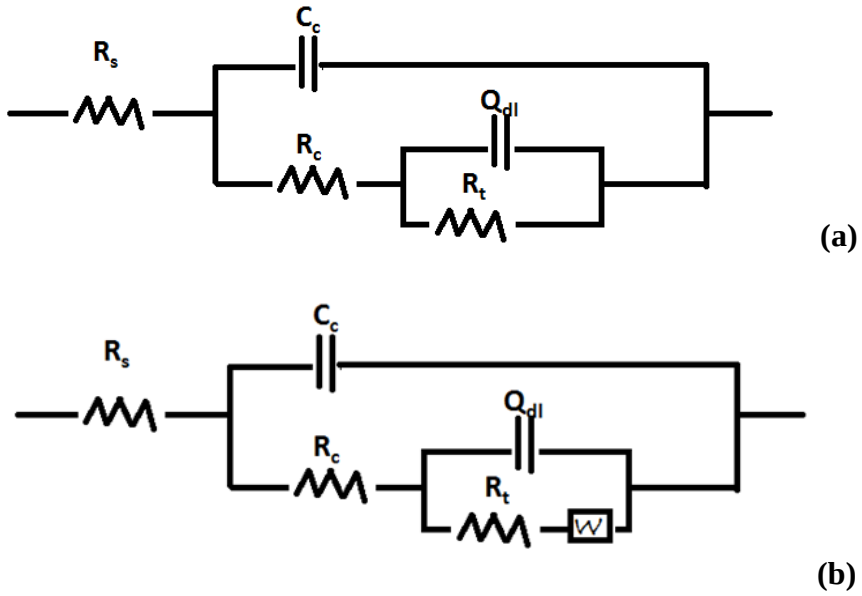

Fig. 4.43: Equivalent electrical circuit for Pani-PAmAc/Epoxy coatings (a) At initial immersion (b) After 30 days immersion

Fig. 4.44 shows the coating capacitance (C_c) of Pani0.5PAmAc/Epoxy, Pani1PAmAc/Epoxy, Pani1.5PAmAc/Epoxy and Pani2PAmAc/Epoxy coatings with respect to immersion time in 0.6M NaCl. The coating capacitance of Pani-PAmAc/Epoxy coatings increased with immersion time. The coating capacitance value of Pani0.5PAmAc/Epoxy was increased from 0.1 $nFcm^{-2}$ to 4 $nFcm^{-2}$ during 480 h of immersion due to diffusion of electrolyte into the coating. After that it reached to saturation level and finally reached to value 9 $nFcm^{-2}$ after 1200 h of immersion. The initial value of coating capacitance of Pani0.5PAmAc/Epoxy, Pani1PAmAc/Epoxy, Pani1.5PAmAc/Epoxy and Pani2PAmAc/Epoxy coatings after 24 h of immersion was 0.1 $nFcm^{-2}$, 0.3 $nFcm^{-2}$, 0.4 $nFcm^{-2}$ and 5 $nFcm^{-2}$, respectively. The final value of coating capacitance of Pani0.5PAmAc/Epoxy, Pani1PAmAc/Epoxy, Pani1.5PAmAc/Epoxy and Pani2PAmAc/Epoxy coatings after 1200 h of immersion was 9

$nFcm^{-2}$, 470 $nFcm^{-2}$, 3300 $nFcm^{-2}$ and 68000 $nFcm^{-2}$, respectively. On increasing the molar ratios of Pani-PAmAc into the coating, increased in diffusion of electrolyte through the coating was observed and lead to more corrosion product formation.

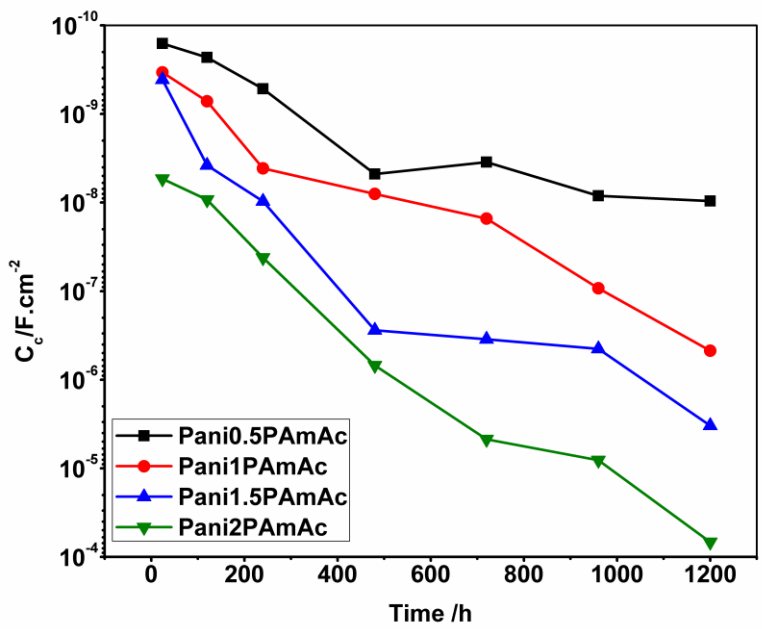

Fig. 4.44: Coating capacitance of the Pani-PAmAc/Epoxy coatings with respect to immersion time in 0.6M NaCl solution

Fig. 4.45 shows the coating resistance (R_c) of the Pani0.5PAmAc/Epoxy, Pani1PAmAc/Epoxy, Pani1.5PAmAc/Epoxy and Pani2PAmAc/Epoxy coatings with respect to immersion time in 0.6M NaCl. R_c is related to electrical resistance to ionic transfer through the coating pores, which reflects the permeability of coating to the electrolyte solution. The value of coating resistance of the Pani0.5PAmAc/Epoxy coating slowly decreased from 59000 MΩ cm^2 to 3400 MΩ cm^2 at initial immersion upto 240 h. After that it reached to saturation level and finally reached to value 110 MΩ cm^2 after 1200 h of immersion. The initial value of coating resistance of Pani0.5PAmAc/Epoxy, Pani1PAmAc/Epoxy, Pani1.5PAmAc/Epoxy and Pani2PAmAc/Epoxy coatings after 24 h of immersion was 59000 MΩ cm^2, 8300 MΩ cm^2, 7900 MΩ cm^2 and 910 MΩ cm^2, respectively. The final value of coating capacitance of Pani0.5PAmAc/Epoxy, Pani1PAmAc/Epoxy, Pani1.5PAmAc/Epoxy and Pani2PAmAc/Epoxy coatings after 1200 h of immersion was 110MΩ cm^2, 4 MΩ cm^2 0.3 MΩ cm^2 and 0.06 MΩ cm^2, respectively. On increasing the molar ratios of Pani-PAmAc into the coating, increased in diffusion of electrolyte through the coating was observed due to more pore formation on the coating surface.

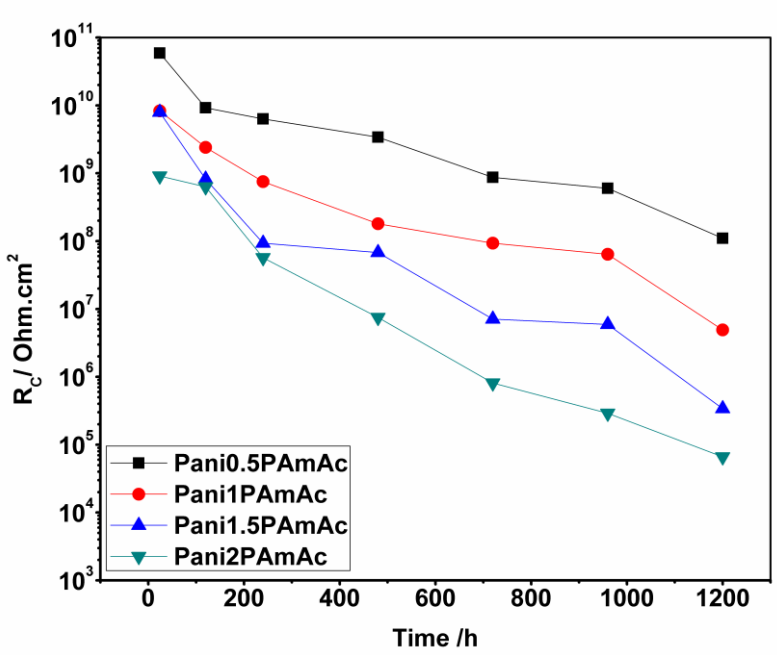

Fig. 4.45: Coating resistance of the Pani-PAmAc /Epoxy coatings with respect to immersion time in 0.6M NaCl solution

Fig. 4.46 shows the charge transfer resistance, R_t of the Pani0.5PAmAc/Epoxy, Pani1PAmAc/Epoxy, Pani1.5PAmAc/Epoxy and Pani2PAmAc/Epoxy coatings with respect to immersion time in 0.6M NaCl. The value of charge transfer resistance, R_t is a measure of the resistance to the electron transfer across the metal surface and is inversely proportional to corrosion rate [34]. The value of R_t for the Pani0.5PAmAc coating decreased slowly from 62 GΩ cm^2 to 1 GΩ cm^2 after 480 h of immersion and reached to final value 0.2 GΩ cm^2 after 1200 h of immersion. For the Pani1PAmAc coatings the value of R_t gradually decreased from 9 GΩ cm^2 to 0.005 GΩ cm^2 after 1200 h of immersion. The value for Pani1.5PAmAc coating was 6 GΩ cm^2 at the initial immersion period, then 0.02 GΩ cm^2 after 720 h and then decreased to 0.0002 GΩ cm^2 at 1200 h immersion. The value for Pani2PAmAc coating was 0.9 GΩ cm^2 at the initial immersion period, then 0.0008 GΩ cm^2 after 720 h and then decreased to 0.00006 GΩ cm^2 at 1200 h immersion. The higher value indicates that the corrosion process become difficult in the case of Pani0.5 PAmAc coating than that of other molar ratio formulations.

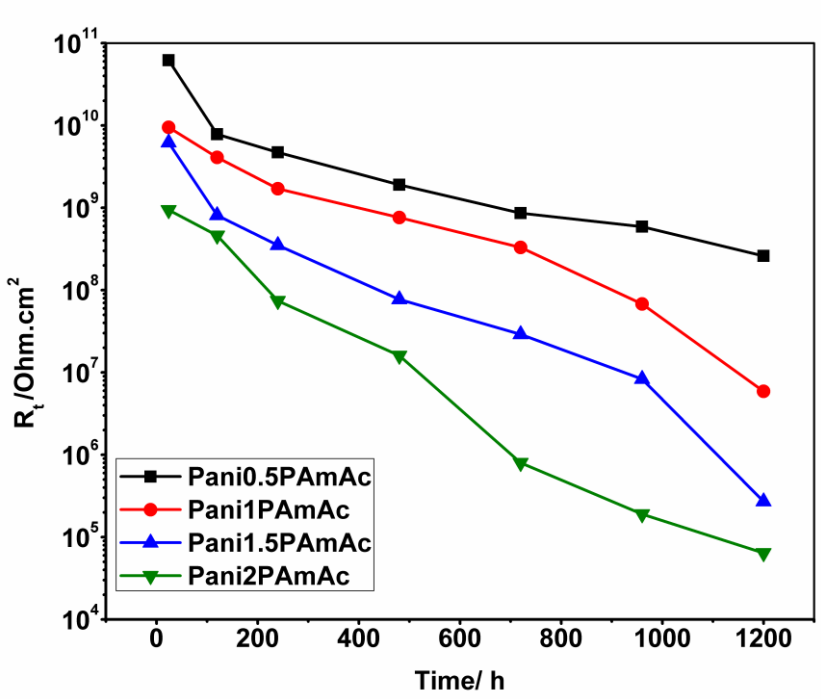

Fig. 4.46: Charge transfer resistance of the Pani-PAmAc /Epoxy coatings with respect to immersion time in 0.6M NaCl solution

4.4.6 Adhesion Test of Pani-PAmAc/Epoxy coating

High adhesion strength of the coatings is a basic requirement for good corrosion protection. The results of adhesion measurements by the crosshatch method are shown in Table 4.5. It is observed that the adhesion strength of Pani-PAmAc/Epoxy coatings were 5B, which is 'Excellent', prior to exposure to 0.6M NaCl. This was due to carboxylic acid present in PAmAc microgel which enhances the adhesion strength of the respective coatings with the substrate. The adhesion strength was also measured after 50 days exposure to 0.6M NaCl. There was decrease in the adhesion strength of Pani1.5PAmAc/Epoxy and Pani2PAmAc/Epoxy coatings after long term immersion. This may be due to swelling of acidic part after long term exposure to electrolyte. However, very less blister formation was observed in Pani1PAmAc/Epoxy and no delamination or blister formation of coating was observed in Pani0.5PAmAc/Epoxy after 50 days exposure to 0.6M NaCl.

Table 4.5: Adhesion test of different molar ratios of Pani-PAmAc/Epoxy coatings

Coating System	Adhesion Test (ASTM 3359)	
	Before exposure	After exposure (0.6M NaCl)
Pani 0.5PAmAc/Epoxy	5B	5B
Pani 1PAmAc/Epoxy	5B	4B
Pani 1.5PAmAc/Epoxy	5B	3B
Pani 2PAmAc/Epoxy	5B	3B

4.4.7 Salt Spray Test of Pani-PAmAc/Epoxy coating

The coated samples were tested in the salt-fog spray chamber for 1200 h as per ASTM B117 as shown in Fig. 4.47.

Fig. 4.47: Photographs of Pani-PAmAc/Epoxy coatings after 1200 h to salt spray exposure

It was observed that Pani0.5PAmAc/Epoxy coating performs much better than the Pani1PAmAc/Epoxy, Pani1.5PAmAc/Epoxy and Pani2PAmAc/Epoxy coatings. As the molar ratio of Pani-PAmAc increases the hydrophilic character of the coating increases which degraded the coating. The high corrosion protection performance was due optimize amount of addition of acrylamide and acrylic acid into the polyaniline. All the formulation shows good results upto 750 h and then degradation of higher molar ratios containing Pani-PAmAc coating starts.

4.4.8 UV-Weatherometer of Pani-PAmAc/Epoxy Coatings

Accelerated weathering of coated specimen was carried out to simulate outdoor weathering using combination of UV light and water condensation (ASTM-G53). Damage caused by the weathering cycle was assessed using visual assessment, colour change and gloss measurement. Visual examination of the exposed specimen shows that there were no white pits of corrosion product, cracking or loss of adhesion (Fig. 4.48). The colour change parameters of Pani-PAmAc/Epoxy coating are shown in Fig. 4.49. The Pani-PAmAc/Epoxy showed less colour change values after 600 h of exposure. The colour change values of all the coatings increases after 1200 h of exposure. The gloss retention parameters of Pani-PAmAc/Epoxy coating are shown in Fig. 4.50. The gloss retention of all the coating was found approximately 80% after 600 h of exposure and ~ 55% after 1200 h of exposure. This shows that there was not drastic change in the gloss of the coatings. The results show that amide group and acidic group in PAmAc moiety act as UV blockers in the Pani-PAmAc/Epoxy system and proved to be effective means for enhancing the weathering resistance of the coatings. Therefore, coating can be used for outdoor application and properties can be enhanced by incorporating various nanoparticles.

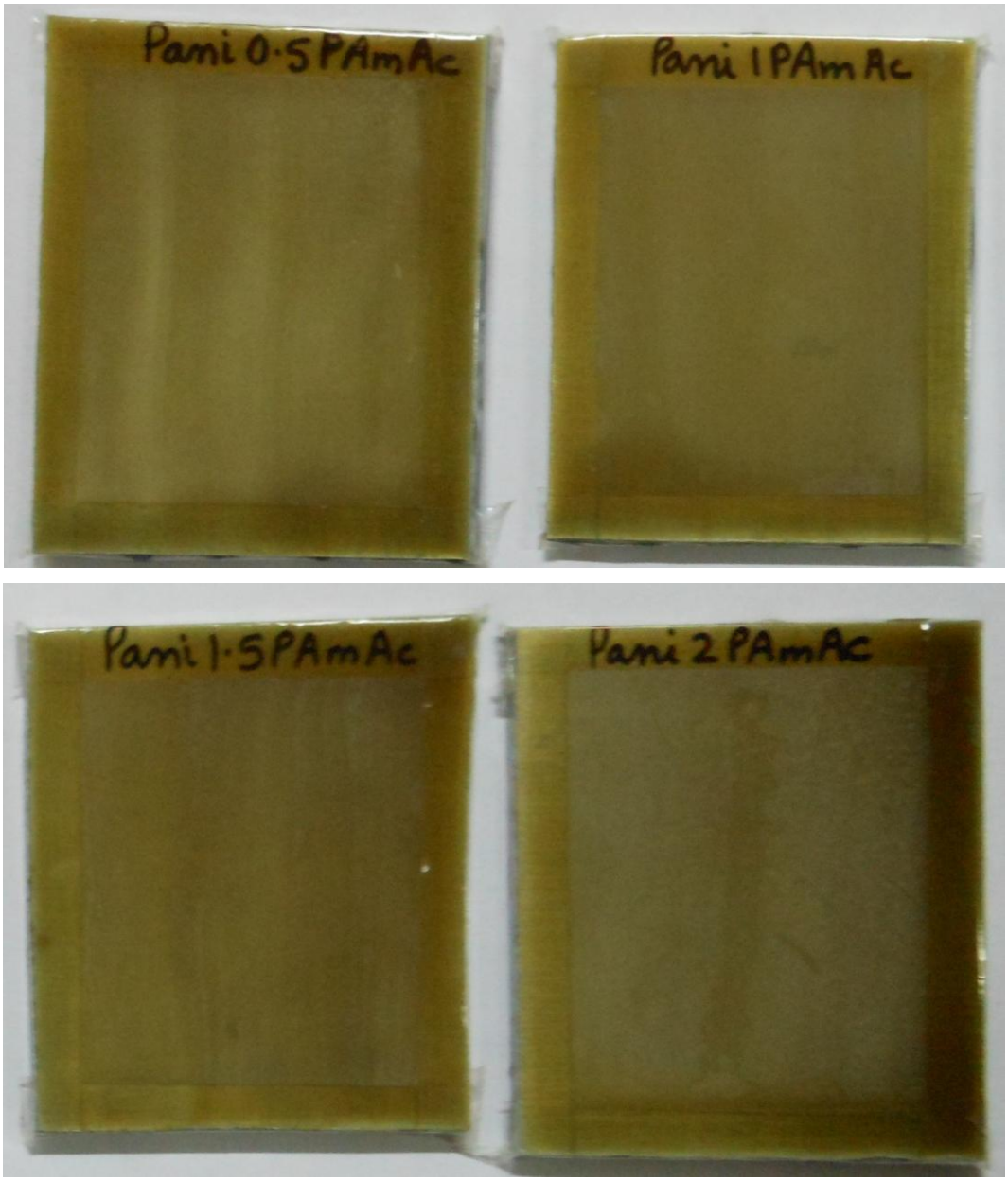

Fig. 4.48: Photographs of Pani-PAmAc/Epoxy coatings after 1200 UV-weatherometer exposure

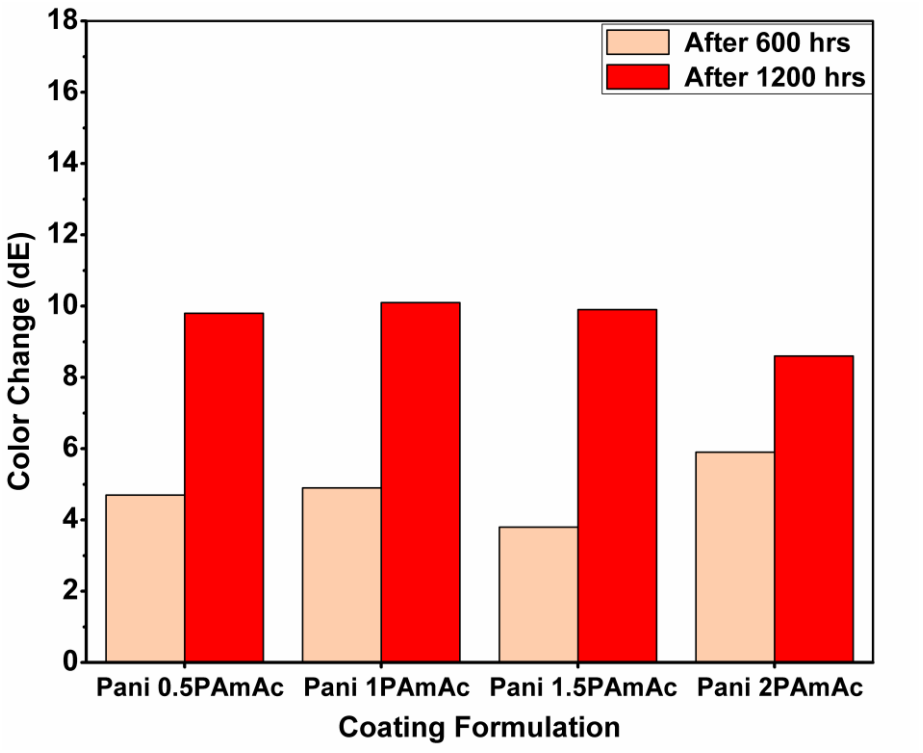

Fig. 4.49: Color change (dE) for Pani-PAmAc/Epoxy coatings

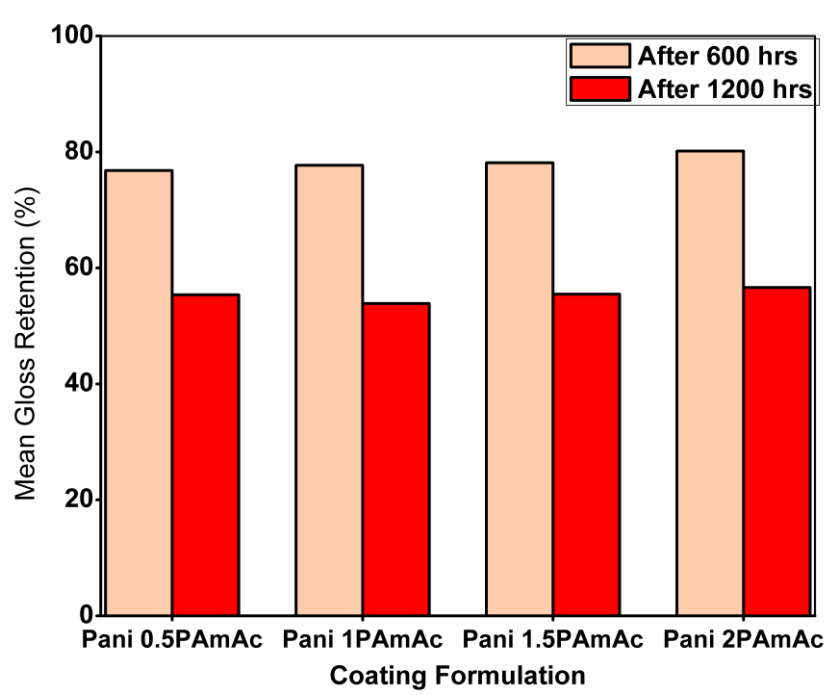

Fig. 4.50: Mean gloss retention (%) of Pani-PAmAc/Epoxy coatings

4.4.9 Mechanical Properties of the Pani-PAmAc/Epoxy Coating

The tensile strength of Pani0.5PAmAc/Epoxy, Pani1PAmAc/Epoxy, Pani1.5PAmAc/Epoxy and Pani2PAmAc/Epoxy films were 6.6, 6.8, 7 and 7.3MPa, respectively as shown in Fig. 4.51. Fig. 4.51 and 4.52 represents the tensile strength and elongation at break against Pani-PAmAc content in the epoxy films. Table 4.6 represents the hardness values of Pani-PAmAc/Epoxy films. It was observed that the increase in molar ratio of Pani and PAmAc resulted in a gradually increase in tensile strength and elongation at break. The increase in properties was attributed to PAmAc copolymer in which acryl amide group act as reinforcing filler for the epoxy matrix and modifies the mechanical properties of the polymer.

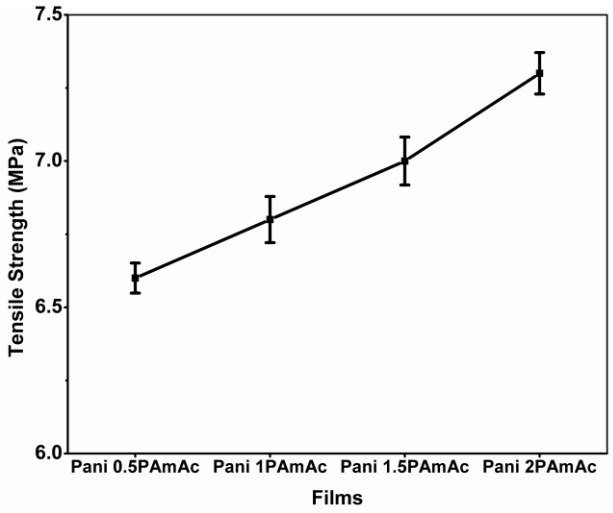

Fig. 4.51: Tensile Strength of Pani-PAmAc/Epoxy films

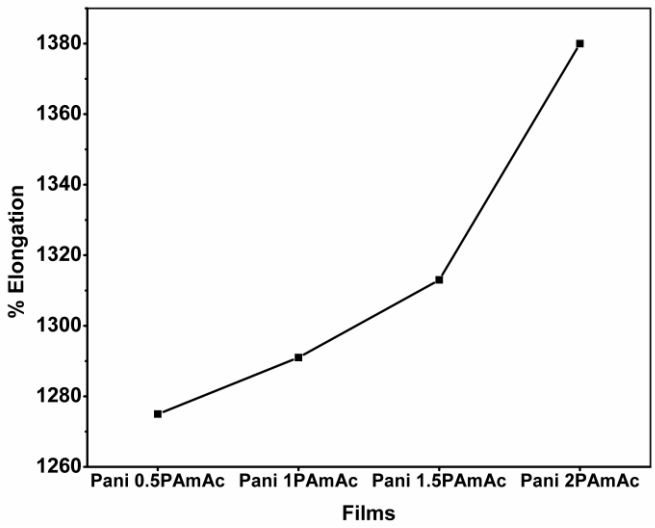

Fig. 4.52: %Elongation of Pani-PAmAc/Epoxy films

Table 4.6: Hardness values of Pani-PAmAc/Epoxy loading films

Coating System	Hardness Values
Pani 0.5PAmAc/Epoxy	HB
Pani 1PAmAc/Epoxy	B
Pani 1.5PAmAc/Epoxy	3B
Pani 2PAmAc/Epoxy	3B

4.5 Characterisation of Pani-PAmAc-Nanoparticles/Epoxy Coating

Nanofiller composition was mentioned in section 3.5 (coating formulation). It was 5 wt % of the coating resin (epoxy and hardner) for each nanocomposite. We also tried 2wt%, 8wt% and 10wt% of nanocomposite in the coating formulation. But above 5wt% the coating particles will not properly dispersed in the coating matrix. So we have chosen 5wt% for all nanocomposites.

4.5.1 Scanning Electron Microscopy of Pani-PAmAc-Nanoparticles/Epoxy coating

The morphology for a coating is very important to understand the filler (dispersed phase) distribution in the matrix (continuous phase) because it is the most important aspect which governs different physical and mechanical properties.

Fig. 4.53 (a-c) shows the SEM of Pani-PAmAc-MMT/Epoxy, Pani-PAmAc- Al_2O_3/Epoxy and Pani-PAmAc-G/Epoxy coatings at 1000x magnification, respectively. Fig. 4.53 exhibited smooth and homogeneous morphology due to uniform distribution of Pani-PAmAc-Nanoparticles into epoxy matrix. No agglomeration of particles was observed. Fig. 4.54 (a-c) shows the SEM of Pani-PAmAc-MMT/Epoxy, Pani-PAmAc- Al_2O_3/Epoxy and Pani-PAmAc-G/Epoxy coatings after 2400 h salt spray exposure at 1000x magnification, respectively.

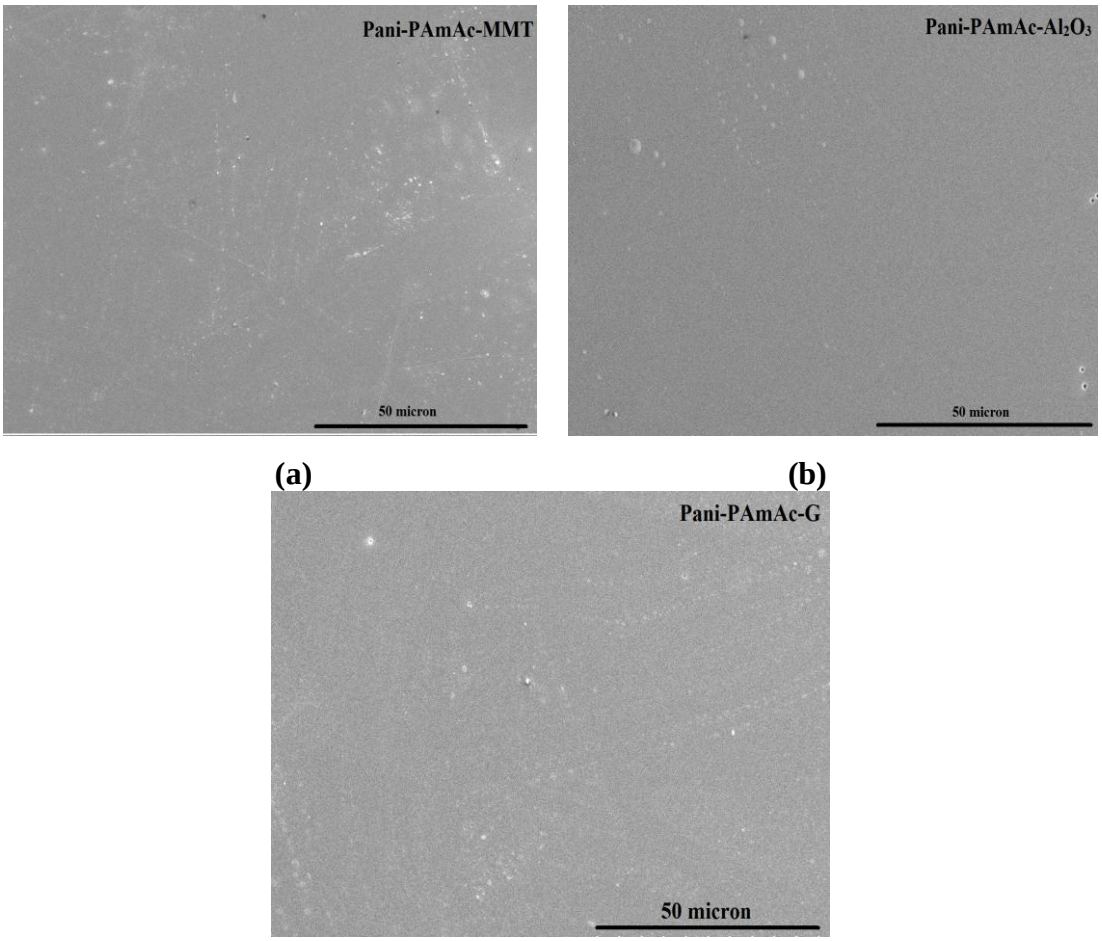

Fig. 4.53: Scanning Electron micrographs of (a) Pani-PAmAc-MMT/Epoxy, (b) Pani-PAmAc- Al_2O_3/Epoxy, (c) Pani-PAmAc-G/Epoxy Coatings (SE at 1000x magnification)

Fig. 4.54a shows that after 2400 h of salt spray exposure Pani-PAmAc-MMT exhibited smooth and homogenous morphology. Very less sign of corrosion was observed with no pits formation. Pani-PAmAc- Al_2O_3/Epoxy coating exhibits the localised pits formation as shown in Fig. 4.54b. Few small corrosion pits and white corrosion product deposits was observed. Pani-PAmAc-G/Epoxy shows the uniform corrosion over the surface (Fig. 4.54c). This shows the initiation of pits formation which leads to surface damaged. It was concluded that the MMT clay particles within the coatings restrict the ingress of electrolyte for longer time period as compared to Al_2O_3 and graphene [106, 107].

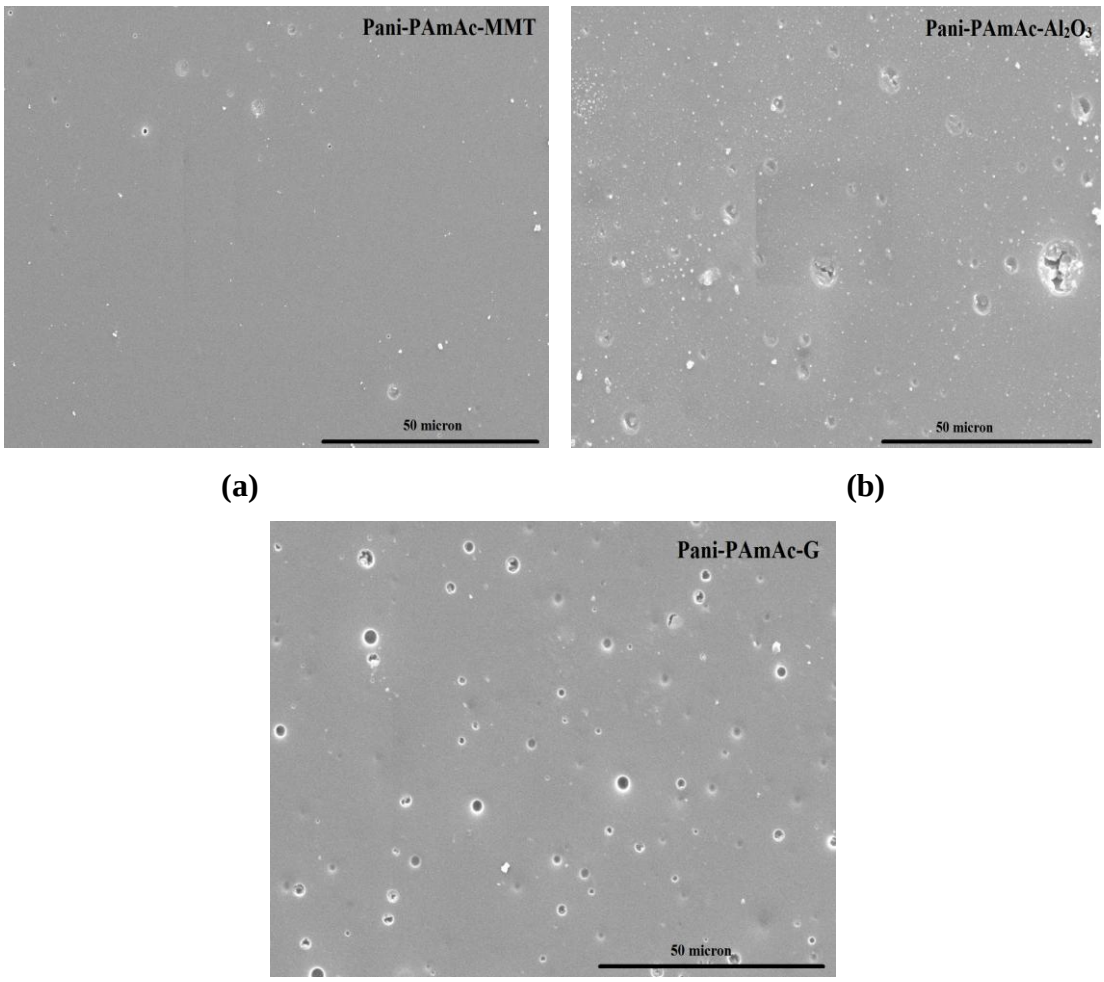

Fig. 4.54: Scanning Electron micrographs of (a) Pani-PAmAc-MMT/Epoxy, (b) Pani-PAmAc- Al_2O_3/Epoxy, (c) Pani-PAmAc-G/Epoxy Coatings after 2400 h salt spray exposure (SE at 1000x magnification)

4.5.2 Atomic Force Microscopy of Pani-PAmAc-Nanoparticles/Epoxy coating

AFM were performed to understand the surface phenomena and morphology of the coatings at the micro and nano level. Fig. 4.55 (a-c) shows the AFM images of Pani-PAmAc-MMT/Epoxy, Pani-PamAc- Al_2O_3/Epoxy and Pani-PamAc-G/Epoxy coatings, respectively. All coatings are crack free and low roughness values. Pani-PamAc-MMT/Epoxy show sharp pyramidal peak like particles that are uniformly distributed throughout the coatings in Fig. 4.55a. It may also be believed that the clay platelets may be covering the system giving it extremely good barrier properties. Pani-PamAc- Al_2O_3/Epoxy exhibits broad hump which seem to be uniformly distributed throughout the coating system. The AFM images of Pani-PamAc-G/Epoxy shows mixed sheets and particles like morphology which was distributed

uniformle to the surface (Fig. 4.55c). The root-mean square (RMS) values of surface roughness determined by AFM were 4.568±0.8, 8.51±0.9 and 3.59±0.7 nm for Pani-PamAc-MMT/Epoxy, Pani-PamAc- Al_2O_3/Epoxy and Pani-PamAc-G/Epoxy coatings, respectively.

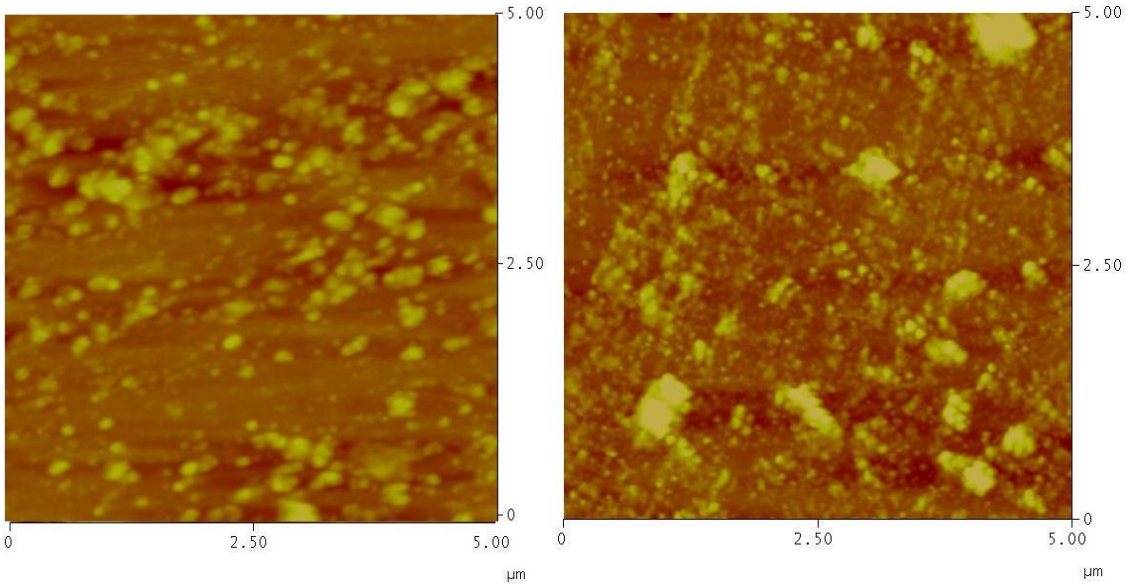

(a) **(b)**

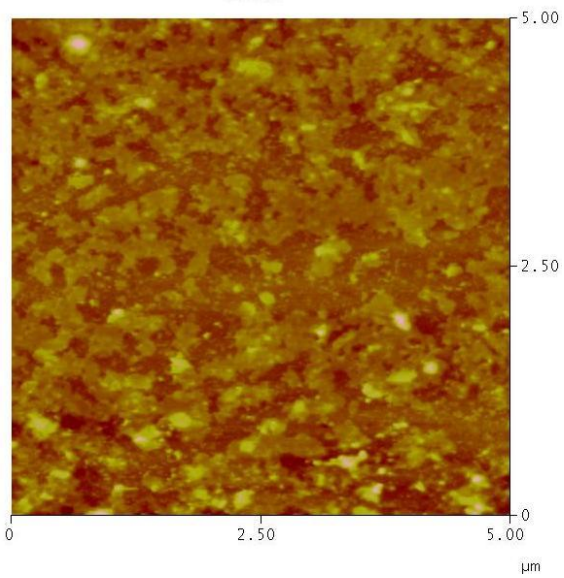

(c)

Fig. 4.55: AFM images of (a) Pani-PAmAc-MMT/Epoxy, (b) Pani-PAmAc- Al_2O_3/Epoxy, (c) Pani-PAmAc-G/Epoxy Coatings (5 microns)

Fig. 4.56 (a-c) shows the AFM images of Pani-PamAc-MMT/Epoxy, Pani-PamAc-Al_2O_3/Epoxy and Pani-PamAc-G/Epoxy coatings after 2400 h salt spray exposure,

respectively. In Fig. 4.56a, Pani-PamAc-MMT exhibited very less sign of corrosion with no pits formation. Pani-PamAc- Al_2O_3/Epoxy coating exhibits the localised pits formation as shown in Fig. 4.56b. Few small corrosion pits and white corrosion product deposits was observed.

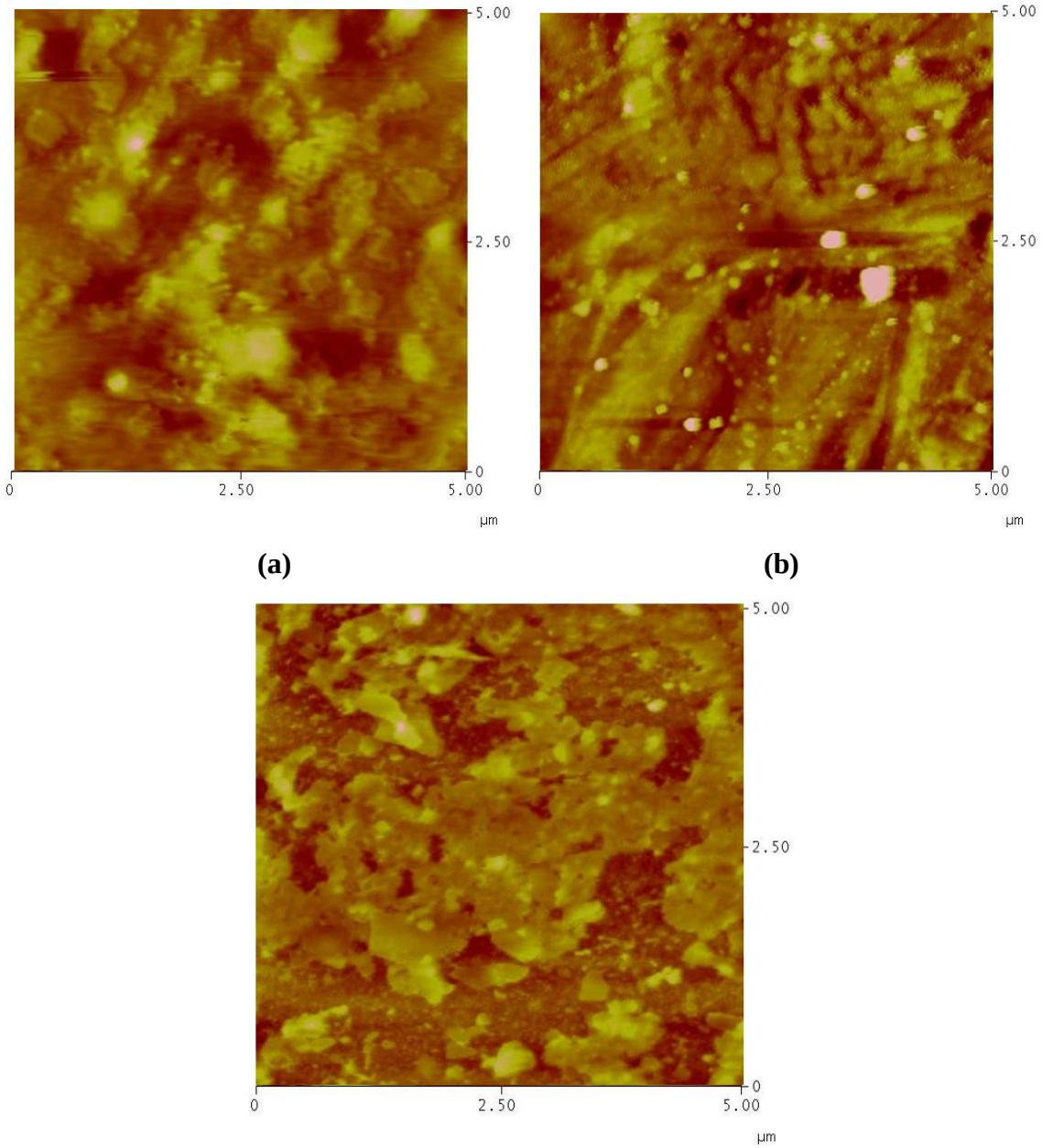

Fig. 4.56: AFM images of (a) Pani-PAmAc-MMT/Epoxy, (b) Pani-PAmAc- Al_2O_3/Epoxy, (c) Pani-PAmAc-G/Epoxy Coatings after 2400 h salt spray exposure (5 microns)

The AFM study detected the presence of pores widespread on the surface of Pani-PamAc-G/Epoxy. It was found that blisters or some uniform pits formed on the coating surface after 2400 h of salt spray exposure (Fig. 4.56c). The RMS values increases due to corrosion product and pits/blisters formation on the surface. The RMS values were 12.45±0.6, 27.36±1.2 and 19.05±0.9 nm for Pani-PamAc-MMT/Epoxy, Pani-PamAc- Al_2O_3/Epoxy and Pani-PamAc-G/Epoxy coatings, respectively.

4.5.3 TGA Analysis of Pani-PAmAc-Nanoparticles/Epoxy coating

TGA curves of Pani-PAmAc-MMT/Epoxy, Pani-PAmAc- Al_2O_3/Epoxy and Pani-PAmAc-G/Epoxy blends are presented in Fig. 4.57. All curves show a typical behavior of the epoxy coating and the degradation temperature of the particles increases when it mixed with epoxy blend. The decomposition process of Pani-PAmAc-MMT starts at 160^0C with subsequent decays being observed at 300^0C, 440^0C and 730^0C.

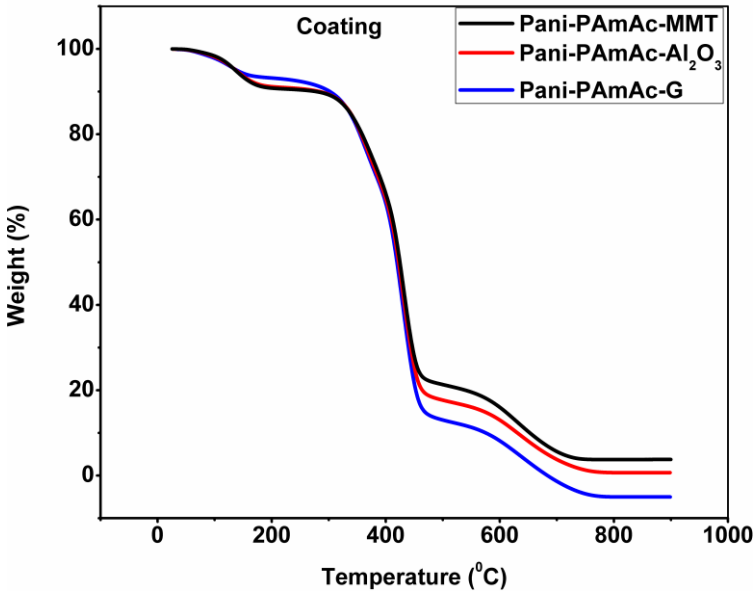

Fig. 4.57: TGA curves of Pani-PAmAc-MMT/Epoxy, Pani-PAmAc- Al_2O_3/Epoxy and Pani-PAmAc-G/Epoxy Coatings

TGA curves show a small weight loss below 160^0C, caused by the loss of adsorbed water and oligomers. The weight loss between 160^0C to 300^0C corresponds to release of sulfonate and carboxylate groups. The weight loss in the range of 300–440°C temperature may be due to the structural decomposition of PAmAc along with nanoparticles. The thermal stability of Pani-

PAmAc-MMT/Epoxy shows higher as compared to Al_2O_3 and G. The degradation temperature of MMT shifted towards the higher temperature range, which confirms the enhancement of thermal stability of the MMT clay with the polymer matrix. The percentage weight loss at 542^0C of Pani-PAmAc-MMT/Epoxy, Pani-PAmAc- Al_2O_3/Epoxy and Pani-PAmAc-G/Epoxy was observed 68%, 72% and 77%, respectively. This shows the stability of the nanoparticles in the same polymer matrix. Major weight loss occurs at the 542^0C where as complete degradation will take place at 800^0C [108].

4.5.4 Electrical Conductivity of Pani-PAmAc-Nanoparticles/Epoxy coating

The room temperature conductivity of Pani-PAmAc-MMT/Epoxy, Pani-PAmAc-Al_2O_3/Epoxy and Pani-PAmAc-G/Epoxy coatings were 3.60, 2.24 and 8.78 S/cm, respectively as shown in Fig. 4.58. The conductivity of coatings decreases as compared to nanoparticles, on addition of epoxy insulating matrix. Fig. 4.59 shows the temperature dependence on electrical conductivity of Pani-PAmAc-MMT/Epoxy, Pani-PAmAc-Al_2O_3/Epoxy and Pani-PAmAc-G/Epoxy coatings.

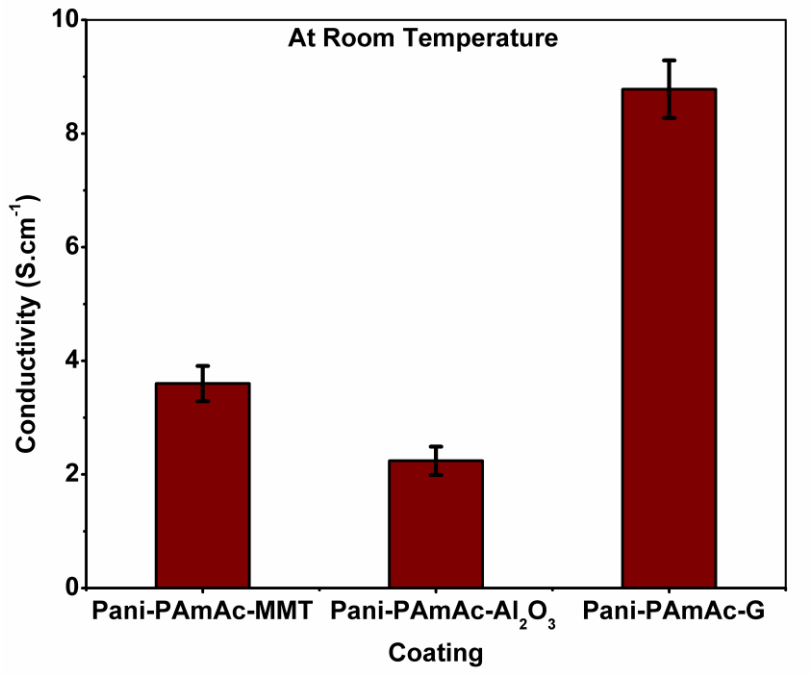

Fig. 4.58: Room temperature conductivity of Pani-PAmAc-MMT/Epoxy, Pani-PAmAc-Al_2O_3/Epoxy and Pani-PAmAc-G/Epoxy coatings

The temperature dependent conductivity was measured from 223 K to 423K. It was noted that the electrical conductivity of the coating increases with the increase in temperature. Pani-PAmAc-MMT/Epoxy and Pani-PAmAc- Al_2O_3/Epoxy coating shows very less conductivity as compared to Pani-PAmAc-G/Epoxy coating. The appreciable improvement in electrical conductivity of Pani-PAmAc-G/Epoxy coating was due to the formation of a conducting network (conjugation) by graphene sheets in the polymer matrix. Electrical properties depend on the polymer matrix, processing method and filler type. On increasing the temperature the movement of electron charge carriers also increases [109]. Graphene particles itself have very good conductivity, movement of electron charge carrier was due to delocalisation of electron even at room temperature. There was not much difference in the conductivity at higher temperature. [104]

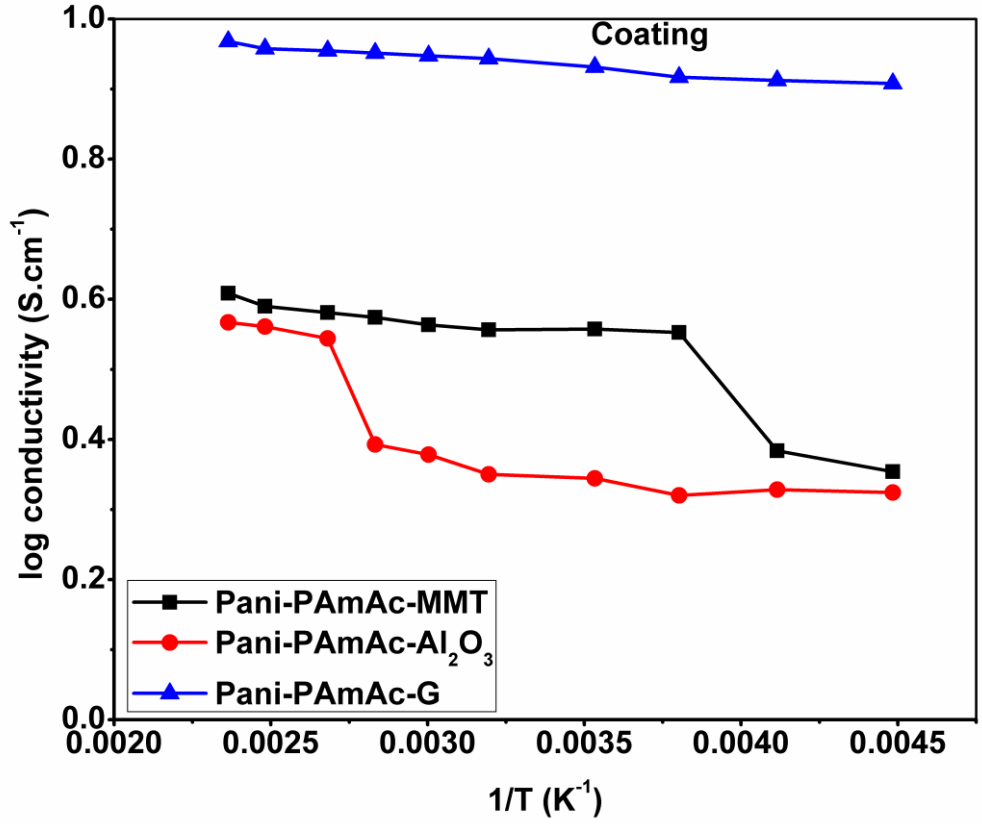

Fig. 4.59: Logarithm of conductivity vs. temperature inverse for Pani-PAmAc-MMT/Epoxy, Pani-PAmAc-Al_2O_3/Epoxy and Pani-PAmAc-G/Epoxy coatings

4.5.5 Corrosion protection properties of Pani-PAmAc-Nanoparticles/Epoxy coating

The corrosion protection behavior of coatings was examined in 0.6M NaCl using potentiodynamic polarization and EIS studies. pH was maintained at 7 for the test solutions.

The potentiodynamic polarization curves for Pani-PAmAc-MMT/Epoxy, Pani-PAmAc-Al_2O_3/Epoxy Pani-PAmAc-G/Epoxy Coated AA2024-T3 panels, at initial immersion in an aqueous 0.6M NaCl solution are shown in Fig. 4.60. The corrosion potential (E_{corr}) for all the three coated AA2024-T3 panels, show noble values than that observed for the bare AA2024-T3, epoxy and Pani/Epoxy and Pani-PAmAc/Epoxy coated AA2024-T3 panels. The E_{corr} values of Pani-PAmAc-MMT/Epoxy and Pani-PAmAc-Al_2O_3/Epoxy was in more positive direction as compared to Pani-PAmAc-G/Epoxy coating as shown in Table 4.7. The positive shift in E_{corr} indicates the more corrosion protection of the AA2024-T3 surface by the formulated coatings (anodic protection). On adding various nanoparticles into the Pani-PAmAc/epoxy coating system the value increased by one to two orders of magnitude. The electrochemical protection is caused by the increase of the corrosion potential, physical barrier effect and the formation of a protective passive layer on AA2024-T3 surface. The values of the corrosion potential (E_{corr}), corrosion current density (i_{corr}) and protection efficiency (PE) obtained from tafel curves of the Pani-PAmAc-nanoparticle/Epoxy coatings are summarized in Table 4.7. It was found that the incorporation of MMT nanoparticles in the Pani-PAmAc/Epoxy matrix promotes the anticorrosive efficiency on AA2024-T3 samples. However enhanced corrosion protection by the Pani-PAmAc-MMT/Epoxy coating over the protection by Pani-PAmAc/Epoxy might result from the silicate nanolayers of clay dispersed in the matrix that increase the tortousity of the diffusion pathway of corrosive agents such as oxygen gas, hydrogen, hydroxide and chloride ions. Whereas Al_2O_3 forms a strong interaction with Pani-PAmAc during synthesis and results in synergistic effect and provide excellent anticorrosion performance. Therefore, the barrier property of coating matrix was improved with the presence of the MMT and Al_2O_3. Pani-PAmAc-G/Epoxy coating also effectively suppresses metal oxidation and oxygen reduction reactions and protects the metal from the aggressive environments [110, 111].

The initial values of the corrosion potential (E_{corr}), corrosion current density (i_{corr}) and protection efficiency (PE) obtained from these curves are given in Table 4.7.

From the measured corrosion current density values, the protection efficiency was obtained from the following equation:

$$\textbf{Protection efficiency (\%)} = (i_{corr}(uc) - i_{corr}(c)) / i_{corr}(uc) * 100$$

where, i_{corr} (uc) and i_{corr} (c) are the corrosion current density values of uncoated and coated samples respectively. All polarisation curves show the insulating effect of epoxy, in that a distinct breakdown potential is not observed, with current gently increasing with increasing anodic potentials. The data reveal (from replicate testing) that the Pani-PAmAc-nanoparticles/Epoxy coating resulted in consistently lower corrosion current and noble corrosion potential being realised. These facts will be more elucidated from the results of electrochemical impedance spectroscopy (EIS).

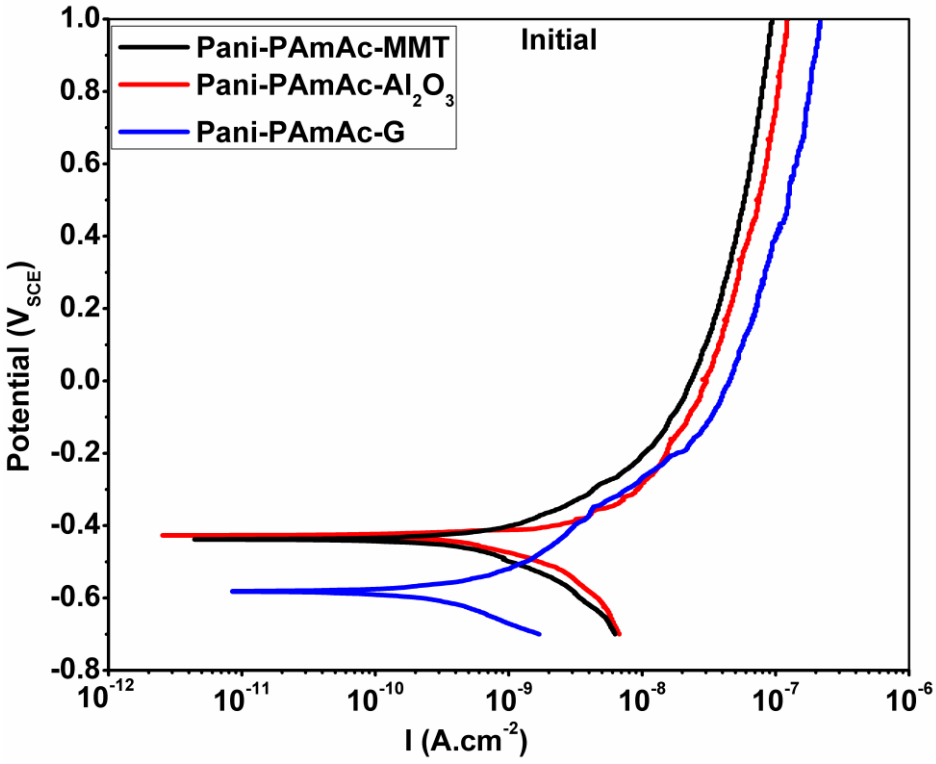

Fig. 4.60: Potentiodynamic polarisation curves of Pani-PAmAc-Nanoparticles/Epoxy coatings at initial immersed stage in 0.6M NaCl solution

Table 4.7: Electrochemical Parameters of Pani-PAmAc-MMT/Epoxy, Pani-PAmAc-Al_2O_3/Epoxy and Pani-PAmAc-G/Epoxy on AA2024-T3 alloy in 0.6M NaCl solution

Compositions	***i_{corr} ($\mu A/cm^2$) (Std. Dev.)***	***E_{corr} (m V $_{SCE}$) (Std. Dev.)***	***P_E (%)***
AA2024-T3 alloy	42.56 (0.16)	-907 (1.2)	-
Pani-PAmAc-MMT/Epoxy	0.001 (0.13)	-435 (0.8)	99.9
Pani-PAmAc- Al_2O_3/Epoxy	0.007 (0.17)	-430 (1.4)	99.9
Pani-PAmAc-G/Epoxy	0.004 (0.24)	-592 (1.6)	99.9

Electrochemical impedance spectroscopy was also used to evaluate the corrosion activity of Pani-PAmAc-nanoparticle/epoxy coatings. Fig. 4.61 shows the impedance behaviour of Pani-PAmAc-MMT/Epoxy, Pani-PAmAc- Al_2O_3/Epoxy Pani-PAmAc-G/Epoxy Coated AA2024-T3 panels at an initial period of immersion in 0.6M NaCl (after 24 h). In the initial immersion, the value of $|Z|_{0.01\ Hz}$ of bare AA2024-T3 alloy was found to be 0.02 MΩ cm^2. The epoxy coated sample has $|Z|_{0.01\ Hz}$ of 0.9 MΩ cm^2, which is one order of magnitude higher than that of bare substrate. For Pani-PAmAc-nanoparticles /epoxy coatings, the values was increased to around four to five orders of magnitude higher than that of epoxy coating. The Pani-PAmAc-MMT/Epoxy, Pani-PAmAc- Al_2O_3/Epoxy and Pani-PAmAc-G/Epoxy coated sample has $|Z|_{0.01\ Hz}$ of 20,000 MΩ cm^2, 10,000 MΩ cm^2 and 7000 MΩ cm^2, respectively [111-113].

Fig. 4.62 shows the impedance of Pani-PAmAc-MMT/Epoxy, Pani-PAmAc- Al_2O_3/Epoxy and Pani-PAmAc-G/Epoxy after 50 days immersion in 0.6M NaCl. The value of $|Z|_{0.01\ Hz}$ of all coating was almost same to initial values instead of Pani-PAmAc-G/Epoxy sample which decreased to 4000 MΩ cm^2 from 7000 MΩ cm2. This was due to diffusion of electrolyte through the coating has taken place. The value of impedance for the other two formulations was almost same. This shows that even after 50 days immersion in 0.6M NaCl, there was no effect on the corrosion protection properties. The EIS results indicated that the corrosion protection of Pani-PAmAc-Nanoparticles/Epoxy coatings were more protective than that of without nanoparticles.

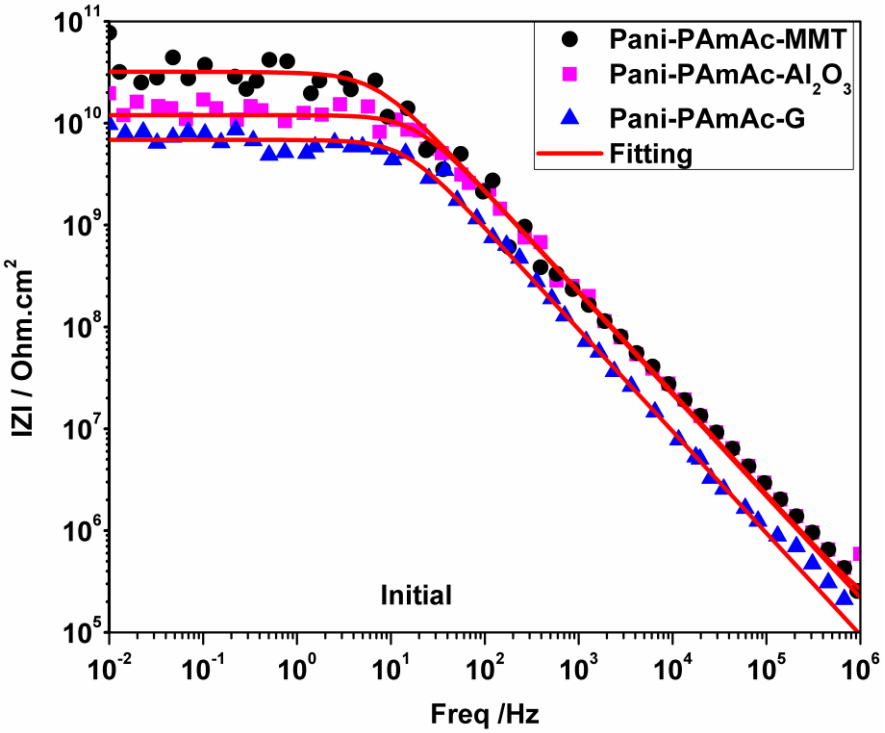

Fig. 4.61: Impedance behavior of Pani-PAmAc-Nanoparticles/Epoxy coatings at initial immersed stage in 0.6M NaCl solution

Fig. 4.63 shows the impedance of Pani-PAmAc-MMT/Epoxy, Pani-PAmAc- Al_2O_3/Epoxy and Pani-PAmAc-G/Epoxy after 100 days immersion in 0.6M NaCl. The value of $|Z|_{0.01\ Hz}$ of coating started decreasing due to diffusion of electrolyte into the coating. The value of Pani-PAmAc-MMT/Epoxy reached to 1000 MΩ cm2, Pani-PAmAc- Al_2O_3/Epoxy to 500 MΩ cm^2 and Pani-PAmAc-G/Epoxy to 70 MΩ cm^2, respectively. This shows that even after 100 days immersion coating still has the protection properties but steadily loses this property. The diffusion process has started but the coating itself has the capability to delay this diffusion process and inhibit the progress of the electrolyte due to inherent modification of double stranded conducting polymer with nanoparticles.

To further interpret the EIS data, curves were fit to the electrical equivalent circuit as shown in Fig. 4.64. The circuits contain two RC circuits representing the coating/electrolyte and coating/metal interfaces, respectively. Where R_s is the solution resistance, which was the resistance between the working electrode and the reference electrode, C_c and R_c represent the coating capacitance and coating pore resistance, respectively. Q_{dl} is the constant phase element representing the double layer capacitance and R_t represents the charge transfer resistance [111, 112].

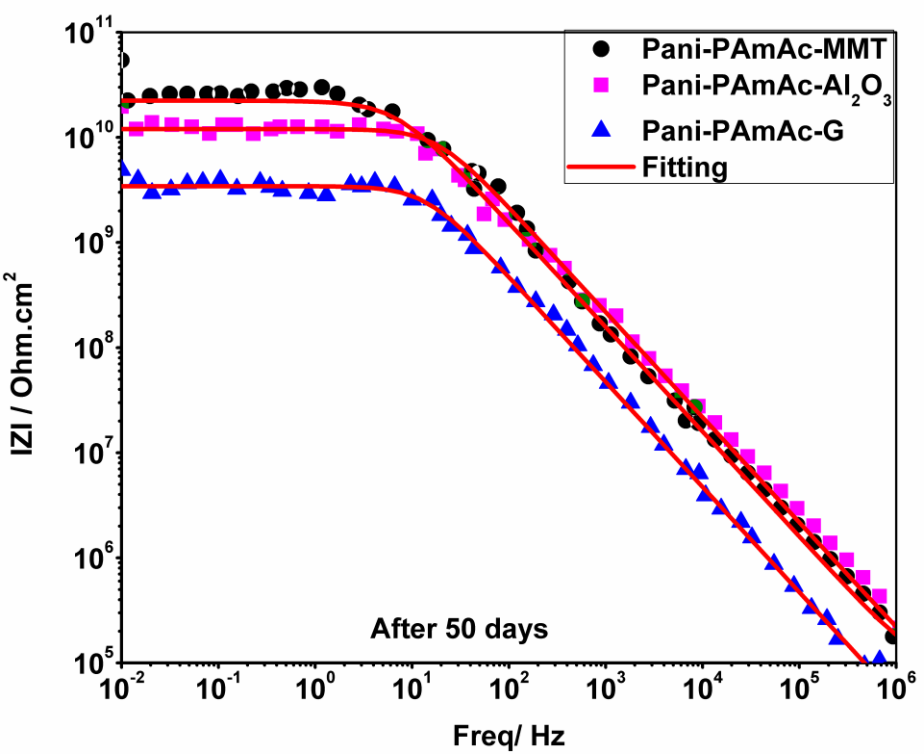

Fig. 4.62: Impedance behavior of Pani-PAmAc-Nanoparticles/Epoxy coatings after 50 days immersion in 0.6M NaCl solution

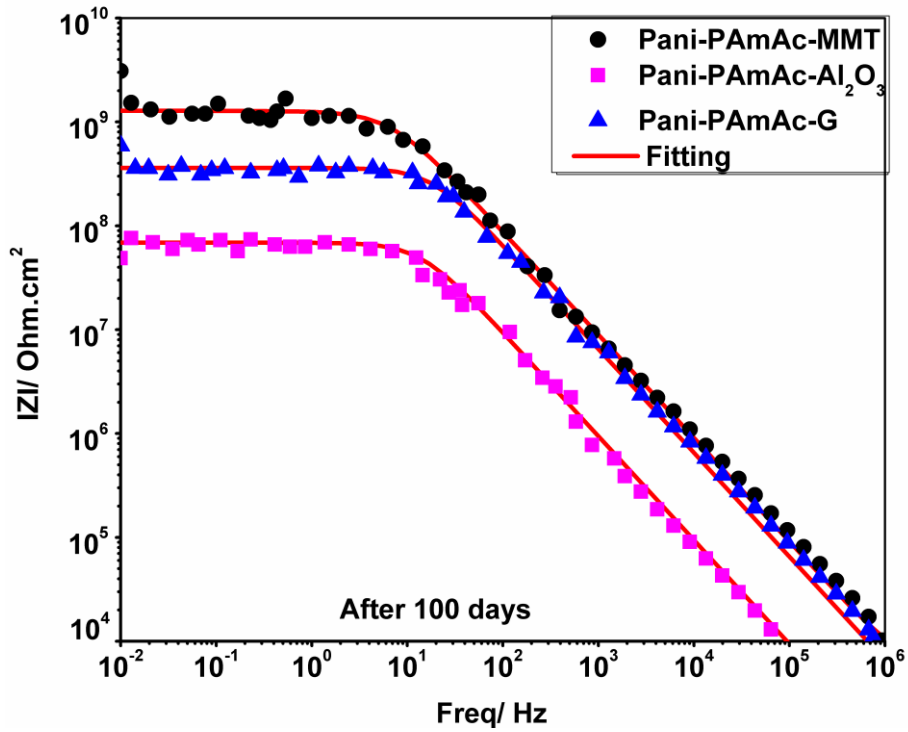

Fig. 4.63: Impedance behavior of Pani-PAmAc-Nanoparticles/Epoxy coatings after 100 days immersion in 0.6M NaCl solution

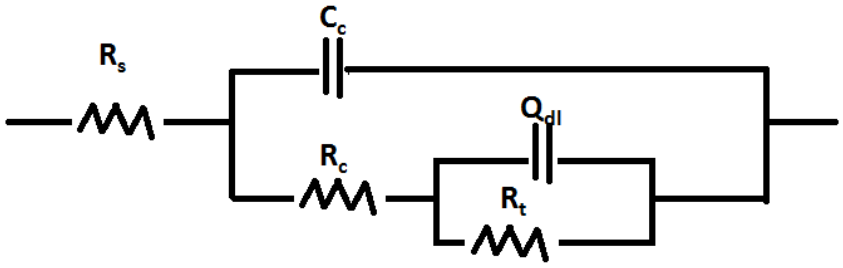

Fig. 4.64: Equivalent electrical circuit for Pani-PAmAc-Nanoparticles/Epoxy coatings

Fig. 4.65 shows the coating capacitance, C_c of Pani-PAmAc-MMT/Epoxy, Pani-PAmAc-Al_2O_3/Epoxy and Pani-PAmAc-G/Epoxy coatings with respect to immersion time in 0.6M NaCl. The coating capacitance of Pani-PAmAc-Al_2O_3 and Pani-PAmAc-G coatings remains almost constant up to 1440 h. Then the value of coating capacitance increased from 0.07 $nFcm^{-2}$ to 0.1 $nFcm^{-2}$ during 1680 h of immersion due to diffusion of water into the coating. After that it reached to saturation level for some time and then reached to value of 1.0 $nFcm^{-2}$ after 2160 h of immersion. At the beginning of the immersion, the value of coating capacitance for Pani-PAmAc-MMT was found to be 0.003 $nFcm^{-2}$ and after immersion to 1200 h, it increased to 0.01 $nFcm^{-2}$. The final value of coating capacitance of Pani-PAmAc-MMT/Epoxy, Pani-PAmAc-Al_2O_3/Epoxy and Pani-PAmAc-G/Epoxy coatings after 2400 h of immersion was 0.03 $nFcm^{-2}$, 0.5 $nFcm^{-2}$ and 1.8 $nFcm^{-2}$, respectively. The result shows that the addition of nanoparticles into the Pani-PAmAc coating matrix decreases the diffusion of electrolyte through the coating and prevents corrosion of the substrate.

Fig. 4.66 shows the coating resistance, R_c of the Pani-PAmAc-MMT/Epoxy, Pani-PAmAc-Al_2O_3/Epoxy and Pani-PAmAc-G/Epoxy coatings with respect to immersion time in 0.6M NaCl. R_c is related to electrical resistance to ionic transfer through the coating pores, which reflects the permeability of coating to the electrolyte solution. The value of coating resistance of the Pani-PAmAc-G coating decreased from 91000 MΩ cm^2 to 5700 MΩ cm^2 after 960 h of immersion. After 960 h immersion, the coating resistance stabilized for some time due to formation of aluminium oxides product which possibly block the pores and finally value decreased to 480 MΩ cm^2. The value of Pani-PAmAc- Al_2O_3 coating was 100000 MΩ cm^2 in the initial immersion period, which was almost equal to Pani-PAmAc-G coating. Then the value decreased to 9800 MΩ cm^2 after 720 h of immersion and finally to 1600 MΩ cm^2. The coating resistance value for the initial immersion value of Rc for the Pani-PAmAc-MMT coating was 130000 MΩ cm^2 which further decreased to 12000 MΩ cm^2 after 2400 h of immersion.

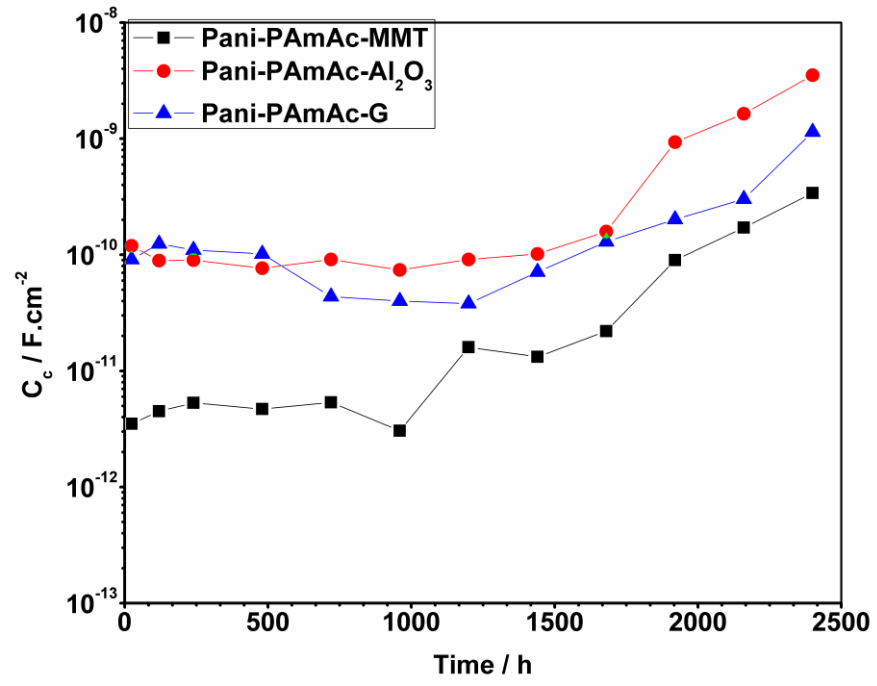

Fig. 4.65: Coating capacitance of the Pani-PAmAc-Nanoparticles/Epoxy coatings with respect to immersion time in 0.6M NaCl solution

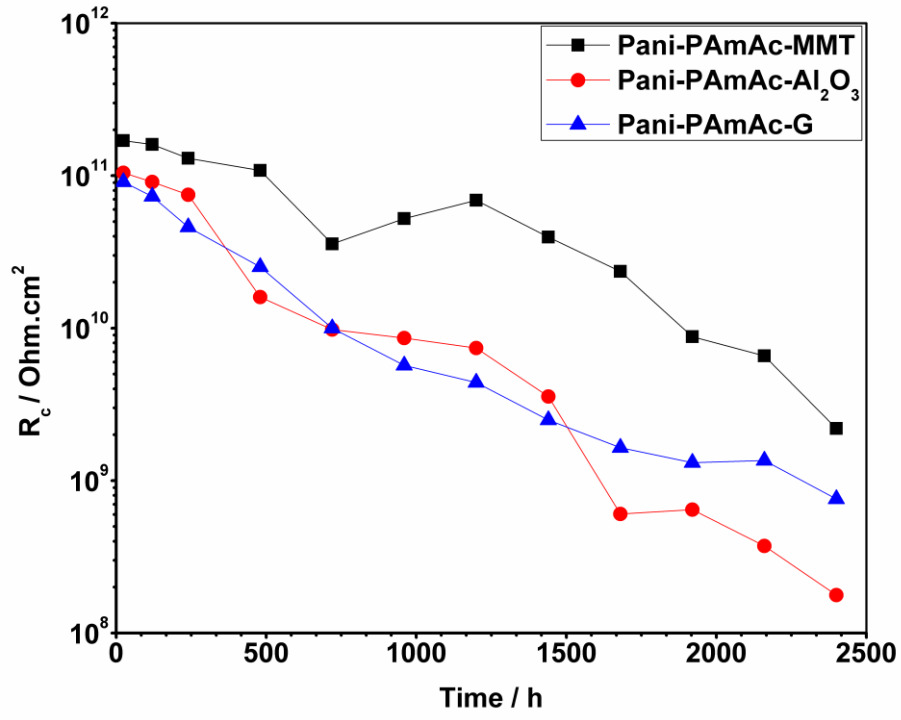

Fig. 4.66: Coating resistance of the Pani-PAmAc-Nanoparticles/Epoxy coatings with respect to immersion time in 0.6M NaCl solution

Fig. 4.67 shows the charge transfer resistance, R_t of the Pani-PAmAc-MMT/Epoxy, Pani-PAmAc- Al_2O_3/Epoxy and Pani-PAmAc-G/Epoxy coatings with respect to immersion time in 0.6M NaCl. The value of charge transfer resistance, R_t is a measure of the resistance to the electron transfer across the metal surface and is inversely proportional to corrosion rate [34]. The value of R_t for the Pani-PAmAc-G coating decreased slowly from 9 GΩ cm^2 to 3 GΩ cm^2 after 1440 h of immersion and reached to final value 6 GΩ cm^2 after 2400 h of immersion. For the Pani-PAmAc- Al_2O_3 coatings the value of R_t gradually decreased from 52 GΩ cm^2 to 10 GΩ cm^2 after 1920 h of immersion. The value for Pani-PAmAc-MMT coating was 110 GΩ cm^2 at the initial immersion period, then 94 GΩ cm^2 after 720 h and then stabilized up to 2160 h and then decreased again. At last the value reached to 64 GΩ cm^2 after 2400 h of immersion, which was of about one order of magnitude higher than that of Pani-PAmAc-G [113, 114].

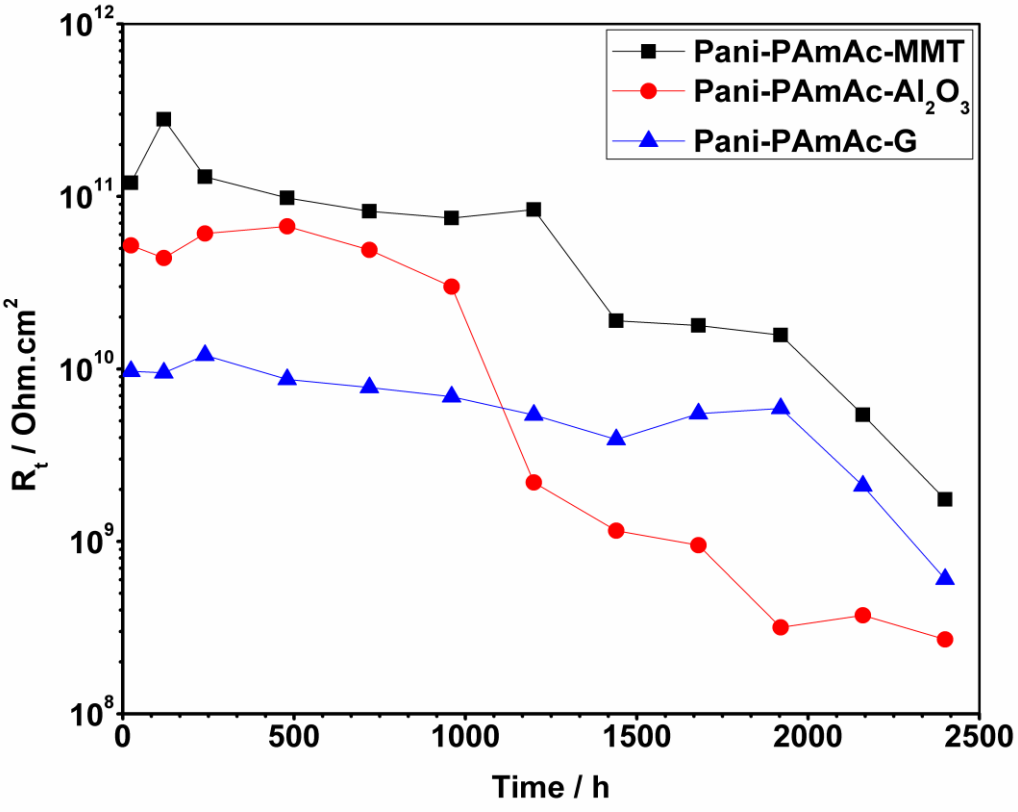

Fig. 4.67: Charge transfer resistance of the Pani-PAmAc-Nanoparticles/Epoxy coatings with respect to immersion time in 0.6M NaCl solution

4.5.6 Adhesion Test of Pani-PAmAc-Nanoparticles/Epoxy coating

High adhesion strength of the coatings is a basic requirement for good corrosion protection. The results of adhesion measurements by the crosshatch method are shown in Table 4.8. It is observed that the adhesion strength of all the nanoparticle containg coatings were 5B, which is 'Excellent', prior to exposure to 0.6M NaCl. The adhesion strength was also measured after 100 days exposure to the 0.6M NaCl. There was no change in the adhesion strength even after long term immersion. No delamination of coating was observed after long term exposure.

Table 4.8: Adhesion test of Pani-PAmAc-MMT/Epoxy, Pani-PAmAc-Al_2O_3/Epoxy and Pani-PAmAc-G/Epoxy coatings

Coating System	Adhesion Test (ASTM 3359)	
	Before exposure	After exposure (0.6M NaCl)
Pani-PAmAC-MMT	5B	5B
Pani-PAmAC-Al_2O_3	5B	5B
Pani-PAmAC-G	5B	5B

4.5.7 Salt Spray Test of Pani-PAmAc-Nanoparticles/Epoxy coating

The coated samples were tested in the salt-fog spray chamber for 2400 h as per ASTM B 117 as shown in Fig. 4.68. It was observed that Pani-PAmAc-MMT/Epoxy coating performs significantly better than the Pani-PAmAc-Al_2O_3/Epoxy and Pani-PAmAc-G/Epoxy coatings. The high corrosion protection performance was due to MMT clay which increases the tortourous path of the coating and resists reaching the electrolyte to the metal. All the formulation shows good results upto 2000 h and then degradation of coating starts.

Fig. 4.68: Photographs of Pani-PAmAc-Nanoparticles/Epoxy coatings after 2400 h to salt spray exposure

4.5.8 UV-Weatherometer of Pani-PAmAc-Nanoparticles/Epoxy coatings

Accelerated weathering of coated specimen was carried out to simulate outdoor weathering using combination of UV light and water condensation (ASTM-G53). Damage caused by the weathering cycle was assessed using visual assessment, colour change and gloss measurement.

Visual examination of the exposed specimen shows that there were no white pits of corrosion product, cracking or loss of adhesion (Fig. 4.69). The colour change parameters of Pani-PAmAc-Nanoparticles/Epoxy coating are shown in Fig. 4.70. The nanoparticles modified Pani-PAmAc/Epoxy showed less colour change values after 1200 h of exposure. The colour change values of all the coatings increases after 2400 h of exposure. The gloss retention parameters of Pani-PAmAc-Nanoparticles/Epoxy coating are shown in Fig. 4.71. The gloss retention of all the coating was found approximately 80% after 1200 h of exposure and ~ 60% after 2400 h of exposure. This shows that there was not drastic change in the gloss of the coatings. These nanoparticles act as UV blockers in the Pani-PAmAc/Epoxy system and proved to be effective means for enhancing the weathering resistance of the coatings. Therefore, coating can be used for outdoor application without modification.

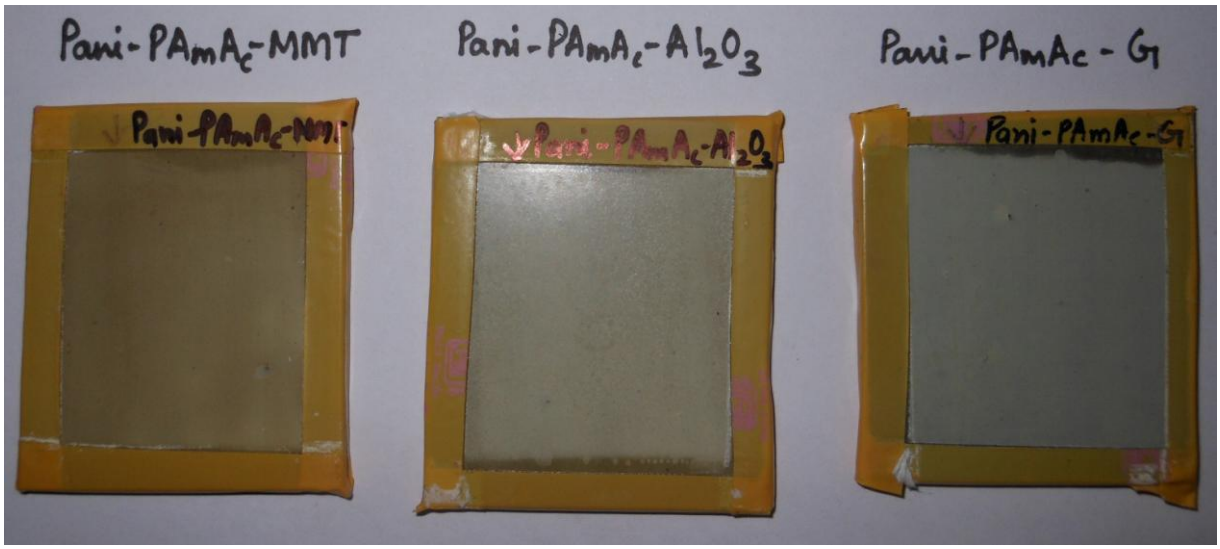

Fig. 4.69: Photographs of Pani-PAmAc-Nanoparticles/epoxy coatings after 2400 UV-weatherometer exposure

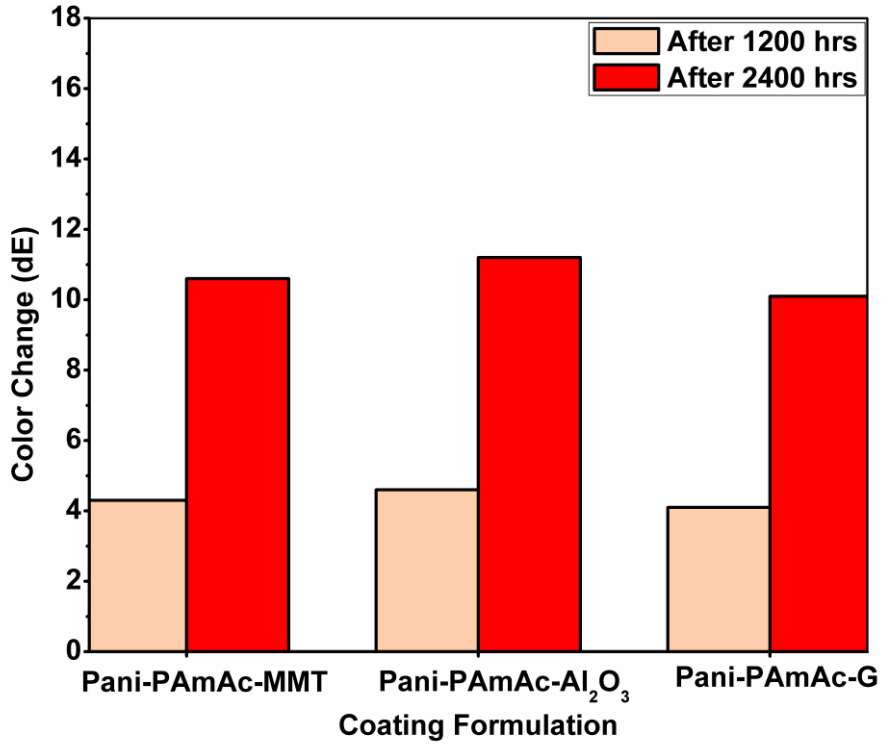

Fig. 4.70: Color change (dE) for Pani-PAmAc-Nanoparticles/Epoxy coatings

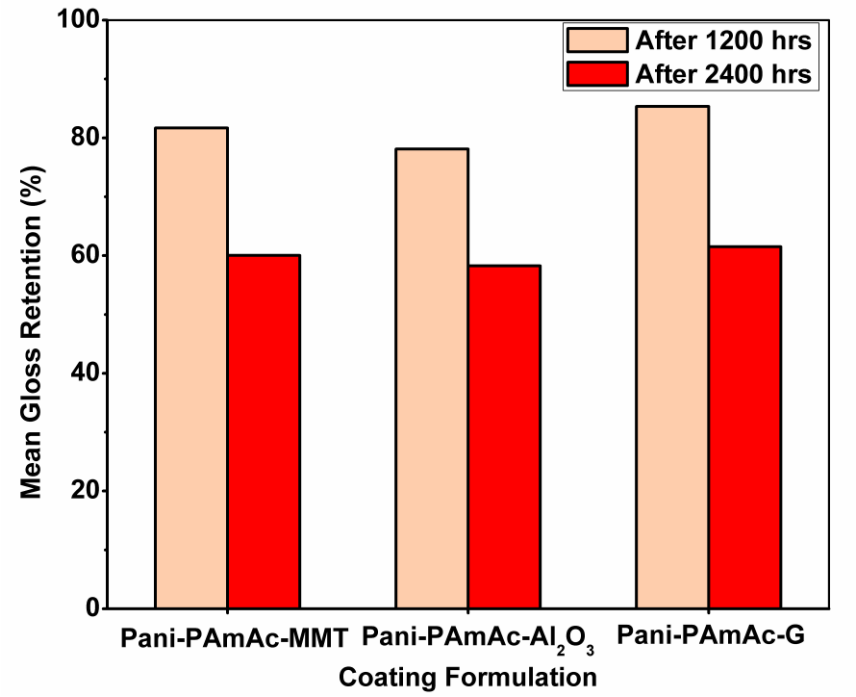

Fig. 4.71: Mean gloss retention (%) of Pani-PAmAc-Nanoparticles/Epoxy coatings

4.5.9 Mechanical Properties of the Pani-PAmAc-Nanoparticle/Epoxy coating

The tensile strength of Pani-PAmAc-MMT/Epoxy, Pani-PAmAc-Al_2O_3/Epoxy and Pani-PAmAc-G/Epoxy films were 5.7, 5.3 and 5.5 MPa, respectively as shown in Fig. 4.72. It was found that there was very less difference in the tensile properties of Pani-PAmAc-MMT/Epoxy, Pani-PAmAc-Al_2O_3/Epoxy and Pani-PAmAc-G/Epoxy films. It was observed that the addition of nanoparticles into the Pani-PAmAc/Epoxy system steadily decreases the tensile strength. The increase in properties of Pani-PAmAc-MMT was ascribed to dispersion of nanosize clay particles which also acts as reinforcing filler for the coating matrix and modifies the mechanical properties of the polymer. Pani-PAmAc-G also imparts good tensile strength and stiffness properties to the epoxy matrix. This was attributed to the large aspect ratio of the graphene sheets, the molecular-level dispersion of graphene sheets in the coating matrix, and the strong interfacial adhesion due to H-bonding between Pani-PAmAc-G and epoxy matrix [115, 116].

The % elongation of Pani-PAmAc-MMT/Epoxy, Pani-PAmAc-Al_2O_3/Epoxy and Pani-PAmAc-G/Epoxy films were 1159, 983 and 1032 respectively as shown in Fig. 4.73. It was found that the higher % elongation of Pani-PAmAc-MMT/Epoxy films can be attributed to

the exfoliation and good dispersion of clay particles that restricts the mobility of polymer chains as well as to the good interfacial adhesion between the particles and the epoxy matrix. Improved in mechanical properties is an indicative of improved mechanical interlocking and adhesion between the nanoparticles, conducting polymer and the polymer matrix. The hardness values of Pani-PAmAc-MMT/Epoxy, Pani-PAmAc-Al_2O_3/Epoxy and Pani-PAmAc-G/Epoxy films were 4H, 4H and 3H respectively as shown in Table 4.9. Improvement in the mechanical properties of polymer nanocomposites is not only dependent on the properties of nanoparticles but also on the properties of the host polymer matrixes. As a result, the degree of improvement in all these properties varies for different nanocomposites.

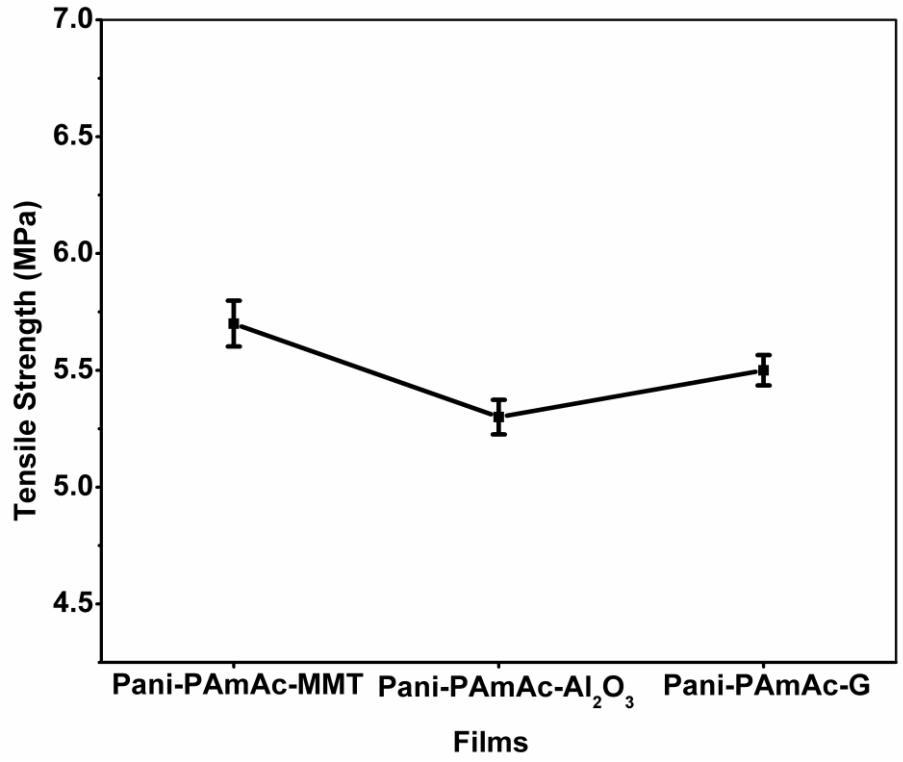

Fig. 4.72: Tensile Strength of Pani-PAmAc-Nanoparticles/epoxy films

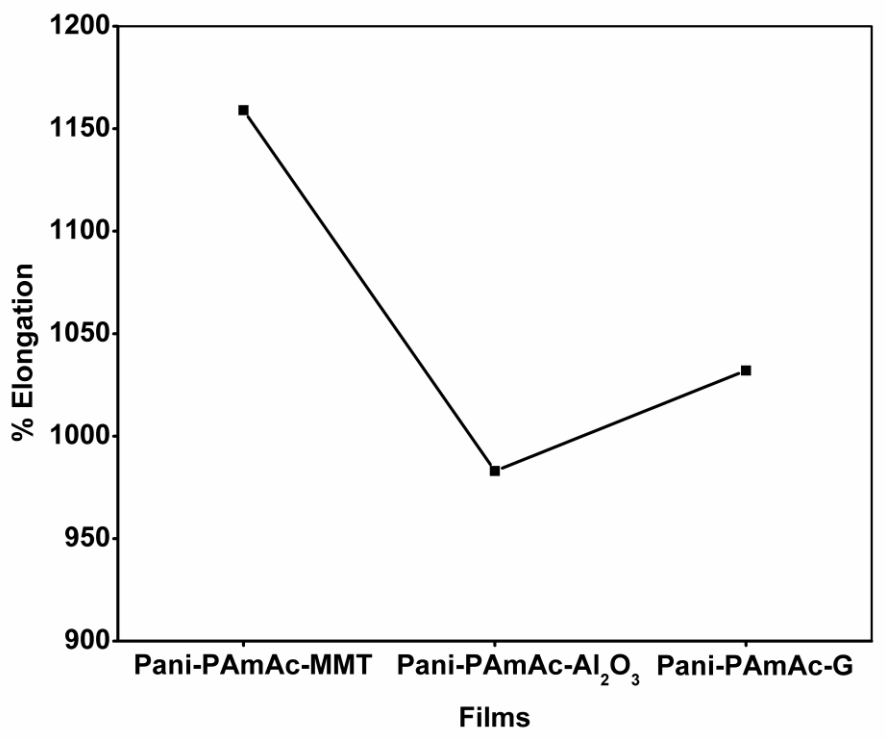

Fig. 4.73: % Elongation of Pani-PAmAc-Nanoparticles/epoxy films

Table 4.9: Hardness values of Pani-PAmAc-MMT/Epoxy, Pani-PAmAc-Al_2O_3/Epoxy and Pani-PAmAc-G/Epoxy films

Coating System	**Pencil Hardness Values (ASTM D3363)**
Pani-PAmAC-MMT	4H
Pani-PAmAC-Al_2O_3	4H
Pani-PAmAC-G	3H

Chapter 5 Corrosion Protection Mechanism

Mechanism of corrosion protection using polyaniline coatings

Two mechanisms have been proposed for the corrosion protection of the AA2024-T3 alloy using lignosulfonate doped polyaniline coatings.

(i) Physical barrier effect

Pani-LGS/Epoxy coating works as a barrier against the diffusion of the electrolyte and aggressive ions, protecting the substrate metal (i.e. a better barrier than epoxy alone).

(ii) Anodic protection

Under immersion conditions, oxidation of metal can act as a trigger for the reduction of the polyaniline coating i.e. Pani (ES) to Pani (EB), leading to the formation of a passive, protective aluminium hydroxide layer [117, 118].

$$2Al^{+3} + \text{Pani-LGS (ES)} + 3H_2O \longrightarrow 2Al(OH)_3 + \text{Pani-LGS (EB)} + 6H^{+} \text{--- (Eq 1)}$$

In a quiescent 0.6M NaCl environment, conversion of Pani-LGS (EB) to Pani-LGS (ES) takes place via the oxygen reduction reaction.

$$2O_2 + 4H_2O + \text{Pani-LGS (EB)} \longrightarrow \text{Pani-LGS (ES)} + 8OH^{-} \text{---------- (Eq 2)}$$

The mechanism may change depending upon whether the coating is defect free or having minor or major defect or on the modifications of the coating (use of dopant, polyelectrolyte and nanoparticles).

5.1 Pani-LGS/Epoxy coating on AA2024-T3 alloy

Case 1: Defect free coating

Initial corrosion protection of AA2024-T3 alloy is due to formation of aluminium hydroxide layer beneath the epoxy based Pani-LGS coating. The coating provides barrier protection and remains intact till it is not exposed to corrosive environment. However, when a sample is exposed to corrosive environment (0.6 M NaCl), initially there is no defect due to conducting nature of the coating. As long as the Pani-LGS is in conducting (ES) form, it can provide protection to the base alloy and this persists whilst there are no defects in the coating. Fig. 5.1 shows the mechanism of protection of AA2024-T3 using lignosulfonate doped polyaniline epoxy coating in 0.6M NaCl.Coating will start deteriorating usually after 15-20 days exposure.

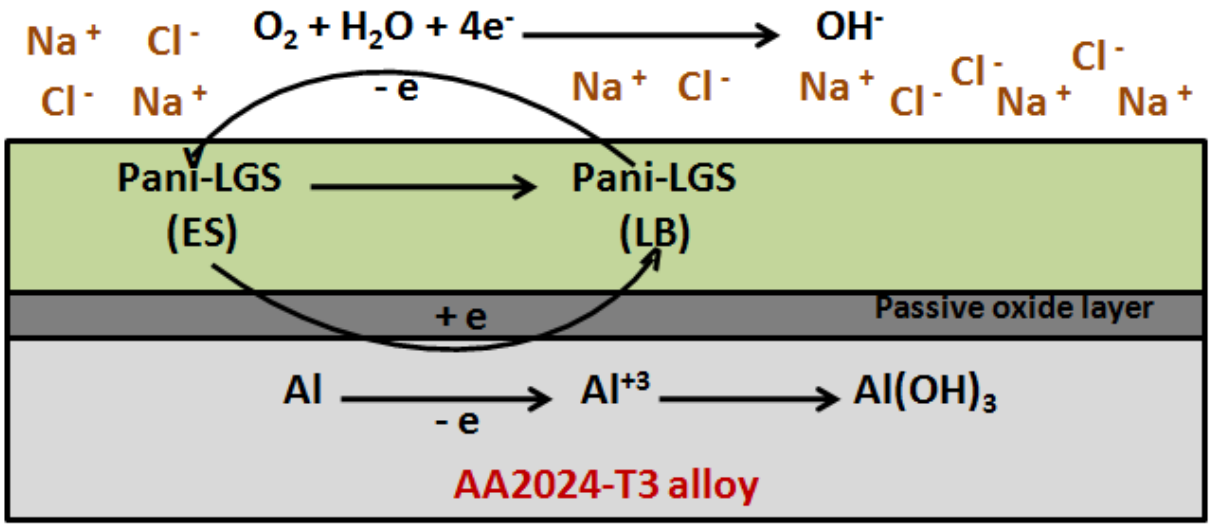

Fig. 5.1: Mechanism of Pani-LGS/Epoxy coating in 0.6M NaCl solution (defect free coating)

Case 2: Coating with minor defects (After 15-20 days exposure)

After 15 days exposure, when minor defects start forming; lignosulfonate dopant reaches at the defect site and helps to protect the metal from corrosion as shown in Fig 5.2 [119-121]. Lignosulfonate anions which exhibit corrosion inhibiting properties [40] are present in the coating to compensate the positive charge of the oxidized polyaniline backbone. After 15-20

days immersed condition when migration of chloride through the coating takes place and this may result in small defects, resulting in coating deterioration Pani-LGS/Epoxy coatings can also exhibit self-healing property during short term immersion, in which the passive oxide is spontaneously repaired after it develops small defects. This is because when the coating and passive oxide damage locally, sulfonate ions of lignosulfonate migrate and reach at the defect site [122, 123]. This will also lead to the inhibition of the cathodic reaction and will slow down the production of hydroxyl ions and thus decrease the rate of delamination. The sulfonate ions react with Al^{+3} ions at the defect site to produce the metal-sulfonate complex which will further prevent corrosion. This hypothesis was well supported by the EIS and FTIR spectra with a peak, at 1084 cm^{-1} of metal dopant complex.

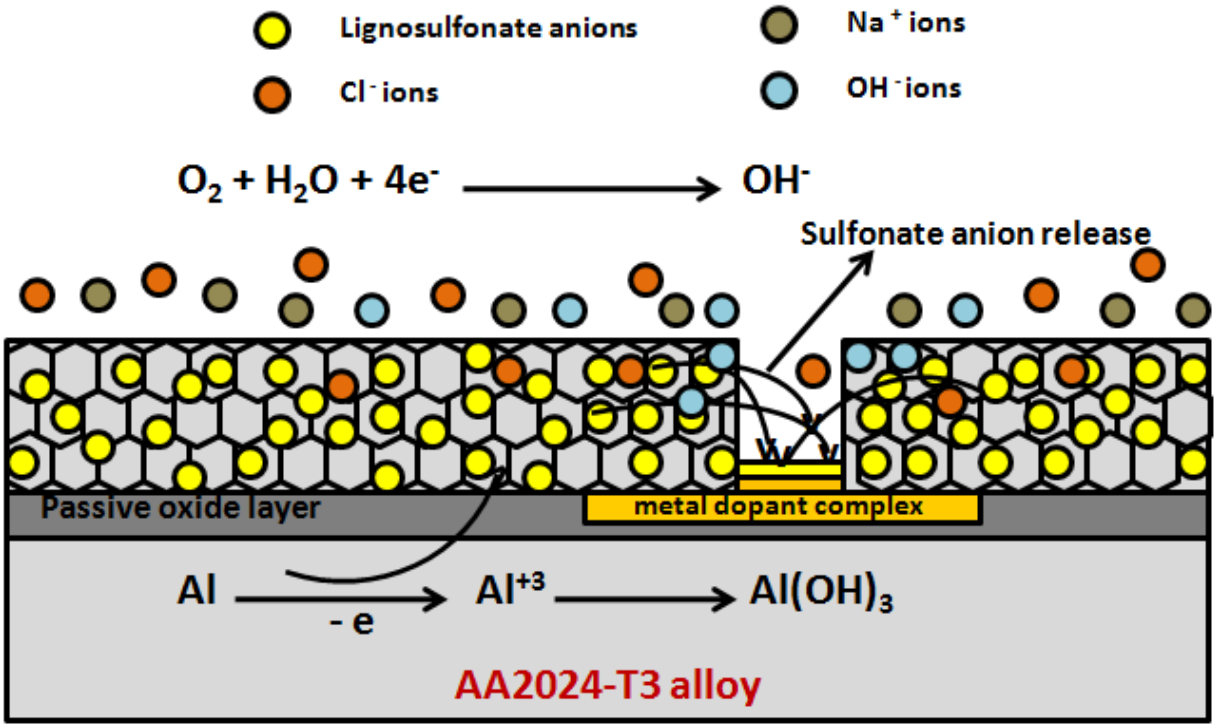

Fig. 5.2: Mechanism of Pani-LGS/Epoxy coating in 0.6M NaCl solution (During 10-25 days immersed condition)

Case 3: Coating with major defects (After 30 days exposure)

After 30 days of immersion in 0.6M NaCl, Pani-LGS/Epoxy coating is no longer an effective corrosion resistant coating as shown in Fig 5.3. All lignosulfonate dopants are consumed by the defects. Coating at this stage loses its conductivity and defects keeps on increasing in aggressive environment. Pani-LGS coating now behaves just as a barrier coating which is not sufficient to protect alloy in the aggressive environment and this lead to enhance corrosion

reaction. The delay in corrosion product formation also depends on the polyaniline concentration. However, at the optimum concentration (5wt%), the Pani-LGS coating shows protective nature due to sufficient amount of LGS and Pani in the epoxy coating. For corrosion protection, the coating must be able to counter small defects.

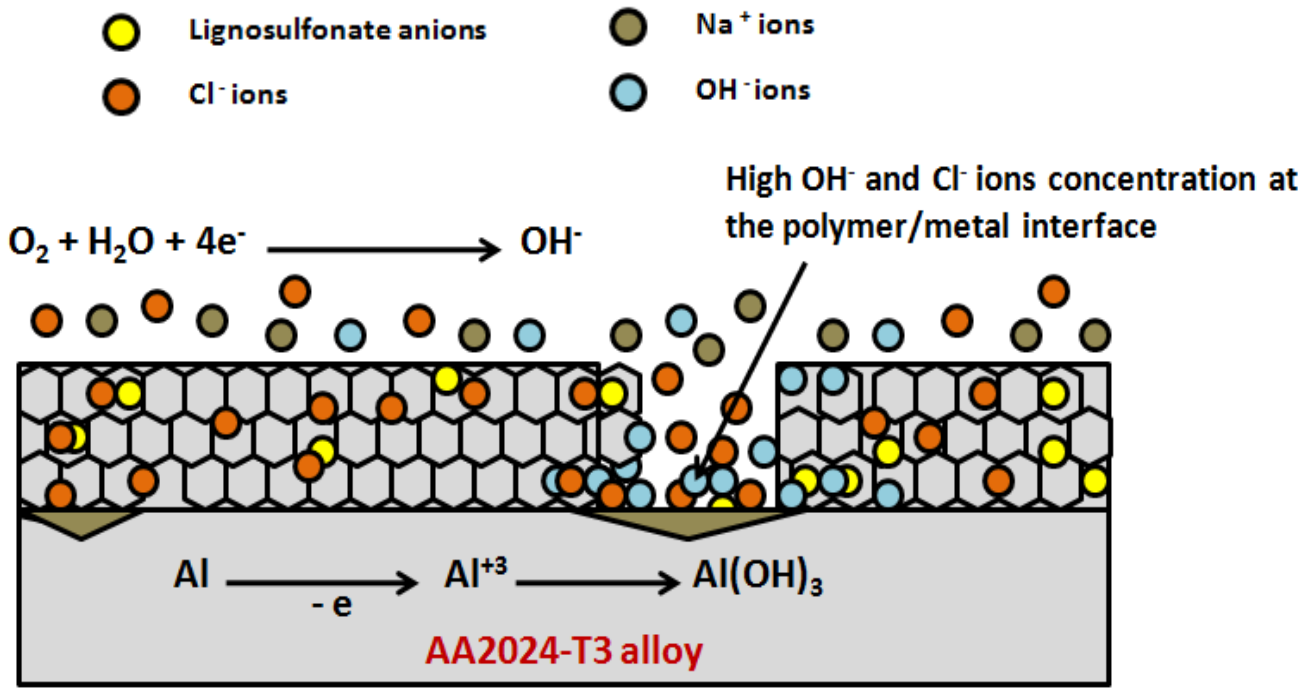

Fig. 5.3: Mechanism of Pani-LGS/Epoxy coating in 0.6M NaCl solution (After 30 days immersed condition)

5.2 Pani-PAmAc/Epoxy coating on AA2024-T3 alloy

The synthesised microgels (poly(acrylamide co acrylic acid)) were capable of forming a uniform dispersion in water media, and the active acidic groups present in the microgels adsorb the monomer units of aniline and helped in the polymerization within the microgel environment itself and also promoted adhesion to metal substrates. In addition, the free polymerised particles present in the solvent were probably deposited over the micellar network, making the interaction more intimate. This schematic diagram (Fig. 5.4) shows how Pani-LGS is incorporating into a poly (acrylamide co acrylic acid) microgel structure and formed composites.

During polarisation of double stranded conducting polymer, deprotonation of the carboxylic group occurs resulting in a net negative charge in the conductive polymer. This was balanced to maintain electro neutrality. One positive ion to balance the negative charge would be the Al^{+3} ions from dissolution of the substrate. The carboxylic ions in the conductive polymer would bind the aluminium ions in the passive layer in a fashion similar to the binding between multidentate polymer and a positively charged ion. An electrostatic attraction between the opposite polarity ions would stabilize the passive layer and essentially block the metal ions from penetrating through the conducting polymer. The difficulty of the aluminium ions being dissolved in the solution is probably the reason for the formation of a tight and stable passive layer. The formation of an aluminium hydroxide layer provides protection to the metal and prevents it from corrosion. As long as it is in conducting (ES) form, it can provide protection to the metal and this can persist whilst there are no defects in the coating. The polarisation data indicate that the corrosion potential shifted to noble direction (anodic protection) which was due to a redox activity of Pani-PAmAc coating. Higher impedance of Pani-PAmAc coating was observed as compared to Pani-LGS. This could delay the diffusion of electrolyte through the coating. Even after 50 days immersion in 0.6M NaCl, Pani-PAmAc/Epoxy coating will able to provide corrosion protection to the metal - due to polyelectrolyte, which prevent from dopant loss and provide electrical conductivity to the polymer backbone. EIS results show that after 50 days immersion in 0.6M NaCl, impedance of epoxy and Pani-LGS coating reaches to very lower values, whereas Pani-PAmAc coating show still higher impedance values. Salt spray test and adhesion test results are also in support of this mechanism.

Case 1: Defect free coating

The one draw-back with the LGS doped Pani/epoxy coatings are that these anionic dopants are easily lost or segregated after long term exposure to heat, moisture, and rain water. Dopants are utilized at the defect site for the protection and once all the dopants reaches at the defect site, the conductivity of polymer decreases, resulting in the loss of corrosion resistance. A double stranded conducting polymer comprising of polyaniline and a functional co-polymer poly (acrylamide co-acrylic acid) was synthesized in the presence of lignosulfonate and incorporated in epoxy matrix and studied for its properties.

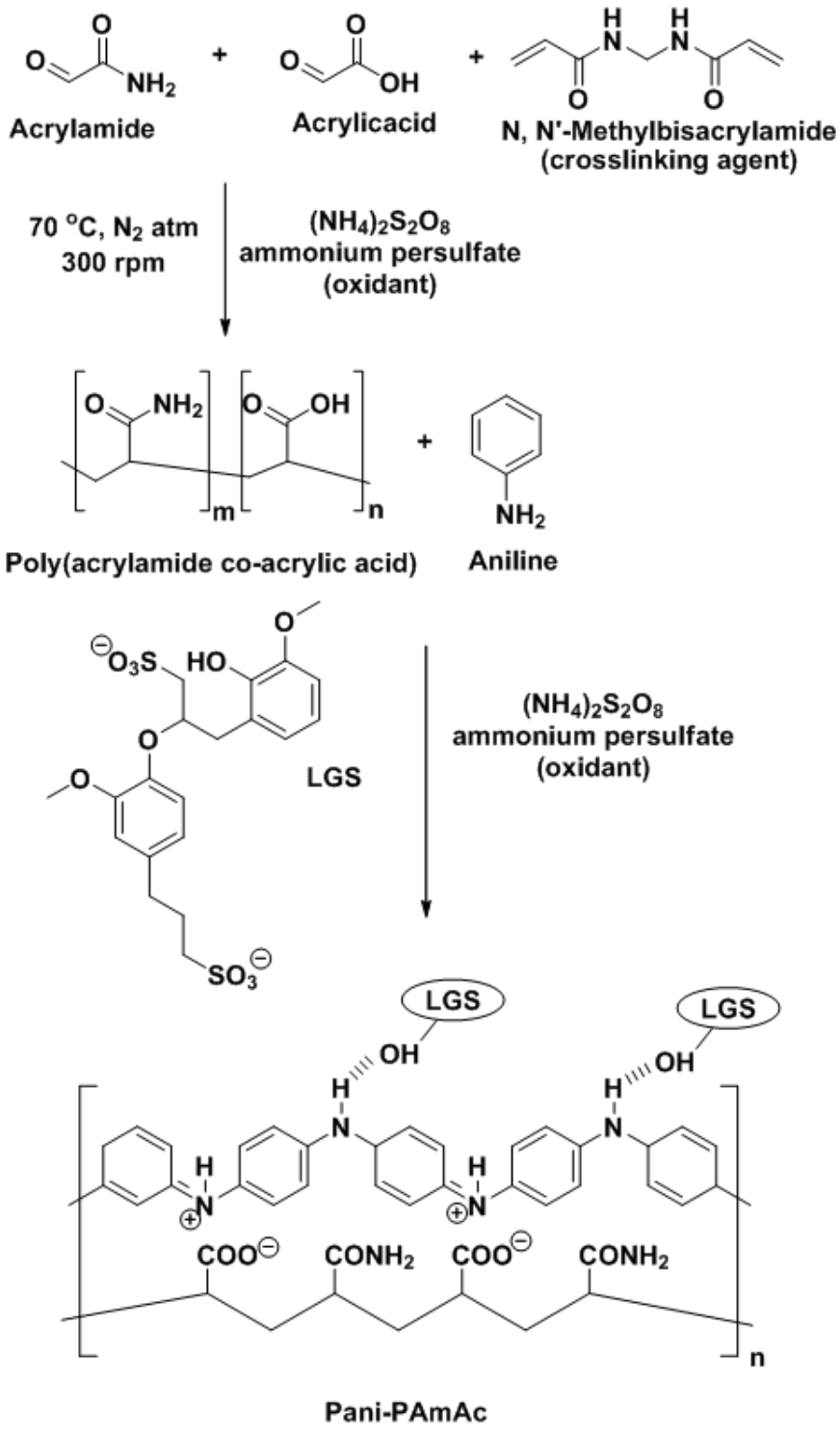

Fig. 5.4: Schematic synthesis of lignosulphonate doped Polyaniline-Poly(acrylamide co-acrylic acid) [Pani-PAmAc]

In Pani-PAmAc coating formulation, free lignosulfonate anions and bound poly (acryl amide co acrylate) anions are present to compensate the positive charge of the oxidized polyaniline backbone. At initial immersed condition, the coating behaviour is same as Pani-LGS coating.

Case 2: Coating with minor defects (After 15-20 days exposure)

In case of small defects in the coating, free lignosulfonate anions are released from the coating by the reduction of the polyaniline, induced by the oxidation of the metal [118-120]. Their release passivates an exposed defect, leading to slowing down the corrosion process as shown in Fig. 5.5. Whereas bound poly(acryl amide co-acrylic acid) polymeric dopant are maintaining the electrical conductivity of the coating.

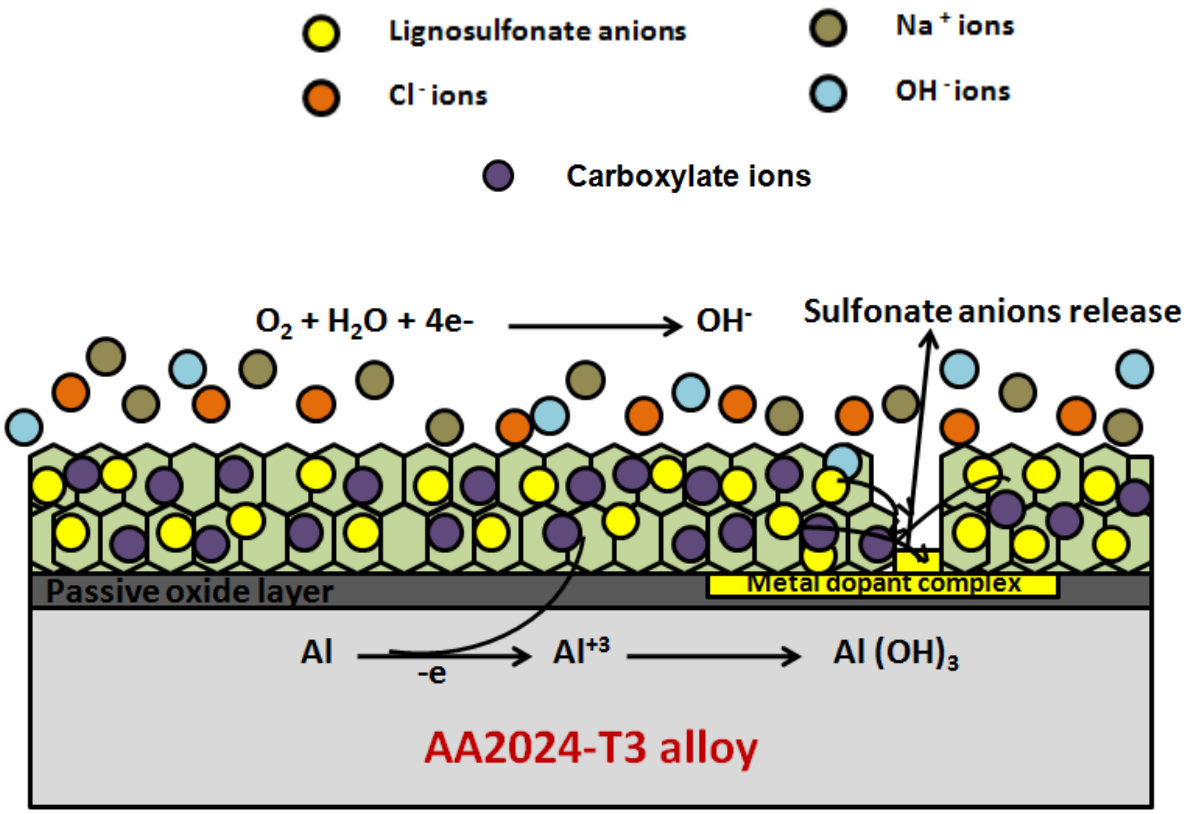

Fig. 5.5: Mechanism of Pani-PAmAc/Epoxy coating in 0.6M NaCl solution (During 15-20 days immersed condition)

After 30 days exposure, when all the free lignosulfonate ions are utilized by the defect site for the metal protection, the carboxylate ions of the poly (acrylamide co-acrylate) then come into to protect the base alloy from corrosion in aggressive environment. Polyaniline is still in conducting form even after loss of the free lignosulfonate dopant. Now the conductivity of the polyaniline is maintained by the poly (acrylamide co-acrylate) ions. Once the free lignosulfonate ions are used up then the carboxylate helps in the corrosion protection as shown in Fig. 5.6. Pani-PAmAc/Epoxy coatings can provide the protection for longer time as compared to the Pani-LGS coating.

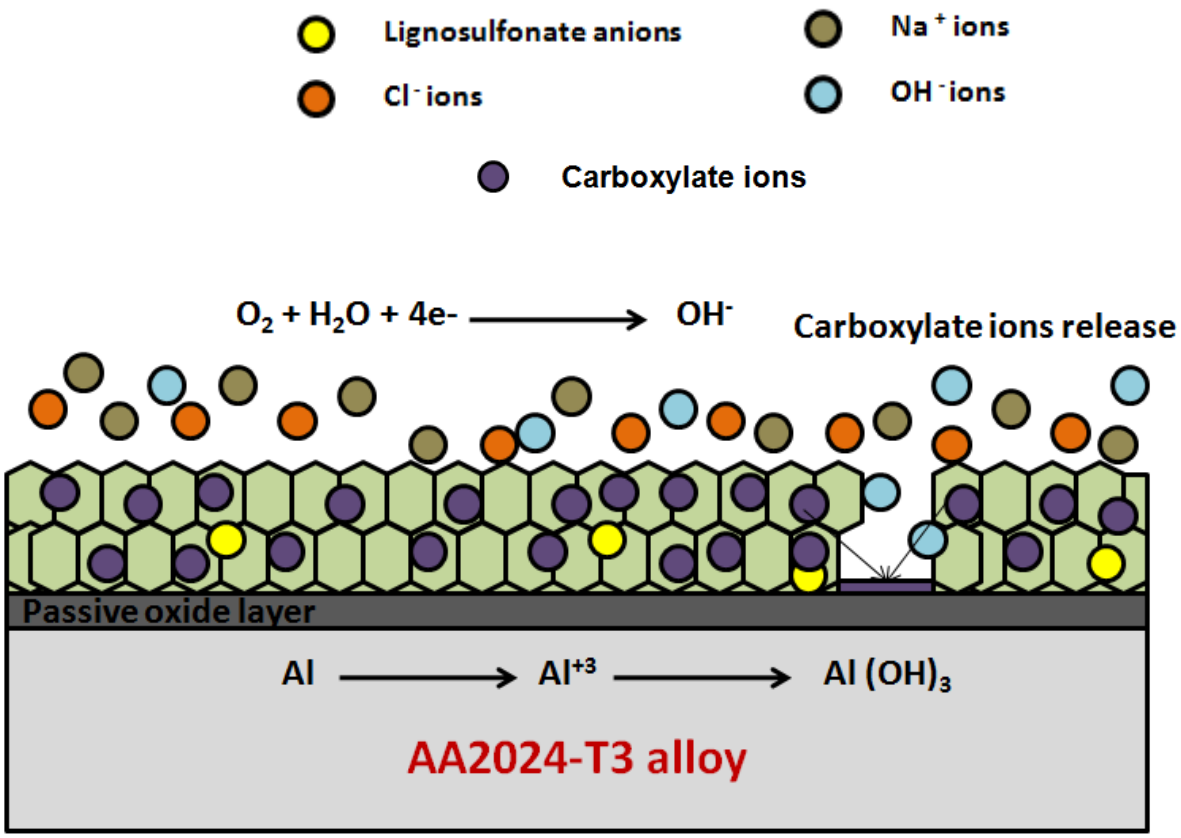

Fig. 5.6: Mechanism of Pani-PAmAc/Epoxy coating in 0.6M NaCl solution (During 30-45 days immersed condition)

Case 3: Coating with major defects (50 days exposure)

After 50 days of immersion in 0.6M NaCl, Pani-PAmAc/Epoxy coating will not be able to provide corrosion protection to the metal - due to utilisation of both free lignosulfonate and bound poly(acrylamide co acrylate) ions by the defect site, as a result of which no redox activity of polyaniline coating was observed and coating losses its conductivity. Now the coating will behave as non conducting (EB) and act just as a normal barrier coating. An aggressive ion reaches to the metal through the coating leading to enhanced corrosion as shown in Fig. 5.7. High concentration of these aggressive ions is a key reason that leads to corrosion product formation and disbondment of the coating.

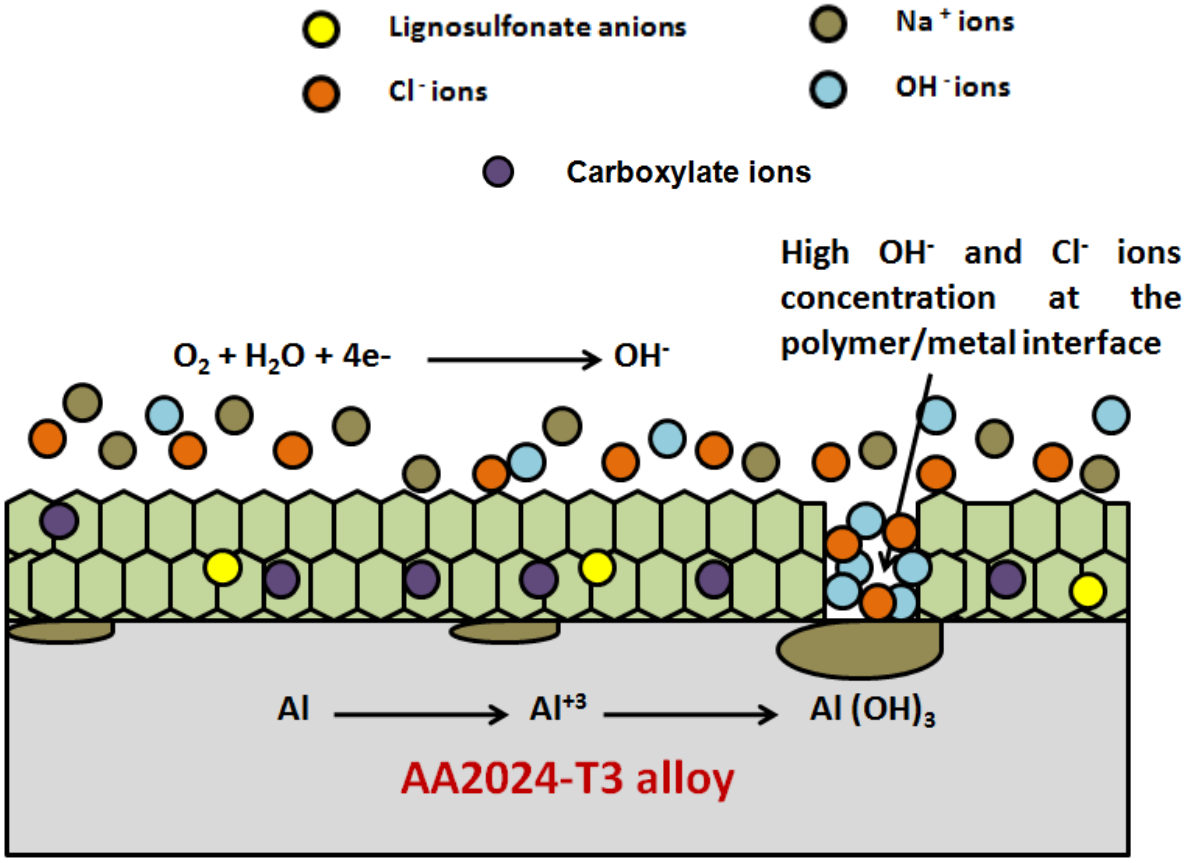

Fig. 5.7: Mechanism of Pani-PAmAc/Epoxy coating in 0.6M NaCl solution (after 50 days immersed condition)

5.3 Pani-PAmAc-Nanoparticles/Epoxy coating on AA2024-T3 alloy

Nanoparticles in the Pani-PAmAc coating retard the diffusion process and protect the metal for longer time as compared to above formulated coatings. The diffusion process of electrolyte will be delayed due to increase in torturous path of the coating because of the well dispersed nanoparticles and resulting in improvement of corrosion resistance. Due to large surface area, nanoparticles are more efficient than microparticles, required in lower concentration to obtain excellent results. In case of Pani-PAmAc-Nanoparticles/Epoxy coating, initial protection of metal is depending on the diffusion process of electrolyte through the coating. Pani-PAmAc-Nanoparticles coating protect the base alloy for ~ 80 days. After ~80 days of immersion in 0.6M NaCl, Pani-PAmAc/Epoxy coating protection properties start decreasing as shown in Fig 5.8. Pani-PAmAc-MMT/Epoxy shows better protection due to nanoclay which has excellent barrier properties to aggressive environment. Pani-PAmAc-G/Epoxy shows excellent corrosion resistance even after long term immersion due to conducting nature of the graphene which maintain the conductivity of the coating by redox

reaction and helps in protection of the metal. Pani-PAmAc- Al_2O_3/Epoxy also shows good resistance towards the environment due to Al_2O_3 nanoparticles in the coating.

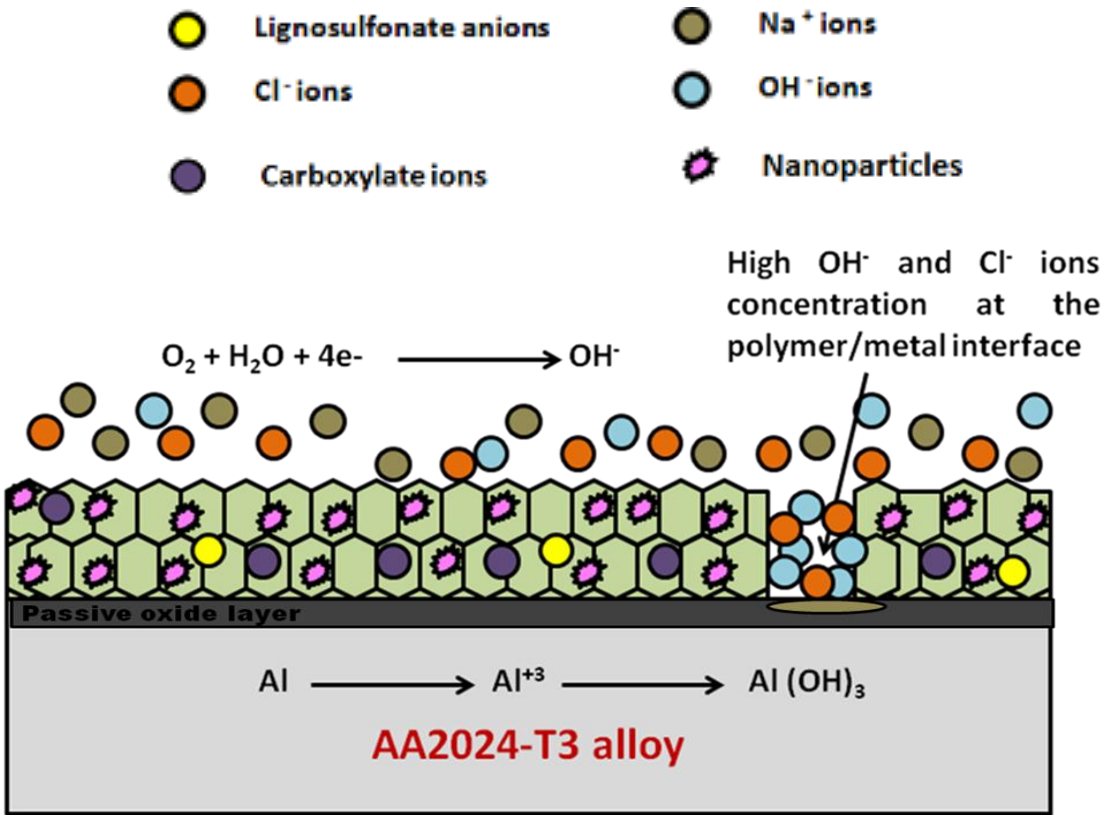

Fig. 5.8: Mechanism of Pani-PAmAc-Nanoparticles/Epoxy coating in 0.6M NaCl solution (~ 80 days immersed condition)

It is difficult to elucidate the nature of interactions of the Pani with different inter metallic particles. As such the data presented in Fig 4.18, 4.39 and 4.60 represent average *E*corr values, comprising contributions from different intermetallic particles such as S-phase, Cu particles and iron rich particles in addition to the Al matrix. However, from previous studies on the stability of ES in contact with oxide-covered metals, it can be predicted that the formation of basic MgO at the surface of Al_2CuMg particles would tend to de-dope ES to form LB. Conversely, ES would be expected to maintain ennoblement of Al–Cu–Fe–Mn intermetallic particles. It might therefore be expected that the presence of ES-induced oxide films on partially dissolved intermetallic particles would hamper local electrochemical activity, such as dealloying and Cu replating, which are implicated in corrosion on AA2024-T3 and also contribute to the overall polyaniline inhibition mechanism [67].

Chapter 6 Conclusion

6.1 Conclusion

An epoxy based anticorrosive polyaniline, modified with polyelectrolyte and nanoparticles coating was developed for aircraft AA2024-T3 alloy. These types of coatings have been developed for the first time. Successful synthesis was possible, and the complementary characterisation methods including SEM, potentiodynamic polarisation, adhesion and salt spray test revealed that formulated coating was smooth and continuous, and capable of imparting significant corrosion protection.

From empirical tests herein, an ~5wt%Pani-LGS coating yielded the highest values of coating pore resistance, an electrical conductivity of 4.88 S/cm and a more compact microstructure as analysed via SEM analysis and best adhesion - even after 30 days immersion; when compared to the other coating formulations herein. A uniform distribution of polyaniline particles decreases the permeability of water and oxygen, increasing the corrosion protection efficiency. Corrosion inhibition was enhanced due to a thickened oxide layer and aided by what is posited to be the release of dopant at the defect site by formation of aluminum–sulfonate complex. Due to dopant loss long term corrosion protection was not possible by Pani-LGS.

Pani-LGS was modified with polyelectrolyte i.e. poly(acrylamide co acrylic acid) (Pani-PAmAc) which resulted in conductivity of 3.9 S/cm, maintain it for longer time and exhibited better corrosion resistance. Potentiodynamic polarisation results indicated a high resistance to electrochemical reactions for Pani-PAmAc/epoxy coatings even after 50 days exposure to 0.6M NaCl; which was physically reconciled from salt spray test data. This was attributed to the synergistic effect of polyaniline with poly(acrylamide co-acrylic acid) which prevents dopant loss and maintains the electrical conductivity of the coating, even after long term exposure to a corrosive environment.

Pani-PAmAc coating system was further modified by addition of nanoparticles (MMT/Al_2O_3/G) to enhance its barrier properties and there was also increase in electrical conductivity to 8.76 S/cm (in case of graphene). Incorporation of nanoparticles i.e. MMT,

Al_2O_3 and G increased the barrier torturous path of the coating and provided excellent corrosion resistance along with excellent mechanical and UV weathering properties. Potentiodynamic polarisation results indicated a lower corrosion rate for Pani-PAmAc-Nanoparticles/epoxy coatings even after 100 days exposure to 0.6M NaCl; which was reconciled from EIS data. This was attributed to the barrier effect of nanoparticles present in the Pani-PAmAc coating. The work also indicates promise for optimisation of this class of coatings for enhanced corrosion protection and potential for further functionalisation to promote self healing aspects – which would be required in order to be a viable chromate replacement.

A suitable corrosion protection mechanism for the developed coatings is proposed which helps in overcoming the defects by both barrier and anodic protection.This developed coating is a potential coating system for the aircraft alloy.

6.2 Suggestions for Future Work

Breakthrough in the use of conducting polymers will come not only from improving the existing materials, but also from creating new ones by the incorporations of other nanoscale fillers. The suggestions of the future work can be in several folds since there is huge potential of development in this new area. The first suggestion is to study the electrical conductivity in depth based on the preliminary results. Electrical conductivity of conducting polymers is always of great interest to scientists working in this area. The effect of incorporation of clay, graphene and carbon nano tubes on the conductivity of conducting polymer is important to the understanding of this kind of material. Our preliminary study of the effect of clay on the electrical conductivity of Pani, as reported in Fig.4.16, showed an interesting result. The interesting phenomenon is that incorporation of clay did not decrease the conductivity of Pani, on the contrary, the conductivity is enhanced. To a certain degree, nano-sized clay platelets carrying a negative charge serves as a dopant in the conducting polymer and facilitates the delocalization of electrons, thus the conductivity is improved. This idea is new and worth to be further verified to better understand this material. The mechanism of intercalation and exfoliation of clay in the nanocomposites needs further study. Attention should be drawn to the structure-property relationship. A full understanding of the behavior of this class of new material will be of benefit to the applications of conducting polymers in various fields.

References

1. Z. Szklarska Smialowska, Pitting corrosion of aluminum, Corros. Sci. 41 (1999) 1743–1767
2. J. Zhao, G. Frankel, R. L. McCreery, Frankel, R.L. McCreery, Corrosion Protection of Untreated AA-2024-T3 in Chloride Solution by a Chromate Conversion Coating Monitored with Raman Spectroscopy, J. Electrochem. Soc. 145 (1998) 2258-2264.
3. P. Leblance, G.S.Frankel, A study of corrosion and pitting initiation of AA2024-T3 using atomic force microscopy, J. Electrochem. Soc. 149 (2002) B239-B247.
4. G. S. Frankel, R. L. McCreery, Inhibition of Al Alloy Corrosion by Chromates, Electrochem. Soc. Interface 10 (2001) 34-38.
5. W. J. Clark, J. D. Ramsey, R. L. McCreery, G. S. Frankel, A galvanic corrosion approach to investigating chromate effects on aluminum alloy 2024-T3, J. Electrochem. Soc. 149(5) (2002) B179-B185.
6. R.G. Buchheit, R.P.Grant, p.f. Hlava, B. McKenzie, G. L. Zender, Local dissolution phenomena associated with S phase (Al_2CuMg) particles in aluminum alloy 2024-T3, J. Electrochem. Soc. 144 (1997) 2621-2628.
7. R.L.Twite, G.P.Bierwagen, Review of alternatives to chromate for corrosion protection of aluminum aerospace alloys, Prog. Org. Coat. 33 (1998) 91-100.
8. M. Rohwerder, A. Michalik, Conducting polymers for corrosion protection: What makes the difference between failure and success? Electrochim. Acta 53(3) (2007) 1300-1313.
9. S. C. Yang, Richard Brown, Water borne polymeric complex and anti corrosive composition, U.S. Patent No. US 6762238 B1 (2004).
10. A. Eftekhari, Nanostructured Conductive Polymers, Wiley, 2010, ISBN: 0470745851.
11. M.S. Nooshabadi, S.M.Ghoreishi, M. Behpour, Electropolymerised polyaniline coatings on aluminum alloy 3004 and their corrosion protection performance, Electrochim. Acta 54 (2009) 6989-6995.
12. K.G. Conroy, C.B. Breslin, The electrochemical deposition of polyaniline at pure aluminum: electrochemical activity and corrosion protection properties, Electrochim. Acta 48 (2003) 721-732.

13. D.E. Tallman, C. Vang, G.G. Wallace, G.P. Bierwagen, Direct electrodeposition of polypyrrole on aluminum and aluminum alloy by electron transfer mediation, J. Electrochem Soc. 149(3) (2002) C173- C179.
14. D. E.Tallman, G. Spinks, A. Dominis, G. G.Wallace, Electroactive conducting polymers for corrosion control, Part1. General Introduction and a review of nonferrous metals, J. Solid State Electrochem 6 (2002) 73-84.
15. D.E. Tallman, Y. Pae, G.P. Bierwagen, Conducting polymers and corrosion Pat 2: Polyaniline on aluminum alloys, Corrosion 56 (2000) 401-410.
16. L. Cecchetto, R. Ambat, A.J. Davenport, D. Delabouglise, J.P. Petit, O. Neel, Emeraldine base as corrosion protective layer on aluminum alloy AA5182: effect of the surface microstructure, Corros. Sci. 49 (2007) 818-829.
17. M. Kendig, M. Hon, L.Warren, 'Smart' corrosion inhibiting coatings, Prog. Org. Coat. 47 (2003) 183-189.
18. D. W. DeBerry, Modification of the electrochemical and corrosion behavior of stainless steel with electroactive coating, J. Electrochem. Soc. 132 (1985) 1022-1026.
19. A. Talo, P. Passiniemi, O. Forsen, S. Ylasaari, Polyaniline/epoxy coatings with good anti-corrosion properties, Synth. Met. 85 (1997) 1333-1334.
20. N. Ahmad, A.G. MacDiarmid, Inhibition of corrosion of steels with the exploitation of conducting polymers, Synth. Met. 78 (1996) 103-110
21. N. B.Panah, I. Danaee, Study of the anticorrosive properties of polypyrrole/polyaniline bilayer via electreochemical techniques, Prog. Org. Coat. 68 (2010) 214–218.
22. N.C.T. Martins, T. Moura e Silva, M.F. Montemor, J.C.S. Fernandes, M.G.S. Ferreira, Polyaniline coatings on aluminum alloy 6061-T6: electrosynthesis and characterization, Electrochim. Acta 55 (2010) 3580–3588.
23. M.R. Bagherzadeh, F. Mahdavi, M. Ghasemi, H. Shariatpanahi, H.R. Faridi, Using nanoemeraldine salt-polyaniline for preparation of a new anticorrosive water-based epoxy coating, Prog. Org. Coat. 68 (2010) 319–322.
24. R. Vera, P. Verdugo, M. Orellana, E. Munoz, Corrosion of aluminum in copper-aluminum couples under a marine environment: Influence of polyaniline deposited onto copper, Corros. Sci. 52 (2010) 3803-3810.
25. A. Sakhri, F.X. Perrin, E. Aragon, S. Lamouric, A. Benaboura, Chlorinated rubber paints for corrosion prevention of mild steel: a comparison between zinc phosphate and polyaniline pigments, Corros. Sci. 52 (2010) 901–909.

26. H.M. Wang, R. Akid, M. Gobara, Scratch-resistant anticorrosion sol–gel coating for the protection of AZ31 magnesium alloy via a low temperature sol–gel route, Corr. Sci. 52 (8) (2010) 2565-2570.
27. N.D. Nam, J.G. Kim, Y.J. Lee, Y.K. Son, A study on the corrosion protection of polyaniline coating in acidic solution using electrochemical methods, Corros. Sci. 51 (2009) 3007–3013.
28. J. Lu, K.S. Moon, B.K. Kim, C.P. Wong, High dielectric constant polyaniline/epoxy composites via in situ polymerization for embedded capacitor applications, Polymer 48 (2007) 1510–1516.
29. W. Jia, R. Tchoudakov, E. Segal, M. Narkis, A. Siegmann, Electrically conductive composites based on epoxy resin containing polyaniline-DBSA and polyaniline-DBSA-coated glass fibres, J. Appl. Polym. Sci. 91 (2004) 1329–1334.
30. P. Tsotra, K. Friedrich, Thermal Mechanical & Electrical Properties of Epoxy resin/polyaniline-dodecylbenzene sulphonic acid blends, Synth.Met. 143 (2004) 237-242.
31. P. Tsotra, O. Gryshchuk, K. Friedrich, Morphological studies of epoxy/polyaniline blends, Macromol. Chem. Phys. 206(7) (2005) 787–793.
32. P. Tsotra, K. Friedrich, Short carbon fiber reinforced epoxy resin/polyaniline blends: their electrical and mech- anical properties, Compos. Sci. Technol. 64(15) (2004) 2385–2391.
33. W. Jia, R. Tchoudakov, E. Segal, R. Joseph, M. Narkis, A. Siegmann, Electrically conductive composites based on epoxy resin with polyaniline-DBSA fillers, Synth. Met. 132 (2003) 269–278.
34. V.X. Moreira, F.G. Garcia, B.G. Soares, Conductive epoxy/amine system containing polyaniline doped with dodecylbenzenesulfonic acid, J. Appl. Polym. Sci. 100(5) (2006) 4059–4065.
35. T. Jeevananda, S. Palaniappan, Siddaramaiah, Spectral and Thermal Studies on Polyaniline-Epoxy Novolac Resin Composite Materials, J. Appl. Polym. Sci. 74 (1999) 3507–3512.
36. L. Shao, J.H. Qiu, H.X. Feng, M.Z. Liu, G.H. Zhang, J.B. An, C. M. Gao, H. L. Lin, Structural investigation of lignosulfonate doped Polyaniline, Synth. Met. 159 (2009) 1761-1766.

37. C. Yang, P. Liu, Water dispersed conductive polypyrroles doped with Lignosulfonate & the weak temperature dependence of electrical conductivity, Ind. Eng. Chem. Res 48 (2009) 9498-9503.
38. S. Roy, J. M. Fortier, R. Nagarajan, S. Tripathy, J. Kumar, L.A. Samuelson, F. F. Bruno, Biomimetic synthesis of a water soluble conducting molecular complex of polyaniline and lignosulfonate, Biomacromolecules 3(5) (2002) 937-941.
39. A. A. Chirkunov, Yu. J. Kuznetsov, M.A. Gusakova, Protection of low carbon steel in aqueous solutions by lignosulphonate inhibitors, Protection of Metal 43 (2007) 367-372.
40. X. Ouyang, X. Qiu, H. Lou, D. Yang, Corrosion & Scale inhibition properties of sodium lignosulfonate & its potential application in recirculating cooling water system, Ind. Eng. Chem. Res. 45(16) (2006) 5716-5721.
41. J.C. Seegmiller, J.E.Pereira da Silva, D.A.Buttry, S.I. Cordoba de Torresi, R.M. Torresi, Mechanism of action of corrosion protection coating for AA2024-T3 based on poly (aniline)-poly (methylmethacrylate) blend, J. Electrochem. Soc. 152 (2005) B45-B53.
42. J. Yun Kwon, E. Y. Kim, H. D. Kim, Preparation & Properties of Waterborne – Polyurethane Coating Materials Containing Conductive Polyaniline, Macromol. Res. 12(3) (2004) 303-310.
43. D. Zaarei, A. Sarabi, F. Sharif, M. M. Gudarzi, S. M. Karsiriha, Corrosion resistant Epoxy nanocomposite coatings containing sub micron emeraldine-base polyaniline and organo modified montmorrilonite", U.S.Patent No. US 2010/0010119 A1 (2010).
44. M.G. Hosseini, M.Raghibi-Boroujeni, I. Ahadzadeh, R.Najjar & M.S.Seyed Dorraji, Effect of Polypyrrole-montmorillonite nanocomposites powder addition on corrosion performance of epoxy coatings on Al 5000, Prog. Org. Coat. 66 (2009) 321-327.
45. C. Basavaraja, R. Pierson, T. K. Vishnuvardhan, D. S. Huh, Characterization and Electrical Behavior of Polyaniline–Poly-N-isopropylacrylamide-co-acrylic acid/Alumina Aqueous Dispersions in the presence of Dodecyl benzenesulfonic acid" European Polymer Journal 44 (2008) 1556-1566.
46. J. M. Gustavsson, P.C. Innis, J. He, G.G.Wallace, D.E.Tallman, Processible Polyaniline-HCSA/poly(Vinyl Acetate-co-Butyl Acrylate) Corrosion Protection Coatings for AA2024-T3: A SVET and Raman study, Electrochim. Acta 54(5) (2009) 1483-1490.
47. G. P.Porebska, M. Stratmann, M. Rohwerder, U. Rammelt, L. M.Duc, W. Plieth, Release mechanism of electrodeposited polypyrrole doped with corrosion inhibitor anions, J. Solid State Electrochem. 10(9) (2006) 730-736.

48. M. Rohwerder, L.M. Duc, A. Michalik, In-situ investigation of corrosion localised at the buried interface between metal and conducting polymer based on composite coatings, Electrochim. Acta 54 (2009) 6075-6081.
49. M. Rohwerder, S.I.Uppenkamp, C.A.Amarnath, Application of the Kelvin Probe method for screening the interfacial reactivity of conducting polymer based coatings for corrosion protection, Electrochim. Acta 56 (2011) 1889–1893.
50. J.H.Huh, E.J.Oh, J.H.Cho, Corrosion characteristics of electrochemically prepared phosphate doped polyaniline films in acidic chloride environments, Synth. Mat. 153 (2005) 13-16.
51. K. Kamaraj, T. Shiva, S.Sathiyanarayanan, S. Muthukrishnan, G. Venkatachari, Synthesis of oxalate doped polyaniline and its corrosion protection performance, J. Solid State Elect. 16 (2012) 465-471.
52. Y. Dong, Y. Liu, Q. Zhou, Comparative studies on the corrosion protection effect of different ions selective polyaniline coatings, Adv. Mat. Res. 287 (2011) 2464-2469.
53. K.C.Chang, M.C.Lai, C.W.Peng, Y.T.Chen, C.L.Lin, J.C.Yang, Comparative studies on the corrosion protection effect of DBSA-doped polyaniline prepared from in situ emulsion polymerization in the presence of hydrophilic Na^{+}-MMT and organophilic organo-MMT clay platelets, Electrochim. Acta 51 (2006) 5645-5653.
54. S. Nagashima, S. Ando, K. Makino, T. Tsukamoto, H. Ohshima, Size dependence of polymer composition in the surface-layer of poly (acrylamide-co-acrylic acid) hydrogel microspheres, J. Coll. Inter. Sci., 197 (1998) 377-382.
55. J.M Liu, L.Sun, S.C. Yang, "Molecular complex of conductive polymer and polyelectrolyte and a process of producing same" US Patent 5489400 (1996).
56. P.Ghosh, A.Chakrabarti, S.K. Siddhanta, Studies on stable aqueous polyaniline prepared with the use of polyacrylamide as the water soluble support polymer, European Poly. Jour. 35 (1999) 803-813.
57. A.Mathiazhagan, R.Joseph, Inter. J. Chem. Eng. Appl., 2(4) 2011, 225-237.
58. M. A. D. Crespo, E. O. Bustamante, A. M. T. Huerta, F.J. R. Gomez, Morphology and Corrosion Performance of Chromate Conversion Coatings on Different Substrates, J. Mexi. Chem. Soc. 52 (2008) 235-240.
59. H. A. Katzman, G.M. Malouf, R. Bauer, G.W. Stupian, Corrosion protective chromate coatings on aluminium, App. Surf. Sci. 2 (1979) 416-432.

60. Jie He, V. J. Gelling, D.E. Tallman, G.P. Bierwagen, A scanning vibrating electrode study of chromate-epoxy primer on steel and aluminum, J. Electrochem. Soc. 147 (2000) 3661-3666.
61. A.G. MacDiarmid, Synthetic metals: A novel role for organic oolymers (Nobel Lecture), Angewandte Chemie Inter. Ed. 40 (2001) 2581-2590.
62. P. Zarras, J. D. Stenger-Smith, An introduction to corrosion protection using electroactive polymers, In electroactive polymers for corrosion control, P. Zarras, J. D. Stenger-Smith, Y. Wei, ACS Symposium series 843, (2003) 2-17 American Chemical Society, Washington DC; 2003, Chapter 1, 2-17.
63. Swapan Kumar Ghosh, "Self-healing Materials: Fundamentals, Design Strategies, and Applications" Wiley VCH (2009).
64. Bredas J. L., Marder S. R., Salaneck W. R., Macromolecules 35 (2002) 1137-1139.
65. Image from http://homepage.ntlworld.com/colin.pratt/applcp.pdf
66. P. Zarras , N.Anderson, C. Webber, D.J. Irvin, J.A. Irvin, A. Guenthner, J.D. Stenger Smith, Progress in using conductive polymers as corrosion-inhibiting coatings, J. Rad. Phy. Chem. 68 (2003) 387-394.
67. G.Williams, H.N.McMurray, Polyaniline inhibition of filiform corrosion on organic coated AA2024-T3, Electrochim. Acta 54 (2009) 4245-4252.
68. T. Wang, Y.J. Tan, Electrodeposition of polyaniline on aluminium alloys for corrosion prevention-A study using the wire beam electrode (WBE), Mater. Sci. Eng. B 132 (2006) 48-53.
69. K.Shah, Y.R.Zhu, G. S.Akundy , J.O.Iroh, O.Popoola, Corrosion and bonding behaviors of intrinsically conductive polymers on aluminum (Al 2024-T3), Key Eng. Mat. 197 (2001) 111-119.
70. A.G. Macdiarmid, J.C. Chiang, A.F. Richter, A.J. Epstein, Polyaniline: a new concept in conducting polymers, Synth. Met. 18 (1987) 285-290.
71. A.B. Samui, A S Patankar, J. Rangarajan, P.C.Deb, Study of polyaniline containing paint for corrosion protection, Prog. Org. Coat. 47 (2003) 1-7.
72. Wessling B., Corrosion prevention with an organic metal (polyaniline):surface ennobling,passivation, corrosion test results, Mater.Corros. 47 (1996) 439-445.
73. K. G. Shah, G.S. Akundy, J.O. Iroh, Polyaniline coated on aluminium (Al-2024-T3): Characterization and electrochemical studies, J. Appl. Poly. Sci. 85 (2002) 1669-1675.
74. P.Zarras, J.D.Stenger-Smith, Y. Wei, Electroactive Polymers for Corrosion Control, B.C. Berry, A. U. Shaikh, T. Viswanathan, Lignosulfonic doped polyaniline (LIGNO-

PANI)for the corrosion prevention of cold rolles steel, "American Chemical Society, Vol. 843 Chapter 12, 182–195 (2003) [DOI: 10.1021/bk-2003-0843.ch012].

75. P. Chandrasekhar, Conducting polymers: Fundamentals and Applications, Kluwer Academic Publications, Springer (1999) 20-22.
76. B.C. Kim, G.M. Spinks, C.O. Too, G.G. Wallace, Y.H. Bae, N. Ogata, Incorporation of novel polyelectrolyte dopants into conducting polymers, React. Func. Poly. 44 (2000) 245-258.
77. U. Riaz, S. A. Ahmad, S.M. Ashraf, S. Ahmad, Effect of dopant on the corrosion protective performance of environmentally benign nanostructured conducting composite coatings, Prog. Org. Coat. 65 (2009) 405-409.
78. T. Schauer, A. Joos, L. Dulog, C.D. Eisenbach, Protection of iron against corrosion with polyaniline primers, Prog. Org. Coat. 33 (1998) 20–27.
79. R. Racicot, M.N. Alias, R. Brown, R. L. Clark, H.B. Liu, S.C. Yang, Anticorrosion of Aluminum: A novel electroactive undercoat, Mat. Res. Soc. Symp. Proc. 413 (1996) 529-534.
80. R.J.Racicot, S.C.Yang, R.Brown, Evidence of a Passive Layer formation from a conductive polymer coating on aluminum alloys, Mat. Res. Soc. Sym. Proc. 458 (1997) 415-420.
81. S.C.Yang, H.Liu, R.L.Clark, "Conducting polymers for coatings and antielectrostatic applications", USPatent 6656388B1 (2003).
82. R.J.Racicot, R.L.Clark, H.B.Liu, S.C. Yang, M.N.Alias, R.Brown, Thin Film Conductive Polymers on Aluminum Surfaces: Interfacial Charge Transfer and Anti-corrosion Aspects, SPIE-Inter. Soc. Opt. Eng. 2528 (1995) 251-258.
83. L.Sun, H. Liu, R.Clark, S.C. Yang, Double strand polyaniline, Syn. Met. 84 (1997) 67-68.
84. R. Racicot, R. Brown, S. C. Yang, Corrosion Protection of Aluminum Alloys by Double-Strand Polyaniline, Syn. Met. 85 (1997) 1263-1264.
85. Q. Sun, M.C. Park, Y. Deng, Dendritic superstructure formation of polyaniline prepared using a water soluble polyelectrolyte copolymer as the support matrix, Mater. Lett. 61 (2007) 3052-3055.
86. Joseph H. Koo, "Polymer Nanocomposites: Processing, Characterization, and Applications" McGraw-Hill (2006).
87. R. Gangopadhyay, A De, Conducting polymer nanocomposites:a brief overview, Chem. Mater. 12 (2000) 608-622.

88. Ali Eftekhari, “Nanostructured Conductive Polymers” Wiley (2010).
89. S. S. Ray, K. Okamoto, M. Okamoto, Structure-property relationship in biodegradable poly(butylenes succinate)/layered silicate nanocomposites, Macromolecules 36 (2003) 2355-2367.
90. M Alexandre, P Dubois, Polymer-Layered nanocomposites: Pre- paration, Properties and use of a new class of materials, Mater.Sci.Eng. A 28 (2000) 1-63.
91. http://www.nanoclay.com/
92. R. Krishnamoorti, R.A. Vaia, E.P Giannelis, Structure and dynamics of polymer-layered silicate nanocomposites, Chem. Mater. 8 (1996) 1728-1734.
93. J.M.Yeh, S.J. Liou, C.Y. Lai, P.C.Wu, Enhancement of corrosion protection effect in polyaniline via the formation of polyaniline-clay nanocomposite materials, Chem. Mater. 13 (2001) 1131-1136.
94. H.M. Lee, H.J. Choi, Synthesis and characterization of polyaniline-Na^+ montmorillonite nanocomposite by microemulsion polymerization, Mole. Crys. Liq.Crys. 463 (2007) 221-225.
95. N.Shahid, R.G.Villate, A.R.Baron, Chemically functionalized alumina nanoparticle effect on carbon fiber/epoxy composites, Composites Sci. Technology 65 (2005) 2250-2256.
96. W. S. Hummers, R.E. Offeman, Preparation of Graphitic Oxide, J. Am. Chem. Soc. 80 (6) (1958) 1339–1339.
97. T.Kuilla, S.Bhadra, D.Yao, N.H.Kim, S.Bose, J.H.Lee, Recent Advances in Graphene Based Polymer Composites, Prog. Poly. Sci. 35 (2010) 1350-1375.
98. Y. Si, E. T. Samulski, Synthesis of water soluble graphene, Nano Lett., 8 (6) (2008) 1679–1682.
99. A. Liu, C. Li, H. Bai, G. Shi, Electrochemical deposition of polypyrrole/sulfonated graphene composite films, J. Phys. Chem. C 114 (2010) 22783–22789.
100. D.Prasai, J.C.Tuberquia, R.R.Harl, G.K.Jennings, K.I.Bolotin, Graphene: Corrosion inhibiting coating, ACS Nano 6(2) (2012) 1102-1108.
101. S.Chen, L.Brown, M.Levendorf, W.Cai, S.Y.Ju, J.Edgeworth, X. Li , C.W. Magnuson, A. Velamakanni, R.D. Piner, J.Kang, J.Park, R.S. Ruoff, Oxidation resistance of graphene-coated Cu and Cu/Ni alloy, ACS Nano 5(2) (2012) 1321-1328.
102. S. Sreevatsa, A.Banerjee,G.Haim, Graphene as a permeable ionic barrier, ECS Meeting Abstract 901(38) (2009) 1319.

103. N.T.Kirkland, T.Schiller, N.Medhekar, N.Birbilis, Exploring graphene as a corrosion protection barrier, Corros Sci. 56 (2012) 1-4.
104. R.K.S.Raman, P.C.Banerjee, D.E.Lobo, H.Gullapalli, M.Sumandasa, A.Kumar, L.Choudhary, R. Tkacz, P.M.Ajayan, M.Majumder, Protecting copper from electrochemical degradation by graphene coating, Carbon 50 (11) (2012) 4040-4045.
105. E.Armelin, R.Pla, F. Liesa, X. Ramis, J.I. Iribarren, C.Aleman, Corrosion protection with polyaniline and polypyrrole as anticorrosive additives for epoxy paint, Corros Sci. 50 (2008) 721-728.
106. S. de Souza, Smart coating based on polyaniline acrylic blend for corrosion protection of different metals, Surf. Coat. Tech. 201 (2007) 7574-7581.
107. B.H.Kim, J.H. Jung, S.H. Hong, and J. Joo, A. J. Epstein, K. Mizoguchi, J. W. Kim, H. J. Choi, Nanocomposite of polyaniline and Na^+ montmorillonite clay, Macromolecules 35 (2002) 1419-1423.
108. D.Lee, K.Char, S. W. Lee, Y. W. Park, Structural changes of polyaniline/montmorillonite nanocomposites and their effects on physical properties, Mater. Chem. 13 (2003) 2942–2947.
109. F. Sun, Y. Pan, J.Wang, Z. Wang, C. Hu, Q.Dong, Synthesis of conducting polyaniline-montmorillonite nanocomposites via inverse emulsion polymerization in supercritical carbon dioxide, Poly. Comp. 31(1) (2010) 163-172.
110. F. Chen, P. Liu, Conducting polyaniline nanoparticles and their dispersion for waterborne corrosion protection coatings, ACS Appl. Mater. Interfaces 3 (7) (2011) 2694–2702.
111. K. Shah & J. Iroh, Electrochemical synthesis and corrosion behavior of poly(N-ethyl aniline) coatings on Al-2024 alloy, Synth. Met. 132 (2002) 35-41.
112. J. O. Iroh & W. Su, Corrosion performance of polypyrrole coating applied to low carbon steel by an electrochemical process, Electrochim. Acta 46 (2000) 15-24.
113. S. Chaudhari, P.P.Patil, Corrosion-protection aspects of electrochemically synthesized poly(o-anisidine) coatings on mild steel: An electrochemical impedance spectroscopy study, Jour. App. Polymer Sc. 106 (1) (2007) 400-410.
114. A. Cook, A. Gabriel, N. Laycock, On the mechanism of Corrosion Protection of Mild Steel with polyaniline, J. Electrochem. Soc. 151(9) (2004) B529-B535.
115. A.Yasmin, J.L.Abot, I.M. Daniel., Processing of Clay/Epoxy Nanocomposites by Shear Mixing, Scripta Materialia 49 (2003) 81–86.

116. B. G. Soares, M.L. Celestino, M. Magioli, V. X. Moreira, D. Khastgir, Synthesis of conductive adhesives based on epoxy resin and polyaniline-DBSA using the in situ polymerization and physical mixing procedures, Synt. Metals 160 (2010) 1981–1986.
117. R. J. Holness, G. Williams, D. A. Worsley, H. N. McMurray, Polyaniline inhibition of corrosion –driven organic coating cathodic delamination on iron, J. Electrochem. Soc. 152(2) (2005) B73–B81.
118. G. Williams, A. Gabriel, A. Cook, H. N. McMurray, Dopant Anion Effects in the Inhibition by Polyaniline of Corrosion-Driven Organic Coating Delamination on Iron, J. Electrochem. Soc. 153(10) (2006) B425–B433.
119. A. Gabriel, N.J. Laycock, H.N. McMurray, G. Williams, A. Cook, Oxidation States Exhibited by In-coating Polyaniline during Corrosion-driven Coating Delamination on Carbon Steel, Electrochem. Solid State Lett. 9(12) (2006) B57-B60.
120. J.N. Barisci, T.W. Lewis, G.M. Spinks, C.O. Too, G.G. Wallace, Conducting Polymers as a Basis for Responsive Materials Systems, J. Intell. Mater. Syst. Struct. 9 (1998) 723-731.
121. P. J. Kinlen, V. Menon, Y. W. Ding, A mechanistic investigation of polyaniline corrosion protection using the scanning reference electrode technique, J. Electrochem. Soc. 146 (1999) 3690-3695.
122. P. J. Kinlen, Y. Ding, D. C. Silverman, Corrosion protection of mild steel using sulfonic and phosphonic acid-doped polyanilines, Corrosion 58 (2002) 490-497.
123. A. Cook, A. Gabriel, D. Siew, N. Laycock, Curr. Corrosion protection of low carbon steel with polyaniline: passivation or inhibition? Appl. Phys. 4 (2004) 133–136.

List of Publications

1. **G.Gupta**, N.Birbilis, A.B.Cook, A.S.Khanna, "Polyaniline-lignosulfonate/epoxy coating for corrosion protection of AA2024-T3", Corrosion Science, 67 (2013) 256-267

2. **G.Gupta**, N.Birbilis, A.S.Khanna, “An Epoxy Based Lignosulphonate Doped Polyaniline- Poly(Acrylamide Co-Acrylic Acid) Coating for Corrosion Protection of Aluminium Alloy 2024-T3” Int. J. Electrochem. Sci., 8 (2013) 3132 – 3149

3. **G.Gupta**, S.S.Pathak, A.S.Khanna, "Anticorrosion performance of eco-friendly silane primer for coil coating applications", Progress in Organic coating, 74 (1) (2012) 106-114.(M.Tech work)

4. **G.Gupta**, N.Birbilis, A.S.Khanna, oral presentation on "Corrosion resistant double stranded conducting polymer nanocomposite coating for aircraft applications" in 33rd Australasian Polymer Symposium at Hobart, Australia. This paper was published in the 33rd Australasian Polymer Symposium proceedings, ISBN number: 978-0-646-57205-5

5. Publish article "Inorganic-Organic Hybrid Nanocomposites : A Shift in Coating Performance" in Chemical World Magazine in May 2010